Spektroskopische Aufklärung der Photoaddition von Psoralen an DNA

Inaugural-Dissertation

zur Erlangung des Doktorgrades
der Mathematisch-Naturwissenschaftlichen Fakultät
der Heinrich-Heine-Universität Düsseldorf

vorgelegt von

Janina Bertling

aus Braunschweig

Düsseldorf, Mai 2022

aus dem Institut für Physikalische Chemie II
der Heinrich-Heine-Universität Düsseldorf

Gedruckt mit der Genehmigung der
Mathematisch-Naturwissenschaftlichen Fakultät der
Heinrich-Heine-Universität Düsseldorf

Berichterstatter:

1. Prof. Dr. Peter Gilch
2. Prof. Dr. Thomas J. J. Müller
3. Prof. Dr. Karin Hauser

Tag der mündlichen Prüfung: 21. März 2022

Ich versichere an Eides Statt, dass die Dissertation von mir selbständig und ohne unzulässige fremde Hilfe unter Beachtung der „Grundsätze zur Sicherung guter wissenschaftlicher Praxis an der Heinrich-Heine-Universität Düsseldorf“ erstellt worden ist.

Düsseldorf, den 25. Mai 2022

Janina Bertling

Diese Dissertation wurde in der Zeit von November 2017 bis Juni 2021 im Arbeitskreis Femtosekundenspektroskopie des Instituts für Physikalische Chemie II der Mathematisch-Naturwissenschaftlichen Fakultät der Heinrich-Heine-Universität Düsseldorf unter der Leitung von Prof. Dr. Peter Gilch angefertigt.

Danksagung

Ich möchte mich sehr bei Prof. Dr. Peter Gilch bedanken. In erster Linie für die Betreuung dieser Arbeit, also das Beantworten vieler Fragen und das gemeinsame Diskutieren verschiedenster Problemstellungen rund um die geliebten Psoralene. Du hattest aber immer auch ein Ohr für Probleme die nicht im Bereich der Psoralene lagen. Ich hatte außerdem die Möglichkeit meine Arbeit auf der ein oder anderen internationalen Konferenz präsentieren zu dürfen und diese Erfahrung möchte ich nicht missen.

Bei Prof. Dr. Thomas J. J. Müller möchte ich mich für die Übernahme des Zweitgutachtens sowie die gute Zusammenarbeit bedanken. Danke auch an Dr. Sarah Geenen, dass ihr uns Psoralene synthetisiert habt, die nicht langweilig sind, sondern unser Können herausgefordert haben ;)

Bei Prof. Dr. Karin Hauser möchte ich mich für die Übernahme des dritten Gutachtens bedanken.

Ich danke der Jürgen Manchot Stiftung für die Förderung dieser Arbeit durch ein Promotionsstipendium.

Prof. Dr. Wolfgang Zinth und Dr. Julia Gontcharov danke ich für die zeitaufgelösten IR-Messungen und die tolle Zusammenarbeit. Vielen Dank für die Möglichkeit mit meinen Proben eurem Labor in München einen Besuch abzustatten. Der Aufbau ist wirklich beeindruckend gewesen!

Bei Kristoffer A. Thom möchte ich mich für irgendwie alles bedanken: für die Süßigkeitenschublade, die akribischen Diskussionen über die passende Farbgebung bei Abbildungen, die „endlose Geduld“ mit den Psoralenen bei den Nanosekundenmessungen ... etc. pp. Ob ich die Promotion auch ohne dich durchgestanden hätte? Vermutlich schon. Aber es wäre lange nicht so amüsant gewesen. Du bist auf jeden Fall am meisten Schuld daran, dass ich die Promotionszeit vermissen werde.

Allen anderen Mitdoktoranden und Postdocs, Dr. Christian Torres, Dr. Jakob Nixdorf, Dr. Anna Reiffers, Oliver Nolden, Wiebke Haselbach, Mahboubeh Morshedi, Carolin Borbeck, Francisco van Riel Neto und Dr. Babara Elza Nogueira de Faria danke ich für die Zusam-

menarbeit und die lustigen Mittags- und Kuchenpausen (wenn nicht grade eine Pandemie uns davon abgehalten hat). Klaus Kelbert, Veronika Mendorf und Franziska Bergstein danke ich für die Aushilfe in allen organisatorischen Dingen oder wenn mal wieder was „kaputt“ gegangen ist. Ihr seid toll! Bei meinen Bachelorstudenten Hannah Jeuken, Matthias Jantz, Robert Heße, Isabell Theves und Mathieu Kippes möchte ich mich für die gute Zuarbeit zu den Fragestellungen meiner Promotionsarbeit bedanken.

Laura, vielen Dank für die tolle Zeit im Studium! Fürs gemeinsame Vorbereiten auf die Prüfungen, aber vor allem für den Spaß den wir zusammen in Düsseldorf hatten!

Bei meiner Familie möchte ich mich dafür bedanken, dass sie einfach immer für mich da ist. Ich freue mich darauf diese Liebe nun an meine eigene kleine Familie weitergeben zu können. Also Junior, ich hoffe du erwähnst deinen Papa und mich dann auch in deiner Dissertation!

Publikationen und Konferenzbeiträge

Publikationen:

- J. Bertling, K. A. Thom, S. Geenen, H. Jeuken, L. Presser, T. J. J. Müller, P. Gilch: „Synthesis and Photophysics of Water-Soluble Psoralens with Red-Shifted Absorption“, *Photochem. Photobiol.* **2021**, 97, 6, 1534–1547, doi:10.1111/php.13480
- J. Diekmann, I. Theves, K. A. Thom, P. Gilch: „Tracing the Photoaddition of Pharmaceutical Psoralens to DNA“, *Molecules* **2020**, 25, 22, 5242, doi:10.3390/molecules25225242
- J. Diekmann, J. Gontcharov, S. Fröbel, C. Torres Ziegenbein, W. Zinth and P. Gilch: „The Photoaddition of a Psoralen to DNA Proceeds via the Triplet State“, *J. Am. Chem. Soc.* **2019**, 141, 34, 13643-13653, doi:10.1021/jacs.9b06521
- A. Reiffers, C. Torres Ziegenbein, L. Schubert, J. Diekmann, K. A. Thom, R. Kühnemuth, A. Griesbeck, O. Weingart and P. Gilch: „On the large apparent Stokes shift of phthalimides“, *Phys. Chem. Chem. Phys.* **2019**, 21, 4839–4853, doi:10.1039/c8cp07795a

Aktive Konferenzteilnahmen:

- **Short Talk:** J. Diekmann, J. Gontcharov, W. Zinth, P. Gilch: *Tracing the Photoaddition of Psoralen to DNA*, Central European Conference on Photochemistry, Bad Hofgastein (Österreich), 02/2020
- **Poster:** J. Diekmann, O. Nolden, K. Thom, P. Gilch: *Time-resolved Spectroscopy on Chemical and Biological Processes*, ELI Beamlines Ultrafast Spectroscopy User Workshop, Dolní Břežany (Tschechien), 09/2019
- **Lecture:** J. Diekmann, C. Torres Ziegenbein, J. Gontcharov, W. Zinth, P. Gilch: *Photo-Addition of Psoralen to DNA Traced by Time Resolved Spectroscopy*, 34th European Congress on Molecular Spectroscopy, Coimbra (Portugal), 08/2018
- **Short Talk:** J. Diekmann, C. Torres Ziegenbein, P. Gilch, J. Gontcharov, W. Zinth: *Time Resolved Spectroscopy on the Mechanism of PUVA Therapy*, Central European Conference on Photochemistry, Bad Hofgastein (Österreich), 02/2018

– **Short Talk:** J. Diekmann, S. Fröbel, P. Gilch: *Photoaddition of Psoralens to DNA traced by Time-Resolved Spectroscopy*, 28th International Conference on Photochemistry, Strasbourg (Frankreich), 07/2017

Zusammenfassung

Psoralene sind eine Gruppe von Naturstoffen. Sie finden Einsatz in der PUVA-Therapie (Psoralen + UVA), welche zur Behandlung von Hautkrankheiten wie z.B. Psoriasis, Neurodermitis und dem kutanen T-Zell-Lymphom eingesetzt wird. Die Therapie basiert auf der Interkalation der Psoralene in die DNA der erkrankten Zelle. Durch Bestrahlung mit Licht aus dem UV-A-Bereich bindet das Psoralen unter Ausbildung eines Cyclobutanrings kovalent an die DNA-Base Thymin (siehe Abbildung 1). Diese Anbindung führt schlussendlich zur Apoptose, dem programmierten Zelltod. Infolgedessen kann eine Linderung der Symptome festgestellt werden.

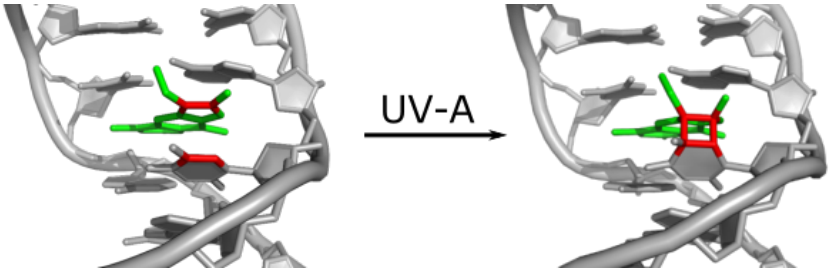

Abbildung 1. – Bei Belichtung mit UV-A-Strahlung bindet das interkalierte Psoralen AMT an die Thymin-Base der DNA.

In vorangegangen Arbeiten konnte mittels Femtosekunden-UV/Vis-Spekroskopie ein photoinduzierter Elektrontransfer (PET) zwischen dem interkalierten Psoralen und einer naheliegenden Guanin-Base festgestellt werden. Der UV-angeregte Zustand des Psoralens wird so innerhalb weniger Pikosekunden gelöscht. Der PET unterdrückt damit die gewünschte Reaktion der Photoanbindung. Durch Wahl einer synthetischen, Guanin-freien DNA konnte in dieser Arbeit mittels Nanosekunden-UV/Vis- und IR-Spekroskopie erstmals die Anbindung des Psoralen-Derivats 4'-Aminomethyl-4,5',8-trimethylpsoralen (AMT) an die DNA im Detail verfolgt werden. Es konnte gezeigt werden, dass die Anbindung im Mikrosekundenbereich stattfindet. Sie verläuft über den lokalen Triplettzustand des Psoralens sowie eines Triplett-Biradikals, bei welchem das Psoralen über eine kovalente Bindung an die Thymin-Base gebunden ist. Für die pharmazeutisch angewandten Derivate 8-Methoxypsoralen (8-MOP) und 4,5',8-Trimethylpsoralen (TMP) konnte ebenfalls eine Anbindung über den Triplett-Zustand nachgewiesen werden.

Zudem wurden vier im Institut für Organische Chemie unter der Leitung von Prof. Dr. Thomas J. J. Müller synthetisierte Psoralene auf ihre photophysikalischen Eigenschaften und

ihrer Tauglichkeit bezüglich der PUVA-Therapie hin untersucht. Mittels Femtosekunden-UV/Vis-Spektroskopie und Cyclovolammetrie konnte gezeigt werde, dass es weiterer Optimierung für einen Einsatz in der PUVA-Therapie bedarf. Basierend auf diesen Ergebnissen konnten Kriterien für die Verbesserung der Psoralen-Derivate formuliert werden.

Abstract

Psoralenes are a group of natural compounds. As active ingredient, they are used in the PUVA (Psoralen + UV-A) therapy to treat skin diseases such as psoriasis, atopic eczema and cutaneous T-cell lymphoma. Psoralenes intercalate into the DNA of the diseased cells. Upon excitation with UV-A light they bind covalently to the thymine base of DNA forming a cyclobutane ring (see Figure 1). This reaction ultimately leads to apoptosis, the programmed cell death of the affected cell. As a result, symptoms of the diseases can be relieved.

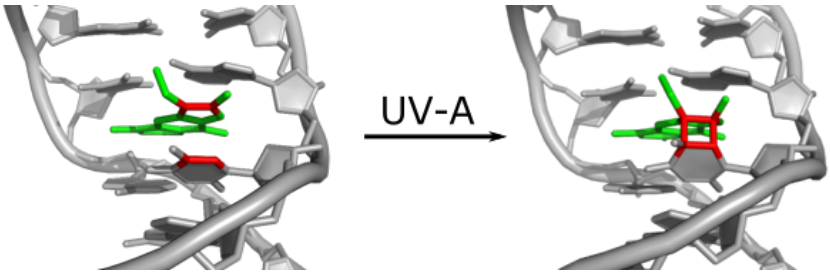

Figure 1. – Upon excitation with UV-A light the intercalated psoralen AMT binds to the thymine base of DNA.

In preceding studies, a photo-induced electron transfer (PET) from a nearby guanine base to the intercalated psoralen could be identified by means of femtosecond UV/Vis spectroscopy. As a results the UV-excited state of the psoralen is quenched within a few picoseconds. The PET, thus, suppresses the desired reaction of the photo-binding. By choosing a synthetic, guanine-free DNA, the binding of the psoralen derivative 4'-aminomethyl-4,5',8-trimethylpsoralen (AMT) to the DNA could be traced in this work for the first time using nanosecond UV/Vis and IR spectroscopy. It can be shown that the binding occurs in the microsecond range. A local triplet state of psoralen and a triplet biradical, in which the psoralen is bound to the thymine base via one covalent bond, are involved in the reaction. For the pharmaceutically applied derivatives 8-methoxypsoralen (8-MOP) and 4,5',8-trimethylpsoralen (TMP), binding via the triplet state could also be proven.

In addition, four new psoralen derivatives were synthesized at the Institute for Organic Chemistry led by Prof. Dr. Thomas J. J. Müller and tested for their photophysical properties and suitability for the PUVA therapy. Femtosecond UV/Vis spectroscopy and cyclovolammetry have shown that further optimization is required for application in PUVA therapy. Based on these results, criteria for improving the psoralen derivatives have been identified.

Abkürzungsverzeichnis

5-MOP *5-Methoxypsoralen*

8-MOP *8-Methoxypsoralen*

AMT *4'-Aminomethyl-4,5',8-trimethylpsoralen*

A *Adenin*

AT-DNA *DNA Oligomer aufgebaut aus zwei Einzelsträngen mit der Sequenz 5'-$(TA)_{20}$-3'*

CPD *Cyclobutan-Pyrimidin-Dimer*

CS *Ladungstrennung (engl.: charge separation)*

DADS *Amplitudenspectrum (engl.: Decay Associated Difference Spectra)*

DNA *Desoxyribonukleinsäure (engl.: deoxyribonucleic acid)*

ECP *Extrakorporale Photopherese*

G *Guanin*

GLA *Global Lifetime Analysis*

IR *Infrarot*

LDA *Lifetime Density Analysis*

LDM *Lifetime Density Map*

PET *Photoinduzierter Elektrontransfer*

PUVA *Psoralen + UV-A*

T *Thymin*

TMP *4,5',8-Trimethylpsoralen*

UV *Ultraviolett*

Inhaltsverzeichnis

1. Motivation

1.1. Photoschädigung der DNA

Ein zweiseitiger Artikel von James Watson und Francis Crick in der Fachzeitschrift *Nature* revolutionierte 1953 die Genetik [1]. Sie entdeckten die doppelhelikale Struktur der Desoxyribonukleinsäure, kurz DNA [2]. Damit konnten sie der Antwort auf die Frage nach der Speicherung und Vervielfältigung unserer Erbinformationen einen großen Schritt näher kommen. Dieses – für diese Arbeit so essentielle Makromolekül – soll daher zunächst im Fokus der Einleitung stehen.

Die doppelhelikale DNA ist aus zwei Einzelsträngen aufgebaut, welche über Wasserstoffbrückenbindungen zusammengehalten werden (siehe Abbildung 1.1). Das Rückgrat ist alternierend aus einem Zucker, der Desoxyribose und einer Phosphateinheit aufgebaut. An dem Zucker ist eine der vier Nukleobasen gebunden. Dabei stehen sich immer zwei Basen der beiden Einzelstränge gegenüber. Guanin und Cytosin bilden ein Basenpaar, sowie Adenin und Thymin. Da es nur diese festgelegte Basenpaarung gibt, legt ein Einzelstrang fest, welche Basenfolge der gegenüberliegende Basenstrang haben muss. Dies ist eine wichtige Eigenschaft, die zudem essentiell für den Mechanismus der Replikation der DNA ist.

Die Replikation ist ein äußerst komplexer Prozess, bei dem es zu Fehlern in der Basenabfolge kommen kann [5]. Dies wird als endogene Ursache für DNA-Schäden bezeichnet. Aber auch exogene Einflüsse können Veränderungen in der DNA hervorrufen. Meist können diese Fehler durch Enzyme repariert werden. Wenn die Reparaturmechanismen fehlschlagen, führt dies zu einer Mutation. Die DNA weist eine Reihe von Schutzmechanismen auf, die Veränderungen durch äußere Einflüsse abwehren sollen. Zusammengefasst werden diese unter dem Begriff DNA Damage Response. 2015 erhielten T. Lindahl, P. Modrich und A. Sancar den Nobelpreis in Chemie für ihre Leistungen zur Aufklärung einiger dieser zelleigenen Reperaturmechanismen [6–8].

Ein weiterer wichtiger äußerer Einflussfaktor ist die UV-Strahlung [9–11]. Die UV-C-Strahlung (200 nm – 280 nm) wird von der Ozonschicht und weiteren Molekülen in der Atmosphäre absorbiert und erreicht die Troposphäre in so geringen Mengen, dass sie unmaßgeblich ist. Auch die UV-B-Strahlung (280 nm – 315 nm) wird zu einem großen Teil absorbiert. Allerdings können besonders in den Teilen der Erde, welche von einer geringen Ozonkonzentration in der Stratosphäre betroffen sind, schnell kritische Dosen an solarer UV-B-Strahlung erreicht werden. Die UV-B-Strahlung kann durch Absorption der Nukleobasen

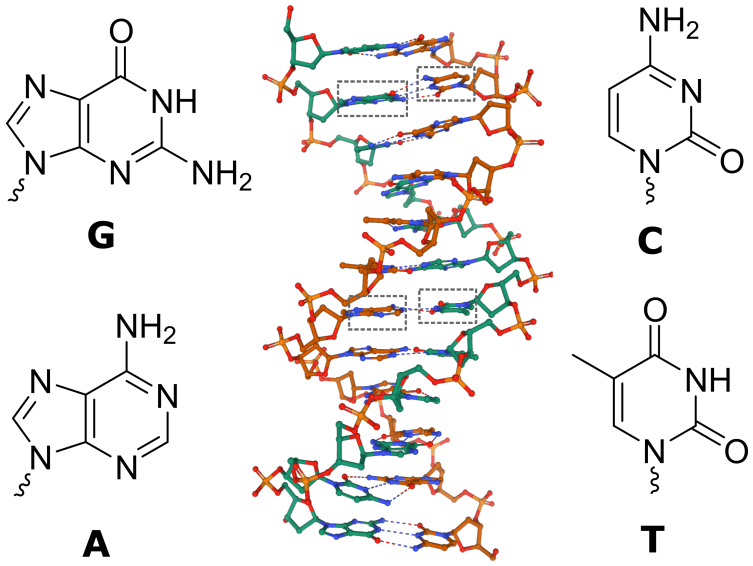

Abbildung 1.1. – Struktur einer DNA-Doppelhelix in B-Konformation. Mit grauen Kästen sind die vier verschiedenen Nukleobasen Guanin (G), Cytosin (C), Adenin (A) und Thymin (T) markiert. Ihre Strukturformeln sind links (Purinbasen) und rechts (Pyrimidinbasen) davon gezeigt. Für die Struktur der DNA wurde der PDB-Eintrag 1BNA [3] und die Software Mol* [4] für die Visualisierung genutzt.

direkt Schäden an der DNA verursachen. Die UV-A-Strahlung (315 nm – 400 nm) wird nicht von der DNA absorbiert. Sie kann allerdings zu sekundären Photoprodukten oder zu indirekter DNA-Schädigung durch Photoreaktion mit anderen durch UV-A-Strahlung angeregten Molekülen führen.

Die häufigsten Photoprodukte der DNA sind Bipyrimidin-Verbindungen [10]. Aus zwei benachbarten Pyrimidinbasen können Cyclobutan-Pyrimidin-Dimere (CPD), 6-4-Photoprodukte (6-4PP) sowie die Dewar-Valenz-Isomere gebildet werden. Der CPD-Schaden zwischen zwei Thyminbasen (siehe Abbildung 1.2) stellt den häufigsten Photoschaden dar [12]. Dennoch ist auch bei diesem Photoprodukt die Quantenausbeute gering (≈ 0.001 in genomischer DNA [13, 14]). Die schnelle Relaxation ($< 1\,\mathrm{ps}$) der angeregten Nukleobasen durch strahlungslose Desaktivierungsprozesse verläuft daher mit großen Ausbeuten [9, 15].

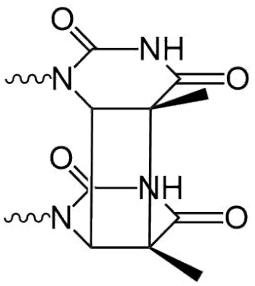

Abbildung 1.2. – Struktur eines Cyclobutan-Pyrimidin-Dimers aus zwei benachbarten Thyminbasen. Dies ist der häufigste direkte Photoschaden an der DNA.

Neben der geringen Photoreaktivität und diversen Reparaturmechanismen durch Enzyme kann auch die Apoptose, der programmierte Zelltod, im Notfall das Erbgut beschützen. Zum Schutz des gesamten Organismus, stirbt die betroffene Zelle ab. Diese Eigenschaft kann sich in Therapien, welche auf die bewusste Photosensibilisierung der DNA abzielen,

zu Nutze gemacht werden [16]. Auf diesem Ansatz basiert auch die PUVA-Therapie [17, 18]. Die photophysikalischen Prozesse der PUVA-Therapie sind Gegenstand dieser Arbeit. In den folgenden Abschnitten wird die Therapie und die aktive Substanz Psoralen näher beschrieben und die Motivation dieser Arbeit erläutert.

1.2. PUVA-Therapie – Eine Erfindung aus dem alten Ägypten?

In dermatologischen Leitlinien zur Behandlung von Psoriasis [19, 20], Neurodermitis [21], Vitiligo [22, 23] und dem kutanen T-Zell-Lymphom [24] findet sich die PUVA-Therapie. Bei der PUVA, kurz für „Psoralen + UV-A“, wird dem Patienten ein Psoralen (Grundkörper siehe Abbildung 1.3) verabreicht und anschließend das betroffene Hautareal mit UV-A-Licht bestrahlt [25]. Ziel ist das Absterben der erkrankten Hautzellen und damit die Linderung der Symptome.

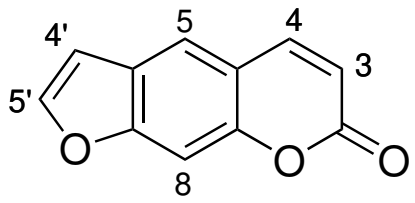

Abbildung 1.3. – Struktur von Psoralen.

Diese Art der Behandlung, welche heute als PUVA-Therapie bezeichnet wird, nahm ihre Anfänge vor über 3000 Jahren. In Ägypten wurde Vitiligo, auch bekannt als Leukoderma („weiße Haut“), mit der Aufnahme eines Extraktes der psoralenhaltigen Pflanze *Ammi majus* und anschließender Exposition der Sonne behandelt [26–28]. Unabhängig davon wurden auch in Indien die psoralenhaltigen Samen der *Psoralea corylifolia* in Kombination mit Sonnenlicht für die Behandlung von Vitiligo verwendet. Viele hundert Jahre später, Ende des 19. Jahrhunderts, veröffentlichte der dänische Dermatologe Niels Ryberg Finsen seine Forschungsergebnisse auf dem Gebiet der Phototherapie. Er wies die positive Wirkung von Sonnenlicht auf die Heilung von Hauttuberkulose nach. Damit galt er als Pionier der Phototherapie und erhielt für seine Forschung 1903 den Nobelpreis für Medizin [28]. Intensive Forschung zur Wirkweise der PUVA begann 1938 mit einer Veröffentlichung von Kuske über die photosensibilisierenden Eigenschaften einiger Psoralene [29]. Der schweizer Arzt isolierte für seine Forschung 5-Methoxypsoralen (5-MOP) (Struktur siehe Abbildung 1.4) aus Bergamottöl. 1947 schafften es die ägyptischen Forscher Fahmy und Abu-Shady an der Universität in Kairo 8-Methoxypsoralen (8-MOP) aus *Ammi majus* zu isolieren [30]. Mit dem isolierten 8-MOP führte der ägyptische Dermatologe El Mofty klinische Untersuchungen zur Behandlung von Vitiligo durch [31]. Eine ägyptische Firma begann anschließend mit der Vermarktung von Psoralenen in flüssiger und in Tablettenform und auch in Europa und Amerika startete intensivere Forschung [26]. Erst 1947 fand 8-MOP Anwendung in der Behandlung von Psoriasis [32]. Zudem entwickelten Parrish et al. eine neue UV-A Lichtquelle, welche die Effektivität im Gegensatz zu den zuvor verwendeten Schwarzlichtquellen deutlich verbesserte. In den folgenden Jahren wurde die moderne Form der PUVA-Therapie von zwei Gruppen von Forschern in Harvard, USA und Wien, Österreich maßgeblich vorangetrieben [27]. Auch eine schwerwiegende Nebenwirkung der PUVA, das Krebsrisiko,

wurde diskutiert [33]. Neben dem Einsatz als Behandlung diverser Hautkrankheiten, fanden die Psoralene weitere Einsatzgebiete. Es wurde festgestellt, dass Psoralene in Kombination mit UV-A-Bestrahlung Viren inaktivieren [34]. Diese Eigenschaft fand Anwendung in der Dekontamination von Blut zur Transfusion [35]. Heute wird hauptsächlich das Psoralen-Derivat Amotosalen für die Pathogeninaktivierung genutzt [36]. 1987 wurde schließlich eine ganz neue Methode, die „extrakorporale Photopherese“ (ECP) vorgestellt [37]. Bei dieser Form der Therapie, welche besonders bei dem kutanen T-Zell-Lymphom Anwendung findet, wird dem Blut außerhalb des Körpers Psoralen zugesetzt, mit UV-A-Licht bestrahlt und anschließend dem Patienten retransfundiert [38]. Es wird angenommen, dass die Immunantwort durch die Psoralen-modifizierten Leukozyten so moduliert wird, dass der Körper gegen die pathogenen T-Zellen effektiv immunisiert und die Produktion weiterer pathogener T-Zellen unterdrückt wird [39]. Auch bei anderen Autoimmunkrankheiten, wie zum Beispiel der Graft-versus-Host-Reaktion, zeigt die ECP eine positive Wirkung [40].

Hinsichtlich des Wirkmechanismus der PUVA-Therapie gibt es allerdings noch einige ungeklärte Fragen. Es herrscht jedoch allgemeiner Konsens, dass das Psoralen-Molekül in die Zelle eindringt [41] und dort mit Biomolekülen interagiert [42]. Das wesentliche Ziel der Psoralene im Hinblick auf die PUVA-Therapie ist die DNA. Psoralene weisen bemerkenswerte Eigenschaften in der Interaktion mit DNA auf, die in den folgenden Abschnitten näher erläutert werden.

1.3. Der Naturstoff Psoralen und seine Derivate

Psoralene sind eine Gruppe von Naturstoffen. Der planare Grundkörper setzt sich aus Cumarin und einem Furanring zusammen (siehe Abbildung 1.3). Anwendung in der Therapie finden die beiden methoxysubstituierten Derivate 8-MOP und 5-MOP sowie 4,5',8-Trimethylpsoralen (TMP) (siehe Abbildung 1.4) [25].

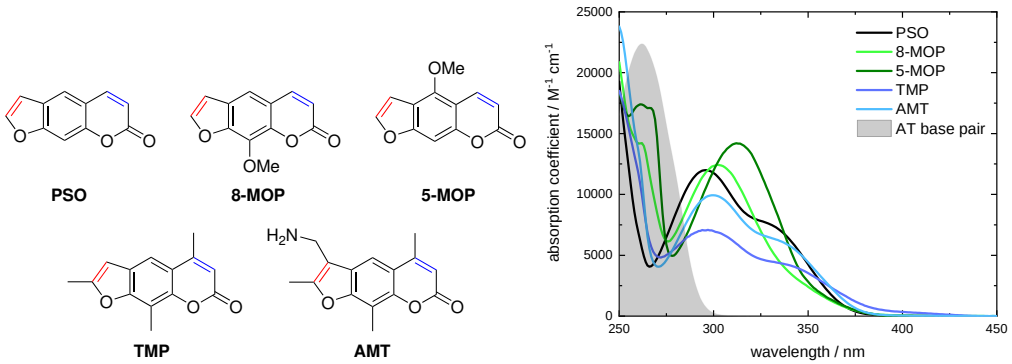

Abbildung 1.4. – Struktur und Absorptionsspektren des Grundkörpers Psoralen (PSO) sowie die in dieser Arbeit relevanten Derivate 8-Methoxypsoralen (8-MOP), 5-Methoxypsoralen (5-MOP), 4,5',8-Trimethylpsoralen (TMP) und 4'-Aminomethyl-4,5',8-trimethylpsoralen (AMT). Links: Die photo-reaktiven Doppelbindungen sind in rot (Furanseite) und blau (Pyronseite) markiert. Rechts: Neben den Absorptionsspektren der Psoralene ist in grau das Absorptionsspektrum eines AT-Basenpaars aus der in dieser Arbeit verwendeten AT-DNA (DNA-Doppelhelix bestehend aus 40 AT-Basenpaaren) dargestellt.

Für die Wirkung im menschlichen Organismus ist die Löslichkeit der Psoralene in Wasser von Bedeutung. Die Wasserlöslichkeit der drei pharmazeutischen Derivate ist gering und reicht von 0.18 mM für 8-MOP bis 2.6 µM für TMP [43]. Liegt DNA in der Lösung vor, so erhöht sich die Konzentration des gelösten Psoralens [34]. Im Zuge dieser Arbeit war allerdings ein Vergleich des photophysikalischen Verhaltens von Psoralen in DNA und Psoralen außerhalb der DNA von großer Bedeutung. Daher wurde das Derivat 4'-Aminomethyl-4,5',8-trimethylpsoralen (AMT), welches eine Wasserlöslichkeit von 34 mM aufweist [44], in den ersten Messungen dieser Arbeit eingesetzt und galt damit auch als Referenz für die folgenden Messungen der anderen Derivate. Die geringe Löslichkeit von beispielsweise TMP macht eine Charakterisierung photophysikalischer Eigenschaften in Wasser mit den hier genutzten Techniken unmöglich. Bei Zugabe von DNA steigt die apparente Löslichkeit allerdings soweit, dass die Eigenschaften von TMP in DNA im Bereich einer messbaren Größenordnung liegen.

Psoralene absorbieren Licht im UV-A-Bereich von 315 nm – 400 nm (siehe Abbildung 1.4). Diese Absorptionsbande kann der Besetzung des S_1-Zustandes zugeordnet werden [45]. Der Übergang hat $\pi\pi^*$-Charakter. Meist wird diese Absorptionsbande als Schulter einer zweiten Bande im Spektrum sichtbar. Diese Bande mit größerer Oszillatorstärke ist der Besetzung des S_3-Zustandes zuzuordnen. Dieser ist ebenfalls ein $\pi\pi^*$-Übergang. Quantenchemische Rechnungen für die Gasphase von Psoralen zeigen, dass der S_2-Zustand energetisch nahe des S_1-Zustands liegt und von $n\pi^*$-Charakter ist. In polar protischen Lösemitteln wie Wasser ist dieser allerdings blauverschoben und liegt energetisch über dem S_3-Zustand [45]. Psoralene fluoreszieren schwach zwischen 380 nm – 600 nm mit Quantenausbeuten von wenigen Prozent [46, 47]. Die Fluoreszenzlebensdauern betragen ca. 1 ns [48]. Die Triplettquantenausbeuten in Wasser liegen für die meisten Derivate zwischen 10 % – 50 % [49, 50]. Tatchen et al. zeigten, dass in polar protischen Lösemitteln ausgehend vom S_1-Zustand mit $\pi\pi^*$-Charakter nur Triplettzustände mit $\pi\pi^*$-Charakter besetzt werden [51]. Die relativ hohen ISC-Quantenausbeuten des El-Sayed verbotenen Übergangs können durch vibronische Spin-Bahn-Kopplungen erklärt werden.

Da langlebige Triplettzustände besetzt werden, können eine große Anzahl verschiedenster Photoreaktionen zwischen zwei Psoralen-Molekülen und auch mit anderen Molekülen, insbesondere Sauerstoff, in Lösung ablaufen [52]. Daher beeinflussen Psoralenkonzentration und Sauerstoffkonzentration die Reaktionsquantenausbeuten und Lebensdauern der angeregten Zustände.

1.4. Interaktion der Psoralene mit DNA

1.4.1. Interkalation der Psoralene in DNA

Die Interkalation bezeichnet die Einlagerung eines Moleküls oder Ions in Zwischenräume größerer Moleküle. Bei dieser Art der nicht-kovalenten Interaktion liegen stets interkalierte und nicht-interkalierte, also freie Moleküle, in einem Gleichgewicht vor. Bei der Interkala-

tion in DNA lagert sich das Fremd-Molekül in den Raum zwischen zwei Basenpaaren ein [53, 54]. Ein bekanntes Beispiel für einen DNA-Interkalator ist Ethydiumbromid. Es wird zur Anfärbung und damit zum Nachweis von DNA verwendet [55]. Psoralene sind ebenfalls dazu in der Lage in DNA zu interkalieren (siehe Abbildung 1.5). Auf Dichroismus basierende Messtechniken (linear-flow dichroism oder CD (circular dichroism)-Spektroskopie) eignen sich besonders gut zum Beweis für die Interkalation der Psoralene [56–58]. Andere Interaktionsarten mit DNA – wie etwa die sogenannten „Groove-Binder“ – lassen sich mit diesen Techniken von denen der Interkalatoren unterscheiden. Darüber hinaus wurden zur Bestimmung von Assoziationskonstanten (bzw. Dissoziationskonstanten) der Interkalation vielfach Gelelektrophorese oder Gleichgewichtsdialyse verwendet [59, 60].

Außerdem lässt sich die Interkalation spektroskopisch über eine Veränderung der Absorptionsbanden der Psoralene im UV-A-Bereich nachweisen [61]. Mit steigendem Verhältnis von DNA zu Psoralen, lässt sich eine Verschiebung der Absorptionsmaxima zu höheren Wellenlängen sowie eine deutliche Abnahme in der Intensität feststellen. Dieser Effekt ist auf die Wechselwirkungen der Übergangsdipolmomente von Psoralen und DNA-Base zurückzuführen [54, 58]. Der hypochrome Effekt kann zur Bestimmung der spezifischen Affinität des Psoralen-Derivats genutzt werden.

Die DNA erfährt durch Interkalation eine leichte Entwindung und damit Streckung und Versteifung der helikalen Struktur [53, 59]. Mit Zugabe von Salzen wie NaCl oder $MgCl_2$ zur Darstellung physiologischer Bedingungen, sinkt die Interkalationsaffinität [60]. Eine signifikante Präferenz der Psoralene für eine Interkalation zwischen AT- oder GC-Basenpaaren konnte nicht gefunden werden [57].

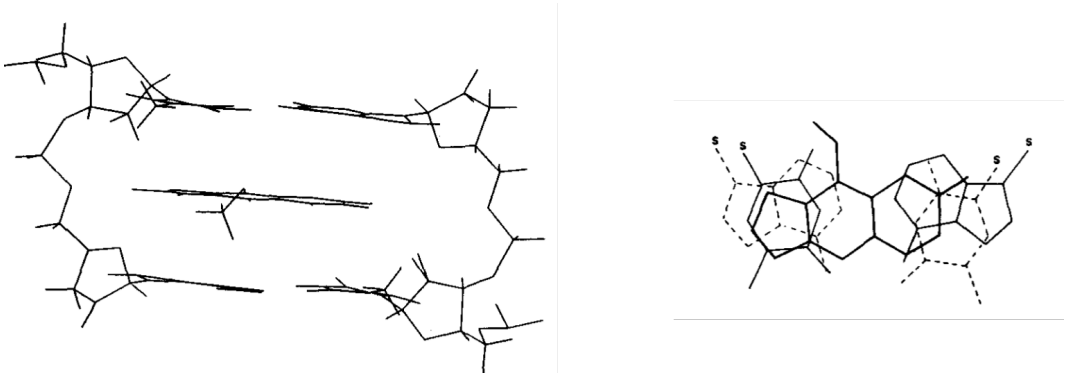

Abbildung 1.5. – Psoralen-Derivat 8-MOP interkaliert in DNA. Links: Ansicht aus der Projektionsebene parallel zur Helixachse. Rechts: Ansicht aus der Projektionsebene orthogonal zur Helixachse. Entnommen aus Demaret et al. [62].

1.4.2. Photoanbindung der Psoralene an DNA

Bei Belichtung des interkalierten Psoralens mit UV-A-Strahlung kann es zu einer Anbindung des Psoralens an die Thymin-Base der DNA kommen (siehe Abbildung 1.6) [63, 64]. Im Gegensatz zur Interkalation ist dieser Prozess nicht reversibel. Das Psoralen bindet entweder über die C4′=C5′-Bindung der Furanseite oder über die C3=C4-Bindung der

Pyronseite an die C5=C6-Bindung der Thyminbase. Dabei handelt es sich formal um eine [2+2]-Cycloaddition. Es entsteht ein Cyclobutanring, welcher das Psoralen und die Thyminbase kovalent verbindet.

Für das Furan- und das Pyronaddukt können jeweils zwei Diastereomere entstehen, je nachdem ob das Psoralen ober- oder unterhalb der Thyminbase lokalisiert ist. Alle vier möglichen Produkte weisen eine *cis-syn*-Stereoisomerie auf. *Cis* bedeutet hier, dass sich Psoralen- und Thymin-Molekül auf derselben Seite des Cyclobutanrings befinden, die Moleküle also „gestapelt“ vorliegen. *Syn* beschreibt in den Furanmonoaddukten, dass sich O1 des Furanrings und N1 der Thyminbase als Substituent am Cyclobutanring direkt gegenüber befinden (markiert mit grauen Pfeilen in Abbildung 1.6). Bei den Pyronmonoaddukten liegen sich C2 des Pyronrings und N1 der Thyminbase gegenüber. Je nach Psoralenderivat können klare Präferenzen für eine Bindung über die Furan- oder Pyronseite gefunden werden. Demaret et al. zeigten, dass die Präferenz zur Anbindung über eine der beiden Seiten mit dem Abstand der reaktiven Psoralen-Doppelbindung zur Thymin-Doppelbindung in Verbindung steht [62]. Durch die geometrische Nähe lässt sich die Tendenz zur Bildung des Pyronmonoaddukts bei dem Psoralenderivat 5-MOP erklären. Bei allen vier anderen untersuchten Psoralenderivaten dagegen – unter anderem 8-MOP – befindet sich die Furan-Doppelbindung näher zur Thymin-Doppelbindung. Zudem scheint eine Methylsubstitution an Position C4 des Psoralens, wie z.B. bei TMP und AMT, eine Pyronadduktbildung fast gänzlich zu verhindern [65]. Dies wird auf sterische Hinderung der 4-Methyl-Gruppe des Psoralens und der 5-Methyl-Gruppe der Thyminbase zurückgeführt. Das Furanmonoaddukt kann ein zweites Photon im UV-A-Bereich absorbieren und über die Pyronseite an eine zweite Thyminbase binden (siehe Abbildung 1.7) [63, 64]. Es entsteht ein sogenannter „Crosslink“, welcher die beiden Einzelstränge der DNA kovalent verbindet.

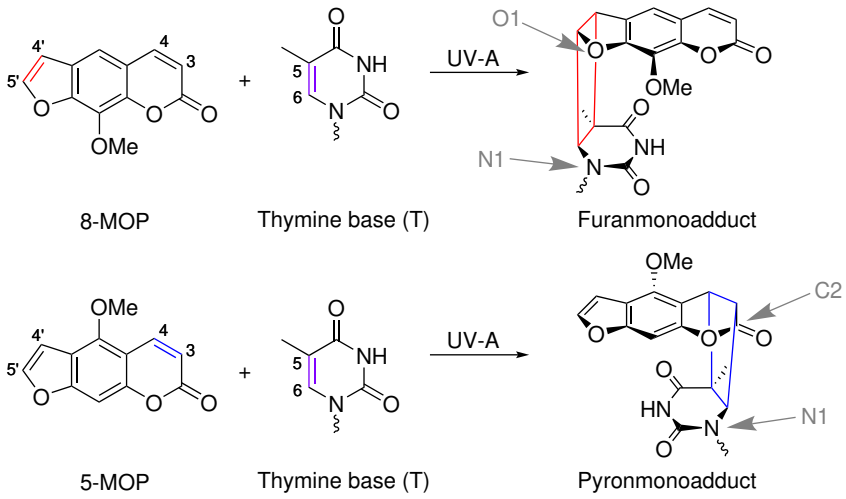

Abbildung 1.6. – Photoanbindung eines Psoralens an die Thymin-Base der DNA. Oben: Das Derivat 8-MOP bindet über die Furanseite (rot) an die Thyminbase. Unten: Das Derivat 5-MOP bindet über die Pyronseite (blau) an die Thyminbase. Es ist jeweils nur eins von zwei möglichen Stereoisomeren gezeigt.

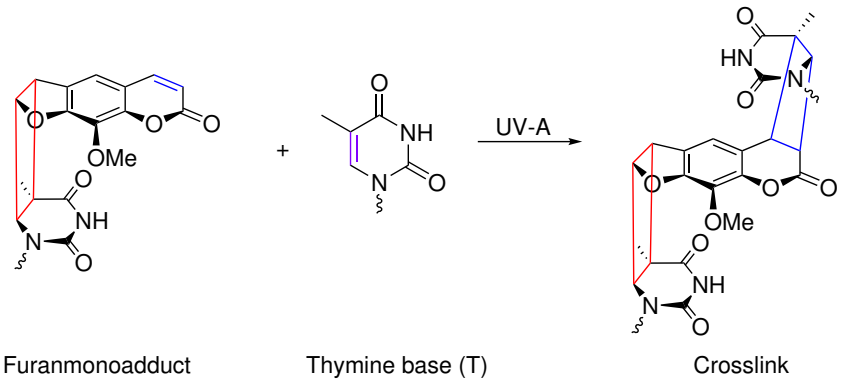

Abbildung 1.7. – Das Furanmonoaddukt, hier von 8-MOP, kann unter Absorption eines zweiten UV-A-Photons über die Pyronseite an eine zweite, gegenüberliegende Thyminbase binden. Es entsteht ein „Crosslink“, welcher die beiden Einzelstränge der DNA kovalent verknüpft.

Die Reaktionsquantenausbeuten unterscheiden sich je nach Psoralen-Derivat und DNA-Sequenz stark. Für natürliche DNA liegen sie im Bereich weniger Prozent [43, 66]. Eine Methylsubstitution am Psoralen führt jedoch beispielsweise zu höheren Quantenausbeuten [66].

Ob ein angeregter Singulett- oder Triplett-Zustand der Precursor der Photoprodukte ist, wurde in der Literatur viel diskutiert. Aufgrund der starken Reduzierung der Triplettquantenausbeute des Psoralens bei Zugabe von DNA sowie einer Reduzierung der Fluoreszenzlebensdauer wurde der angeregte Singulett-Zustand in vielen Publikationen als Vorläufer postuliert [50, 67, 68]. Die Autoren quantenchemischer Studien kommen zu unterschiedlichen Schlüssen [69–72]. Serrano-Pérez et al. publizierten eine Studie basierend auf der CASPT2-Methode und stellten die These auf, dass das Furanmonoaddukt aus dem angeregten Singulett und das Pyronmonoaddukt aus dem Triplett entsteht [70]. Eine TD-DFT-Studie dagegen sagt für beide Monoaddukte eine hohe Barriere für die Anbindung aus dem angeregten Singulett-Zustand voraus [71]. Eine DFT-basierte Publikation aus dem Jahr 2013 von Huang und Zhang unterstützt die These einer Anbindung aus dem Triplett über ein Biradial-Intermediat mit einer kovalenten Bindung zwischen Psoralen und Thyminbase [72].

In einer experimentellen Publikation aus dem Jahr 1987 von Sage und Moustacchi konnte außerdem eine klare Präferenz für die Photoproduktbildung an langen AT-Sequenzen festgestellt werden [73]. Bei Verwendung synthetischer DNA-Sequenzen, welche nur aus dem AT-Basenpaar bestehen, erhöht sich die Quantenausbeute erheblich [74]. 2015 konnte diese Beobachtung von Fröbel et al. im Arbeitskreis Gilch erklärt werden. Der Effekt ist auf einen photoinduzierten Elektronentransfer (PET) von der Base Guanin auf das angeregte Psoralen zurückzuführen [61, 74] (siehe Abbildung 1.8). Es folgt eine Ladungsrekombination innerhalb weniger Pikosekunden. Diese sehr schnelle Konkurrenzreaktion verhindert das effiziente Anbinden des Psoralens über die Cycloaddition. Es erklärt außerdem das starke Quenching des Triplettzustands sowie die Reduzierung der Fluoreszenz in natürlicher DNA. Aufgrund dieser Tatsache war es vermutlich bisher noch nicht möglich den kinetischen Precursor des Photoprodukts experimentell eindeutig zu identifizieren.

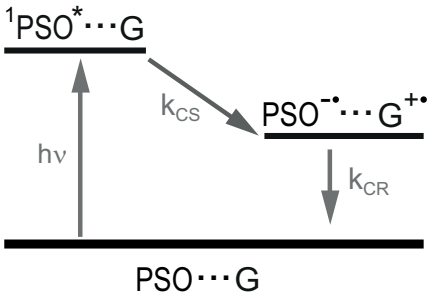

Abbildung 1.8. – Schema des photoinduzierten Elektrontransfers (PET) von der DNA-Base Guanin auf das Psoralen. Interkaliertes Psoralen (PSO) wird durch Absorption eines UV-A-Photons in den S_1 angeregt. Befindet sich eine Guanin-Base (G) in der Nähe des Psoralens, quencht es den angeregten Zustand durch Übertragung eines Elektrons. Die Ladungstrennung (CS) und die Ladungsrekombination (CR) erfolgen in wenigen Pikosekunden.

1.5. Ziele dieser Arbeit – oder: Wie könnte das „perfekte“ Psoralen aussehen?

Wie im vorigen Abschnitt erläutert, konnte der transiente Precursor für die Anbindung eines Psoralens an die DNA noch nicht eindeutig identifiziert werden. Sascha Fröbel ermittelte in seiner Dissertation aus dem Jahr 2016 dazu vielversprechende Strategien [47]. Zunächst wurde deutlich, dass der Einsatz von Guanin-freier DNA essentiell für die Beobachtung der Photoanbindung ist, um den PET auszuschließen. Außerdem wurde deutlich, dass zeitaufgelöste UV/Vis-Spektroskopie alleine nicht zu einer Aufklärung reicht, da sich Signalbeiträge der beteiligten Komponenten überlappen. Daher wurde eine Kooperation mit dem Lehrstuhl für BioMolekulare Optik der Ludwig-Maximilians-Universität München unter der Leitung von Prof. Dr. Wolfgang Zinth angestrebt. Dort können zeitaufgelöst die Änderungen der Absorption im infraroten Bereich aufgenommen werden. Ein IR-Spektrum weist im Gegensatz zum Spektrum im UV/Vis eine große Anzahl schmaler, hochcharakteristischer Banden auf. Außerdem konnte in München mit dieser Technik bereits die Entstehung des CPD-Schadens an DNA-Sequenzen kinetisch verfolgt werden [15]. Daher waren auch für die Anbindung des Psoralens – wie in Abschnitt 1.3 beschrieben fiel die Wahl auf das Derivat AMT – an die Thymin-Base charakteristische Banden zu erwarten. Die Ergebnisse dieser Kooperation sind in Abschnitt 2.1 beschrieben.

Im darauffolgenden Abschnitt 2.2 wurden Techniken der stationären und zeitaufgelösten Spektroskopie auf die Untersuchung der pharmazeutisch genutzten Psoralen-Derivate 8-MOP, 5-MOP und TMP angewendet. Es sollte untersucht werden, ob diese Derivate ein ähnliches oder ein abweichendes Verhalten im Vergleich zu AMT im Hinblick auf die Photoanbindung aufweisen. Aus diesen Ergebnissen können zudem weitere Schlüsse für die Vorhersage zur Effizienz anderer Derivate gezogen werden.

Ziel dieser Arbeit war es nicht nur den Mechanismus der Anbindung aufzuklären, sondern auch Strategien für die Synthese eines Psoralens, welches verbesserte Eigenschaften gegen-

über den zur Zeit applizierten Psoralenen aufweist, zu entwickeln. Das „perfekte“ Psoralen aus der Sicht eines Grundlagenforschers sollte zunächst möglichst effektiv an die DNA anbinden. Eine hohe Wasserlöslichkeit, eine hohe Interkalationsaffinität und eine hohe Reaktionsquantenausbeute gehören damit zu essentiellen Anforderungen. Eigenschaften, welche trotz effektiven Anbindens einem Einsatz in der Therapie entgegenstehen wie z.B. Reaktionen mit anderen Biomolekülen, Unverträglichkeit oder Nebenwirkungen werden in dieser Sichtweise zunächst nicht betrachtet.

In Zusammenarbeit mit dem Lehrstuhl für Organische Chemie der Heinrich-Heine-Universität unter der Leitung von Prof. Dr. Thomas J. J. Müller sind vor diesem Hintergrund erste Psoralen-Derivate erfolgreich synthetisiert und auf ihre photophysikalischen Eigenschaften hin untersucht worden [75–77]. Das übergeordnete Ziel war es, die elektronischen Eigenschaften des pharmazeutisch applizierten 8-MOP durch Substitution so zu verändern, dass der PET nicht auftritt und somit die schnelle Desaktivierung des angeregten Zustands verhindert wird. Der PET kann unterdrückt werden, wenn die freie Standardreaktionsenthalpie ΔG^0_{CS} für die Ladungstrennung größer null ist. Die Standardreaktionsenthalpie kann über die Weller-Gleichung errechnet werden [78]:

$$\Delta G^0_{CS} = e_0(E^0(D^{+\bullet}/D) - E^0(A/A^{-\bullet})) + W - E_{00}. \tag{1.1}$$

Gleichung 1.1 beschreibt den Zusammenhang von freier Standardreaktionsenthalpie und den Standardpotentialen des Donors $E^0(D^{+\bullet}/D)$, in diesem Fall der Guanin-Base der DNA, sowie des Akzeptors $E^0(A/A^{-\bullet})$, in diesem Fall des Psoralen. Ist die Differenz der Potentiale (in Vielfachen der Elementarladung e_0) größer als die Energiedifferenz zwischen den Schwingungsgrundzuständen von S_0 und S_1 des Psoralens (E_{00}), so kann der PET unterdrückt werden. Der Term W (*Work Term*) berücksichtigt die Stabilisierung durch Coulombwechselwirkung des ladungsgetrennten Zustands. Da die Erniedrigung von E_{00}, also eine Rotverschiebung der S_1-Absorptionsbande, den zusätzlichen Vorteil der spektroskopischen Trennung von der DNA-Absorption hat, wurde dieser Ansatz priorisiert. Infolge vergrößert sich das spektroskopische Fenster zur gezielten Anregung des Psoralens. Zur Realisierung dieser Ziele wurde 8-MOP an Position 5 substituiert (siehe Abbildung 1.9). Durch die Vergrößerung des π-Systems wird sich die Rotverschiebung der Absorption erhofft. Die Einbringung ei-

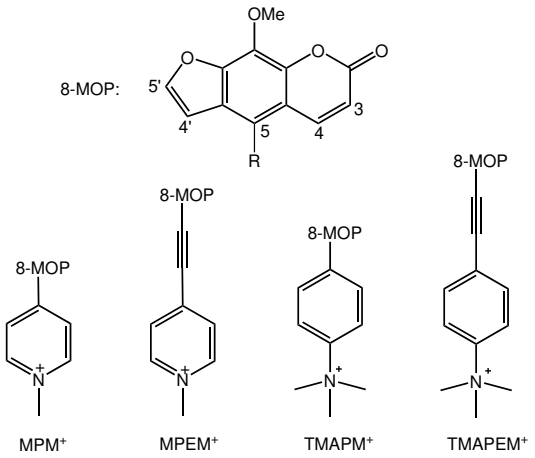

Abbildung 1.9. – Strukturen der wasserlöslichen Psoralene mit rot-verschobener Absorption. Der Grundkörper 8-MOP wurde dafür an Position 5 mit einer der abgebildeten Gruppen substituiert.

ner positiven Ladung hat eine höhere Wasserlöslichkeit sowie höhere Interkalationsaffinität als Ziel. Die Erfolge und Misserfolge dieses Projekts sowie die Lehren daraus werden in Abschnitt 2.3 aufgeführt und erklärt. Aufbauend auf diese, soll eine Strategie zur weiteren Verbesserung der Eigenschaften entwickelt werden, um schlussendlich das „perfekte“ Psoralen ausfindig zu machen.

2. Zeitaufgelöste Spektroskopie an Psoralenen

2.1. Anbindung von AMT an die DNA via Triplettzustand

Der Titel der ersten Publikation dieser Arbeit „The Photoaddition of a Psoralen to DNA Proceeds via the Triplet State“ verrät bereits die zentrale Nachricht an die Leserschaft – die Anbindung des Psoralens AMT and die DNA findet über den Triplettzustand statt. Zu diesem Titel bzw. diesem Ergebnis bedurfte es einer Vielzahl verschiedenster Techniken der Spektroskopie, Quantenchemie, sowie Verfahren der Datenanalyse. Die meisten dieser Techniken sind bereits seit Jahren im Arbeitskreis fest etabliert und daher in zahlreichen Dissertationen ausführlich beschrieben [47, 79–82]. Überraschenderweise war die übliche Methode zur Auswertung der zeitaufgelösten Daten nicht ausreichend für eine zufriedenstellende Interpretation. Die Anbindung des Psoralens an die DNA wies eine unerwartet große Anzahl an Zeitkonstanten und Komplexität auf. Daher wurde eine weitere Methode zur Auswertung dieser Daten herangezogen. Das Prinzip und die Vorzüge der *Lifetime Density Analysis* (LDA) sollen im folgenden Abschnitt erläutert werden.

2.1.1. LDA – Eine Methode der Globalen Datenanalyse

Für die Extraktion der gewünschten Informationen aus einer zeitaufgelösten Messung bedarf es einer auf das Problem abgestimmten Analysemethode. Die hier verwendeten Methoden untersuchen den Datensatz „global“, das heißt, dass alle Zeitspuren simultan ausgewertet werden. Für gewöhnlich kommt dabei die „Global Lifetime Analysis“ (GLA) zum Einsatz [83, 84]. Bei dieser Methode wird der Datensatz $\Delta A(\tilde{\nu}, t)$ mit einer diskreten Anzahl an Exponentialfunktionen genähert.

$$\Delta A(\tilde{\nu}, t) = IRF \otimes \sum_{i=a}^{n} \Delta A_i(\tilde{\nu}) \cdot e^{-\frac{t}{\tau_i}}. \tag{2.1}$$

Das Ergebnis dieser Analyse sind die sogenannten „Decay Associated Difference Spectra“ (DADS) $\Delta A_i(\tilde{\nu})$ mit zugehöriger Lebensdauer τ_i. Ein DADS zeigt die präexpontentielle Amplitude für jede Lebensdauer τ_i. $IRF\otimes$ steht für eine Faltung mit der instrumentellen Antwortfunktion, die hier mit einer Gaussfunktion genähert wird. Zum Auswerten der Daten wurde die IDL-basierte Software z20 [84] benutzt, welche an der LMU München am

Lehrstuhl für BioMolekulare Optik unter der Leitung von Prof. Dr. W. Zinth entwickelt wurde. Essentiell bei dieser Methode ist die Vorgabe einer diskreten Anzahl an Zerfällen durch vorangegangene Betrachtung und Einschätzung durch den Nutzer der Software.

Für Systeme mit komplexer Kinetik, ausgezeichnet durch eine große Anzahl an Zerfällen, kann eine andere Methode zur Auswertung herangezogen werden – die „Lifetime Density Analysis“ (LDA). Obwohl schon länger bekannt, brachte erst die Gruppe um A. Holzwarth vom Max-Planck-Institut für Bioanorganische Chemie in Mülheim Anfang der 2000er mehr Aufmerksamkeit für diese Methode, als sie erstmals auch mittels LDA gewonnene Ergebnisse veröffentlichten [85–88]. Sie nutzten die Methode zur Auswertung und Darstellung von Prozessen in der Photosynthese. Da auch die Anbindung des Psoralens AMT an die DNA ein unerwartet komplexes Verhalten zeigte, wurden die zeitaufgelösten IR-Daten zusätzlich zur GLA mit der LDA ausgewertet. Der entscheidende Unterschied zur GLA ist, dass hier die Vorgabe einer definierten Anzahl an Zerfällen für die Auswertung entfällt. Die Methode basiert auf der Beschreibung der Daten durch ein Integral über eine kontinuierliche Verteilung exponentieller Zerfälle:

$$\Delta A(\tilde{\nu}, t) = \int_0^\infty \Phi(\tilde{\nu}, \tau) \cdot e^{-\frac{t}{\tau}} d\tau. \tag{2.2}$$

Der gemessene Datensatz $\Delta A(\tilde{\nu}, t)$ ist dabei die Laplace-Transformierte der spektralen Wahrscheinlichkeitsdichte $\Phi(\tilde{\nu}, \tau)$. Durch inverse Laplace-Transformation kann die gesuchte präexponentielle Funktion $\Phi(\tilde{\nu}, \tau)$ erhalten werden. In der numerischen Implementierung wird statt des Integrals eine Summe mit einem diskreten, großen Wert n an Lebensdauern τ verwendet.

$$\Delta A(\tilde{\nu}, t) = IRF \otimes \sum_{j=1}^{n} \Phi_j(\tilde{\nu}, \tau_j) \cdot e^{-\frac{t}{\tau_j}}. \tag{2.3}$$

Dieser Wert n beträgt typischerweise ≈ 100 und ist damit wesentlich größer als die erwartete Zahl der Zeitkonstanten. Zudem ist eine Regularisierung notwendig. Ohne Regularisierung führt die Anpassung durch die Methode der kleinsten Quadrate zwar zur optimalen Lösung des Problems, aber da die Anzahl an Lebensdauern – also Parametern – groß ist, führt schon geringes Rauschen in den Daten zur einer Überanpassung („overfitting“). Dies äußert sich in großen, unechten Amplitudenschwankungen, welche die Auswertung bedeutungslos machen. Ein Regularisierungsparameter „bestraft“ (penalizes) große Fitkoeffizienten, also hier Amplituden, und kontrolliert so die Balance zwischen Regularisierung und der Restnorm. Ausführliche Erläuterungen zur Implementierung finden sich in den Referenzen [89–91].

Zum Auswerten wurde die Software OPTIMUS [90] verwendet. Diese wurde von C. Slavov am Institut für Physikalische und Theoretische Chemie der Goethe-Universität Frankfurt unter der Leitung von J. Wachtveitl entwickelt. In OPTIMUS ist die Tikhonov-Regularisierung implementiert. Die Wahl des richtigen Regularisierungsparameters wurde über das L-Curve-Kriterium getroffen. Es wurden die Amplituden zu $n = 250$ gleichmäßig auf einer

logarithmischen Achse verteilten Lebensdauern zwischen 1 ns und 1 ms berechnet und eine fixe IRF von 3 ns verwendet.

Das Ergebnis der LDA ist die Lifetime Density Map (LDM) (siehe Abbildung 2.1). Durch geeignete Darstellung der drei Achsen (Wellenzahl $\tilde{\nu}$, Lebensdauer τ, Amplitude Φ) lässt sich für den Betrachter ein visuell anschauliches Ergebnis darstellen. Den Vorzeichen der Amplitude werden unterschiedliche Farben zugeordnet. In dieser Arbeit wurde für positive Amplituden, die einem Abfall der Absorption entsprechen, die Farbe Rot gewählt, für negative Amplituden, also einer Zunahme der Absorption, die Farbe Blau. Für den Betrachter der LDM kann so unmittelbar ein Eindruck über die ungefähre Anzahl und Lebenszeit der Prozesse gewonnen werden. Mit dieser Information können bei Bedarf anschließend mittels GLA die Amplitudenspektren gewonnen werden.

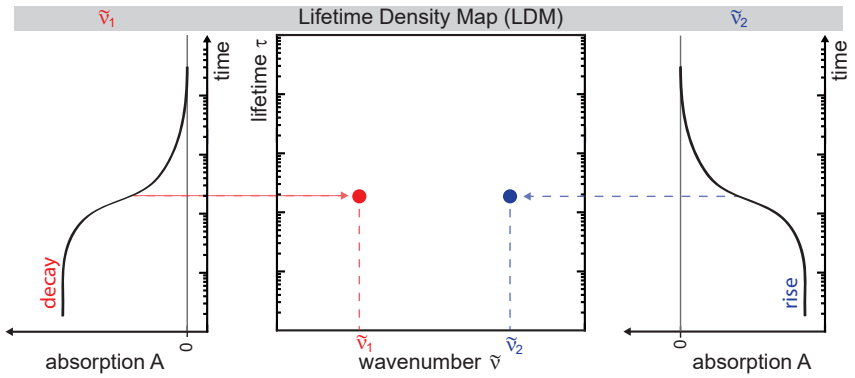

Abbildung 2.1. – Simplifizierte Veranschaulichung der Entstehung einer Lifetime Density Map (LDM). Die Lebensdauer τ des monoexponentiellen Zerfalls für die Wellenzahl $\tilde{\nu}_1$ findet sich dargestellt in rot (für Signalzerfälle) in der LDM wieder. Signalanstiege sind in blau dargestellt. Reale Daten erzeugen in der LDM nicht wie hier dargestellte Deltafunktionen (Punkte), sondern Verteilungen.

2.1.2. Nanosekundenspektroskopie im UV/Vis und IR zur Aufklärung der Photoaddition (Veröffentlichung I)

Title: The Photoaddition of a Psoralen to DNA Proceeds via the Triplet State

Authors: Janina Diekmann, Julia Gontcharov, Sascha Fröbel, Christian Torres Ziegenbein, Wolfgang Zinth, Peter Gilch

Published in: Journal of the American Chemical Society

Year: 2019

Impact Factor: 14.695 (2019)

Eigene Anteile an der Veröffentlichung:

- Durchführung und Auswertung der stationären IR-Messungen und der quantenchemischen Rechnungen
- Großteil der Auswertung zu den zeitaufgelösten UV/Vis und IR-Messungen
- Erstellung der Abbildungen
- Literaturrecherche und Verfassen eines großen Anteils des Manuskripts

JACS
JOURNAL OF THE AMERICAN CHEMICAL SOCIETY
Article
Cite This: J. Am. Chem. Soc. 2019, 141, 13643−13653
pubs.acs.org/JACS

The Photoaddition of a Psoralen to DNA Proceeds via the Triplet State

Janina Diekmann,[†] Julia Gontcharov,[‡] Sascha Fröbel,[†,§] Christian Torres Ziegenbein,[†,∥] Wolfgang Zinth,[‡] and Peter Gilch*[,†]

[†]Institut für Physikalische Chemie, Heinrich-Heine-Universität Düsseldorf, Universitätsstr. 1, 40225 Düsseldorf, Germany
[‡]Lehrstuhl für BioMolekulare Optik, Fakultät für Physik and Center for Integrated Protein Science Munich CIPSM, Ludwig-Maximilians-Universität München, Oettingenstrasse 67, 80538 München, Germany

Supporting Information

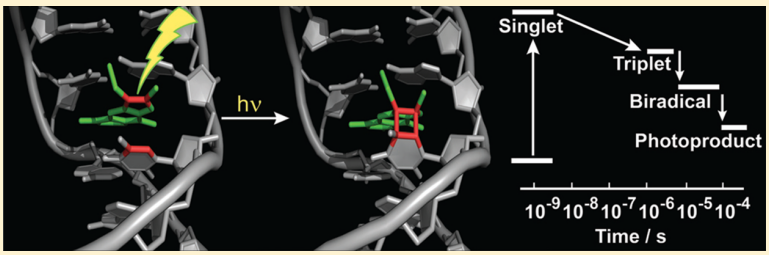

ABSTRACT: Psoralens are natural compounds that serve in the light dependent treatment of certain skin diseases (PUVA therapy). They are DNA intercalators that upon photoexcitation form adducts with thymine bases. For one psoralen derivative, 4′-aminomethyl-4,5′,8-trimethylpsoralen (AMT), the photoreactions are characterized here by nanosecond UV−vis and IR absorption spectroscopy. The triplet state of AMT is identified as the reactive one. On the 1−10 μs time scale this local triplet state transforms into a triplet biradical bearing one single bond between the addends. Within ∼50 μs this biradical forms the final adduct featuring a cyclobutane ring. This kinetic behavior is in stark contrast to the closely related photoaddition of two thymine moieties within the DNA. Origins of the differences are discussed.

INTRODUCTION

Ultraviolet (UV) light can trigger chemical reactions in DNA, which—if not repaired enzymatically—irreversibly damage the carrier of the genetic code.[1] Various of these DNA photolesions have been identified. The most abundant one is the cyclobutane pyrimidine dimer (CPD) formed between two thymine bases adjacent on the DNA strand.[2] The formation of this lesion was traced by femtosecond UV pump infrared (IR) probe spectroscopy.[3,4] The experiments showed that the CPD formation after UV−C absorption occurs within a few 100 fs via an excited singlet state as a precursor. This implies that the ring forms in a concerted Woodward−Hoffmann[5] type way. Studies on the dimerization via the triplet state are hampered by the small quantum yield of this state for direct excitation.[2,6] Higher populations of the thymine triplet state can be attained by sensitization.[7] Experiments with direct[6] and sensitized[7] excitation indicated that the efficiency for dimerization starting from the triplet state is small; i.e., <0.1.

A structural motive closely related to the CPD one is encountered in photoreactions between psoralens and DNA (Scheme 1). Psoralens are natural compounds with a long pharmaceutical history.[8−11] They are utilized in light dependent treatments of skin diseases like psoriasis,[9] vitiligo,[10] and cutaneous T-cell lymphoma.[12,13] These treatments are referred to as PUVA for psoralen and UV-A radiation.[10] A frequently used active agent in PUVA therapy is 8-methoxypsoralen (8-MOP). The derivatives 5-methoxypsoralen (5-MOP) and 4,5′,8-trimethylpsoralen (TMP) are also applied in PUVA treatments.[10] Concerning the molecular background of PUVA there is consensus that psoralens are DNA intercalators,[14] i.e., they insert between the base pairs of DNA. Upon photoexcitation they covalently bind to DNA whereby a cyclobutane

Scheme 1. Structure of the Psoralen Derivative AMT,[a] the Thymine Base of the DNA, and One of the Two Diastereomeric *cis-syn*-Photoadducts on the Furan Side

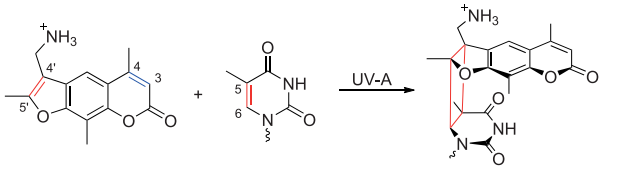

[a]The photoreactive double bond on the furan side is marked in red, and on the pyrone side in blue.

Received: June 19, 2019
Published: August 15, 2019

DOI: 10.1021/jacs.9b06521
J. Am. Chem. Soc. 2019, 141, 13643−13653

ring is formed. The resulting DNA damage can then trigger apoptosis (programmed cell death) of the affected cell.[15]

In DNA psoralens preferentially photobind to thymine bases.[16] Binding to the furan side (Scheme 1) involving the C4′═C5′ double bond as well as to the pyrone side involving the C3═C4 double bond was discussed in the literature.[14] The furan-monoadduct may absorb a second photon to form a cross-link/diadduct via the pyrone side.[17] The selectivity for the two sides depends on the substitution pattern. For the psoralen derivative 4′-aminomethyl-4,5′,8-trimethylpsoralen (AMT) studied here, the addition preferentially occurs at the furan side.[18−20] The adduct adopts the *cis-syn* structure depicted in Scheme 1.[16,20] The psoralen may bind to a thymine in the 3′ direction of the DNA strand or to one in 5′ direction. The resulting adducts are diastereomers.[21] For adducts formed from AMT intercalated into poly(dA-dT), an enzymatic hydrolysis and HPLC analysis showed indications for the formation of both diastereomers.[19] The authors of the study, however, did not quantify the ratio in which they are formed.

The mechanism of this photoaddition was addressed in several quantum chemical studies.[21−24] According to a study using the CASSCF//CASPT2 method furan-side adducts ought to form preferentially with an excited singlet of psoralen as a precursor.[23] However, for the psoralen derivative 8-methoxypsoralen, a TD-DFT study yielded substantial barriers (40 kJ/mol) between the Franck−Condon point of the S_1 surface and the transition region to the ground state of the furan as well as the pyrone side adduct.[24] This indicates that an alternative route to the adduct is taken. On the basis of DFT computation for the electronic ground state S_0 and the lowest triplet T_1, Huang and Zhang[25] suggest that the furan-side adduct forms via a triplet biradical with one C−C single bond connecting the psoralen to the thymine moiety.

Psoralens intercalated into calf thymus DNA were studied by laser flash photolysis.[26,27] Contrary to the situation in solution,[28] no indication for the population of the triplet state was found. This finding may be explained based on femtosecond experiments conducted by some of the present authors.[29,30] For AMT intercalated into DNA containing guanine bases a photoinduced electron transfer (PET) was discovered. Photoexcited AMT hereby acts as an acceptor. The PET seems to occur in competition with the photoaddition. The occurrence of the PET was recently confirmed independently.[31] In A,T-only DNA this PET does not occur.[30] Even more, up to several nanoseconds the spectrotemporal behavior of AMT intercalated into AT-only DNA, AMT_{INT} in the following, strongly resembles the behavior of AMT in aqueous solution. As AMT in AT-only DNA is photoreactive, this shows that the photoaddition occurs on time scales longer than a couple of nanoseconds. This photoaddition has not yet been followed by time-resolved spectroscopy.

Here, the photoaddition is studied by nanosecond laser flash photolysis as well as nanosecond UV pump IR probe spectroscopy. The experiments were conducted on the psoralen derivative AMT as it features a relatively high intercalation affinity.[30] The spectroscopic results will show unequivocally that the addition proceeds via the triplet state of AMT. Evidence will be given that the addition proceeds via a biradical intermediate, which is formed within microseconds. The biradical decays within ∼50 μs to yield the adduct.

RESULTS

In the following, spectroscopic measurements on the photoaddition of AMT intercalated into AT-DNA (AMT_{INT}) will be described (for experimental details see Supporting Information (SI)). The single strands of an alternating copolymer of deoxyadenosine and thymidine, 5′-$(TA)_{20}$-3′, were annealed forming double strand oligomers, which will be referred to as AT-DNA throughout the text. In the following experiments one has to account for the fractions of intercalated and free psoralens. These fractions can be computed based on dissociation constants K_D. For AMT and AT-DNA K_D amounts to 4.4×10^{-4} M.[30] The value refers to DNA base pairs (bp). For the typical concentrations employed in this study, fractions between 0.4 and 0.9 of AMT were intercalated. In the earlier femtosecond studies mentioned in the Introduction, the contribution of free AMT was recorded separately and after suitable scaling subtracted from the measurement of AMT in the presence of DNA.[29,30] This approach cannot be pursued here, since in the nano- to microsecond region the lifetime of AMT is concentration dependent.[27] Contributions of free AMT, thus, have to be considered.

Steady-State UV−Vis Spectroscopy. The absorption spectrum of AMT_{INT} is characterized by a shoulder at 340 nm and an increasing signal toward shorter wavelengths (Figure 1A). For the concentrations employed the fraction of AMT_{INT} amounts to 0.9 and the depicted spectrum is predominantly due to AMT_{INT}. For wavelengths below ∼305 nm the absorption of the DNA bases dominates.[4] Illumination of the sample at 370 nm alters the absorption spectrum. Since DNA

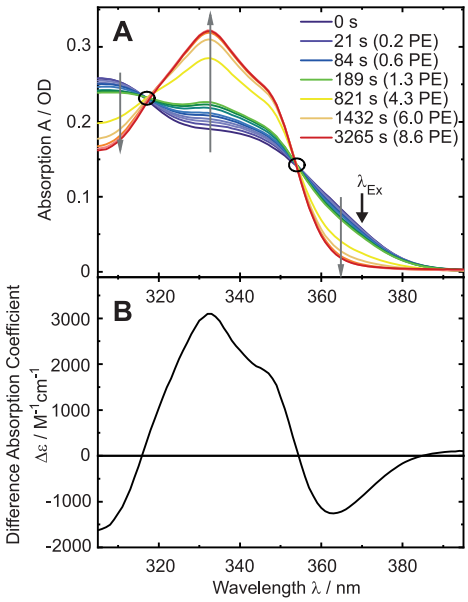

Figure 1. Photoaddition of AMT to AT-DNA traced by UV−vis absorption. (A) Spectrum of AMT (35 μM) and AT-DNA (4 mM, bp) dissolved in an aqueous buffer after indicated illumination times (λ_{Ex} = 370 nm, P = 1.4 mW, V = 2 mL, d = 1 cm). In addition to the illumination times photon equivalents (PE) are indicated (see SI 1.2). The DNA contribution to the absorption was subtracted. Circles mark isosbestic points. (B) Difference spectrum obtained from the data set given on the top. The first spectrum (violet) was subtracted from the last one (red).

DOI: 10.1021/jacs.9b06521
J. Am. Chem. Soc. 2019, 141, 13643−13653

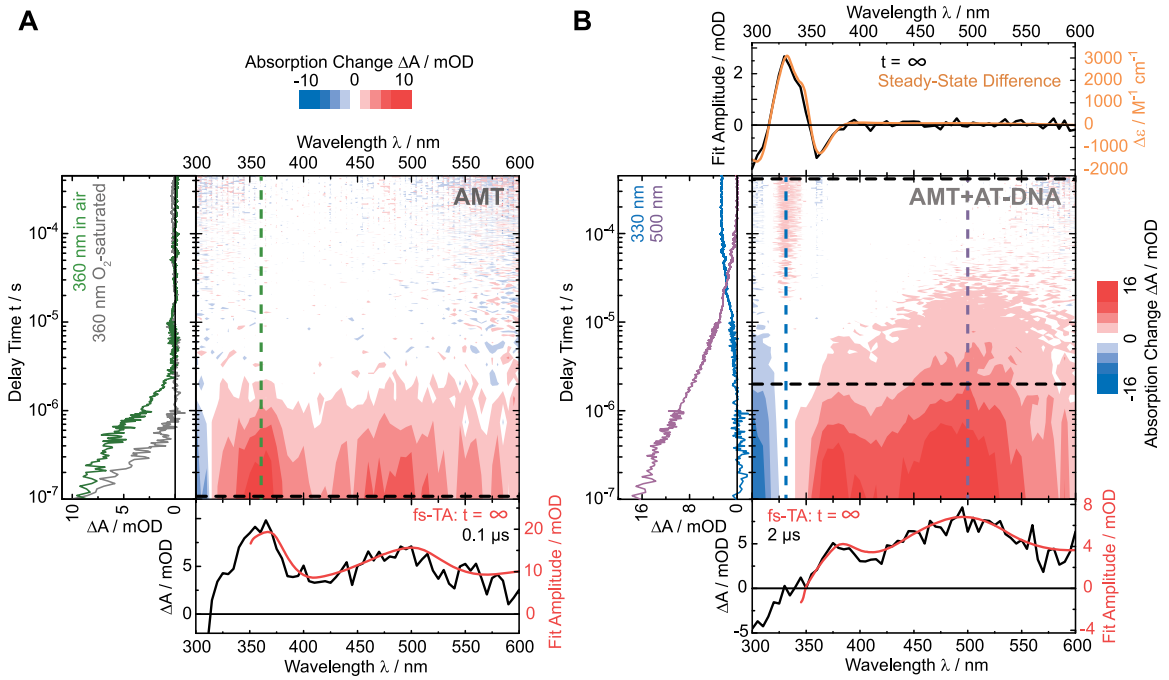

Figure 2. Nanosecond transient absorption of AMT and AMT with AT-DNA in the UV−vis. (A) Nanosecond UV−vis data on AMT (0.14 mM) in aerated H_2O after excitation at 355 nm. The green dashed line in the contour plot indicates the time trace at 360 nm shown on the left side. The same measurement conducted after saturating the AMT-water-solution with O_2 (1 bar) gives the gray time trace for 360 nm. Below the contour plot is the spectrum after 0.1 μs in comparison to the fs-UV−vis spectrum for "infinite" delay time. (B) Nanosecond UV−vis data on AMT (0.12 mM) and AT-DNA (0.4 mM, bp) in aerated H_2O with buffer after excitation at 355 nm. The blue and violet dashed lines in the contour plot indicate the time traces at 330 and 500 nm shown on the left side. Below the contour plot is the spectrum after 2 μs in comparison with the spectrum for "infinite" delay time of the fs-UV−vis-experiment. On top of the contour plot is the spectrum for "infinite" delay time of the ns-UV−vis-experiment in comparison with the steady-state-difference spectrum.

does not absorb in the UV-A, the changes of the absorption spectrum must involve AMT. Around 330 nm the absorption increases whereas for wavelengths below 318 nm and above 355 nm the absorption decreases. Isosbestic points are located at 318 and 355 nm. Their occurrences render a secondary photochemistry unlikely. The increase around 330 nm is an indication for the furan side monoadduct.[19] From these spectral changes and the amount of absorbed photons, a reaction quantum yield Φ_R of 0.12 is derived. The value is in good agreement with an earlier report.[30] The reaction quantum yield of free AMT is much smaller[32] and its contribution was, thus, neglected. After illuminating the samples for about 3000 s (photon equivalent of 8.6) no further changes are observed. For this exhaustive irradiation the concentration of photoadducts ought to equal the initial concentration of AMT_{INT}. With this input, difference absorption coefficients $\Delta\epsilon(\lambda)$ may be computed (Figure 1B).

Nanosecond Laser Flash Photolysis. A solution of AMT in aerated water was excited with nanosecond laser pulses centered at 355 nm (Figure 2A). The usage of a flow cell and the chosen sample amount ensured negligible transients due to the excitation of photoproducts. This applies to AMT and AMT_{INT}. Around time zero the excitation generates a difference absorption signal with positive bands peaking at 370 and 500 nm. For wavelengths smaller than 315 nm ground state bleach is observed. The difference spectrum agrees well with the "infinity" decay-associated difference spectrum (DADS) retrieved from a femtosecond experiment (Figure 2A, bottom).[29] The spectral pattern matches the one assigned to the triplet state of AMT.[27] The difference absorption decays to zero throughout the spectral range covered with a lifetime of ca. 1 μs. The lifetime is affected by the concentrations of oxygen and AMT. For water saturated with oxygen (1 bar) instead of air the lifetime is reduced to 0.2 μs (Figure 2A, left). Quenching experiments with varying concentrations of AMT and oxygen yielded self-quenching ($k_q^S = 1 \times 10^9$ M^{-1} s^{-1}), oxygen-quenching ($k_q^{O_2} = 3.3 \times 10^9$ M^{-1} s^{-1}) and intrinsic rate constants ($k_0 = 5 \times 10^4$ s^{-1}). Whereas the quenching constants are in line with earlier findings,[27] the intrinsic rate constant is by a factor of 5 larger. This could be due to residual oxygen in the solution.

Addition of AT-DNA to the AMT solution alters the decay kinetics of AMT (Figure 2B). For technical reasons low concentrations of AMT (0.12 mM) and AT-DNA (0.4 mM, bp) were employed. These concentrations correspond to a fraction of AMT_{INT} of only 0.44. Intercalated and free AMT, thus, contribute to the time dependent signals. For a qualitative assignment of the results the difference spectrum recorded 2 μs after photoexcitation is first considered. According to the measurement on AMT in absence of DNA the contribution of free AMT has mostly decayed after 2 μs. The spectrum at 2 μs agrees well with the one obtained by femtosecond spectroscopy for "infinite" delay times, which was assigned to the triplet state of AMT_{INT} (Figure 2B, bottom).[30] This spectroscopic signature decays on the 10 μs time scale giving way to a difference spectrum with a positive band at 330 nm adjacent to the ground state bleach observed for wavelengths smaller than 320 nm. The pattern agrees very well with the steady-state difference spectrum (Figure 2B, top). This gives clear evidence that after a few 100 μs, at latest, the photoadduct has been

DOI: 10.1021/jacs.9b06521
J. Am. Chem. Soc. 2019, 141, 13643−13653

formed. To obtain more quantitative information on the kinetics the results were subject to a global multiexponential analysis. A trial function with three exponentials and an offset to account for the photoadduct was necessary to describe the data. The fit yields time constants of 1, 6, and 49 μs. To identify the contribution of free AMT the measurement was repeated with oxygen saturated solutions (data not shown). Intercalated chromophores are expected to be shielded from oxygen by the DNA and thus their kinetics should not be affected strongly by oxygen.[33] In the O_2-saturated solution an *additional* time constant of 0.2 μs shows up. The value matches expectations based on the quenching experiment in free AMT (see above). Therefore, the 1 μs time constant in *aerated* solution is related to both, AMT and AMT_{INT}. The three time constants of 1, 6, and 49 μs can thus be attributed to AMT_{INT}. They will be assigned in conjunction with the IR data.

Steady-State IR Spectroscopy. For reasons of IR transparency all IR spectra were recorded in D_2O solutions. In D_2O, hydrogen−deuterium exchange occurs and thus NH and NH_2 functions of the AMT and DNA bear deuterons.[34] Neither an ND nor an ND_2 vibration is expected in the covered region.[35] In the spectral window left open by D_2O, AMT features a strong IR band at 1684 cm^{-1} (Figure 3A). Due

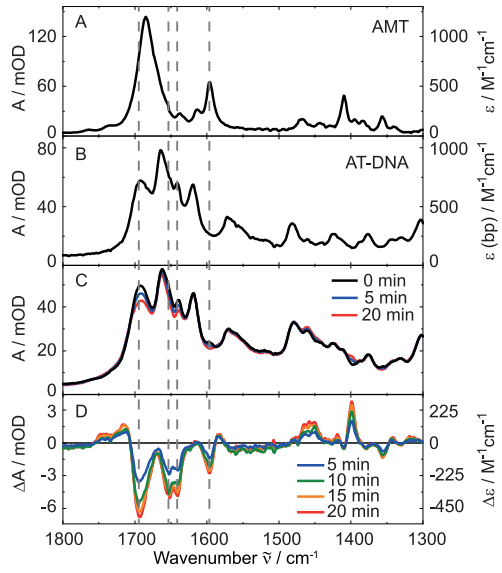

Figure 3. Steady-state IR spectra of the reaction of AMT and AT-DNA. (A) IR spectrum of AMT (12 mM) in D_2O. (B) IR spectrum of AT-DNA (7.7 mM, bp) in D_2O with buffer. (C) IR spectra of AMT (1.5 mM) in AT-DNA (6.5 mM, bp) in D_2O with buffer for indicated illumination periods (λ_{Ex} = 375 nm). (D) Computed difference spectra from C. From each spectrum the first spectrum (black) was subtracted. For the exhaustive irradiation (red) the concentration of photoadducts ought to equal the initial concentration of intercalated AMT. With this input, difference absorption coefficients $\Delta\epsilon(\lambda)$ were computed (right axis refers to difference spectrum plotted in red).

to position and strength the band can be assigned to the carbonyl stretching vibration.[36] The assignment finds support from quantum chemical computations (see below). Another prominent peak is located at 1596 cm^{-1} and is due to a C═C stretching vibration of the psoralen moiety. In the fingerprint region,[36] a strong band at 1410 cm^{-1} due to a CH_3 deformation is observed. In the region covered, the strong bands of the IR spectrum of AT-DNA (Figure 3B) between 1700 and 1600 cm^{-1} are due to nucleobase vibrations.[35] The bands at 1693 and 1663 cm^{-1} can be assigned to C═O stretching vibrations of the thymine base, the one peaking at 1641 cm^{-1} to a thymine ring deformation and at 1619 cm^{-1} to an adenine ring deformation.

The initial spectrum of AMT with AT-DNA before illumination is dominated by the DNA vibrations due to its higher concentration. For the concentrations employed in the IR experiment, the fraction of AMT_{INT} amounts to 0.9. Irradiation at 375 nm causes significant changes in the IR-spectrum (Figure 3C and D). Between 1700 and 1600 cm^{-1} the bleaching of four bands can be observed. The band bleaching at ∼1693 cm^{-1} can be assigned to both AMT and AT-DNA. The two closely spaced ones at ∼1650 cm^{-1} must be of AT-DNA since AMT has no pronounced absorption in this wavenumber range. As DNA is not photoexcited with 375 nm light, the bleach of an IR band of DNA gives clear evidence of a photoreaction involving excited AMT and DNA. The band at 1595 cm^{-1} indicates AMT bleach. Over 1700 cm^{-1} and below 1600 cm^{-1} positive absorption changes are visible. These are the vibration bands of the photoproduct. A sharp band at 1399 cm^{-1} and a broad band at 1470−1440 cm^{-1} forms. In this fingerprint region,[36] an assignment to a specific vibration of the photoproduct is difficult; hence, no assignment is made here.

Nanosecond UV Pump IR Probe. A solution of AMT in D_2O was excited with nanosecond laser pulses peaking at 355 nm. The resulting absorption changes in the IR were probed in the range 1750−1375 cm^{-1} (Figure 4A). As in the nanosecond laser flash experiments, a flow system was used to avoid contributions of photoproducts to the transients. In the time range up to 1 μs, absorption bleach is detected for the AMT-bands around 1684, 1596, and 1410 cm^{-1} (cf. Figure 3A). A pronounced positive band is located at 1625 cm^{-1}. In addition, a spectrally flat positive contribution is observed throughout most of the spectral region covered. The strong positive band at 1625 cm^{-1} may be assigned to the red-shifted C═O stretching vibration of AMT in the triplet state. Such red-shifts are common for triplet states of carbonyl compounds.[37,38] The shift is also in line with quantum chemical computations (see below). Positive and negative features decay to essentially zero on the microsecond time scale. For a quantitative evaluation of the decay kinetics, lifetime density analysis (LDA) and global lifetime analysis (GLA) were used (detailed description of these methods in the SI 1.5). For the simple kinetics of AMT, LDA is not necessary. It is performed here to contrast it with the analysis for AMT with DNA. In LDA, one determines spectral amplitudes associated with a certain exponential lifetime τ_x. A component with a certain lifetime τ_x with positive and negative amplitude will represent a signal decay and rise, respectively. In the lifetime density map (LDM) the largest features are found around 0.5 μs, which can be attributed to the reformation of the ground state of AMT (Figure 4C). The results obtained by LDA concur with a global single exponential fit yielding a time constant of 0.5 μs and DADS matching the LDA pattern (Figure 4C). The lifetime is shorter than the one determined by nanosecond UV−vis spectroscopy (1 μs). This can be explained by an increased concentration quenching due to the higher AMT concentration employed in the IR experiments.

When AT-DNA is added to the solution (Figure 4B) the time-resolved IR signature shows strong changes. With the

DOI: 10.1021/jacs.9b06521
J. Am. Chem. Soc. 2019, 141, 13643−13653

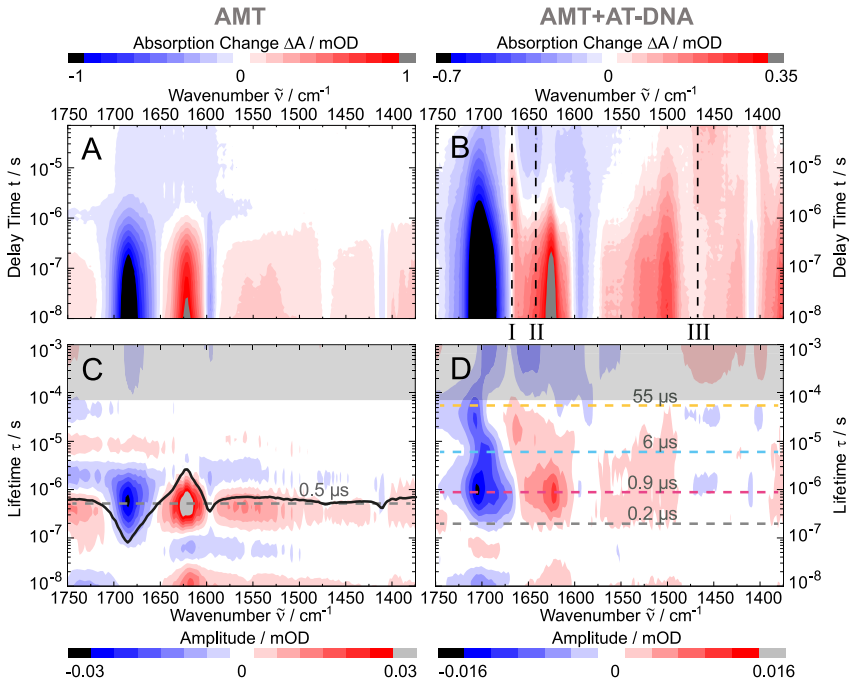

Figure 4. Transient IR absorption of AMT and AMT in AT-DNA after excitation at 355 nm. (A,B) IR transient absorption signals on AMT (1.1 mM) dissolved in D_2O (A) and on AMT (1.1 mM) with AT-DNA (6.6 mM, bp) in buffered D_2O (pD 7.8) (B). The color coding gives the absorption change in mOD. Dashed vertical lines mark the spectral location of time traces plotted in Figure 5. (C,D) Lifetime density maps (LDM). Red (blue) hue represents decaying (rising) signals. The gray shaded area marks an extrapolation beyond the time window covered in the measurement. The LDM for AMT (C) also contains the DADS for a time constant of 0.5 μs. In the LDM for AMT in AT-DNA (D), the horizontal lines represent the time constants derived from a multiexponential global analysis.

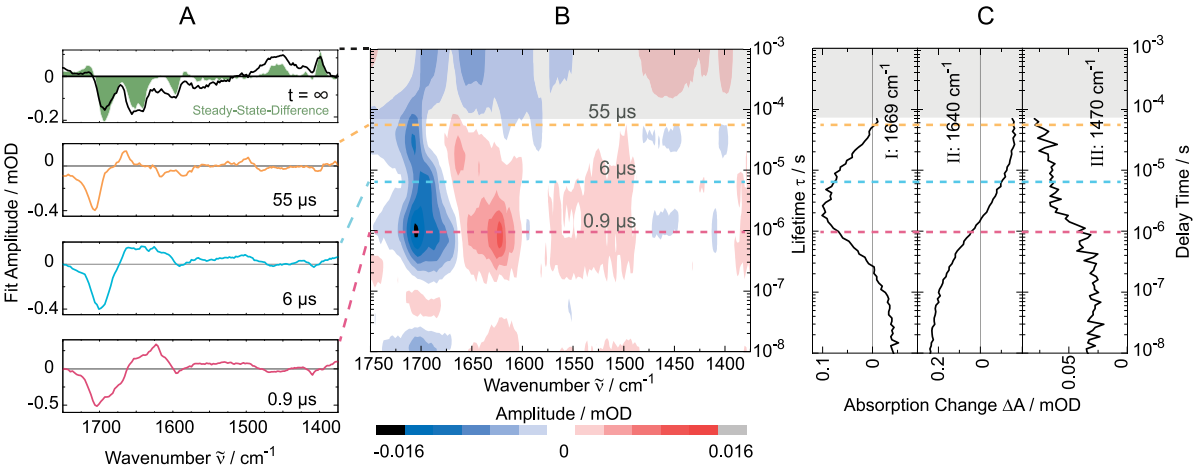

Figure 5. Analysis of the transient IR absorption data of AMT in AT-DNA. (A) DADS from the multiexponential global analysis. (B) LDM (Figure 4D). (C) Time dependence of the IR absorption change for given wavenumbers. At 1669 cm^{-1} an intermediate formed after the AMT triplet state is clearly visible in the time trace. At 1640 cm^{-1} the triplet decay and the bleach of DNA are dominant. At 1470 cm^{-1} the photoproduct formation becomes evident at late delay times.

high concentrations of DNA employed here (6.6 mM in base pairs), the fraction of AMT_{INT} is high (ca. 0.9). At early times absorption bleaches are detected at 1703, 1593, and 1410 cm^{-1}. The bleaching band of the carbonyl stretching vibration (1703 cm^{-1}) is blue-shifted in comparison to free AMT (1684 cm^{-1}). A pronounced positive absorption change occurs at 1625 cm^{-1} and less pronounced positive features are observed throughout the major part of the investigated spectral region. In the late microsecond time range, another positive feature appears at around 1669 cm^{-1}. The respective time dependence (Figure 5C, trace I) shows a rise of the absorption for $t < 2$ μs and a decrease after ca. 6 μs. At around 1640 cm^{-1} (Figure 5C, trace II) a negative absorption change is discernible after $t = 2$ μs. By comparison with the steady-state experiment (cf. Figure 3) this can be assigned to a bleach of DNA bands. At 1470 cm^{-1} (Figure 5C, trace III) the signal increases slightly at around 1 μs giving way to a broad absorption band (1470−1440 cm^{-1}) of the photoproduct. At very late delay times the spectral pattern strongly resembles the steady-state difference spectra (Figure 5A, top). This similarity

DOI: 10.1021/jacs.9b06521
J. Am. Chem. Soc. 2019, 141, 13643−13653

shows that the photoaddition, traced by time-resolved IR, is finished on the 10 μs time scale.

To resolve the reaction kinetics an LDA analysis of the transient data was performed. The respective plot (Figure 4D and 5B) underscores the qualitative observation that the kinetics of AMT_{INT} are more complex than the one of AMT in solution. In the LDA plot large negative amplitudes are seen around 1700 cm^{-1} and from 0.1 μs onward. These are due to ground state recovery as well as signal rises upon the formation of intermediates and of the final photoproduct. The negative feature changes its spectral position with time, indicating that multiple kinetic processes are involved. Between 1675 and 1500 cm^{-1} positive amplitudes are observed from ~0.1 μs until 10 μs. A pronounced feature located at 1625 cm^{-1} points to a lifetime of some microseconds. A comparison with the same feature in Figure 4C indicates that the pattern is associated with the decay of the AMT triplet. A second weaker one is located at 1669 cm^{-1} and observed for lifetimes of several tens of microseconds. The patterns points to intermediates being involved in the formation of the photoadduct. The experimental data and LDA analysis show that a multiexponential trial function is required to describe the experimental results with GLA. Fits with increasing number of exponential terms showed that at least four components together with an offset are required for a satisfying modeling of the data. The time constants are 0.2, 0.9, 6, and 55 μs. Corresponding DADS are shown in Figure 5A.

The amplitudes of the DADS with the shortest time constant of 0.2 μs (given in the SI, Figure S1) are much smaller than those of the other DADS. On the basis of the small amplitude this DADS could be due to contributions of nonintercalated AMT. The time constant of 0.2 μs, however, does not match expectations of the lifetime of free AMT (Figure 4C). A clear assignment is therefore not possible at this point. All DADS (Figure 5A) show a negative amplitude around ~1700 cm^{-1}. As in the LDA, negative amplitudes are due to an absorption increase, which may be due to recovery of ground-state absorption or the absorption upon the formation of intermediates or the final photoproduct. Because of an overlay of ground state, intermediate and product bands, a clear assignment for the negative amplitude in this region to either recovery or formation is not possible. Recoveries and formations seem to contribute to the negative amplitude around 1700 cm^{-1} of all three DADS. Positive amplitudes are especially pronounced in the range of 1670−1600 cm^{-1}. These can be ascribed to the decay of the excited triplet state and also to the decay of an additional intermediate. Small negative amplitudes around 1450 and 1400 cm^{-1} indicate the formation of the photoproduct. The DADS for $\tau = \infty$ overlays well with the steady-state difference spectrum (Figure 5A) underscoring the statement that the photoadduct formation ends on the 10 μs time scale.

Computed IR Spectra. To identify the intermediates found in the nanosecond transient IR spectra, quantum chemical computations were performed. The DFT method with the B3LYP density functional and the 6-31+G* basis set as implemented in Gaussian 09 was used.[39] The solvent environment was taken into account implicitly using the SCRF method (dielectric constant of 78 for water). AMT_{INT} is expected to experience a lower dielectric constant due to the surrounding DNA. Reported constants range from $\epsilon_r = 8$ of dry DNA,[40] 20 for the minor groove[41] to 55 for the major groove.[42] Neither the value for the minor nor the major groove should apply for a DNA intercalator like AMT. The dielectric constant experienced by AMT should be comparable to the constant of a heterocyclic solvent like pyridine. Its dielectric constant (ϵ_r = 13) is not so far from the one of dry DNA. Therefore, computations were also performed using the dielectric constant of pyridine (see Figure S2 in the SI). The resulting spectroscopic patterns are essentially identical to the ones described in the following. Exchangeable protons were replaced by deuterons. In the computation, the structures were first geometry-optimized. Wavenumbers and IR transition strengths of the vibrations were then computed within the harmonic approximation. The obtained wavenumbers were scaled by a factor of 0.96.[43] In the computations only the photoreactive parts were considered, i.e., the DNA surrounding AMT was not included. To model the attachment of the thymine base to the deoxyribose moiety of DNA, computations were performed for 1-methylthymine and the respective adducts.

Stick spectra resulting from the computations are compiled in Figure 6. As expected,[36] the most intense bands for all species considered have strong C═O stretching contributions. For AMT in its electronic ground state (Figure 6A) the computation places the band at 1656 cm^{-1}. This is somewhat smaller than the experimental value of 1684 cm^{-1}. Also the wavenumber of the second highest band is smaller in the computation (1557 cm^{-1}) than in the experiment (1596 cm^{-1}). The band is due to C═C stretching vibrations of the aromatic ring system. For 1-methylthymine, the computation places the carbonyl stretching vibrations at

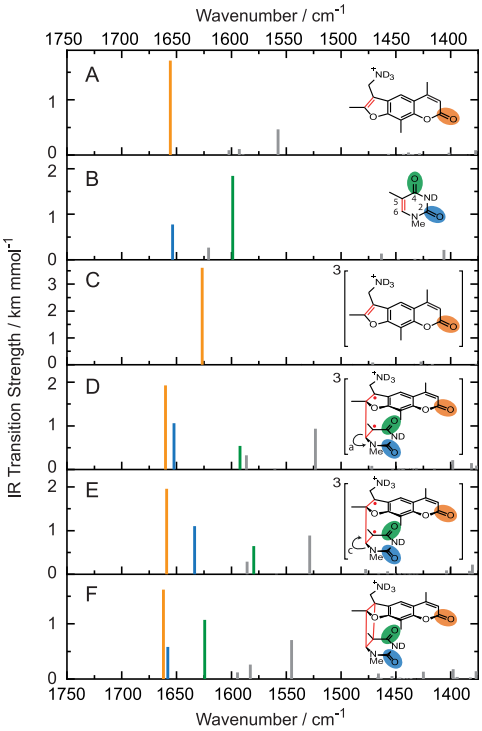

Figure 6. Computed IR stick spectra of AMT and 1-methylthymine derived species. The positions of the bars represent the corrected (scaling factor of 0.96) wavenumbers and their heights the IR transition strength. In the structural formulas on the right the C═O bands contributing predominantly to the strongest IR bands are color coded.

DOI: 10.1021/jacs.9b06521
J. Am. Chem. Soc. 2019, 141, 13643−13653

1655 and 1599 cm^{-1}.[35,44] Again, the experimental values (1693 and 1663 cm^{-1}) are somewhat higher. In the calculated triplet spectrum of AMT the C═O stretching vibration is downshifted to 1626 cm^{-1}. The band exceeds other ones in terms of transition strength by a factor of ∼10. Both, the downshift in frequency and the predominance over the other bands are in accordance with the experiment. For AMT and AMT_{INT} one observes one pronounced positive band in the early IR difference spectra (cf. Figure 4). The band is located at wavenumbers smaller than the negative signal due to the bleach of ground state C═O vibration. For AMT, the positive band and the bleach decay simultaneously due to the depletion of the triplet state.

For AMT_{INT}, the decay of the positive band due to triplet excitation gives way to a band peaking at 1669 cm^{-1}. Guided by the quantum chemical study of Huang and Zhang[25] we hypothesize that this peak can be assigned to a biradical intermediate with a structure as depicted in Figure 6D and E. In this intermediate AMT and thymine are connected by a single bond between positions 5′ of AMT and 6 of thymine (cf. Scheme 1). For the quantum chemical computation, the starting geometry of the biradical was derived from an NMR structure[45] of a closely related photoadduct. By rotation around the 5′-6 bond a start geometry was obtained. Anticlockwise ($^3(AMT^{\bullet}-T^{\bullet})_a$, Figure 6D) and clockwise rotations ($^3(AMT^{\bullet}-T^{\bullet})_c$, Figure 6E) were performed. The respective optimized conformers differ in energy by 0.03 eV, which is of the order of the thermal energy. So both conformers might coexist. A preference for one of these two could result from constraints due to the surrounding DNA. Such constraints were not accounted for in the computation. In the computed IR spectra of the anticlockwise conformer $^3(AMT^{\bullet}-T^{\bullet})_a$ and clockwise conformer $^3(AMT^{\bullet}-T^{\bullet})_c$ the C═O vibration of the AMT moiety adopts wavenumbers (1660 cm^{-1}) close to the one of the AMT ground state. The impact of biradical formation is larger for the C═O vibrations of the thymine part. The C4═O vibration is shifted to smaller wavenumbers (1592 cm^{-1} for $^3(AMT^{\bullet}-T^{\bullet})_a$ and 1580 cm^{-1} for $^3(AMT^{\bullet}-T^{\bullet})_c$). The response of the C2═O vibration is less pronounced for $^3(AMT^{\bullet}-T^{\bullet})_a$ and its wavenumber is hardly changed (1652 cm^{-1}). For $^3(AMT^{\bullet}-T^{\bullet})_c$ it is lowered to 1634 cm^{-1}. In comparison with the thymine ground state, the ordering of the transition strengths is inverted in the biradical. Now, the C2═O vibration carries a higher transition strength. It is this vibration that we associated with the 1669 cm^{-1} band observed in the time-resolved IR experiment on AMT_{INT}. In the computed spectrum of the final photoadduct (Figure 6F) the C═O vibration of the AMT part is slightly higher in wavenumber (1662 cm^{-1}) than in the starting material. Also the C═O vibrations of the thymine moiety are up-shifted in wavenumber (1658 and 1624 cm^{-1}). The upshift of the C═O vibration of AMT and the C2═O one of thymine is in accordance with the steady-state difference spectrum (cf. Figure 3). For wavenumbers larger than 1700 cm^{-1} positive absorption changes are detected. Moving to smaller wavenumbers, first, only absorption bleaches are seen. This is in line with the computations that yielded smaller transitions strengths for the respective vibrations of the photoadduct in comparison to ones of the starting materials. Notably, the computation predicts a strong positive signature at 1545 cm^{-1}. This finds its counterpart at 1583 cm^{-1} in the experiment. The distinct positive experimental features at 1450 and 1399 cm^{-1} are difficult to associate clearly with computed bands.

DISCUSSION

The experimental results presented here clearly show that the photoaddition of a psoralen to thymine leaves a strong signature in IR spectra. Thanks to this signature the kinetics of this addition may be traced in time. From the respective time-resolved IR spectra it may safely be deduced that this addition proceeds on the microsecond time scale. For AMT_{INT} the singlet excitation was shown to persist for a few nanoseconds.[29,30] This gives evidence that the precursor of the photoadduct is the triplet state.

Analysis of the time-resolved UV−vis as well as IR experiments have shown that the addition proceeds in a multiexponential fashion with time constants spreading from 0.2 to 50 μs. Partially, this can be related to the observation of an intermediate in the time-resolved IR experiment (cf. Figures 4 and 5) and thereby to consecutive kinetics. Such an intermediate is expected to form during the decay of the AMT_{INT} triplet state. The kinetic description of this process requires one time constant. The transformation of this intermediate to the photoadduct calls for another time constant. The fact that more than two time constants are derived might point to additional intermediates. Inspection of the LDM derived from the time-resolved IR spectra (cf. Figure 5) gives no clear spectroscopic indication for an *additional* intermediate. Centered around ∼1 μs, one observes one stripe of spectral features. The most prominent among these features is the positive signature at 1625 cm^{-1}. With the aid of the quantum-chemical computation this feature is assigned to the decay of the triplet state. The second stripe is located around 20 μs. The dominant positive signature is situated at higher wavenumbers than the one of the triplet state. This matches expectations based on the formation of a biradical intermediate. If an additional intermediate is unlikely, a kinetic heterogeneity should be considered. Such a heterogeneity might result from intercalation sites of AMT_{INT} differing in distance and orientation with respect to the thymine bases to which it photoattaches. These differences might then translate into different rate constants for the addition. The finding mentioned in the Introduction that different diastereomers can form during the photoaddition[21] is in line with this kinetic heterogeneity. The lifetimes in the range 1−6 μs are therefore assigned to the decay of the AMT_{INT} triplet state. The biradical intermediate forming during its decay persists for 50 μs (Figure 7). Spectroscopically and quantum chemically derived energies for the species involved in the reaction cascade indicate that all processes are downhill.

For the present conditions, the quantum yield Φ_R for the addition of AMT_{INT} to thymine amounts to 0.12, i.e., most excitations decay nonreactively. The finding that the reaction proceeds via the triplet state implies that $\Phi_R = \Phi_T \cdot \eta_R^T$. Hereby, η_R^T is the efficiency ($\eta_R^T \leq 1$) with which $^3AMT_{INT}$ forms the photoproduct. The triplet yield Φ_T for AMT_{INT} has not yet been determined. For AMT in water a value of 0.2 was reported.[27] On the basis of this triplet yield an efficiency of 0.6 results. However, femtosecond UV−vis experiments on AMT and AMT_{INT} point to a higher triplet yield Φ_T for AMT_{INT}—though the value was not quantified.[30] A higher Φ_T implies a lower efficiency η_R^T. Indeed, an analysis of the time-resolved IR spectra (see SI) affords a triplet yield Φ_T of 0.44 for AMT_{INT} and an efficiency η_R^T of 0.27.

DOI: 10.1021/jacs.9b06521
J. Am. Chem. Soc. 2019, 141, 13643−13653

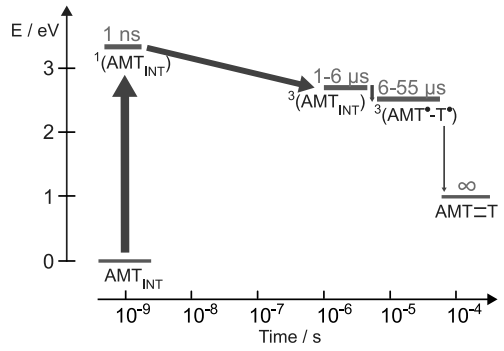

Figure 7. Lifetimes of detected transient species involved in the photoaddition of AMT_{INT} to thymine. The relative efficiency for the formation of the consecutive species is expressed by the thickness of the arrows. The energy scale on the left refers to the equilibrium energies of the species with respect to the one of the addends. The energy of $^1AMT_{INT}$ was derived from spectroscopic data.[30] The other energies were obtained quantum chemically.

Regardless of the determination method, the efficiency η_R^T is smaller than unity. Thus, either during the transition from the triplet state to the biradical intermediate and/or during the transformation of the latter to the photoadduct, repopulation of the starting material occurs. Bleach recovery contributions in the 0.9 and 6 μs DADS at 1593 and 1410 cm^{-1} absent in the 55 μs one suggest that more population is lost during the formation of the biradical (Figure 5A or Figure S1 in the SI).

The photoadduct formed by AMT_{INT} and thymine and the CPD lesion formed between two thymine moieties, are structurally closely related. Yet, their formation kinetics are very different. The CPD predominantly forms with the excited singlet state as a precursor.[3,4] The photoaddition thereby has to compete with the ultrafast (~1 ps) nonradiative decay of thymine singlet states.[46,47] The singlet lifetime of AMT is 3 orders of magnitude longer.[29,30] Still, no evidence for a reaction via this state was seen. This implies that the rate constant for the photoaddition via the singlet channel is at least 3 orders of magnitude smaller for the AMT_{INT} addition than the one for the CPD formation. Also concerning the photoaddition with a triplet precursor very pronounced differences are observed. Thymine features a small triplet quantum yield Φ_T of the order of 0.01,[48] which is more than an order of magnitude smaller than the value for AMT_{INT} (see above). So, trivially, triplet processes are more likely in AMT_{INT} as compared to thymine. The triplet deactivation of thymine in an all thymine DNA single strand $(dT)_{18}$ was compared with the behavior of an isolated thymine moiety (dT).[6] The time-resolved IR study showed that the triplet state in $(dT)_{18}$ is strongly quenched. The triplet lifetime for $(dT)_{18}$ amounts to only 10 ns.[6] For isolated thymine moieties the triplet lifetime is in the microsecond range.[49] The quenching observed in $(dT)_{18}$ was attributed to the formation of a biradical in which two thymine moieties are linked by one single bond (^{3}(T$^•$−T$^•$)). Because of the strong quenching the measured time constant of 10 ns equals the time constant of the reaction. The present results point to the formation of an analogous biradical starting from AMT_{INT} (^{3}(AMT$^•$−T$^•$)). For the AMT_{INT} triplet a distribution of lifetimes in the microsecond range was found. Therefore, the time constant for the reaction is of the order of microseconds or larger and thereby at least 2 orders of magnitude larger than for $(dT)_{18}$. Also the lifetimes of the biradicals differ largely. The biradical ^{3}(T$^•$−T$^•$) persists for 60 ns, ^{3}(AMT$^•$−T$^•$) for ~50 μs. They also differ in reactivity. The biradical ^{3}(T$^•$−T$^•$) mostly decays by reformation of the starting material—a fraction of less than 0.1[6] (0.04 according to Liu et al.[7]) of the ^{3}(T$^•$−T$^•$) forms the CPD. For ^{3}(AMT$^•$−T$^•$) this fraction is at least as high as 0.27 (see SI) since this fraction has to be equal or exceed the efficiency η_R^T for which a range of 0.27−0.6 was obtained for AMT_{INT}.

On a qualitative level some of these differences can be explained by considering the pertinent frontier orbitals. Small barriers and thereby large rate constants are expected for a singlet (2 + 2) photoaddition if the highest occupied molecular orbitals (HOMOs) and lowest unoccupied molecular orbitals (LUMOs) of the reaction partners feature high amplitudes at the reacting positions.[50,51] Frontier orbitals for thymine[52−56] and psoralen[57] derivatives were computed with different quantum chemical approaches. The orbitals obtained by these methods are very similar in terms of nodal structures and density distributions. For sake of comparison, orbitals resulting from the DFT computations are considered here (Figure 8). For our CPD formation interactions of two thymine units at the positions 5 and 6 have to be considered. HOMO and LUMO of the thymine moiety feature high amplitudes here. So if for two properly aligned thymine moieties one is in the excited singlet state, strong HOMO−HOMO and LUMO−LUMO interactions result. These interactions favor a fast cycloaddition, which matches the experimental observation[3] and results of nonadiabatic molecular dynamics computations.[58] For the addition of photoexcited AMT_{INT} to a thymine moiety, frontier orbitals of AMT and thymine should be inspected. For a furan side addition the positions 4′ and 5′ of AMT are decisive. The HOMO of AMT has nonvanishing amplitude here, yet it is smaller than the respective value at the thymine moiety. So a smaller HOMO−

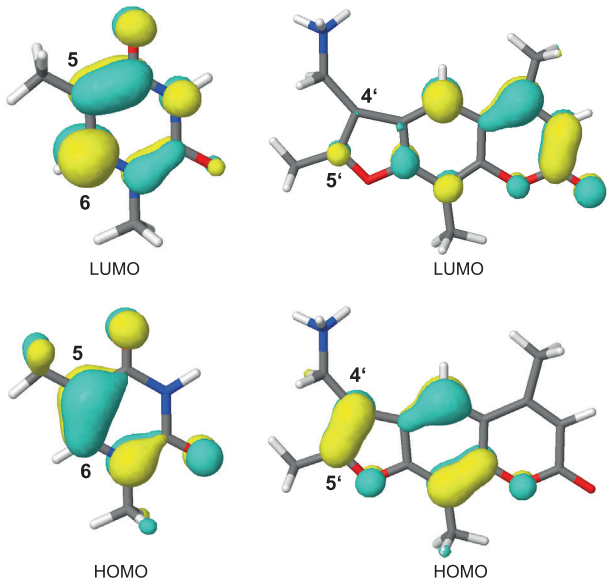

Figure 8. Highest occupied (HOMO) and lowest unoccupied (LUMO) molecular orbitals of 1-methylthymine and AMT. (S_0 geometry and state, B3LYP functional, 6-31+G* basis set, isoline = 0.05). The numbering of the relevant atoms is included.

DOI: 10.1021/jacs.9b06521
J. Am. Chem. Soc. 2019, 141, 13643−13653

HOMO interaction is expected. The LUMO exhibits very small amplitudes at the positions 4′ and 5′ and thus LUMO−LUMO interactions will not contribute. This might explain why for AMT_{INT} the singlet photoaddition is so slow that it cannot compete with the nonreactive decay of the AMT singlet excitation. Matching this argument, a quantum chemical study on a psoralen derivative predicted a large barrier (40 kJ/mol) for the formation via the excited singlet state.[24]

Also concerning the addition via the triplet channel inspection of frontier orbitals can be informative.[51] The presence of the biradicals $^3(T^\bullet-T^\bullet)$ and $^3(AMT^\bullet-T^\bullet)$ indicate that respective moieties are first connected by one single bond. For the formation of $^3(T^\bullet-T^\bullet)$ a quantum-chemical study revealed a preference for a single bond between the position 6 of the two thymine moieties.[59] The respective frontier orbitals exhibit large amplitudes at this position. Yet, this also applies to the neighboring position 5. The biradical $^3(AMT^\bullet-T^\bullet)$ is thought to feature a single bond between the position 5′ of AMT and 6 of thymine.[25] The HOMO of AMT exhibits a large amplitude here and thus a substantial HOMO−HOMO interaction is possible. However, the LUMO of AMT has a very small amplitude here and therefore only a weak LUMO−LUMO interaction is expected. On the basis of the frontier orbitals of AMT the preference for the 5′ position is understandable. Concerning the thymine part, position 5 and 6 seem plausible. Irrespective of the preference, the smaller LUMO−LUMO interaction for AMT and thymine versus thymine−thymine could explain why the formation of $^3(T^\bullet-T^\bullet)$ is faster than the one of $^3(AMT^\bullet-T^\bullet)$.

The lifetime of $^3(AMT^\bullet-T^\bullet)$ exceeds the one of $^3(T^\bullet-T^\bullet)$ by 3 orders of magnitude. The 60 ns lifetime of $^3(T^\bullet-T^\bullet)$ matches the characteristic time scale for hyperfine induced triplet−singlet transitions in biradicals.[6] Thus, in $^3(AMT^\bullet-T^\bullet)$, processes other than triplet−singlet transitions seem to be rate limiting. In a DFT study for a biradical, closely related to $^3(AMT^\bullet-T^\bullet)$, an energy difference of 57.7 kJ/mol between the singlet−triplet transition point and the equilibrium geometry of the biradical was computed.[25] With such an activation energy one expects lifetimes of the biradical of 0.1−1 ms depending on the pre-exponential factor. This magnitude is close to the one of the experimental value (∼50 μs). The DFT computation also suggests that the triplet biradical does not revert back to the addends, the respective barrier being 83.7 kJ/mol. This would imply that most biradicals transform into the photoadduct. The efficiency η_R^T is less than one because most triplet excitation of AMT_{INT} do not form the biradical. For $^3(T^\bullet-T^\bullet)$ it is the other way round. These experimental findings should be further scrutinized by quantum chemistry.

The observed addition of AMT_{INT} to thymine via the triplet state matches the early finding[29,30] that presence of guanine in the vicinity of AMT_{INT} reduces its photoreactivity. AMT_{INT} in its excited singlet is quenched by PET with a guanine base as a donor. Due to this quenching the triplet state of AMT_{INT} is not populated and the photoaddition cannot occur. On the basis of these observations, criteria for psoralens efficient in PUVA therapy may be formulated: Excitation energies and redox properties should be such that PET will not occur even if guanine is present. The psoralen should feature a high triplet quantum yield. Synthetic and spectroscopic efforts to identify such psoralens are presently undertaken.

CONCLUSIONS

Nanosecond laser flash photolysis combined with nanosecond UV pump IR probe spectroscopy and quantum chemical calculations allowed to characterize the photoinduced addition of the psoralen AMT to a thymine moiety. The spectroscopic results show unequivocally that the addition proceeds via the triplet channel. The reaction occurs on the microsecond time scale and involves an intermediate, presumably a biradical. The kinetics of this photoaddition are strongly slowed down—by orders of magnitude—as compared to the corresponding photoaddition of two thymine moieties within the DNA. Yet, the reaction quantum yield is considerably higher for the psoralen AMT. Partially, these experimental findings can be rationalized using qualitative MO considerations. Similarities in the spectrotemporal behavior of AMT and other psoralens, among them the therapeutically used 8-MOP,[30] suggest that the present findings bear relevance for all PUVA agents. The results could pave the way toward better PUVA agents.

ASSOCIATED CONTENT

Supporting Information

The Supporting Information is available free of charge on the ACS Publications website at DOI: 10.1021/jacs.9b06521.

Experimental procedures; ns-IR: DADS of AMT with AT-DNA; Computed IR spectra in pyridine; Reaction efficiency of the triplet state (PDF)

AUTHOR INFORMATION

Corresponding Author

*gilch@hhu.de

ORCID

Peter Gilch: 0000-0002-6602-9397

Present Addresses

[§]Covestro Deutschland AG, Kaiser-Wilhelm-Allee 60, 51373 Leverkusen, Germany.

[∥]TÜV Rheinland Industrie Service GmbH, Am Grauen Stein, 51105 Köln, Germany.

Notes

The authors declare no competing financial interest.

ACKNOWLEDGMENTS

Financial support by Deutsche Forschungsgemeinschaft (project GI 349/6-1) is gratefully acknowledged. Janina Diekmann thanks the Jürgen Manchot Stiftung for a scholarship. Wolfgang Zinth and Julia Gontcharov were supported by the Deutsche Forschungsgemeinschaft through the Clusters of Excellence "Center for Integrated Protein Science Munich" and "Munich-Centre for Advanced Photonics".

REFERENCES

(1) Cadet, J.; Vigny, P. In *Bioorganic Photochemistry*; Morrison, H., Ed.; John Wiley & Sons: New York, 1990; pp 1−272.

(2) Cadet, J.; Mouret, S.; Ravanat, J. L.; Douki, T. Photoinduced damage to cellular DNA: Direct and photosensitized reactions. *Photochem. Photobiol.* **2012**, *88*, 1048−1065.

(3) Schreier, W. J.; Schrader, T. E.; Koller, F. O.; Gilch, P.; Crespo-Hernández, C. E.; Swaminathan, V. N.; Carell, T.; Zinth, W.; Kohler, B. Thymine dimerization in DNA is an ultrafast photoreaction. *Science* **2007**, *315*, 625−629.

(4) Schreier, W. J.; Gilch, P.; Zinth, W. Early Events of DNA Photodamage. *Annu. Rev. Phys. Chem.* **2015**, *66*, 497−519.

DOI: 10.1021/jacs.9b06521
J. Am. Chem. Soc. 2019, 141, 13643−13653

(5) Hoffmann, R.; Woodward, R. B. Selection Rules for Concerted Cycloaddition Reactions. *J. Am. Chem. Soc.* **1965**, *87*, 2046−2048.
(6) Pilles, B. M.; Bucher, D. B.; Liu, L.; Clivio, P.; Gilch, P.; Zinth, W.; Schreier, W. J. Mechanism of the decay of thymine triplets in DNA single strands. *J. Phys. Chem. Lett.* **2014**, *5*, 1616−1622.
(7) Liu, L.; Pilles, B. M.; Gontcharov, J.; Bucher, D. B.; Zinth, W. Quantum Yield of Cyclobutane Pyrimidine Dimer Formation Via the Triplet Channel Determined by Photosensitization. *J. Phys. Chem. B* **2016**, *120*, 292−298.
(8) Bethea, D.; Fullmer, B.; Syed, S.; Seltzer, G.; Tiano, J.; Rischko, C.; Gillespie, L.; Brown, D.; Gasparro, F. P. Psoralen photobiology and photochemotherapy: 50 years of science and medicine. *J. Dermatol. Sci.* **1999**, *19*, 78−88.
(9) Almutawa, F.; Alnomair, N.; Wang, Y.; Hamzavi, I.; Lim, H. W. Systematic review of UV-based therapy for psoriasis. *Am. J. Clin. Dermatol.* **2013**, *14*, 87−109.
(10) Ling, T. C.; Clayton, T. H.; Crawley, J.; Exton, L. S.; Goulden, V.; Ibbotson, S.; McKenna, K.; Mohd Mustapa, M. F.; Rhodes, L. E.; Sarkany, R.; Dawe, R. S. British Association of Dermatologists and British Photodermatology Group guidelines for the safe and effective use of psoralen-ultraviolet A therapy 2015. *Br. J. Dermatol.* **2016**, *174*, 24−55.
(11) Knobler, R.; Berlin, G.; Calzavara-Pinton, P.; Greinix, H.; Jaksch, P.; Laroche, L.; Ludvigsson, J.; Quaglino, P.; Reinisch, W.; Scarisbrick, J.; Schwarz, T.; Wolf, P.; Arenberger, P.; Assaf, C.; Bagot, M.; Barr, M.; Bohbot, A.; Bruckner-Tuderman, L.; Dreno, B.; Enk, A.; French, L.; Gniadecki, R.; Gollnick, H.; Hertl, M.; Jantschitsch, C.; Jung, A.; Just, U.; Klemke, C.-D.; Lippert, U.; Luger, T.; Papadavid, E.; Pehamberger, H.; Ranki, A.; Stadler, R.; Sterry, W.; Wolf, I. H.; Worm, M.; Zic, J.; Zouboulis, C. C.; Hillen, U. Guidelines on the use of extracorporeal photopheresis. *J. Eur. Acad. Dermatol. Venereol.* **2014**, *28*, 1−37.
(12) Humme, D.; Nast, A.; Erdmann, R.; Vandersee, S.; Beyer, M. Systematic review of combination therapies for mycosis fungoides. *Cancer Treat. Rev.* **2014**, *40*, 927−933.
(13) Child, F. J.; Mitchell, T. J.; Whittaker, S. J.; Scarisbrick, J. J.; Seed, P. T.; Russell-Jones, R. A randomized cross-over study to compare PUVA and extracorporeal photopheresis in the treatment of plaque stage (T2) mycosis fungoides. *Clin. Exp. Dermatol.* **2004**, *29*, 231−236.
(14) Kitamura, N.; Kohtani, S.; Nakagaki, R. Molecular aspects of furocoumarin reactions: Photophysics, photochemistry, photobiology, and structural analysis. *J. Photochem. Photobiol., C* **2005**, *6*, 168−185.
(15) Johnson, R.; Staiano-Coico, L.; Austin, L.; Cardinale, I.; Nabeya-Tsukifuji, R.; Krueger, J. G. PUVA treatment selectively induces a cell cycle block and subsequent apoptosis in human T-lymphocytes. *Photochem. Photobiol.* **1996**, *63*, 566−571.
(16) Kanne, D.; Straub, K.; Hearst, J. E.; Rapoport, H. Isolation and Characterization of Pyrimidine-Psoralen-Pyrimidine Photodiadducts from DNA. *J. Am. Chem. Soc.* **1982**, *104*, 6754−6764.
(17) Hearst, J. E. Photochemistry of the Psoralens. *Chem. Res. Toxicol.* **1989**, *2*, 69−75.
(18) Kanne, D.; Rapoport, H.; Hearst, J. E. 8-Methoxypsoralen-nucleic acid photoreaction. Effect of methyl substitution on pyrone vs. furan photoaddition. *J. Med. Chem.* **1984**, *27*, 531−534.
(19) Oroskar, A.; Olack, G.; Peak, M. J.; Gasparro, F. P. 4′-Aminomethyl-4,5′,8-trimethylpsoralen photochemistry: the effect of concentration and UVA fluence on photoadduct formation in poly(dA-dT) and calf thymus DNA. *Photochem. Photobiol.* **1994**, *60*, 567−73.
(20) Hearst, J. E.; Isaacs, S. T.; Kanne, D.; Rapoport, H.; Straub, K. The reaction of the psoralens with deoxyribonucleic acid. *Q. Rev. Biophys.* **1984**, *17*, 1.
(21) Cimino, G. D.; Gamper, H. B.; Isaacs, S. T.; Hearst, J. E. Psoralens as photoactive probes of nucleic acid structure and function. *Annu. Rev. Biochem.* **1985**, *54*, 1151−1193.
(22) Serrano-Pérez, J. J.; Serrano-Andrés, L.; Merchán, M. Photosensitization and phototherapy with furocoumarins: A quantum-chemical study. *Chem. Phys.* **2008**, *347*, 422−435.
(23) Serrano-Pérez, J. J.; Merchán, M.; Serrano-Andrés, L. Photoreactivity of Furocoumarins and DNA in PUVA Therapy: Formation of Psoralen-Thymine Adducts. *J. Phys. Chem. B* **2008**, *112*, 14002−14010.
(24) Omar, S.; Eriksson, L. A. Interaction and photobinding between 8-methoxypsoralen and thymine. *Chem. Phys. Lett.* **2009**, *471*, 128−132.
(25) Huang, X.; Zhang, R. A. Theoretical Rationale why Furan-side Monoadduct is More Favorable Toward Diadduct Formation in 8-Methoxypsoralen and Thymine Complexes. *Photochem. Photobiol.* **2013**, *89*, 891−899.
(26) Beaumont, P. C.; Parsons, B. J.; Navaratnam, S.; Phillips, G. O.; Allen, J. C. The reactivities of furocoumarin exicted states with DNA in solution. A laser flash photolysis and fluorescence study. *Biochim. Biophys. Acta, Nucleic Acids Protein Synth.* **1980**, *608*, 259−265.
(27) Salet, C.; Macedo De Sa E Melo, T.; Bensasson, R.; Land, E. J. Photophysical properties of aminomethylpsoralen in presence and absence of DNA. *Biochim. Biophys. Acta, Nucleic Acids Protein Synth.* **1980**, *607*, 379−383.
(28) Bensasson, R. V.; Land, E. J.; Salet, C. Triplet excited state of furocoumarins: reaction with nucleic acid bases and amino acids. *Photochem. Photobiol.* **1978**, *27*, 273−80.
(29) Fröbel, S.; Reiffers, A.; Torres Ziegenbein, C.; Gilch, P. DNA Intercalated Psoralen Undergoes Efficient Photoinduced Electron Transfer. *J. Phys. Chem. Lett.* **2015**, *6*, 1260−1264.
(30) Fröbel, S.; Levi, L.; Ulamec, S. M.; Gilch, P. Photoinduced Electron Transfer between Psoralens and DNA: Influence of DNA Sequence and Substitution. *ChemPhysChem* **2016**, *17*, 1377−1386.
(31) Paul, S.; Samanta, A. Ground- and Excited-State Interactions of a Psoralen Derivative with Human Telomeric G-Quadruplex DNA. *J. Phys. Chem. B* **2018**, *122*, 2277−2286.
(32) Isaacs, S. T.; Shen, C.-K. J.; Hearst, J. E.; Rapoport, H. Synthesis and characterization of new psoralen derivatives with superior photoreactivity with DNA and RNA. *Biochemistry* **1977**, *16*, 1058−1064.
(33) Berkoff, B.; Hogan, M.; Legrange, J.; Austin, R. Dependence of oxygen quenching of intercalated methylene blue triplet lifetime on DNA base-pair composition. *Biopolymers* **1986**, *25*, 307−316.
(34) Banyay, M.; Sarkar, M.; Gräslund, A. A library of IR bands of nucleic acids in solution. *Biophys. Chem.* **2003**, *104*, 477−488.
(35) Lee, C.; Cho, M. Vibrational dynamics of DNA. II. Deuterium exchange effects and simulated IR absorption spectra. *J. Chem. Phys.* **2006**, *125*, 114509.
(36) Socrates, G. *Infrared and Raman Characteristic Group Frequencies*, 3rd ed.; John Wiley & Sons: Chichester, 2001.
(37) Hare, P. M.; Middleton, C. T.; Mertel, K. I.; Herbert, J. M.; Kohler, B. Time-resolved infrared spectroscopy of the lowest triplet state of thymine and thymidine. *Chem. Phys.* **2008**, *347*, 383−392.
(38) Srivastava, S.; Yourd, E.; Toscano, J. P. Structural Differences between $\pi\pi^*$ and $n\pi^*$ Acetophenone Triplet Excited States as Revealed by Time-Resolved IR Spectroscopy. *J. Am. Chem. Soc.* **1998**, *120*, 6173−6174.
(39) Frisch, M. J.; Trucks, G. W.; Schlegel, H. B.; Scuseria, G. E.; Robb, M. A.; Cheeseman, J. R.; Scalmani, G.; Barone, V.; Mennucci, B.; Petersson, G. A.; Nakatsuji, H.; Caricato, M.; Li, X.; Hratchian, H. P.; Izmaylov, A. F.; Bloino, J.; Zheng, G.; Sonnenberg, J. L.; Hada, M.; Ehara, M.; Toyota, K.; Fukuda, R.; Hasegawa, J.; Ishida, M.; Nakajima, T.; Honda, Y.; Kitao, O.; Nakai, H.; Vreven, T.; Montgomery, J. A., Jr.; Peralta, J. E.; Ogliaro, F.; Bearpark, M.; Heyd, J. J.; Brothers, E.; Kudin, K. N.; Staroverov, V. N.; Kobayashi, R.; Normand, J.; Raghavachari, K.; Rendell, A.; Burant, J. C.; Iyengar, S. S.; Tomasi, J.; Cossi, M.; Rega, N.; Millam, J. M.; Klene, M.; Knox, J. E.; Cross, J. B.; Bakken, V.; Adamo, C.; Jaramillo, J.; Gomperts, R.; Stratmann, R. E.; Yazyev, O.; Austin, A. J.; Cammi, R.; Pomelli, C.; Ochterski, J. W.; Martin, R. L.; Morokuma, K.; Zakrzewski, V. G.; Voth, G. A.; Salvador, P.; Dannenberg, J. J.; Dapprich, S.; Daniels, A. D.; Farkas, O.; Foresman, J. B.; Ortiz, J. V.; Cioslowski, J.; Fox, D. J. *Gaussian 09*, Revision A.02; Gaussian, Inc.: Wallingford, CT, 2016.

DOI: 10.1021/jacs.9b06521
J. Am. Chem. Soc. 2019, 141, 13643−13653

(40) Cuervo, A.; Dans, P. D.; Carrascosa, J. L.; Orozco, M.; Gomila, G.; Fumagalli, L. Direct measurement of the dielectric polarization properties of DNA. *Proc. Natl. Acad. Sci. U. S. A.* **2014**, *111*, E3624−E3630.
(41) Jin, R.; Breslauer, K. J. Characterization of the minor groove environment in a drug-DNA complex: bisbenzimide bound to the poly[d(AT)].poly[d(AT)]duplex. *Proc. Natl. Acad. Sci. U. S. A.* **1988**, *85*, 8939−8942.
(42) Barawkar, D. A.; Ganesh, K. N. Fluorescent d-(CGCGAATTCGCG): Characterization of major groove polarity and study of minor groove interactions through a major groove semantophore conjugate. *Nucleic Acids Res.* **1995**, *23*, 159−164.
(43) Koch, W.; Holthausen, M. C. *A Chemist's Guide to Density Functional Theory*; Wiley-VCH Verlag GmbH: Weinheim, 2001; Vol. 3.
(44) Taniguchi, H.; Saito, M. The effect of water on infrared spectra of DNA. *J. Phys.: Condens. Matter* **2009**, *21*, 064242.
(45) Spielmann, H. P.; Dwyer, T. J.; Hearst, J. E.; Wemmer, D. E. Solution Structures of Psoralen Monoadducted and Cross-Linked DNA Oligomers by NMR Spectroscopy and Restrained Molecular Dynamics. *Biochemistry* **1995**, *34*, 12937−12953.
(46) Pecourt, J. M.; Peon, J.; Kohler, B. DNA excited-state dynamics: Ultrafast internal conversion and vibrational cooling in a series of nucleosides. *J. Am. Chem. Soc.* **2001**, *123*, 10370−10378.
(47) Middleton, C. T.; de La Harpe, K.; Su, C.; Law, Y. K.; Crespo-Hernández, C. E.; Kohler, B. DNA Excited-State Dynamics: From Single Bases to the Double Helix. *Annu. Rev. Phys. Chem.* **2009**, *60*, 217−239.
(48) Banyasz, A.; Douki, T.; Improta, R.; Gustavsson, T.; Onidas, D.; Vayá, I.; Perron, M.; Markovitsi, D. Electronic excited states responsible for dimer formation upon UV absorption directly by thymine strands: Joint experimental and theoretical study. *J. Am. Chem. Soc.* **2012**, *134*, 14834−14845.
(49) Salet, C.; Bensasson, R.; Becker, R. S. Triplet Excited States of Pyrimidine Nucleosides and Nucleotides. *Photochem. Photobiol.* **1979**, *30*, 325−329.
(50) Caldwell, R. A. A Predictor of Reactivity in Allowed Photodimerizations and Photocycloadditions. *J. Am. Chem. Soc.* **1980**, *102*, 4004−4007.
(51) Fleming, I. *Molecular Orbitals and Organic Chemical Reactions*; John Wiley & Sons, Ltd.: Chichester, UK, 2010.
(52) Gustavsson, T.; Bányász, Á.; Lazzarotto, E.; Markovitsi, D.; Scalmani, G.; Frisch, M. J.; Barone, V.; Improta, R. Singlet Excited-State Behavior of Uracil and Thymine in Aqueous Solution: A Combined Experimental and Computational Study of 11 Uracil Derivatives. *J. Am. Chem. Soc.* **2006**, *128*, 607−619.
(53) Dargiewicz, M.; Biczysko, M.; Improta, R.; Barone, V. Solvent effects on electron-driven proton-transfer processes: Adenine-thymine base pairs. *Phys. Chem. Chem. Phys.* **2012**, *14*, 8981−8989.
(54) Souri, M.; Mohammadi, A. K. Investigation of solvent effect on adenine-thymine base pair interaction. *J. Mol. Liq.* **2017**, *230*, 169−174.
(55) Marian, C. M.; Schneider, F.; Kleinschmidt, M.; Tatchen, J. Electronic excitation and singlet-triplet coupling in uracil tautomers and uracil-water complexes: A quantum chemical investigation. *Eur. Phys. J. D* **2002**, *20*, 357−367.
(56) Etinski, M.; Marian, C. M. Ab initio investigation of the methylation and hydration effects on the electronic spectra of uracil and thymine. *Phys. Chem. Chem. Phys.* **2010**, *12*, 4915.
(57) Tatchen, J.; Kleinschmidt, M.; Marian, C. M. Electronic excitation spectra and singlet-triplet coupling in psoralen and its sulfur and selenium analogs. *J. Photochem. Photobiol., A* **2004**, *167*, 201−212.
(58) Rauer, C.; Nogueira, J. J.; Marquetand, P.; González, L. Cyclobutane Thymine Photodimerization Mechanism Revealed by Nonadiabatic Molecular Dynamics. *J. Am. Chem. Soc.* **2016**, *138*, 15911−15916.
(59) Zhang, R. B.; Eriksson, L. A. A triplet mechanism for the formation of cyclobutane pyrimidine dimers in UV-irradiated DNA. *J. Phys. Chem. B* **2006**, *110*, 7556−7562.

DOI: 10.1021/jacs.9b06521
J. Am. Chem. Soc. 2019, 141, 13643−13653

2.2. Photoaddition der pharmazeutisch genutzten Psoralene an DNA (Veröffentlichung II)

Title: Tracing the Photoaddition of Pharmaceutical Psoralens to DNA

Authors: Janina Diekmann, Isabell Theves, Kristoffer A. Thom, Peter Gilch

Published in: Molecules

Year: 2020

Impact Factor: 3.267 (2019)

Eigene Anteile an der Veröffentlichung:

- Konzeptualisierung
- Auswertung der stationären UV/Vis und IR-Messungen sowie der quantenchemischen Rechnungen
- Planung und Auswertung der zeitaufgelösten UV/Vis Messungen
- Erstellung der Abbildungen
- Literaturrecherche und Verfassen eines großen Anteils des Manuskripts

molecules

MDPI

Article

Tracing the Photoaddition of Pharmaceutical Psoralens to DNA

Janina Diekmann, Isabell Theves, Kristoffer A. Thom and Peter Gilch *

Institut für Physikalische Chemie, Heinrich-Heine-Universität Düsseldorf, Universitätsstr. 1, 40225 Düsseldorf, Germany; janina.diekmann@hhu.de (J.D.); isabell.theves@hhu.de (I.T.); kristoffer.thom@hhu.de (K.A.T.)
* Correspondence: gilch@hhu.de

Received: 30 September 2020; Accepted: 7 November 2020; Published: 10 November 2020

Abstract: The psoralens 8-methoxypsoralen (8-MOP), 4,5′,8-trimethylpsoralen (TMP) and 5-methoxypsoralen (5-MOP) find clinical application in PUVA (psoralen + UVA) therapy. PUVA treats skin diseases like psoriasis and atopic eczema. Psoralens target the DNA of cells. Upon photo-excitation psoralens bind to the DNA base thymine. This photo-binding was studied using steady-state UV/Vis and IR spectroscopy as well as nanosecond transient UV/Vis absorption. The experiments show that the photo-addition of 8-MOP and TMP involve the psoralen triplet state and a biradical intermediate. 5-MOP forms a structurally different photo-product. Its formation could not be traced by the present spectroscopic technique.

Keywords: psoralen; 8-MOP; TMP; 5-MOP; DNA damage; PUVA; photochemistry; UV/Vis spectroscopy; IR spectroscopy; time-resolved spectroscopy

1. Introduction

The light-dependent PUVA (psoralen + UVA) therapy is a well-established symptomatic treatment of skin diseases like psoriasis [1,2], atopic eczema [3], vitiligo [4,5] and cutaneous T-cell lymphoma [6,7]. In the treatment, patients are administered psoralen derivatives and the affected skin regions are exposed to UVA radiation [8]. Concerning the molecular mechanism of the therapy, it was shown that the uptake of psoralens in the cellular nuclei is the first step [9]. While the main targets of the psoralen are the nucleic acids, minor interactions with other biomolecules like lipids and proteins in other parts of the cell can take place [10]. Concerning DNA as a target, there is consensus that psoralens intercalate into DNA, that is, they insert themselves between the base pairs. Upon photo-excitation, the intercalated psoralens may bind to the DNA base thymine (see Scheme 1). A cyclobutane ring forms involving the 4′ and 5′ positions of the psoralen (furan side) and the five and six positions of the thymine base [11–13]. The formation of a cyclobutane ring involving the three and four positions of the psoralen (pyrone side) was also found. The ratio of the two adducts depends on the substitution pattern [14]. Photo-excitation of the furan side adduct can trigger another photoaddition which results in DNA crosslinking. The damage done to DNA by (mono-) adducts and crosslinks can induce apoptosis of the affected cells, ultimately resulting in the relief of symptoms [15].

The mechanism of this photoaddition was addressed by steady-state [11] and time-resolved spectroscopy [16–18] as well as quantum chemistry [19–22]. In a recent study, we traced the photo-addition of psoralen to DNA in real-time [23]. The study addressed the derivative 4′-aminomethyl-4,5′,8-trimethylpsoralen (AMT) and a DNA double-strand consisting of alternating adenine (A) and thymine (T) bases (AT-DNA in the following). AMT was selected as it features a high water solubility [24], a relatively high intercalation affinity (see below) and a high quantum yield for the photoaddition of 0.12 [25]. For AMT intercalated into DNA bearing guanine (G) and cytosine (C) base pairs, a photo-induced electron transfer (PET) was observed. This PET reduces the propensity for

the photoaddition [26]. Therefore, experiments were conducted with AT-DNA. AMT predominantly forms the furan side adduct. With nanosecond UV/Vis and IR spectroscopy, it was shown that the photo-addition of AMT proceeds via a local triplet state. This state features lifetimes in the range 1–10 µs. The spread is presumably due to heterogeneity of the sample. The decaying local triplet state feeds a triplet biradical in which the AMT moiety is connected with a thymine base via a C-C single bond. Formation of the second bond and thereby the final photo-product takes ~50 µs. AMT has favorable properties for a spectroscopic characterization and potentially for clinical use. However, AMT has no approval for clinical applications. Psoralens which received approval are 8-methoxypsoralen (8-MOP), 4,5′,8-trimethylpsoralen (TMP) and 5-methoxypsoralen (5-MOP) [8]. In most countries, the commonly used psoralen is 8-MOP [7]. While in the United States, 8-MOP is the only derivative available for clinical use [6], in some European countries TMP and 5-MOP find application [1,4]. Yet, TMP and 5-MOP are less studied and only rarely administered [8].

Here, it will be investigated in how far the mechanistic picture derived from experiments on AMT can be transferred to psoralens (8-MOP, TMP and 5-MOP) used in clinics. While for AMT a combination of time-resolved UV/Vis and time-resolved infrared (IR) spectroscopy was used to resolve the kinetics of the photo-addition, herein we use solely the technique of time-resolved UV/Vis spectroscopy available in our lab. The small quantum yields and/or water solubilities of these derivatives are very challenging for the small signals in time-resolved IR spectroscopy. It will be shown that for a comparison between derivatives the not as demanding and less resource-intensive method of time-resolved UV/Vis spectroscopy can still show distinct similarities and differences between derivatives. To this end, dissociation constants characterizing the intercalation, reaction quantum yields, spectroscopic patterns as well as kinetic parameters of the photo-addition were recorded. Based on the results, some guidelines for the rational improvement of PUVA agents shall be given.

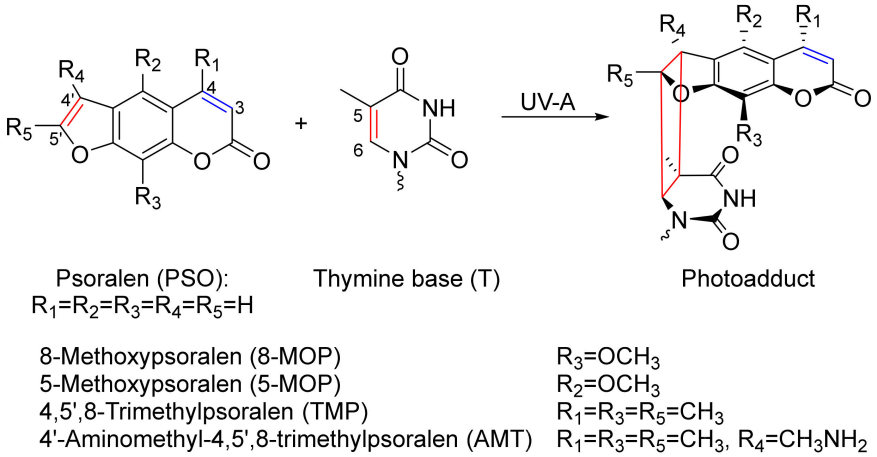

Scheme 1. Structures of relevant psoralen derivatives and their photoaddition to DNA. Reaction via the 4′-5′-double-bond results in the furan monoadduct. The DNA is represented by the thymine base.

2. Results

The following results show spectroscopic measurements on psoralen derivatives with and without DNA. Synthetic DNA double strands with alternating adenine (A) and thymine (T) bases, AT-DNA in the following, were employed. They were formed by annealing 5′-$(TA)_{20}$-3′ single strands. All three psoralen derivatives have, as opposed to AMT, low water solubility ranging from few micromolar for TMP to a few hundred micromolar for 8-MOP [27]. The apparent solubility increases when the psoralen can intercalate into DNA [28].

2.1. Intercalation

Intercalation of psoralens into DNA is a prerequisite for the photoaddition and, thus, has to be characterized. The propensity for intercalation is commonly quantified by the dissociation constant K_D [24]:

$$K_D = \frac{c_{Pso,free} \cdot c_{DNA,free}}{c_{Pso,int}}. \quad (1)$$

$c_{Pso,free}$ is the concentration of free (non-intercalated) psoralen, $c_{Pso,int}$ stands for the concentration of intercalated psoralen and $c_{DNA,free}$ the concentration of DNA base pairs which are not hosting a psoralen. All concentrations refer to equilibrium conditions. A small K_D value represents a strong intercalation affinity. The dissociation constant K_D can be determined by a titration experiment [25,29] which relies on the hypochromic effect in the UV/Vis absorption of psoralens upon intercalation [30]. In the titration, the total concentration of psoralen $c_{Pso,free} + c_{Pso,int}$ was kept constant and the total DNA concentration c_{DNA} gradually reduced (see Reference [25] for details). Results of such a titration for 8-MOP and AT-DNA are summarized in Figure 1. In the respective UV/Vis absorption for wavelengths larger than 300 nm—the spectral region below cannot be covered due to the high DNA absorption—the impact of DNA on the 8-MOP absorption is clearly visible. For high DNA concentration and thereby a large fraction of intercalated 8-MOP the absorption is relatively small. For low DNA concentration and thereby mostly free 8-MOP the absorption is higher. This is in line with the hypochromic effect of intercalation. From the dependence of the absorption at 302 nm on the total DNA concentration the dissociation constant K_D can be determined. The procedure relies on Equation (1) as well as Beer's law and is specified in Reference [25]. The K_D value of 8-MOP and AT-DNA derived thereby amounts to 1.1×10^{-3} M. For 8-MOP and calf thymus DNA, Isaacs et al. have determined a similar value of 1.3×10^{-3} M [27]. Deviation in K_D values can be expected for differing DNA sequences and ionic strength of the sample [31]. For AMT and AT-DNA, a somewhat smaller value of 4.4×10^{-4} M [25] was reported. With the same procedure (data not shown) a dissociation constant K_D of 1.8×10^{-4} M for 5-MOP and AT-DNA was determined. A higher intercalation affinity compared to 8-MOP is in line with early reports [32]. The low solubility of TMP in water renders a K_D determination by the above procedure difficult. Therefore, only the order of magnitude is estimated for the constant K_D. For this estimate solid TMP was added to a solution of AT-DNA in amounts exceeding its solubility. Under these conditions the concentration $c_{Pso,free}$ ought to equal the saturation concentration of TMP. The concentration of intercalated TMP $c_{Pso,int}$ was determined photometrically. From these values, a K_D value of the order of 10^{-4} M was estimated.

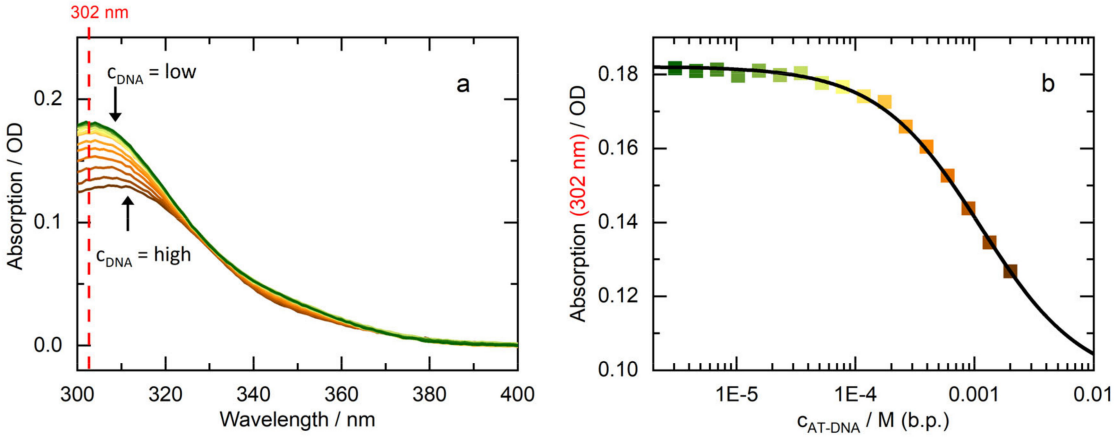

Figure 1. Intercalation behavior of 8-MOP: (**a**) UV/Vis absorption spectra of 8-MOP (15 µM) with increasing concentration of AT-DNA in phosphate-buffered saline (PBS). The contribution of DNA to the absorption was subtracted; (**b**) Absorption at 302 nm versus the concentration of AT-DNA. A fit yields the dissociation constant K_D of 1.1×10^{-3} M.

2.2. UV/Vis Absorption Signatures of the Photoadditions

All three psoralen derivatives absorb light in the UVA range (315–400 nm). The absorption coefficients are high at the lower end of the UVA (5000–15,000 M^{-1} cm^{-1}) and low or close to zero around 400 nm. The DNA has very low to zero absorption in this range. The spectrum of 8-MOP intercalated into AT-DNA shows an absorption up to 400 nm (Figure 2a, green). Irradiation at 390 nm causes changes to the absorption spectrum. The irradiation times are converted into photon equivalents (PE) which is a measure of the light dose (see Materials and Methods). A PE value of one implies that each molecule has absorbed one photon. With the irradiation time or PE value, the absorption between 322–366 nm increases and below 322 and above 366 nm decreases. The last spectrum, the spectrum of the photoproduct, features a maximum at 340 nm and a shoulder at ~352 nm. These features indicate the formation of the furan monoadduct [12,33–35]. Longer irradiation at 390 nm causes the absorption to decrease throughout the whole UVA spectrum (not shown here). Even though the absorption of the monoadduct is almost zero at 390 nm, the small absorption seems to cause the formation of a secondary photoproduct, presumably a crosslink. Neither the pyrone monoadduct nor the crosslink absorb light in the UVA range [12]. Difference absorption coefficients for the monoaddition were extracted from these spectra. A plot of the absorption versus irradiation time (not shown here) indicates that after ~150 min the monoaddition is terminated. Therefore, the concentration of the photo-product ought to equal the initial concentration of intercalated 8-MOP. From that, the difference absorption coefficients can be computed (Figure 2d). The spectrum has a maximal difference absorption coefficient of ~4000 M^{-1} cm^{-1} and the spectral pattern is red-shifted by 8 nm with respect to that of AMT [23]. With the knowledge of the light power impinging on the sample, a reaction quantum yield Φ_R of 0.04 was computed. The value is higher than yields determined for 8-MOP in calf thymus DNA (0.013 [27], 0.0065 [36] and 0.0046 [37]). The difference could be related to the PET quenching occurring in the DNA-samples bearing guanine.

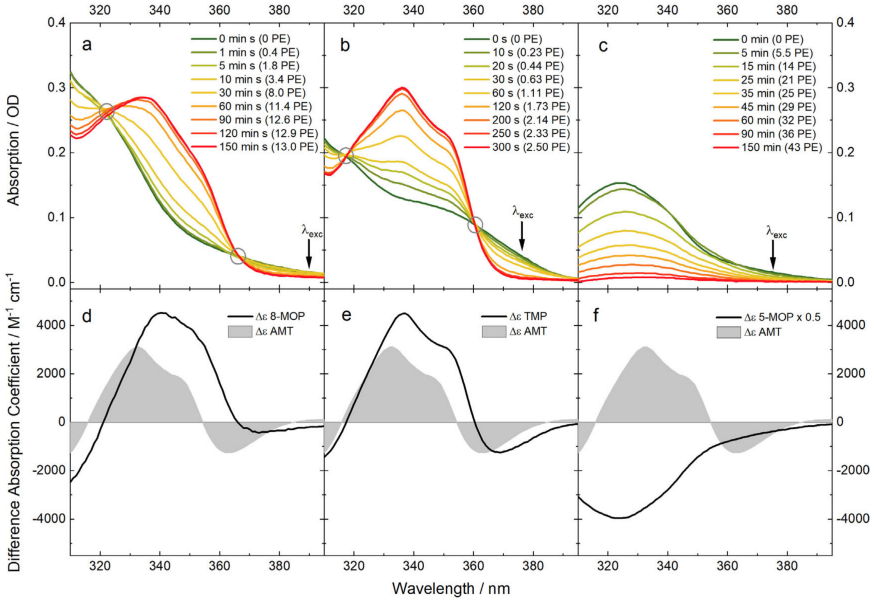

Figure 2. Photoaddition of psoralens to AT-DNA traced by UV/Vis absorption. Irradiation intervals are given in seconds and in photon equivalents (PE). Circles mark isosbestic points. Absorption contributions of the DNA were subtracted: (**a**) Spectra of 8-MOP (33 µM) and AT-DNA (4 mM) in PBS buffer after indicated irradiation times (λ_{exc} = 390 nm, P = 9.5 mW, V = 2.2 mL, d = 1 cm); (**b**) Spectra of TMP (38 µM) and AT-DNA (3.3 mM) in PBS buffer after indicated irradiation times (λ_{exc} = 375 nm, P = 7.5 mW, V = 2.4 mL, d = 1 cm); (**c**) Spectra of 5-MOP (18.4 µM) and AT-DNA (2 mM) in PBS buffer after indicated irradiation times (λ_{exc} = 375 nm, P = 15 mW, V = 2 mL, d = 1 cm); (**d**–**f**) Difference absorption spectra obtained from the data above are compared to the one of AMT with AT-DNA [23].

Similar spectroscopic signatures are observed for the photoaddition of TMP to AT-DNA (see Figure 2b). Upon irradiation with 375 nm light, absorption increases are observed between 317 and 360 nm and decreases beyond these values. In comparison to 8-MOP, the isosbestic points are better defined. This might be related to a lower propensity of TMP to form crosslinks [33,35]. Assuming that after 300 s or a PE of 2.5 the monoadduct formation has come to a halt, a difference spectrum was computed (see Figure 2e). The spectrum is very similar to the one of the AMT furan monoadduct. A reaction quantum yield Φ_R of 0.4 was determined. Therefore, the psoralene derivative TMP is three times more efficient in binding to AT-DNA then AMT with a quantum yield Φ_R of 0.12 [23]. A higher reaction quantum yield for TMP in comparison to AMT is consistent with the previous studies [27,31]. In these studies, the photoaddition to calf thymus DNA was examined, allowing for no direct comparison of the values.

The spectral changes caused by the irradiation of intercalated 5-MOP are very different from the two discussed above (Figure 2c). The absorption spectrum of intercalated 5-MOP is similar to the one of 8-MOP, although slightly red-shifted. Upon irradiation with 375 nm light a decrease of the absorption in the whole spectral range covered is observed. With increasing irradiation time or PE value the spectrum decays to essentially zero. The difference spectrum is therefore nothing else than the inverted absorption spectrum of intercalated 5-MOP. As such it bears no resemblance with the difference spectra of TMP and 8-MOP. The reaction quantum yield Φ_R was determined to 0.017. The spectral changes may be explained by the formation of the pyrone monoadduct. The pyrone monoadduct does not absorb light in the shown UVA region [38]. In comparison to TMP and 8-MOP there are less studies on the photoproducts of 5-MOP. The results shown here are in agreement with the assumption that for 5-MOP the pyrone side monoadduct seems more favorable [38,39].

2.3. IR Absorption Signatures of the Photoaddition

Due to the low water solubility, the signals of intercalated TMP in the IR are very small in relation to the noise. Hence, the focus will be on 8-MOP and 5-MOP here. The IR spectra of 8-MOP and 5-MOP without DNA were recorded in deuterated acetonitrile because of solubility reasons (Figure 3a,b). The spectrum of 8-MOP features one very strong vibration band at 1732 cm^{-1}. It is attributed to the carbonyl stretching vibration [40,41]. One broad band at 1632 cm^{-1} and a more distinct one at 1591 cm^{-1} are attributed to C=C stretching vibrations. The spectrum of 5-MOP features a strong vibration band at 1733 cm^{-1} which can be attributed to the carbonyl stretching vibration [41]. The bands at 1631, 1609, 1581 and 1549 cm^{-1} can be assigned to C=C stretching vibrations. For the reason of IR transparency AT-DNA and 8-MOP were studied using buffer solutions based on D_2O. This causes exchangeable protons of DNA to be replaced by deuterons, that is, NH vibrations are not to be expected. AT-DNA features four distinct bands in the upper-frequency range (Figure 3c). The bands at 1693 cm^{-1} and 1663 cm^{-1} can be assigned to carbonyl stretching vibrations of the thymine base and the one at 1641 cm^{-1} and 1619 cm^{-1} to C=C stretching vibrations of the thymine and adenine base respectively [42]. In a solution of 8-MOP (1.3 mM) and AT-DNA (20 mM) in buffer, roughly 95% of 8-MOP is intercalated. When irradiated with an LED emitting at 375 nm, the absorption changes (Figure 3e). Distinct negative absorption changes can be seen at 1701 cm^{-1}, 1653 cm^{-1}, 1641 cm^{-1} and at 1590 cm^{-1}. Sharp positive absorption changes are located at 1671 cm^{-1}, 1626 cm^{-1} and 1411 cm^{-1}. A broad one is located around 1750 cm^{-1} as well as between 1480–1440 cm^{-1}. For the assignment to certain vibrations of the reagents one has to keep in mind, that the IR spectrum of 8-MOP was recorded in deuterated acetonitrile and that the frequencies and transition strengths of the vibrations also differ between intercalated and free psoralen [23]. Negative absorption changes around 1700 cm^{-1} are probably due to the bleach of carbonyl stretching vibrations of 8-MOP as well as thymine. The absence of strong bands of 8-MOP around 1650 cm^{-1} suggests that bleaches at 1653 cm^{-1} and 1641 cm^{-1} are due to thymine. A more detailed assignment can be achieved with the help of quantum chemical calculations (see below). The positive band at around 1750 cm^{-1} features a slight shift to higher wavenumbers with longer irradiation time (Figure 3E). This temporal behavior suggests that this

feature is due to secondary photochemistry, that is, crosslink formation. The propensity of 8-MOP for crosslinks was already observed by UV/Vis spectroscopy (see above). The difference spectrum for 8-MOP after 20 min of irradiation is very similar to the one obtained for AMT (Figure 3g), except for positive difference absorption bands at 1671 and 1626 cm^{-1} which are not visible for AMT. After 70 min of irradiation, the spectra differ at 1750 cm^{-1} indicating that crosslink formation is more likely for 8-MOP than for AMT.

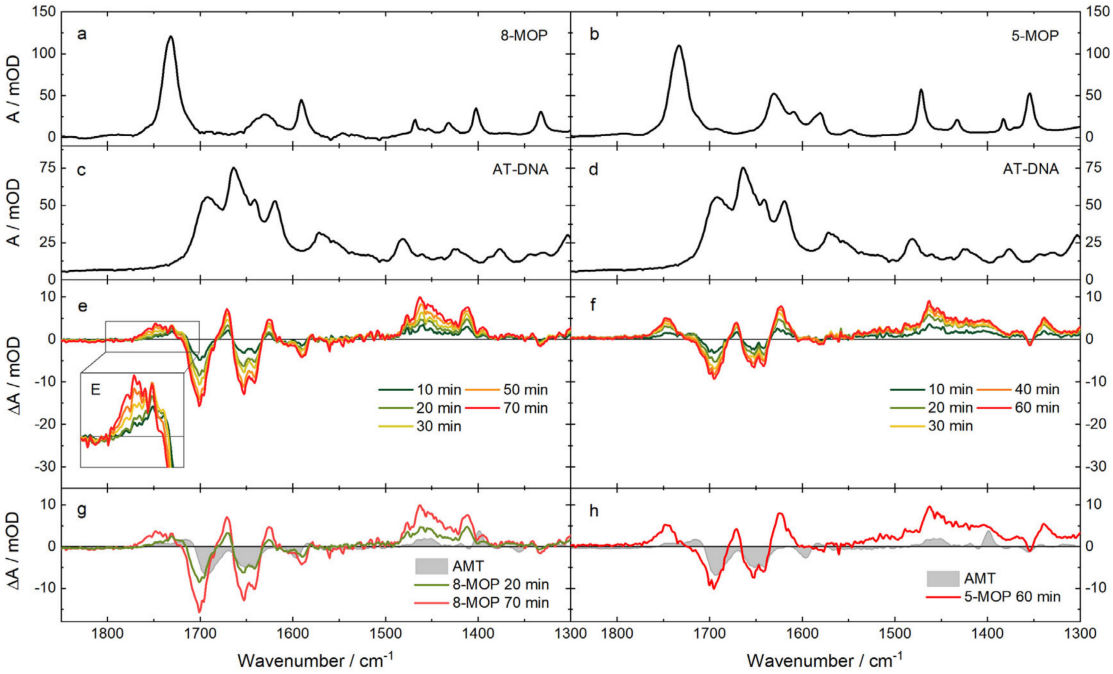

Figure 3. Steady-state IR spectra of the photoaddition of 8-MOP (left) and 5-MOP (right) to AT-DNA: (**a**) 8-MOP (11 mM) in acetonitrile-d3; (**b**) 5-MOP (10 mM) in acetonitrile-d3; (**c**,**d**) AT-DNA (7.7 mM) in PBS buffered D_2O; (**e**) Difference spectra of the irradiation of 8-MOP (1.3 mM) with AT-DNA (20 mM) in PBS buffered D_2O (λ_{exc} = 375 nm, P = 26 mW). (**e**) Magnification of the marked range; (**f**) Difference spectra of the irradiation of 5-MOP (0.7 mM) with AT-DNA (20 mM) in PBS buffered D_2O (λ_{exc} = 375 nm, P = 26 mW); (**g**,**h**) Comparison of difference spectra obtained from the data in (**e**,**f**) with the one of AMT (1.5 mM) with AT-DNA (6.5 mM) (λ_{exc} = 375 nm, P = 15 mW) [23].

In a solution of 5-MOP (0.7 mM) and AT-DNA (20 mM), 99% of 5-MOP is intercalated. At first sight, changes due to irradiation with a 375 nm LED (Figure 3f) are similar to the ones of 8-MOP. A shift in absorption is not visible, which is an indication that no secondary photoreaction took place. The difference spectrum of 5-MOP features similar bleaching bands as the one of AMT (Figure 3h). The positive difference absorption for 5-MOP, which is very similar to the one of 8-MOP after 70 min of irradiation, indicates a different photoreaction, which is presumably the pyrone adduct formation.

2.4. Quantum Chemical Computations of the IR Signatures

Quantum chemical calculations support the interpretation of the experimental infrared spectra. Spectra were computed relying on density functional theory (DFT) using the B3LYP functional and a 6–31 + G* basis set as implemented in Gaussian 09 [43]. The self-consistent reaction field (SCRF) method accounted for the solvent environment implicitly. The DNA environment was not treated explicitly in the computation. Instead, a continuum approach was applied. Hereby, the dielectric constant of pyridine (~13) was chosen to approximate the DNA environment. Water, with a dielectric constant of 78, gave similar results, albeit the carbonyl stretching vibrations being located at slightly lower wavenumbers ($\Delta\tilde{\nu}$~−7 cm^{-1}). Acidic protons were exchanged for deuteron. After

geometry-optimization, the wavenumbers and IR transitions strength were computed. The harmonic frequencies were scaled by a factor of 0.96 [44].

For the calculation of the IR spectra of 8-MOP, Cambridge Structural Database (CSD) entry XANTOX was used as starting geometry [45]. The carbonyl stretching vibration at 1670 cm^{-1} features the highest transitions strength (Figure 4a, green). Three weaker bands are located at 1595, 1588 and 1553 cm^{-1} and can be assigned to C=C stretching vibrations. The computed spectrum shows high similarity to the experimental one in acetonitrile-d3 (compare Figure 3a), though the experimental spectrum is shifted to higher wavenumbers by ~+60 cm^{-1}. No attempts to treat (a part of) the double-stranded DNA by quantum chemistry were made. Instead only the IR spectrum of 1-methylthymine was computed. Three bands at 1661, 1624 and 1608 cm^{-1} can be seen. The ones with higher transition strengths are the carbonyl stretching vibrations, while the one at 1624 cm^{-1} can be assigned to a ring deformation mode [42]. Base pairing and stacking as well as other effects influence the vibrations of thymine as part of DNA [46], explaining the difference in frequency and strength of the vibrations in the experimental spectrum of AT-DNA (compare Figure 3b). For the structure of the monoadduct Protein Data Bank (PDB) entry 203D, which is based on nuclear magnetic resonance (NMR) measurements, was used as starting geometry [47]. Hereby, the DNA part was reduced to the respective 1-methylthymine moiety. The carbonyl vibration of 8-MOP at 1671 cm^{-1} experienced almost no shift. The carbonyl vibrations of thymine at 1667 and 1637 cm^{-1} are shifted by +6 and +29 cm^{-1} respectively. At 1591, 1584 and 1546 cm^{-1} the C=C stretching vibrations of 8-MOP can be seen, although the one at 1591 cm^{-1} has lost in strength as it is almost not visible. A synthetic difference spectrum was obtained by subtracting the computed 8-MOP and 1-methylthymine spectrum from the computed adduct spectrum. If one neglects the fact that the computed pattern is located at lower wavenumbers by ~−40 cm^{-1}, the two patterns match rather well. The bleach at 1702 cm^{-1}, although not as pronounced in the calculation, is due to the shifts in the carbonyl vibration of 8-MOP and one of the carbonyl vibrations of thymine. The positive feature around 1670 cm^{-1} in the experiment can be explained with the shift of the other thymine carbonyl vibration to higher wavenumbers. The bleach contributions at 1653 cm^{-1} and 1641 cm^{-1} seen in the experimental difference spectra are according to the computation due to carbonyl and C=C stretching vibrations of thymine. The fingerprint region is not very well matched, which at this level of calculation is plausible.

In the case of TMP, CSD entry LINTUX served as a starting geometry for calculating IR spectra [48]. The carbonyl stretching vibration is located at 1658 cm^{-1} and features the highest transition strength (Figure 4c, green). Frequencies and transition strengths of C=C vibrations of TMP and TMP as part of the furan monoadduct are very similar to the ones of 8-MOP and its furan monoadduct (compare Figure 3a,c). The synthetic difference spectra are almost identical (compare Figure 3b,d). The experimental difference absorption is, as explained above, due to the low signal to noise ratio not discussed in detail. The region around 1700 cm^{-1} matches rather well, which supports the furan side product formation.

For the calculation of the IR spectra of 5-MOP, CSD entry ARARIW was used as starting geometry [49]. The carbonyl stretching vibration at 1669 cm^{-1} features the highest transition strength (Figure 4e, green). Bands at 1587, 1580, 1543 and 1530 cm^{-1} are attributed to C=C vibrations. All these bands can be found in the experimental spectrum in acetonitrile-d3 as well (compare Figure 3b). The starting geometry for the pyrone monoadduct was extracted from PDB entry 204D [47]. The carbonyl vibration of 5-MOP experiences a major shift (+37 cm^{-1}). The thymine vibrations are shifted by +10 and +33 cm^{-1} respectively. Bands at 1590 and 1570 cm^{-1} are attributed to C=C stretching vibrations of 5-MOP. The synthetic difference spectrum shows high similarity to the experimental one, with exception of the fingerprint region. The positive difference absorption around 1750 cm^{-1} is due to the shift of the 5-MOP carbonyl vibration, which cannot be seen in the calculation of the furan monoadducts. Hence, it can be seen as an indicator of the photoaddition on the pyrone side.

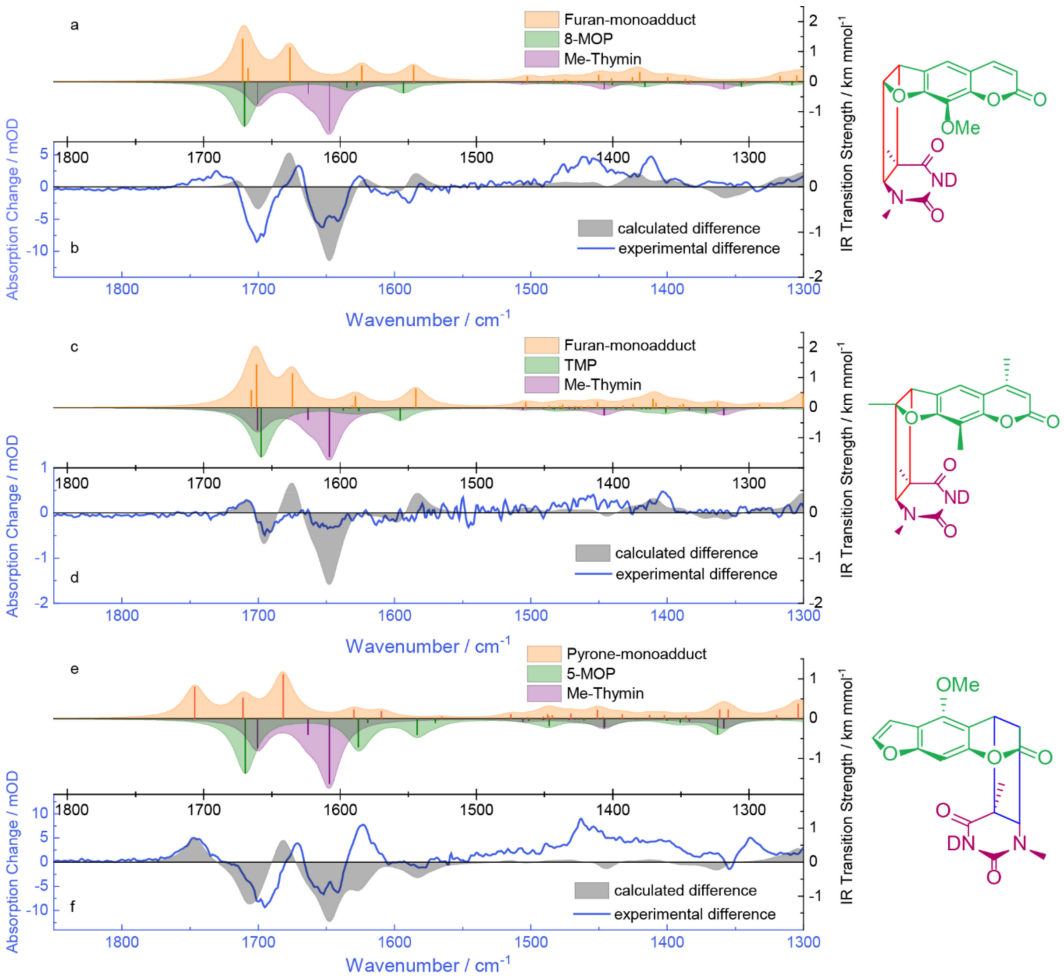

Figure 4. IR signatures of photoaddition computed by quantum chemistry in comparison with the experimental data: (**a**,**c**,**e**) IR spectra of psoralens, 1-methylthymine and their respective photo-products obtained from a DFT calculation with the B3LYP functional and a 6-31 + G* basis set (scaling factor 0.96). Stick spectra were converted into the presented ones by convolution with Lorentzians (full width at half maximum (FWHM) of 20 cm^{-1}). The spectra of the psoralens and 1-methylthymine are inverted to highlight possible bleach contributions; (**b**,**d**,**f**) Comparison of calculated difference and experimental difference absorption. The blue X-axes (experimental difference) is shifted by 40 cm^{-1} to higher wavenumbers relative to the black X-axes (computational differences). Structures of the respective photo-products are depicted on the right.

2.5. Nanosecond Transient UV/Vis Absorption Signatures of the Photoaddition

Solutions of 8-MOP and TMP with AT-DNA were excited with UVA laser pulses and probed in the UV/Vis region. Due to the lack of spectroscopic signatures of the 5-MOP photo-product in the accessible UV/Vis region, only 8-MOP and TMP are treated in the following.

A solution of 8-MOP and AT-DNA in buffered water was excited with nanosecond laser pulses centered at 355 nm (Figure 5). At these concentrations ~70% of 8-MOP is intercalated. For the absorptions employed, the detection wavelengths below 340 nm were not accessible. The spectral pattern around time zero, featuring an absorption band peaking at ~360 nm, is similar to the one reported for the triplet state of non-intercalated 8-MOP [50,51]. So, it is very likely that the time zero signature is due to the triplet state of intercalated and partly due to non-intercalated 8-MOP. For the conditions employed here, the measurement reveals a triplet decay time of 0.6 µs for non-intercalated 8-MOP (see Figure 5, violet). The value is in good agreement with the literature [51], if one takes the intrinsic first-order decay (2.5×10^5 s^{-1}), self-quenching (3.8×10^9 M^{-1} s^{-1}) and quenching by oxygen

(4×10^9 M^{-1} s^{-1}) into account. For non-intercalated 8-MOP the signal at large delay times is essentially zero. For these delay times, the intercalated 8-MOP features a distinct difference absorption signal at wavelengths smaller than 360 nm.

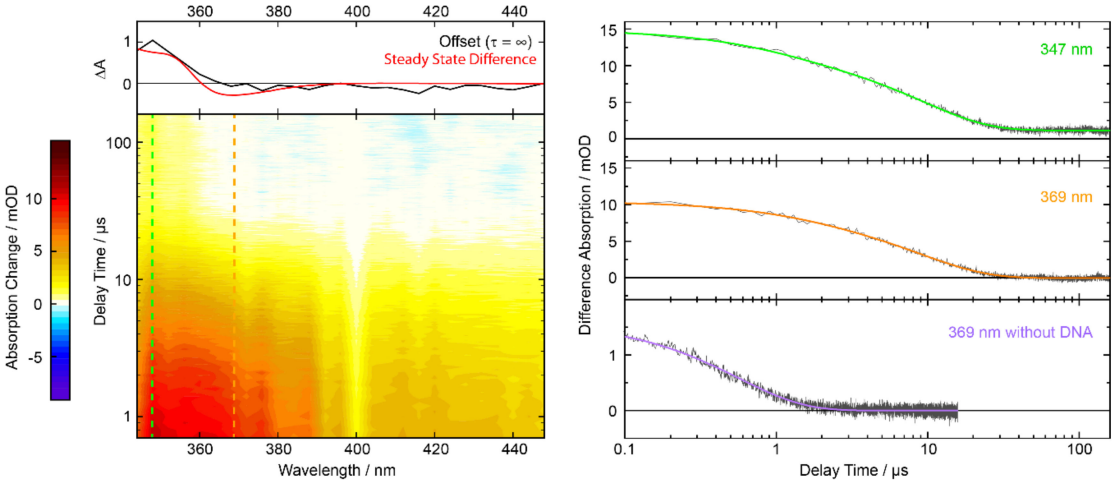

Figure 5. Nanosecond transient absorption of 8-MOP (0.3 mM) with AT-DNA (3 mM) in aerated buffer solution after excitation at 355 nm. Left: The transient absorption in the contour plot is color-coded. The dashed lines mark the respective time trace shown on the right. On top is the offset spectrum in comparison with the steady-state signature (red, scaled to match the offset spectrum) after irradiation at 390 nm. Right: Time traces at 347 and 369 nm. The third time trace shows 8-MOP (0.2 mM) without DNA in water. The colored lines show bi-exponential (green and orange) or single exponential (violet) fits of the data.

The decay pattern of intercalated 8-MOP (see Figure 5, green and orange) is also in stark contrast to the behavior of non-intercalated one (Figure 5, violet). The decay is bi-exponential with time constants of τ_1 = 1 µs and τ_2 = 10 µs (values obtained by global analysis). In the time traces for intercalated 8-MOP, no indications for a tri-exponential decay are observed. One could therefore reason, that the time constant τ_1 of 1 µs is due to residual non-intercalated 8-MOP which features a time constant close to 1 µs. However, in an oxygen-saturated solution (~1 bar) of 8-MOP and AT-DNA (data not shown), the 1 µs time constant persists. Since one expects significant oxygen quenching for non-intercalated 8-MOP [52], the time constant τ_1 of ~1 µs can be attributed to intercalated 8-MOP.

The respective decay associated difference spectra (DADS) of the data above are shown in Figure 6. Both bear resemblance with the 8-MOP triplet spectrum [50,51]. The global analysis also yields an offset spectrum ($\tau_3 = \infty$) which matches the steady-state difference spectrum of the photo-addition (cf. Figure 5, top).

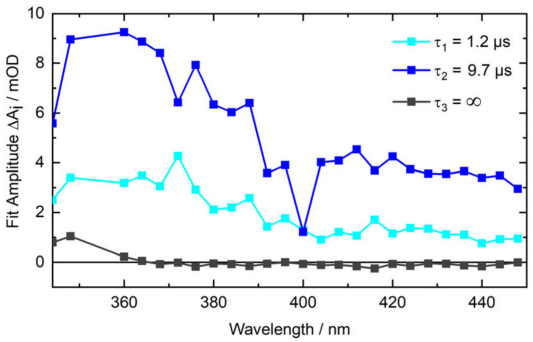

Figure 6. DADS from a multi-exponential global analysis of the nanosecond transient absorption data of 8-MOP with AT-DNA. The time trace at excitation wavelength 355 nm was not included in the fit.

The photoreaction of TMP and AT-DNA was traced by the same approach. A solution of TMP and AT-DNA in buffered water was excited with nanosecond laser pulses centered at 355 nm (Figure 7). Due to the low solubility of TMP, signal levels are smaller than those of 8-MOP. Furthermore, the higher reaction quantum yield Φ_R of TMP compared to 8-MOP implies that the reactants are converted to photo-product after fewer scans. We, therefore, covered only the spectral region centered around 350 nm. In this range, the signature of the photo-product is expected. Around time zero a negative transient absorption for wavelengths smaller than ~320 nm is observed. This is due to ground state bleach. For longer wavelengths, a positive signal is detected. The signature is in line with the triplet signatures of non-intercalated TMP. The respective spectra feature a maximum around 470 nm [17]. Indeed, a single wavelength scan at 470 nm (see Figure 7, orange) reveals a relatively strong time zero signal. For non-intercalated TMP the signal decays to essentially zero within ~1 µs. The decay for intercalated TMP proceeds bi-exponentially with time constants of τ_1~1 µs and τ_2~40 µs. This decay goes along with the built-up of an offset signal between 320–360 nm, which matches the steady-state difference spectrum of the photo-addition. Relative to the time zero signal the offset signal is higher than the one of 8-MOP. This matches the expectation based on the reaction quantum yield Φ_R.

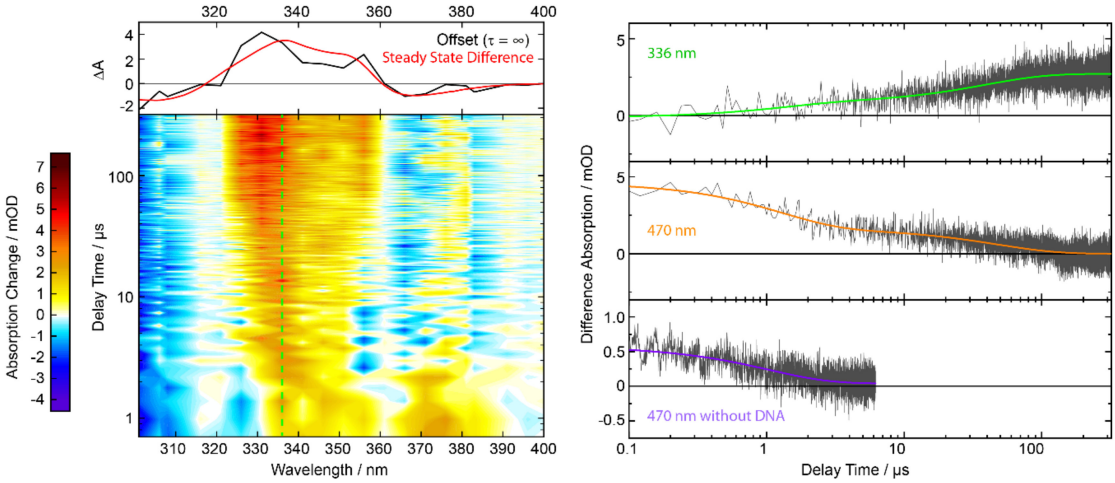

Figure 7. Nanosecond transient absorption of TMP (17 µM) with AT-DNA (1.6 mM) in aerated buffer solution after excitation at 355 nm. Left: The transient absorption in the contour plot is color-coded. The green line marks the respective time trace (336 nm) shown on the right. On top is the offset spectrum in comparison with the steady-state signature (red, scaled to match the offset spectrum) after irradiation at 375 nm. Right: Time traces at 336 and 470 nm. The third time trace shows TMP (6 µM) without DNA in water. The colored lines show bi-exponential (green and orange) or single exponential (violet) fits of the data.

3. Discussion

Our previous results on the furan side photo-addition of AMT to AT-DNA [23] showed that this addition proceeds via the local triplet state of AMT and a triplet biradical. The present study indicates that this mechanism also applies to 8-MOP and TMP.

For 8-MOP intercalated into AT-DNA a bi-exponential decay with time constants of τ_1~1 µs and τ_2~10 µs were observed. We assign the time constant τ_1 to the decay of the 8-MOP triplet state, which presumably goes along with the formation of a triplet biradical in which the psoralen at 5′ position (see Scheme 1) is connected with the thymine moiety at position 6 by a single bond. The time constant τ_2 would then be associated with the decay of the biradical and formation of the final product. Seemingly in conflict with this interpretation is the observation that the spectral signatures do not change much during the τ_1 process (cf. Figure 6). Presumably, this is due to similar spectral signatures of the local triplet state and the triplet biradical. Such similarity was already observed for AMT and

AT-DNA [23]. For this system, the intermediary of a triplet biradical found strong support from time-resolved IR spectroscopy.

For a triplet state as a precursor, the reaction quantum yield Φ_R is given by the triplet quantum yield Φ_T times the reaction efficiency of the triplet state $\eta_R^T \leq 1$, that is, $\Phi_R = \Phi_T \cdot \eta_R^T$. The reaction quantum yield Φ_R for the addition of 8-MOP to AT-DNA was determined to be 0.04. The triplet yield Φ_T of non-intercalated 8-MOP was reported to be 0.06 [51]. If this value also applies to intercalated 8-MOP, the efficiency η_R^T amounts to 0.67. A similar value is derived from a different approach. The efficiency η_R^T can be obtained from

$$\eta_R^T = \frac{c_{PP}}{c_T} = \frac{c^{t=\infty}}{c^{t=0}}, \tag{2}$$

c_{PP} is the concentration of the photo-product in the time-resolved experiment. This concentration is measured at "infinite" times ($c^{t=\infty}$). c_T is the triplet concentration which is measured at time zero ($c^{t=0}$). Concentrations c_{PP} and c_T can be obtained from the respective difference absorption signals ΔA and coefficients $\Delta\varepsilon$,

$$\eta_R^T = \frac{\Delta A^{t=\infty}_{347\ \mathrm{nm}}}{\Delta \varepsilon^{PP}_{347\ \mathrm{nm}}} \cdot \frac{\Delta \varepsilon^{T}_{370\ \mathrm{nm}}}{\Delta A^{t=0}_{370\ \mathrm{nm}}}. \tag{3}$$

For the photo-product the signal $\Delta A^{t=\infty}_{347\ \mathrm{nm}}$ and coefficient $\Delta \varepsilon^{PP}_{347\ \mathrm{nm}}$ at 347 nm, as determined here, were inserted. For the triplet state the signal $\Delta A^{t=0}_{370\ \mathrm{nm}}$, corrected for the intercalated fraction and coefficient $\Delta \varepsilon^{T}_{370\ \mathrm{nm}}$ at 370 nm [51] were used. The coefficient $\Delta \varepsilon^{T}_{370\ \mathrm{nm}}$ refers to 8-MOP in water. With these values an efficiency η_R^T of ~0.6 results. This implies that–compared to AMT–the 8-MOP triplet is somewhat more reactive (η_R^T of AMT: 0.3–0.4 [23]). Due to the smaller triplet yield Φ_T of 8-MOP its overall reaction quantum yield Φ_R is smaller (Φ_R of AMT: 0.12).

Also, for TMP a bi-exponential decay pattern is observed. The time constants of τ_1 = 1 µs and τ_2 = 40 µs are very close to the one reported for AMT intercalated into AT-DNA [23]. Taking the structural similarity of AMT and TMP into account, this is not surprising. It is therefore also likely that like with intercalated AMT the time constant τ_1 describes the decay of the local triplet state accompanied by the biradical formation. The time constant τ_2 is therefore assigned to the biradical decay and the formation of the photo-product. The high reaction quantum yield Φ_R of 0.4 is somewhat surprising. The reported triplet yield Φ_T of non-intercalated TMP is ~0.1 in methanol [17]. This would imply an unphysical efficiency $\eta_R^T > 1$. Our present interpretation of this is that the triplet yield Φ_T of intercalated TMP is substantially larger than the one for non-intercalated TMP. Indications for that were already observed for AMT [23].

The behavior of 5-MOP is qualitatively different for the one of AMT, 8-MOP and TMP. In line with earlier studies, our UV/Vis and IR measurements indicate that the photo-addition proceeds via the pyrone side of the psoralen and not the furan side. Unfortunately, due to the lack of a spectroscopic signature of this adduct in the accessible UV/Vis range, the formation could not be traced in real-time. Time-resolved IR experiments ought to be conducted to clarify this in the future.

4. Materials and Methods

4.1. Samples

8-MOP and 5-MOP were purchased from TCI (Tokyo, Japan, >98%) and TMP from Sigma-Aldrich (Steinheim, Germany, ≥98%). The lyophilized oligonucleotide 5′-$(TA)_{20}$-3′ was purchased from Sigma-Aldrich. The manufacturer purified the sample by HPLC. Annealing of the oligonucleotide strands in solution was performed within 24 h before the measurements by heating the solution in a water bath up to 93 °C and letting it cool down to room temperature within several hours. Solvents used were pure water (Fisher Chemical, Loughborough, UK, HPLC gradient grade), deuterium oxide (Deutero GmbH, Kastellaun, Germany, 99.9% D) and acetonitrile-d3 (Sigma-Aldrich, ≥99.8% D).

Solutions of the oligonucleotides were buffered with PBS (Sigma Aldrich, one tablet dissolved in 200 mL yielded 10 mM phosphate buffer, 2.7 mM potassium chloride, 137 mM sodium chloride, pH 7.4 at 25 °C).

4.2. Steady-State Spectroscopy

Absorption spectra in the UV/Vis were recorded with a Lambda 19 spectrometer from Perkin Elmer. Fused silica cuvettes with path lengths of 0.1, 1 and 5 cm from Hellma were employed. Absorption spectra in the IR were recorded with an FT-IR-spectrometer Vertex 80v from Bruker Optik. A custom-made cuvette with a Teflon spacer for a path length of 0.1 mm was used. CaF_2 windows of 3 mm thickness from Korth Kristalle were employed. The spectra were corrected for the absorption of aqueous vapor and HDO, if necessary. All measurements were performed at room temperature.

For the irradiation in the steady-state experiments, LEDs emitting at 375 nm or 390 nm were used. For the determination of the quantum yield in the UV/Vis experiments the solutions were stirred while irradiating. With the light power P and the irradiation time t photon equivalents PE were computed via the equation:

$$PE(t) = \frac{n_{abs}(t)}{n_{Pso}} = \frac{I_0 \cdot \int_0^t \left(1 - 10^{-A_{Ex}(t)}\right) dt}{n_{Pso}} = \frac{P \cdot \int_0^t \left(1 - 10^{-A_{Ex}(t)}\right) dt}{h \cdot \frac{c}{\lambda_{Ex}} \cdot N_A \cdot n_{Pso}}. \quad (4)$$

Here, n_{abs} is the amount of the absorbed photons and n_{Pso} the amount of psoralen molecules. A_{Ex} refers to the absorption at excitation wavelength λ_{Ex}. h is defined as the Planck's constant, c as the speed of light and N_A as Avogadro's number. A PE of one implies that on average each psoralen molecule has absorbed one photon.

4.3. Nanosecond Transient Absorption in the UV/Vis

The nanosecond transient absorption data were acquired with a laser flash photolysis spectrometer LP980 from Edinburgh Instruments in a right-angle geometry. The frequency tripled output (355 nm) of a Nd:YAG laser (Spitlight 600, InnoLas, Germany) with a repetition rate of 5 Hz and a pulse duration of 12 ns (FWHM) was utilized for photoexcitation. The excitation energy ranged from 4–17 mJ per pulse. The diameter of the pump beam was ~8 mm. A pulsed xenon lamp (Osram XBO 150 W/CR OFR) generated the probe light. Fused silica flow-through cuvettes from Hellma with different path lengths in pump and probe direction were employed. To gain the best signal to noise ratio while keeping the turnover rate low, cuvettes with different dimensions (1.5 × 3 mm, 2 × 10 mm or 5 × 10 mm) were used, depending on the sample. The transmitted probe light was dispersed by a grating monochromator and detected by a photomultiplier (Hamamatsu, Japan, R928). The signal was digitized by an oscilloscope (MDO 3022, Tektronix, Beaverton, OR, USA) and the absorption change was calculated based on measurements with and without laser excitation. For every time trace three sets of 8 consecutive measurements were averaged. If indicated, solutions were purged with oxygen or nitrogen (99.999%, Air Liquide, Düsseldorf, Germany). The measurements were performed at 17 °C.

4.4. Data Analysis

The time-resolved data were analyzed with a global multi-exponential fit function

$$\Delta A(\lambda, t) = IRF \otimes \sum_{i=1}^{n} \Delta A_i(\lambda) \cdot e^{-\frac{t}{\tau_i}}, \quad (5)$$

which is convoluted with an instrumental response function (IRF). The IRF was approximated by a Gaussian with an FWHM of 0.1 µs. The fit yields time constants τ_i and decay associated difference spectra (DADS) $\Delta A_i(\lambda)$ [53].

5. Conclusions

The photoaddition of three pharmaceutical psoralens (5-MOP, 8-MOP and TMP) to AT-DNA was studied by steady-state and time-resolved spectroscopy. IR spectroscopy proved to be useful in distinguishing pyrone side (5-MOP) and furan side (8-MOP and TMP) photoadditions. The furan side additions were shown to proceed via a local triplet state and a triplet biradical. The present results, thus, underscore the importance of triplet states for the photo-reactivity. Once this state is populated, the investigated psoralens add to thymine with high efficiency. So, when optimizing psoralens for the PUVA therapy, a small dissociation constant K_D [54], a low propensity for PET quenching by guanine [25] and a high triplet yield should be aimed at. Optimizations along these lines are presently undertaken by us.

Author Contributions: Conceptualization, J.D. and P.G.; methodology, J.D. and P.G.; formal analysis, J.D.; investigation, J.D., I.T. and K.A.T.; data curation, J.D.; writing—original draft preparation, J.D. and P.G.; writing—review and editing, J.D. and P.G.; visualization, J.D.; supervision, P.G.; project administration, P.G.; funding acquisition, J.D. and P.G. All authors have read and agreed to the published version of the manuscript.

Funding: This research was funded by the Deutsche Forschungsgemeinschaft, grant number GI 349/6-1 and the Jürgen Manchot Stiftung (scholarship for J.D.).

Acknowledgments: Computational infrastructure and support were provided by the Centre for Information and Media Technology at Heinrich Heine University Düsseldorf. The authors thank Klaus Kelbert for technical support.

Conflicts of Interest: The authors declare no conflict of interest. The funders had no role in the design of the study; in the collection, analyses, or interpretation of data; in the writing of the manuscript, or in the decision to publish the results.

References

1. Pathirana, D.; Ormerod, A.; Saiag, P.; Smith, C.; Spuls, P.; Nast, A.; Barker, J.; Bos, J.; Burmester, G.-R.; Chimenti, S.; et al. European S3-Guidelines on the systemic treatment of psoriasis vulgaris. *J. Eur. Acad. Dermatol. Venereol.* **2009**, *23*, 1–70. [CrossRef] [PubMed]
2. Menter, A.; Korman, N.J.; Elmets, C.A.; Feldman, S.R.; Gelfand, J.M.; Gordon, K.B.; Gottlieb, A.; Koo, J.Y.M.; Lebwohl, M.; Lim, H.W.; et al. Guidelines of care for the management of psoriasis and psoriatic arthritis. *J. Am. Acad. Dermatol.* **2010**, *62*, 114–135. [CrossRef] [PubMed]
3. Sidbury, R.; Davis, D.M.; Cohen, D.E.; Cordoro, K.M.; Berger, T.G.; Bergman, J.N.; Chamlin, S.L.; Cooper, K.D.; Feldman, S.R.; Hanifin, J.M.; et al. Guidelines of care for the management of atopic dermatitis. *J. Am. Acad. Dermatol.* **2014**, *71*, 327–349. [CrossRef] [PubMed]
4. Taieb, A.; Alomar, A.; Böhm, M.; Dell'Anna, M.L.; De Pase, A.; Eleftheriadou, V.; Ezzedine, K.; Gauthier, Y.; Gawkrodger, D.J.; Jouary, T.; et al. Guidelines for the management of vitiligo: The European Dermatology Forum consensus. *Br. J. Dermatol.* **2013**, *168*, 5–19. [CrossRef] [PubMed]
5. Oiso, N.; Suzuki, T.; Wataya-kaneda, M.; Tanemura, A.; Tanioka, M.; Fujimoto, T.; Fukai, K.; Kawakami, T.; Tsukamoto, K.; Yamaguchi, Y.; et al. Guidelines for the diagnosis and treatment of vitiligo in Japan. *J. Dermatol.* **2013**, *40*, 344–354. [CrossRef] [PubMed]
6. Olsen, E.A.; Hodak, E.; Anderson, T.; Carter, J.B.; Henderson, M.; Cooper, K.; Lim, H.W. Guidelines for phototherapy of mycosis fungoides and Sézary syndrome: A consensus statement of the United States Cutaneous Lymphoma Consortium. *J. Am. Acad. Dermatol.* **2016**, *74*, 27–58. [CrossRef]
7. Knobler, R.; Berlin, G.; Calzavara-Pinton, P.; Greinix, H.; Jaksch, P.; Laroche, L.; Ludvigsson, J.; Quaglino, P.; Reinisch, W.; Scarisbrick, J.; et al. Guidelines on the use of extracorporeal photopheresis. *J. Eur. Acad. Dermatol. Venereol.* **2014**, *28*, 1–37. [CrossRef]
8. Ling, T.C.; Clayton, T.H.; Crawley, J.; Exton, L.S.; Goulden, V.; Ibbotson, S.; McKenna, K.; Mohd Mustapa, M.F.; Rhodes, L.E.; Sarkany, R.; et al. British Association of Dermatologists and British Photodermatology Group guidelines for the safe and effective use of psoralen-ultraviolet A therapy 2015. *Br. J. Dermatol.* **2016**, *174*, 24–55. [CrossRef]
9. Sasaki, M.; Meguro, F.; Kumazawa, E.; Fujita, H.; Kakishima, H.; Sakata, T. Evidence for uptake of 8-methoxypsoralen and 5-methoxypsoralen by cellular nuclei. *Mutat. Res. Mol. Mech. Mutagen.* **1988**, *197*, 51–58. [CrossRef]

10. Schmitt, I.M.; Chimenti, S.; Gasparro, F.P. Psoralen-protein photochemistry—A forgotten field. *J. Photochem. Photobiol. B Biol.* **1995**, *27*, 101–107. [CrossRef]
11. Hearst, J.E.; Isaacs, S.T.; Kanne, D.; Rapoport, H.; Straub, K. The reaction of the psoralens with deoxyribonucleic acid. *Q. Rev. Biophys.* **1984**, *17*, 1. [CrossRef] [PubMed]
12. Cimino, G.D.; Gamper, H.B.; Isaacs, S.T.; Hearst, J.E. Psoralens as photoactive probes of nucleic acid structure and function. *Annu. Rev. Biochem.* **1985**, *54*, 1151–1193. [CrossRef] [PubMed]
13. Kitamura, N.; Kohtani, S.; Nakagaki, R. Molecular aspects of furocoumarin reactions: Photophysics, photochemistry, photobiology, and structural analysis. *J. Photochem. Photobiol. C Photochem. Rev.* **2005**, *6*, 168–185. [CrossRef]
14. Kanne, D.; Rapoport, H.; Hearst, J.E. 8-Methoxypsoralen-nucleic acid photoreaction. Effect of methyl substitution on pyrone vs. furan photoaddition. *J. Med. Chem.* **1984**, *27*, 531–534. [CrossRef] [PubMed]
15. Vowels, B.R.; Yoo, E.K.; Gasparro, F.P. Kinetic Analysis of Apoptosis Induction in Human Cell Lines by UVA and 8-MOP. *Photochem. Photobiol.* **1996**, *63*, 572–576. [CrossRef] [PubMed]
16. Bensasson, R.V.; Land, E.J.; Salet, C. Triplet excited state of furocoumarins: Reaction with nucleic acid bases and amino acids. *Photochem. Photobiol.* **1978**, *27*, 273–280. [CrossRef]
17. Beaumont, P.C.; Parsons, B.J.; Phillips, G.O.; Allen, J.C. A laser flash photolysis study of the reactivities of the triplet states of 8-methoxypsoralen and 4,5′,8-trimethylpsoralen with nucleic acid bases in solution. *Biochim. Biophys. Acta Nucleic Acids Protein Synth.* **1979**, *562*, 214–221. [CrossRef]
18. Beaumont, P.C.; Parsons, B.J.; Navaratnam, S.; Phillips, G.O.; Allen, J.C. The reactivities of furocoumarin exicted states with DNA in solution. A laser flash photolysis and fluorescence study. *Biochim. Biophys. Acta* **1980**, *608*, 259–265. [CrossRef]
19. Serrano-Pérez, J.J.; González-Luque, R.; Merchán, M.; Serrano-Andrés, L. The family of furocoumarins: Looking for the best photosensitizer for phototherapy. *J. Photochem. Photobiol. A Chem.* **2008**, *199*, 34–41. [CrossRef]
20. Serrano-Pérez, J.J.; Merchán, M.; Serrano-Andrés, L. Photoreactivity of Furocoumarins and DNA in PUVA Therapy: Formation of Psoralen−Thymine Adducts. *J. Phys. Chem. B* **2008**, *112*, 14002–14010. [CrossRef]
21. Omar, S.; Eriksson, L.A. Interaction and photobinding between 8-methoxypsoralen and thymine. *Chem. Phys. Lett.* **2009**, *471*, 128–132. [CrossRef]
22. Huang, X.; Zhang, R. A Theoretical Rationale why Furan-side Monoadduct is More Favorable Toward Diadduct Formation in 8-Methoxypsoralen and Thymine Complexes. *Photochem. Photobiol.* **2013**, *89*, 891–899. [CrossRef] [PubMed]
23. Diekmann, J.; Gontcharov, J.; Fröbel, S.; Torres Ziegenbein, C.; Zinth, W.; Gilch, P. The Photoaddition of a Psoralen to DNA Proceeds via the Triplet State. *J. Am. Chem. Soc.* **2019**, *141*, 13643–13653. [CrossRef] [PubMed]
24. Isaacs, S.T.; Shen, C.-K.J.; Hearst, J.E.; Rapoport, H. Synthesis and characterization of new psoralen derivatives with superior photoreactivity with DNA and RNA. *Biochemistry* **1977**, *16*, 1058–1064. [CrossRef] [PubMed]
25. Fröbel, S.; Levi, L.; Ulamec, S.M.; Gilch, P. Photoinduced Electron Transfer between Psoralens and DNA: Influence of DNA Sequence and Substitution. *ChemPhysChem* **2016**, *17*, 1377–1386. [CrossRef]
26. Fröbel, S.; Reiffers, A.; Torres Ziegenbein, C.; Gilch, P. DNA Intercalated Psoralen Undergoes Efficient Photoinduced Electron Transfer. *J. Phys. Chem. Lett.* **2015**, *6*, 1260–1264. [CrossRef] [PubMed]
27. Isaacs, S.T.; Chun, C.; Hyde, J.E.; Rapoport, H.; Hearst, J.E. A Photochemical Characterization of Reactions of Psoralen Derivatives with DNA. In *Trends in Photobiology*; Springer US: Boston, MA, USA, 1982; pp. 279–294.
28. Musajo, L.; Rodighiero, G.; Colombo, G.; Torlone, V.; Dall'Acqua, F. Photosensitizing furocoumarins: Interaction with DNA and photo-inactivation of DNA containing viruses. *Experientia* **1965**, *21*, 22–24. [CrossRef]
29. El-Gogary, T.M.; El-Gendy, E.M. Noncovalent attachment of psoralen derivatives with DNA: Hartree–Fock and density functional studies on the probes. *Spectrochim. Acta Part A Mol. Biomol. Spectrosc.* **2003**, *59*, 2635–2644. [CrossRef]
30. Dougherty, G.; Pigram, W.J. Spectroscopic Analysis of Drug-Nucleic Acid Interaction. *Crit. Rev. Biochem.* **1982**, *12*, 103–132. [CrossRef]
31. Hyde, J.E.; Hearst, J.E. Binding of psoralen derivatives to DNA and chromatin: Influence of the ionic environment on dark binding and photoreactivity. *Biochemistry* **1978**, *17*, 1251–1257. [CrossRef]

32. Isaacs, S.T.; Wiesehahn, G.; Hallick, L.M. In vitro characterization of the reaction of four psoralen derivatives with DNA. *Natl. Cancer Inst. Monogr.* **1984**, *66*, 21–30. [PubMed]
33. Kanne, D.; Straub, K.; Rapoport, H.; Hearst, J.E. Psoralen-Deoxyribonucleic Acid Photoreaction. Characterization of the Monoaddition Products from 8-Methoxypsoralen and 4,5′,8-Trimethylpsoralen. *Biochemistry* **1982**, *21*, 861–871. [CrossRef] [PubMed]
34. Straub, K.; Kanne, D.; Hearst, J.E.; Rapoport, H. Isolation and Characterization of Pyrimidine-Psoralen Photoadducts from DNA. *J. Am. Chem. Soc.* **1981**, *103*, 2347–2355. [CrossRef]
35. Oroskar, A.; Olack, G.; Peak, M.J.; Gasparro, F.P. 4′-Aminomethyl-4,5′,8-trimethylpsoralen photochemistry: The effect of concentration and UVA fluence on photoadduct formation in poly(dA-dT) and calf thymus DNA. *Photochem. Photobiol.* **1994**, *60*, 567–573. [CrossRef]
36. Tessman, J.W.; Isaacs, S.T.; Hearst, J.E. Photochemistry of the Furan-Side 8-Methoxypsoralen-Thymidine Monoadduct Inside the DNA Helix. Conversion to Diadduct and to Pyrone-Side Monoadduct. *Biochemistry* **1985**, *24*, 1669–1676. [CrossRef]
37. Rodighiero, G.; Musajo, L.; Dall'acqua, F.; Marciani, S.; Caporale, G.; Ciavatta, L. Mechanism of skin photosensitization by forucoumarins. *Biochim. Biophys. Acta Nucleic Acids Protein Synth.* **1970**, *217*, 40–49. [CrossRef]
38. Anselmino, C.; Voituriez, L.; Cadet, J. Characterization of the cis-syn and cis-anti Diastereoisomers of 5-Methoxypsoralen Pyrone-Side Monocycloadducts to Thymidine. *Chem. Res. Toxicol.* **1993**, *6*, 858–865. [CrossRef]
39. Demaret, J.-P.; Brunie, S.; Ballini, J.-P.; Vigny, P. Geometry of Intercalation of Psoralens in DNA Approached by Molecular Mechanics. *Photochem. Photobiol.* **1989**, *50*, 7–21. [CrossRef]
40. Finkelstein, N.; Albrecht, C.F.; van Jaarsveld, P.P. Isolation and structure elucidation of xanthotoxin, a phototoxic furanocoumarin, from Peucedanum galbanum. *South African J. Bot.* **1993**, *59*, 81–84. [CrossRef]
41. Masuda, T.; Takasugi, M.; Anetai, M. Psoralen and other linear furanocoumarins as phytoalexins in Glehnia littoralis. *Phytochemistry* **1998**, *47*, 13–16. [CrossRef]
42. Lee, C.; Cho, M. Vibrational dynamics of DNA. II. Deuterium exchange effects and simulated IR absorption spectra. *J. Chem. Phys.* **2006**, *125*, 114509. [CrossRef] [PubMed]
43. Frisch, M.J.; Trucks, G.W.; Schlegel, H.B.; Scuseria, G.E.; Robb, M.A.; Cheeseman, J.R.; Scalmani, G.; Barone, V.; Petersson, G.A.; Nakatsuji, H.; et al. *Gaussian 09, Revision A.02*; Gaussian, Inc.: Wallingford, CT, USA, 2016.
44. Koch, W.; Holthausen, M.C. *A Chemist's Guide to Density Functional Theory*; Wiley-VCH Verlag GmbH: Weinheim, Germany, 2001; Volume 3, ISBN 3527303723.
45. Stemple, N.R.; Watson, W.H. The crystal and molecular structure of xanthotoxin, $C_{12}H_8O_4$. *Acta Crystallogr. Sect. B Struct. Crystallogr. Cryst. Chem.* **1972**, *28*, 2485–2489. [CrossRef]
46. Lee, C.; Park, K.H.; Cho, M. Vibrational dynamics of DNA. I. Vibrational basis modes and couplings. *J. Chem. Phys.* **2006**, *125*, 114508. [CrossRef] [PubMed]
47. Spielmann, H.P.; Dwyer, T.J.; Hearst, J.E.; Wemmer, D.E. Solution Structures of Psoralen Monoadducted and Cross-Linked DNA Oligomers by NMR Spectroscopy and Restrained Molecular Dynamics. *Biochemistry* **1995**, *34*, 12937–12953. [CrossRef] [PubMed]
48. Fujii, I.; Aoyama, N.; Miike, A.; Hirayama, N. Crystal Structure of a Potent Pigmentation Agent Trioxsalen. *Anal. Sci.* **1998**, *14*, 871–872. [CrossRef]
49. Bauri, A.K.; Foro, S.; Nhu Do, Q.N. Crystal structure of bergapten: A photomutagenic and photobiologically active furanocoumarin. *Acta Crystallogr. Sect. E Crystallogr. Commun.* **2016**, *72*, 1194–1196. [CrossRef]
50. Sloper, R.W.; Truscott, T.G.; Land, E.J. The Triplet State of 8-Methoxypsoralen. *Photochem. Photobiol.* **1979**, *29*, 1025–1029. [CrossRef]
51. Craw, M.; Bensasson, R.V.; Ronfard-Haret, J.C.; Melo, M.T.S.; Truscott, T.G. Some Photophysical Properties of 3-Carbethoxypsoralen, 8-Methoxypsoralen and 5-Methoxypsoralen Triplet States. *Photochem. Photobiol.* **1983**, *37*, 611–615. [CrossRef]
52. Berkoff, B.; Hogan, M.; Legrange, J.; Austin, R. Dependence of oxygen quenching of intercalated methylene blue triplet lifetime on DNA base-pair composition. *Biopolymers* **1986**, *25*, 307–316. [CrossRef]

53. Satzger, H.; Zinth, W. Visualization of transient absorption dynamics—Towards a qualitative view of complex reaction kinetics. *Chem. Phys.* **2003**, *295*, 287–295. [CrossRef]
54. Buhimschi, A.D.; Gooden, D.M.; Jing, H.; Fels, D.R.; Hansen, K.S.; Beyer, W.F.; Dewhirst, M.W.; Walder, H.; Gasparro, F.P. Psoralen Derivatives with Enhanced Potency. *Photochem. Photobiol.* **2020**, 1014–1031. [CrossRef] [PubMed]

Sample Availability: Samples of all compounds are not available from the authors.

Publisher's Note: MDPI stays neutral with regard to jurisdictional claims in published maps and institutional affiliations.

2.3. Photophysikalische Eigenschaften von Psoralenen mit rotverschobener Absorption (Veröffentlichung III)

Title: Synthesis and Photophysics of Water-Soluble Psoralens with Red-Shifted Absorption

Authors: Janina Bertling, Kristoffer A. Thom, Sarah Geenen, Hannah Jeuken, Lysander Presser, Thomas J. J. Müller, Peter Gilch

Published in: Photochemistry and Photobiology

Year: 2021

Impact Factor: 2.721 (2019)

Eigene Anteile an der Veröffentlichung:

- stationäre Messungen zu $TMAPM^+$ und $TMAPEM^+$
- Auswertung der stationären Messungen
- Planung und Auswertung der zeitaufgelösten UV/Vis Messungen
- Erstellung der Abbildungen
- Literaturrecherche und Verfassen eines großen Anteils des Manuskripts

Photochemistry and Photobiology, 2021, 97: 1534–1547

Research Article

Synthesis and Photophysics of Water-Soluble Psoralens with Red-Shifted Absorption

Janina Bertling[1,‡], Kristoffer A. Thom[1], Sarah Geenen[2], Hannah Jeuken[1], Lysander Presser[2], Thomas J. J. Müller[2]* and Peter Gilch[1]*

[1]Institut für Physikalische Chemie, Heinrich-Heine-Universität Düsseldorf, Düsseldorf, Germany
[2]Institut für Organische Chemie und Makromolekulare Chemie, Heinrich-Heine-Universität Düsseldorf, Düsseldorf, Germany

Received 15 April 2021, accepted 24 June 2021, DOI: 10.1111/php.13480

ABSTRACT

8-Methoxypsoralen (8-MOP) serves as a PUVA (psoralen + UV-A) agent in the treatment of certain skin diseases. Derivatives of 8-MOP with cationic aromatic substituents at the five positions were synthesized and characterized by steady-state, femtosecond and nanosecond spectroscopy as well as cyclic voltammetry. The aromatic substituents' positive charge increases the water solubility and the affinity toward intercalation into DNA. The aromatic substituents were supposed to lower the psoralen S_1 energy and thereby suppress a photo-induced electron transfer (PET) with guanine-bearing DNA. Such a suppression of this PET is expected to increase the propensity of psoralens to photo-addition to DNA. For derivatives bearing methylpyridinium residues, femtosecond spectroscopy revealed an intramolecular PET occurring on the picosecond time scale. This PET precludes the population of the triplet state. As triplet states are the precursor state for the photo-addition to DNA, their intermolecular PET renders these derivatives ineffective in terms of PUVA. For two derivatives bearing trimethylphenylammonium moieties, such an intramolecular PET does not occur and the triplet state is populated. Surprisingly, these compounds also exhibit no PUVA activity. Based on these findings, implications for further optimization of PUVA agents are discussed.

INTRODUCTION

Psoralens are heteroaromatic compounds, which are commonly used in photosensitizing treatments (1,2). As active agent in the PUVA therapy (**P**soralen + **UV-A**), they are used to treat skin diseases such as psoriasis, atopic eczema and cutaneous T-cell lymphoma (3). Psoralens are decent DNA intercalators (4). Upon photoexcitation, intercalated psoralens can bind to the adjacent thymine base of the DNA, forming a cyclobutane ring. This involves the 4′ and 5′ (furan side) or the 3 and 4 positions (pyrone side) of the psoralen and the 5 and 6 double bond of thymine (see Fig. 1a). This alteration in the DNA can trigger apoptosis of the whole cell leading to relief of symptoms of the mentioned diseases when applied to affected skin cells (5).

A commonly applied and well-researched psoralen derivative is 8-methoxypsoralen (8-MOP) (6–9). It is a naturally occurring derivative with overall superior characteristics compared to other natural derivatives tested in clinical studies to this day (3). In this study, we want to introduce new psoralen derivatives and discuss criteria to synthesize more effective psoralens. The actual quality of a drug, where relief of symptoms and side effects are weighted, can only be measured in clinical studies. This study will focus on criteria, we think, will ultimately lead to a high effectiveness of a psoralen binding to the DNA.

A first criterion is the water solubility of the psoralen. 8-MOP has a solubility of only 0.2 mM (10). Another derivative well represented in research is 4′-aminomethyl-4,5′, 8-trimethylpsoralen (AMT) with a solubility around 30 mM, showcasing the advantage of ions (11). Another important characteristic is the affinity to intercalate into DNA. Suitably placed cationic residues can promote the intercalation as the residues can interact with the negatively charged sugar-phosphate backbone of DNA. Bulky substituents may impair the intercalation (10). In addition to these ground state properties, also photophysical and photochemical ones need to be considered. For several psoralens, it was shown by nanosecond UV/Vis and IR absorption spectroscopy that the furan side addition to DNA proceeds via their triplet state (12,13). An efficient PUVA agent should, thus, feature a high triplet quantum yield Φ_T. Femtosecond UV/Vis absorption spectroscopy revealed a photo-induced electron transfer (PET) involving the intercalated psoralens (14,15). The base guanine (G) was identified as the electron donor and the psoralen derivative in its S_1 state as the acceptor. For G in close proximity to the intercalated psoralen—either directly adjacent or a few base pairs apart—the PET occurs within picoseconds. The PET suppresses the triplet formation and, thus, strongly reduces the photoreactivity. In line with that, for AT-only DNA, the quantum yields Φ_R for the cycloaddition are higher than for DNA-bearing AT and GC base pairs (15). In a pharmaceutical context, DNA containing only AT base pairs of course does not occur.

*Corresponding authors' email: gilch@hhu.de (Peter Gilch), ThomasJJ.Mueller@hhu.de (Thomas J.J. Müller)
Dedicated to Heinrich G. Gilch on the occasion of his 90th birthday.
‡née Diekmann

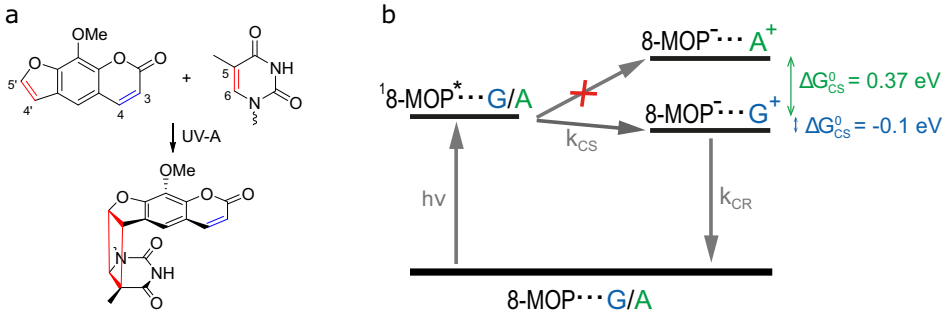

Figure 1. Photoaddition of the psoralen derivative 8-MOP to DNA (a) and photo-induced electron transfer involving 8-MOP (b). a: After excitation, the psoralen derivative 8-MOP can bind to the thymine base of DNA via the furan (red) or the pyrone side (blue, photoproduct not shown). b: Energetic scheme of the photo-induced electron transfer from guanine (G) to 8-MOP. Absorption of an UV-A-photon populates the S_1 state of intercalated 8-MOP (^{1}8-MOP*). Guanine, in close proximity, quenches the S_1 state by transfer of an electron with a rate constant k_{CS} for the charge separation. Charge recombination with the rate constant k_{CR} leads to recovery of the psoralen ground state. With adenine (A) as a donor, the PET is endergonic. ΔG^0_{CS} values were taken from ref. (15).

PET can be suppressed by changing the thermodynamics of the process (cf. Fig. 1b). A suppression may be achieved if the change of Gibbs free energy for charge separation (CS) resulting from the PET is positive, $\Delta G^0_{CS} \gtrsim 0$. It can be determined via the Weller equation (eq. 1) (16).

$$\Delta G^0_{CS} = e_0\left(E^0(D^{+\cdot}/D) - E^0(A/A^{-\cdot})\right) - E_{00} + W \qquad (1)$$

The equation includes the standard electrode potentials of the donor cation radical $E^0(D^{+\cdot}/D)$ (guanine) and the acceptor $E^0(A/A^{-\cdot})$ (psoralen derivative) as well as the 0-0 energy E_{00} of the psoralen S_1 state. e_0 is the elementary charge. The work term W accounts for the stabilization of the CS state by electrostatic attraction. Details concerning the work term for the DNA-psoralen PET can be found in ref. (15). For 8-MOP as an acceptor, the ΔG^0_{CS} value amounts to +0.37 eV for the electron transfer from the purine base adenine and –0.10 eV for the transfer from guanine. These values explain why PET can be observed with guanine but not with adenine. In the case of 8-MOP, the ΔG^0_{CS} value would have to increase by at least 0.1 eV to change the reaction from exergonic to endergonic. Yet, also for a slightly positive ΔG^0_{CS} value, a PET might play a role, provided that the rate constant for charge recombination k_{CR} is high. According to eq. (1), the PET can be suppressed by lowering the psoralen S_1 energy E_{00} and/or shifting the potential $E^0(A/A^{-\cdot})$ toward more negative values. Lowering the excitation energy E_{00} has the additional advantage that the spectroscopic separation of the psoralen and DNA absorption bands increases. This is supportive of a selective excitation of psoralens in DNA.

We, thus, extended the π-system of the well-established PUVA agent 8-MOP. To this end, aryl moieties were placed at its 5 position (see Scheme 1). For reasons of water solubility and intercalation affinity, these moieties bear quaternized nitrogen atoms. We note that this quaternization might compromise the PET suppression at it tends to shift $E^0(A/A^{-\cdot})$ toward more positive values. In the following, synthesis and photophysics of four water-soluble 8-MOP derivatives will be presented. The compounds were characterized by steady-state absorption and emission spectroscopy as well as cyclic voltammetry. By means of femtosecond UV/Vis spectroscopy, compounds with nonvanishing triplet quantum yields were identified. All compounds turned out to be decent DNA intercalators. Surprisingly, none of the compounds photo-bind to DNA. Reasons for that and strategies for future improvements will be discussed.

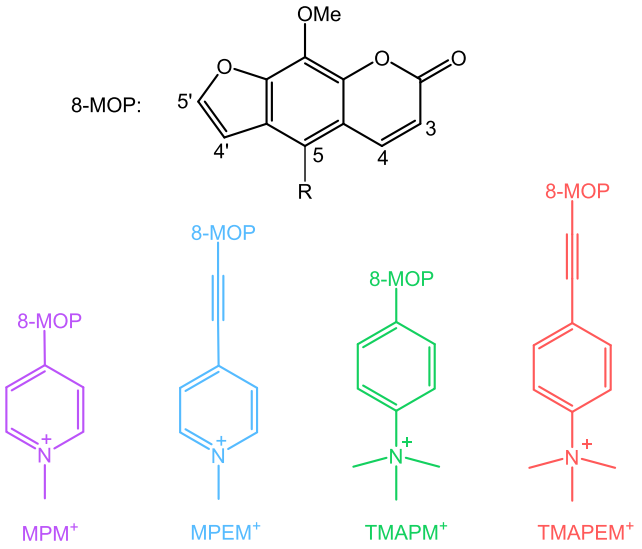

Scheme 1. Structures of the synthesized and characterized psoralen derivatives MPM^+, $MPEM^+$, $TMAPM^+$ and $TMAPEM^+$ based on the therapeutically applied 8-MOP. The substituents are covalently bound to 8-MOP at position 5.

MATERIALS AND METHODS

Samples and general conditions. 8-MOP was purchased from TCI (>98%). Coumarin 102 was supplied by Radiant Laser Dyes and thioxanthone (97%) as well as 1-methylpyridinium iodide by Sigma-Aldrich. Pure water (Fisher Chemical, HPLC gradient grade) and ethanol (Sigma-Aldrich, absolute, >99.8%) were used as solvents. The lyophilized oligonucleotide 5′-$(TA)_{20}$-3′ (AT-DNA in the following) was purchased from Sigma-Aldrich. Solutions of the oligonucleotide were buffered with PBS (Sigma-Aldrich, one tablet dissolved in 200 ml yields 10 mM phosphate buffer, 2.7 mM potassium chloride, 137 mM sodium chloride, pH 7.4 at 25°C). Annealing of the oligonucleotide strands in solution was performed within 24 h before the measurements. The solution was heated in a water bath up to 93°C and cooled down to room temperature within several hours. Psoralen precursors **1** and **2** for quaternization were synthesized by Suzuki or Sonogashira coupling from 5-bromo-8-methoxy psoralen according to our previously published protocol (17) and 4-ethynyl-1-methylpyridinium triflate (MPE triflate) was synthesized according to literature (18). All measurements were performed at room temperature (~ 20°C).

Steady-state spectroscopy. The UV/Vis absorption spectra were recorded with a two-beam Lambda 19 spectrometer from Perkin Elmer GmbH. Fused silica cuvettes with path lengths of 0.1 or 1 cm from Hellma were employed.

The fluorescence spectra were recorded in right-angle detection with a FluoroMax-4 from Horiba Scientific. The absorption at the excitation wavelength was ~ 0.05 at a path length of 1 cm to avoid inner filter effects. The spectra were corrected for the spectral sensitivity of the instrument. As reference for the determination of fluorescence quantum yields coumarin 102 in ethanol, $\Phi_{fl} = 0.80$ (19,20), was employed.

For the conversion into the wavenumber representation, fluorescence spectra recorded with constant wavelength band pass were multiplied by the respective wavelength squared (21). Absorption and fluorescence spectra were multiplied by $\tilde{\nu}^{-1}$ and $\tilde{\nu}^{-3}$, respectively, to account for intrinsic frequency dependences (22). The 0-0 energy E_{00} was determined as the intersection of the converted and normalized absorption and fluorescence spectra.

The photoreactivity of the psoralens was investigated with an LED (NSPU510CS, Nichia) emitting at 375 nm as a light source. The solution was stirred during the illumination. The ratio of absorbed photons n_{abs} and psoralen molecules n_{Pso} gives the photon equivalents (PE):

$$\mathrm{PE}(t) = \frac{n_{\mathrm{abs}}(t)}{n_{\mathrm{Pso}}} = \frac{P \cdot \int_0^t \left(1 - 10^{-A_{\mathrm{Ex}}(t)}\right) dt}{h \cdot \frac{c}{\lambda_{\mathrm{Ex}}} \cdot N_A \cdot n_{Pso}} \tag{2}$$

The light power P impinging on the sample was measured using a thermopile sensor (PS19, Coherent). The term $\left(1 - 10^{-A_{Ex}(t)}\right)$ accounts for the fraction of this light power absorbed by the sample. h is the Planck constant, c the speed of light, and N_A the Avogadro's number.

Femtosecond transient absorption spectroscopy. The fs transient absorption (fs-TA) setup has been described elsewhere in more detail (23). A 1 kHz Ti:Sa laser amplifier system (Coherent Libra) served as pulse source. The output wavelength is 800 nm, and the pulse duration is 100 fs. Part of its output was converted by a noncollinear OPA (TOPAS-white, Light Conversion) to 610 nm and then frequency-doubled in a β-barium borate crystal to yield the pump wavelengths of 300 nm or 317 nm. To yield the 400 nm pump beam, the 800 nm laser output was frequency-doubled. The pump pulse energy was adjusted to ~ 1 μJ, and the pump beam had a focal size of 160 μm (full width at half maximum (FWHM)) at the sample. The absorption change was probed with a white light continuum generated in CaF_2 with a diameter of 100 μm on the sample. The relative polarization of the pump and probe beam was set to the magic angle. The time resolution was ~ 180 fs. The spectra were recorded at 139 time delay settings between –1 to 1 ps on a linear and from 1 ps to 3.4 ns on a logarithmic scale. For every delay setting, 2000 spectra were recorded and the data were averaged over 2 or 4 succeeding delay scans. The solution was pumped through a fused silica flow cell (custom made, Hellma Analytics) with 0.5 mm path length. To remove signal contributions of the solvent, a separate measurement of the solvent was subtracted with proper scaling. The instrumental time-zero shift was determined via the optical Kerr effect as a function of wavelength and corrected for.

Nanosecond transient absorption spectroscopy. The nanosecond transient absorption (ns-TA) data were acquired with a laser flash photolysis spectrometer LP980 from Edinburgh Instruments in a right-angle geometry. The fourth harmonic of the output wavelength (266 nm) of a Nd:YAG laser (Spitlight 600, InnoLas) with a repetition rate of 5 Hz and a pulse duration of 12 ns (FWHM) was utilized for photoexcitation. The average pulse energy amounted to 5 mJ. The diameter of the pump beam was ~ 8 mm. A pulsed xenon lamp (Osram XBO 150 W/C OFR) was used as a probe beam. Fused silica flow-through cuvettes from Hellma with a path length of 5 mm in pump and 10 mm in probe direction were employed. The absorption per path length was set to 0.7 per cm at the excitation wavelength. The transmitted probe light was dispersed by a grating monochromator and detected by a photomultiplier (Hamamatsu, R928). The signal was digitized by an oscilloscope (MDO3022, Tektronix). To obtain transient spectra, every 5 nm kinetic traces were recorded and averaged over 400 acquisitions.

Time-correlated single photon counting. Time-correlated single photon counting was performed on a FluoTime 300 from PicoQuant. A supercontinuum picosecond laser (SuperK Extreme equipped with SuperK Extend-UV, NKT Photonics) tuned to 380 nm served as excitation source. Emission was detected at 524 nm under magic angle conditions. The repetition rate was set to 78 MHz. Sample solutions with an absorption at the excitation wavelength below 0.1 were measured until a peak value of 10 000 counts was achieved. The instrumental response function was measured with scattered light.

Electrochemistry. Cyclic voltammetry experiments (EG&G Princeton Applied Research Model 263A potentiostat; software: PowerSuite Revision 2.12.1.) were performed under argon atmosphere in dry and degassed acetonitrile at 293 K using n-Bu_4NPF_6 (0.1 M) as electrolyte. The three-electrode array consists of a working electrode with a 2 mm platinum disk (A = 0.031416 cm^2), a platinum wire counter electrode and an Ag|AgCl (3.0 M NaCl) reference electrode. Scan rates v of 100, 250, 500 and 1000 mVs^{-1} were employed. Cyclic voltammograms can be found in the Supporting Information. All potentials are reported versus the normal hydrogen electrode (NHE).

Data analysis. Wavelength-dependent time-resolved data were analyzed globally using a multi-exponential trial function convoluted with the instrumental response function (IRF) (24):

$$\Delta A(\lambda, t) = \mathrm{IRF} \otimes \sum_{i=1}^{n} \Delta A_i(\lambda) \cdot e^{-\frac{t}{\tau_i}} \tag{3}$$

The fit yields a decay-associated difference spectrum (DADS) $\Delta A_i(\lambda)$ for each time constant τ_i. TCSPC data sets were fitted with a multi-exponential trial function convoluted with the IRF:

$$S(t) = \mathrm{IRF} \otimes \sum_{i=1}^{n} A_i \cdot e^{-\frac{t}{\tau_i}} \tag{4}$$

RESULTS

Synthesis

Upon treatment of compounds **1** and **2** (17) with trimethyloxonium tetrafluoroborate (Meerwein's salt) (25) in dichloromethane at 0°C for 15 min and at room temperature for 24–48 h, the quaternized derivatives were obtained in 62–67% yield as crystalline solids (Scheme 2).

The structures of all compounds were unambiguously assigned by ^1H, ^{13}C NMR and IR spectroscopy, as well as by high-resolution mass spectrometry.

Steady-state characteristics

All derivatives show water solubilities higher than 1 mM, proving the advantage of ionized psoralen derivatives. The solubility of 8-MOP in comparison is 0.2 mM (10). The absorption spectra of all derivatives dissolved in water are depicted in Fig. 2a. Respective spectra for dichloromethane solutions can be found in the Supporting Information. Spectra of all derivatives are red-shifted with respect to 8-MOP. In all spectra, except for $MPEM^+$, the S_1 absorption bands are visible as shoulders. According to quantum chemical computations on psoralens and derivatives, at least two allowed electronic transitions are expected above 300 nm (26,27). To extract peak wavelengths λ_{abs} and absorption coefficients ε_{max} of the lowest transition, absorption signals as a function of the wavelength were subject to a fit with a Gaussian, for the retrieved parameters see Table 1. The peak absorption coefficients are of a similar order for MPM^+, $TMAPM^+$ and 8-MOP (~ 1000 M^{-1} cm^{-1}) and higher for $MPEM^+$ and $TMAPEM^+$ (~ 10 000 M^{-1} cm^{-1}).

The fluorescence spectra cover a similar spectral region with maximal emission wavelengths λ_{em} around 520 nm (see Fig. 2b). All derivatives feature large Stokes shifts in the range of 8000–11 000 cm^{-1}. The shift is smaller for the ones with red-shifted absorption. The 0-0 energies E_{00} are similar or slightly lower than the one for 8-MOP. The E_{00} energies were determined using the assumption that the vertical absorption and emission

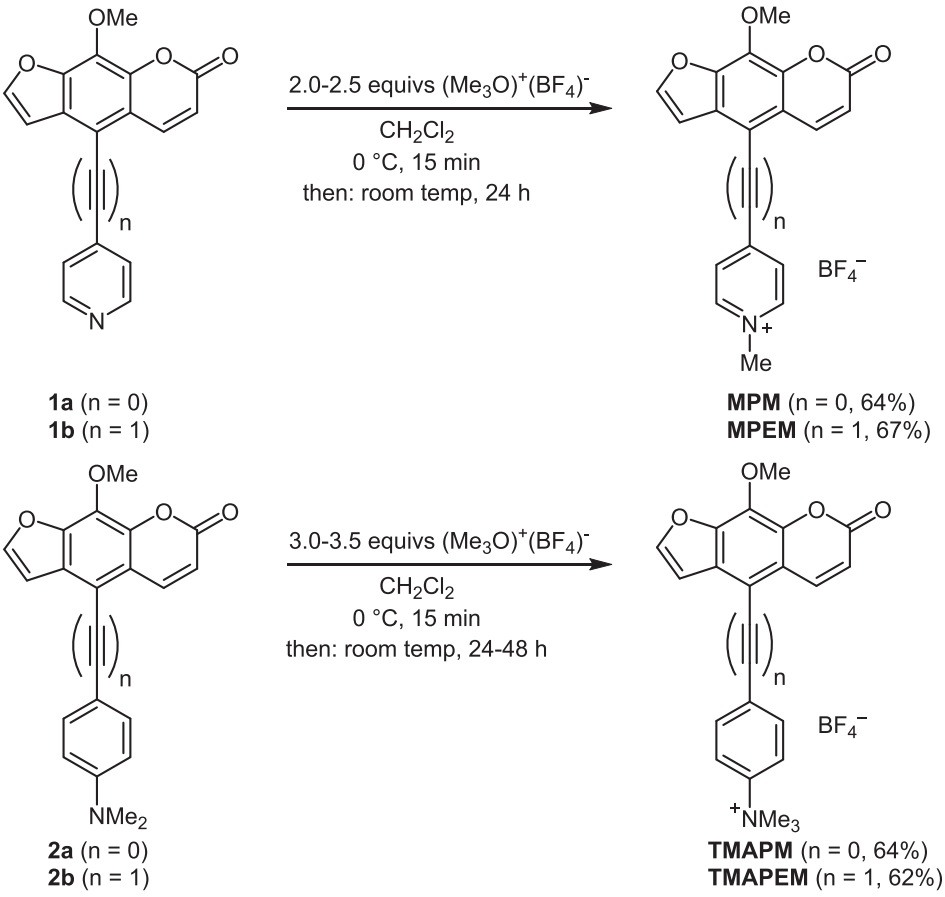

Scheme 2. Synthesis of quaternized psoralen derivatives.

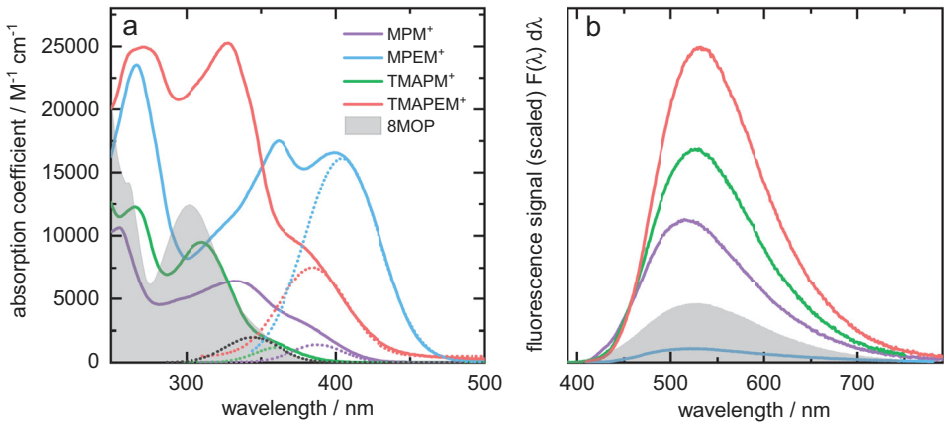

Figure 2. Absorption coefficients (a) and emission spectra (b) of investigated psoralen derivatives in H_2O as well as 8-MOP as a reference. The dotted lines represent the absorption band lowest in energy derived from a Gaussian fit. The emission spectra were scaled to be proportional to the respective fluorescence quantum yield.

energies are "symmetric" with respect to the E_{00} value. Quantum chemical computations suggest deviations from this at least for the parent compound psoralen (26). The fluorescence quantum yields Φ_{fl} of all derivatives are low, ranging from 0.001 to 0.02. Using absorption and fluorescence spectra as an input, the radiative rate constant k_{rad}^{SB} was computed relying on the Strickler-Berg relation (22,28). In this analysis, an integration over the absorption band lowest in energy has to be performed. As for most derivatives studied here, this band overlaps with the transition to a higher state. Therefore, the integration was performed using the Gaussians given in Fig. 2. This might introduce a systematic error in the Strickler-Berg analysis. With this approach, a radiative rate constant k_{rad}^{SB} of $0.55 \cdot 10^7$ s^{-1} was derived for 8-MOP (see Table 1). MPM^+ and $TMAPM^+$ feature rate constants k_{rad}^{SB} of the same magnitude. The ones for $MPEM^+$ and $TMAPEM^+$ are one order of magnitude larger. With the rate constants

Table 1. Spectral properties of the investigated psoralen derivatives in H_2O.

	MPM^+	$MPEM^+$	$TMAPM^+$	$TMAPEM^+$	8-MOP
λ_{abs}/nm	388	404	361	385	344
$\tilde{\nu}_{abs}$/cm^{-1}	25 887	24 364	27 471	25 671	28 394
ε_{max}/M^{-1} cm^{-1}	1404	16 120	1194	7518	1976
λ_{em}/nm	515	524	526	530	528
$\tilde{\nu}_{em}$/cm^{-1}	17 986	17 212	17 794	17 606	17 483
$\tilde{\nu}_{Stokes}$/cm^{-1}	7901	7152	9695	8065	10 911
E_{00}/eV	2.8	2.7	2.9	2.7	2.9
Φ_{fl}	0.009	0.001	0.013	0.019	0.004[†]
$k_{rad}^{SB}/10^7$ s^{-1}	0.27	5.94	0.29	2.46	0.55
$\tau_{fl}^{SB}/10^{-9}$ s	3.37	0.02	4.54	0.77	0.73
$\tau_{fl}/10^{-9}$ s	0.23	0.002	1.2	0.8	0.9[15]

Peak absorption wavelengths λ_{abs} and wavenumbers $\tilde{\nu}_{abs}$ for the band lowest in energy as well as absorption coefficient ε_{max} are derived from a Gaussian fit. The values λ_{abs} and λ_{em} were obtained from measurements with constant wavelength bandpass. The values given in wavenumbers and electronvolts are derived from spectra corrected for physical effects. Fluorescence quantum yields Φ_{fl} were determined with coumarin 102 in ethanol as a reference. A Strickler-Berg analysis yields a radiative rate constant k_{rad}^{SB}. A prediction for the fluorescence lifetime τ_{fl}^{SB} is obtained via $\tau_{fl}^{SB} = \frac{\Phi_{fl}}{k_{rad}^{SB}}$. Femtosecond transient absorption experiments give actual fluorescence lifetimes τ_{fl}. [†]Value by Shim et al. is 0.0028 (47).

k_{rad}^{SB} and the fluorescence quantum yields Φ_{fl} as an input, predictions for the fluorescence lifetimes τ_{fl}^{SB} are possible using $\tau_{fl}^{SB} = \frac{\Phi_{fl}}{k_{rad}^{SB}}$. These predictions will be compared with results from actual measurements below.

Transient states

The fate of the photo-excited psoralens was traced by femtosecond and nanosecond transient absorption spectroscopy. Such a study on the "benchmark" molecule 8-MOP had revealed an S_1 lifetime of 0.9 ns (15) matching the value (0.7 ns) derived from the steady-state spectra (cf. Table 1). The S_1 decay is accompanied by the population of the triplet state. Its quantum yield Φ_T amounts to 0.06 (8).

MPM^+. A solution of MPM^+ in water was excited with femtosecond laser pulses centered at 400 nm and probed in the UV/Vis region. Around time zero, a prominent positive absorption band around 425 nm is discernable (see Fig. 3). The maximum of a negative difference absorption band shifts from ~ 500 nm at time zero to ~ 540 nm within 2 ps. Between 2 and 100 ps, the absorption changes slightly, clearly evident around 500 nm with a change from negative to positive difference absorption. After 100 ps, the difference absorption decays to zero within the time range covered. Accounting for the initial dynamic Stokes shift and the decay behavior later on requires a trial function with five exponentials and an offset. As shown for instance by Marciniak and Lochbrunner (29), parametrizing dynamic Stokes shifts with the present approach requires several exponentials. The first three time constants of $\tau_1 = 30$ fs, $\tau_2 = 400$ fs and $\tau_3 = 2$ ps fall in the range of the dielectric relaxation of water (30). The respective DADS (see Fig. 4) feature negative contributions in the short wavelength range and positive ones in the long wavelength range. This is the pattern expected for a band shifting to the red (29). The DADS ΔA_4 (time constant $\tau_4 = 12$ ps) is different in nature. It exhibits a negative amplitude almost throughout the spectral range covered. The DADS ΔA_5 associated with the longest time constant τ_5 of 230 ps features a negative amplitude around 550 nm, which can be assigned to stimulated emission (see Fig. 5). The offset spectrum is essentially zero throughout the complete spectral range. The changes on the 100 ps time scale can therefore be attributed to the decay of electronic excitation and recovery of the ground state. No electronically excited state with a lifetime exceeding ~ 200 ps seems to be involved in the photophysics of MPM^+. On the other hand, the analysis of the steady-state spectra afforded a fluorescence lifetime of 3.4 ns (see Table 1). This suggests that the electronic state from which the emission originates features a higher oscillator strength than the one inferred from the absorption spectrum. As will be argued in the following, an *intramolecular* electron transfer from the 8-MOP part to the methylpyridinium residue of the molecule could result in the formation of this state.

Such an electron transfer ought to generate a charge shifted state with a rate constant k_{CS}. This state would then recombine to yield the ground state with a rate constant k_{CR}. One could associate $1/k_{CS}$ with τ_4=12 ps and $1/k_{CR}$ with $\tau_5 = 230$ ps. After the charge shift process, one ought to observe spectroscopic signatures of oxidized 8-MOP and reduced methylpyridinium moieties (see Fig. 5). Indeed, oxidized 8-MOP ($8\text{-}MOP^+$) features an absorption band at ~ 650 nm (9) where a peak is observed in the DADS ΔA_5. The neutral radical derived from methylpyridinium (concerning its generation see Supporting Information) features a very broad absorption band with a peak around 450 nm. If one further considers the ground state bleach and the stimulated emission, the DADS ΔA_5 can be reconstructed (see Fig. 5). An analysis of the relative signal height of the stimulated emission in relation to the signal contribution of $8\text{-}MOP^+$ suggests that this charge shifted state is a stronger emitter than the one initially excited. This might resolve the discrepancy between the measured and predicted fluorescence lifetimes (cf. Table 1). The transition from the primarily excited state to the charge shifted one increases the peaks absorption (or gain) coefficient ε_{max} from ~ 1000 M^{-1} cm^{-1} to ~ 5000 M^{-1} cm^{-1}. This increase will raise the radiative rate constant k_{rad}^{SB}, which can explain the shorter fluorescence lifetime.

Cyclic voltammetry suggests that a photo-induced charge shift process might be thermodynamically feasible (see Supporting Information). Although all spectroscopic data were recorded with water as a solvent, for cyclic voltammetry acetonitrile served as a solvent. Therefore, somewhat other potential values than those reported here might be applicable for the processes occurring in water. As most of the reductions/oxidations are chemically irreversible, the given standard potentials are estimated from the peak potentials as described in the SI. A standard electrode potential E_{MPM^{2+}/MPM^+} of +1.9 V vs NHE (all potentials are reported versus the normal hydrogen electrode, NHE) was determined. The value matches the +1.9 V determined for 8-MOP under identical conditions (31). For the reduction of MPM^+, a standard potential of $E_{MPM^+/MPM}$ of –0.8 V vs NHE was derived. For methylpyridinium itself, in acetonitrile a value of −1.2 V vs NHE (in water a value of −1.4 V vs NHE was reported (32)) was determined. The standard potentials and the E_{00} energy of 2.8 eV (see Table 1) imply a change of Gibbs free energy ΔG_{CS}^0 of ~ +0.1 eV. Keeping in mind that somewhat different values for potentials (determined in acetonitrile) might apply in water, the charge shift process could be slightly exergonic.

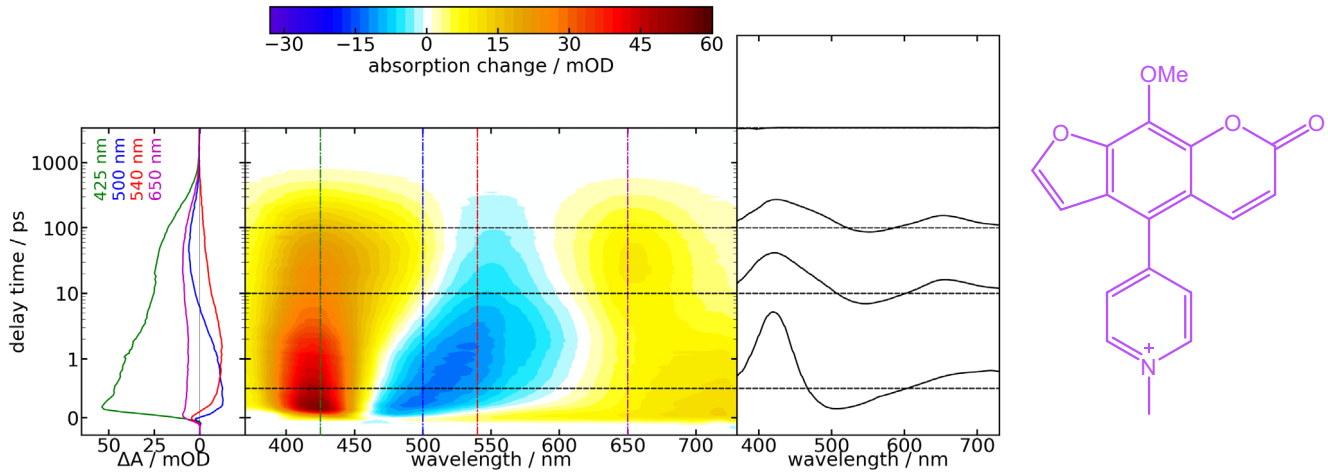

Figure 3. Femtosecond transient absorption of MPM^+ (6.5 mM) in H_2O after excitation at 400 nm. The difference absorption of MPM^+ is color-coded. Vertical lines in the contour plot give the wavelengths of the time traces shown on the left. Horizontal lines give the delay time of the transient spectra depicted on the right.

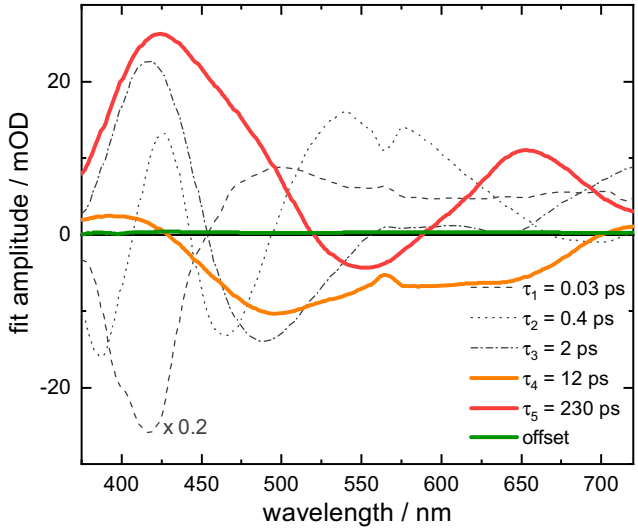

Figure 4. DADS retrieved for the femtosecond transient absorption experiment on MPM^+ (Fig. 3).

Concerning the PET from guanine to MPM^+, a change of Gibbs free energy ΔG^0_{CS} of –0.9 eV can be calculated via eq. 1 with $E^0(D^{+\cdot}/D)$ of +1.47 V for guanine (33), $E^0(A/A^{-\cdot})$ of –0.8 V for MPM^+, an E_{00} of 2.8 eV and a work term W of –0.34 eV (15). This shows that an intermolecular electron transfer with guanine as electron donor could quench the S_1 state as well. The observed transient behavior after excitation as well as the electrochemical characteristics indicate that MPM^+ does not seem to be a candidate for a PUVA drug. The excited singlet state is quenched intramolecularly and hence no population of the triplet state visible. Experiments involving DNA will confirm this assumption (see below).

$MPEM^+$. A solution of $MPEM^+$ in water was excited with femtosecond pulses centered at 400 nm and probed in the UV/Vis. Around time zero negative absorption changes around 370 and 575 nm as well as positive changes below 350 nm and around 470 nm are discernable (see Fig. 6). With reference to the steady-state spectra (see Fig. 2), the negative signal centered at 370 nm can be attributed to a ground state bleach and the one at 575 nm to stimulated emission. The stimulated emission persists for only a few picoseconds. The other signals decay to zero on the time scale of several 100 ps. A global fit of the data requires five time constants. The first two time constants (τ_1 = 30 fs, τ_2 = 700 fs) are presumably associated with solvation dynamics in water (30). In the DADS ΔA_3 (time constant τ_3 = 2 ps), a negative band centered at 575 nm is visible (see Fig. 7). Comparison with a converted fluorescence spectrum of $MPEM^+$ (see Supporting Information) shows that this band is due to the decay of the stimulated emission and thereby the depletion of the S_1 state. The DADS ΔA_4 (time constant τ_4 = 29 ps) features a negative amplitude in the region of the ground state absorption, which could indicate ground state recovery, and a broad positive one. The DADS ΔA_5 (time constant τ_5 = 300 ps) is characterized by a negative band centered at 368 nm and two positive ones at 470 and 660 nm. The offset spectrum is essentially zero through the spectral range covered indicating that no transient state persists for more than some 100 ps.

The time constant τ_3 = 2 ps with which the stimulated emission decays is shorter than the prediction based on the steady-state results (see Table 1). As revealed by TCSPC, the fluorescence decay is tri-phasic (see Supporting Information). In addition to a fast decay not resolved by the TCSPC instrument, two weak components with time constants of 0.6 and 2.9 ns are detected. This tri-phasic behavior results in the longer (average) lifetime obtained from the steady-state measurements. This large spread in fluorescence lifetimes and the finding that the ground state recovery occurs with at least two time constants (τ_4 and τ_5) might be due to the coexistence of many rotamers in the ground state of $MPEM^+$. $MPEM^+$ is a diaryl substituted acetylene. These feature rotational barriers of the order of thermal energy at room temperature (34,35). So, a large conformational space is expected to be populated in the ground state. The different conformers might exhibit different excited state decays.

As with MPM^+, the fast quenching of the primarily singlet state (time constant τ_3 = 2 ps) could be explained with an

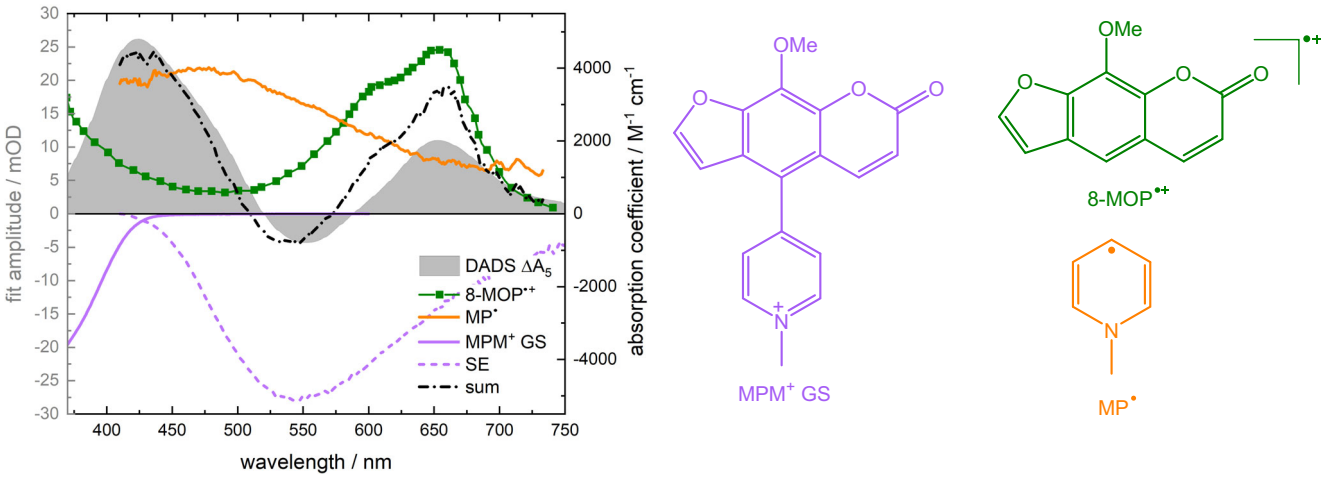

Figure 5. Decomposition of the DADS ΔA_5 of MPM^+ (gray, from Fig. 4) into signatures of its constituents. The absorption spectrum of MPM^+ in ground state (GS, violet) as well as the stimulated emission (SE, violet dashed) are inverted to demonstrate the assignment to the negative contribution in the DADS. The absorption spectrum and coefficients of the 8-MOP cation were obtained from Solar et al. (9) The spectrum of the methylpyridinium (MP) radical was obtained from an fs-TA measurement of MP^+ iodide. The sum of all contributions (black) is compared to the DADS ΔA_5 (gray). The stimulated emission and the MP radical spectrum were scaled such that the sum of all contributions best matches DADS ΔA_5.

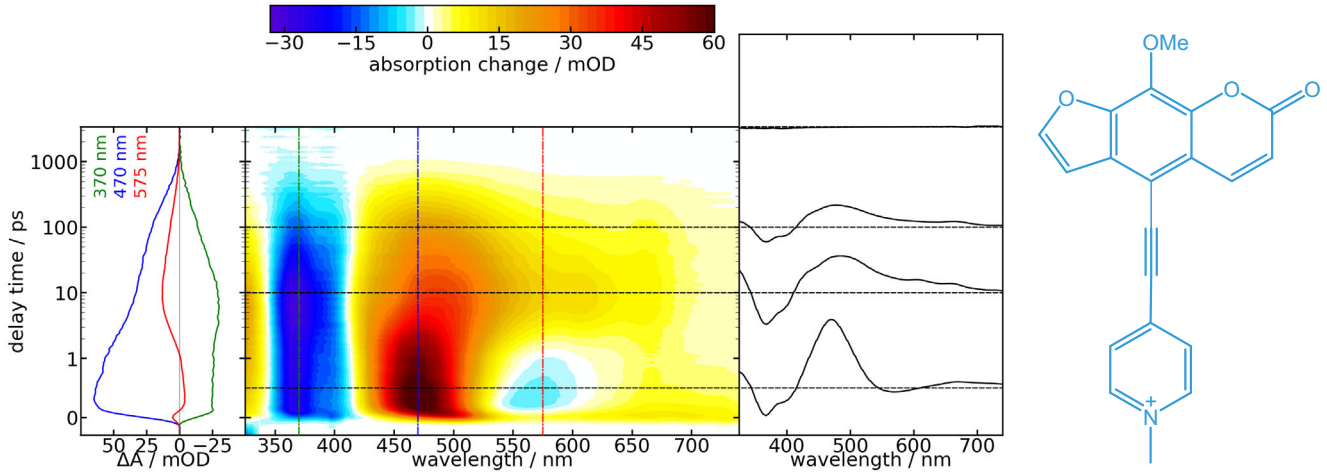

Figure 6. Femtosecond transient absorption of $MPEM^+$ (1.2 mM) in H_2O after excitation at 400 nm. The difference absorption of $MPEM^+$ is color-coded. Vertical lines in the contour plot give the wavelengths of the time traces shown on the left. Horizontal lines give the delay time of the transient spectra depicted on the right

intramolecular electron transfer from the 8-MOP to the methylpyridinium part. Spectroscopic and electrochemical measurements support this notion. Concerning the spectroscopic support, the DADS ΔA_5, which ought to be associated with the decay of the charge shifted state, is scrutinized (Fig. 8). The spectrum of ground state $MPEM^+$ contributes below ~ 450 nm as a bleach signal. A spectrum of the 8-MOP cation can be found in ref. (9). The reduced substituent MPE, the MPE radical ($MPE^\bullet$, for its generation see Supporting Information), features a transient spectrum with an absorption maximum at ~ 535 nm. Summing the contributions of $8\text{-}MOP^+$ and $MPE^\bullet$ as well as the ground state bleach yields a reconstructed spectrum similar to the DADS ΔA_5 of $MPEM^+$. Note that contrary to MPM^+, no stimulated emission had to be included. The peak at 665 nm in the DADS ΔA_5 is well reproduced by the reconstructed spectrum, while the one at 480 nm is at smaller wavelengths than predicted (535 nm). The reconstruction is of course based on the assumption that the two moieties are completely decoupled. As this does not apply, differences between the DADS ΔA_5 and the reconstructed spectrum are not so surprising. The presence of $8\text{-}MOP^+$ and $MPE^\bullet$ contributions show that an intramolecular electron transfer is the cause of the fast S_1 quenching. Cyclic voltammetry supports this hypothesis. The voltammogram of $MPEM^+$ in acetonitrile shows standard potentials $E_{MPEM^{2+}/MPEM^+}$ of +1.9 V and $E_{MPEM^+/MPEM}$ of –0.7 V vs NHE. MPE^+ itself features the same standard potential of –0.7 V vs NHE. With an E_{00} energy of 2.7 eV (see Table 1), the change in Gibbs free energy amounts to –0.1 eV. This magnitude could also explain why components with time constants exceeding 2 ps show up in the TCSPC experiment despite the fact that no stimulated emission contributions occur in the DADS ΔA_5. For a free energy difference of this magnitude, E-type delayed fluorescence (36)

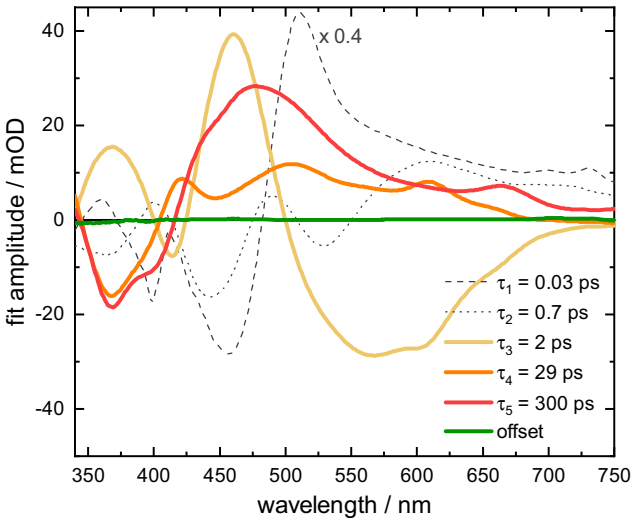

Figure 7. DADS retrieved for the femtosecond transient absorption experiment on $MPEM^+$ (Fig. 6).

involving the S_1 and the charge shifted state might occur. The free energy difference translates into a relative population of the S_1 state after equilibration of ~ $5{\cdot}10^{-4}$. The ratio between the fast and the slow fluorescence decay amplitudes observed by TCSPC is of a similar magnitude. So, indeed, the longer-lived fluorescence component could be due to delayed fluorescence.

Regarding a PET from guanine to $MPEM^+$, a Gibbs free energy ΔG^0_{CS} of –0.9 eV results with $E^0(A/A^{-\cdot})$ of –0.7 V and an E_{00} of 2.7 eV, showcasing again that E_{00} is not low enough to compensate for the less negative reduction potential.

TMAPM$^+$. A solution of $TMAPM^+$ in water was excited with femtosecond laser pulses centered around 300 nm and probed in the UV/Vis. The spectral pattern around time zero is similar to the one of 8-MOP (15) with broad bands around 380–480 nm and 600 to 700 nm (see Fig. 9). This initial signal persists for up to ~ 1 ns. It then gives way to a weak residual signal. A fit with two exponential functions and an offset is necessary to fit the data. One time constant with $\tau_1 = 1$ ps can be attributed to solvation effects in water (30). The DADS ΔA_2 (time constant $\tau_2 = 1200$ ps) features a positive amplitude with broad bands around 425 and 650 nm and can be attributed to the S_1 decay (see Fig. 10). The offset spectrum reveals that a species with a longer lifetime is present. The time constant τ_2 of 1200 ps is shorter than the value of 4.5 ns derived from the steady-state results (cf. Fig. 2). A plausible explanation for that discrepancy cannot be given at this point.

The fate of the carrier of the offset spectrum was traced by nanosecond transient absorption spectroscopy (see Fig. 11). For technical reasons, the sample solution was excited with 266 nm light pulses and not with 400 nm ones as in the femtosecond experiment. Early on, a negative signal around 310 nm due to ground state bleach and a positive signal with maximum at 370 nm are visible. This spectral pattern closely resembles the fs-TA offset spectrum (see Fig. 11, top). A single exponential fit reveals a decay with a time constant of 1.5 µs. Note that the intrinsic lifetime is presumably longer since no attempts were made to exclude oxygen quenching. The spectral pattern is similar to the one of the 8-MOP triplet state (6,8). It is thus assigned to the T_1 state of $TMAPM^+$. The triplet yield Φ_T could be determined to be 0.15 and the difference absorption coefficient at maximum $\Delta\varepsilon_T$ (370 nm) to be 10 400 M^{-1} cm^{-1} with thioxanthone as a reference (details in the SI).

Regarding a PET from guanine to $TMAPM^+$ a Gibbs free energy ΔG^0_{CS} of –0.6 eV results with $E^0(A/A^{-\cdot})$ of –1.2 V and an E_{00} of 2.9 eV.

TMAPEM$^+$. A solution of $TMAPEM^+$ in water was excited with femtosecond laser pulses centered at 400 nm and probed in the UV/Vis (see Fig. 12). Around time zero, the difference spectrum features an absorption maximum at 520 nm. A decay with small amplitude change around 520 nm with about 10 ps is followed by a strong decrease in signal throughout the spectrum within ~ 1 ns. A small, positive absorption feature is visible for long

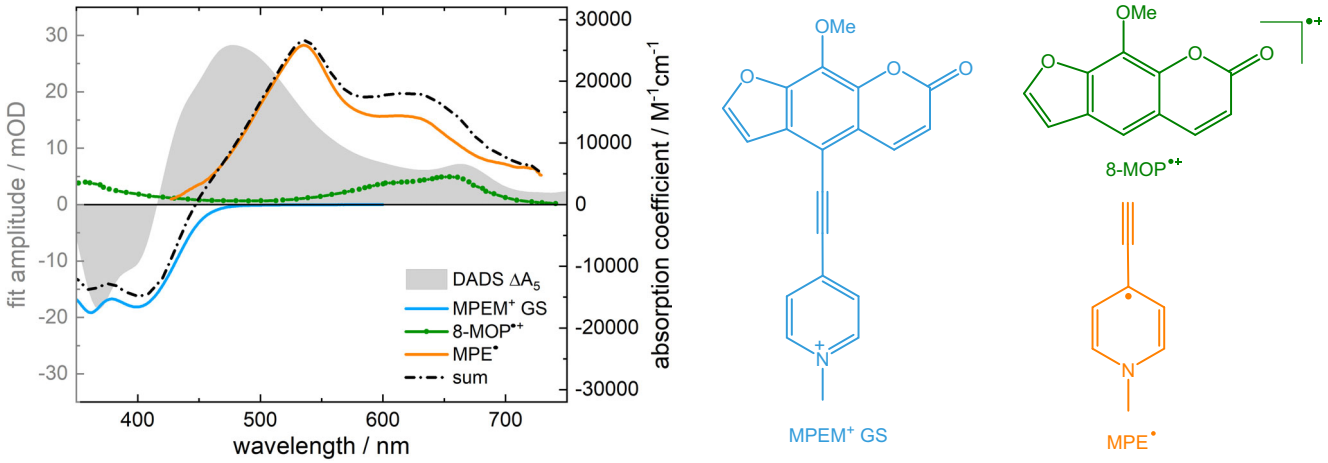

Figure 8. Decomposition of the DADS ΔA_5 of $MPEM^+$ (from Fig. 7) into signatures of its constituents. The absorption spectrum of $MPEM^+$ in ground state (GS, blue) is inverted to demonstrate the assignment to the negative contribution in the DADS. The absorption spectrum and coefficients of the 8-MOP cation were obtained from Solar et al. (9). The spectrum of the MPE radical was obtained from an fs-TA measurement of MPE^+ iodide and scaled to fit the maximum OD of the gray one. The sum of all contributions (black) is compared to the DADS ΔA_5 (gray).

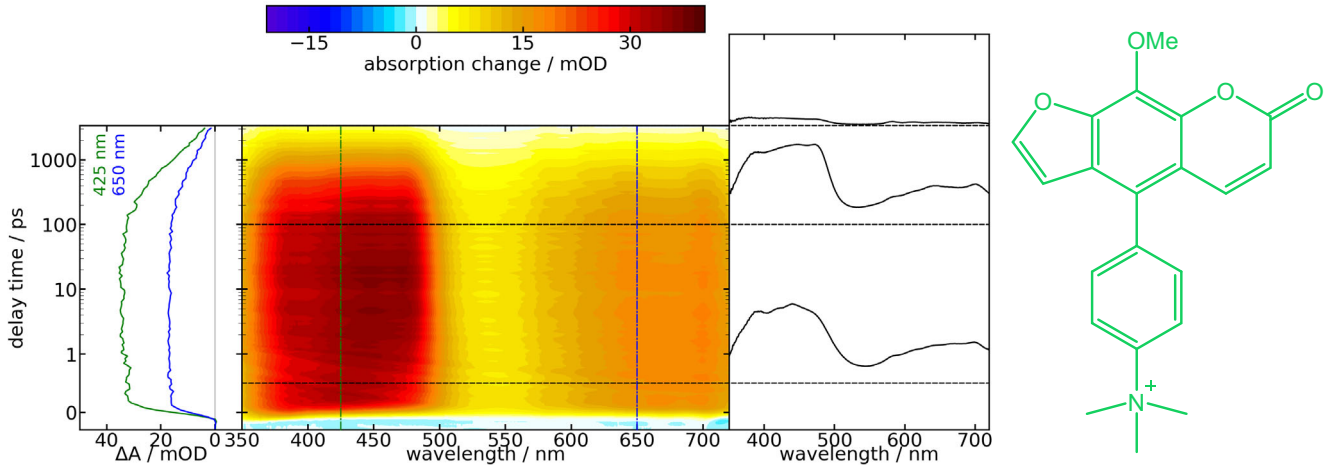

Figure 9. Femtosecond transient absorption of $TMAPM^+$ (3.2 mM) in H_2O after excitation at 300 nm. The difference absorption of $TMAPM^+$ is color-coded. Vertical lines in the contour plot give the wavelengths of the time traces shown on the left. Horizontal lines give the delay time of the transient spectra depicted on the right.

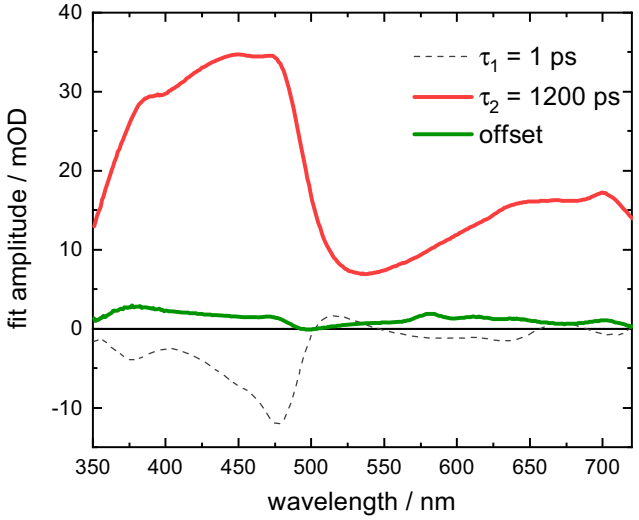

Figure 10. DADS retrieved for the femtosecond transient absorption experiment on $TMAPM^+$ (Fig. 9).

delay times. Five exponentials and an offset are needed to fit the data. The two shortest ones (τ_1 = 10 fs and τ_2 = 1 ps) can be attributed to dielectric relaxation in water (30). The DADS of τ_3 = 12 ps features a small positive amplitude around 525 nm and τ_4 = 130 ps a broad band with small amplitudes throughout the spectral range (see Fig. 13). The largest time constant of τ_5 = 1000 ps can be assigned to the decay of the S_1 state. The offset spectrum features a broad band with a maximum around 550 nm. The lifetime for the S_1 state reported here is in good agreement with the value retrieved from the steady-state spectra (cf. Table 1). Attempts were made to trace the further fate of excited $TMAPEM^+$ by nanosecond transient absorption. Unfortunately, due to low signal level no reproducible data could be obtained. Therefore, also no triplet yield Φ_T can be reported. Comparing the relative magnitude of the femtosecond offset spectra of $TMAPM^+$ and $TMAPEM^+$ suggests a substantially smaller triplet yield Φ_T for the latter.

A PET with guanine might be feasible since the Gibbs free energy ΔG^0_{CS} amounts to +0.1 eV with a standard potential $E^0(A/A^{-\cdot})$ of –1.7 V and an E_{00} of 2.7 eV.

Interaction with DNA

As outlined in the Introduction, a good PUVA agent ought to feature a high intercalation affinity and a high quantum yield for the addition to DNA. The affinity for intercalation is commonly quantified with the dissociation constant K_D (11):

$$K_D = \frac{c_{\mathrm{Pso,\,free}} \cdot c_{\mathrm{DNA,\,free}}}{c_{\mathrm{Pso,int}}}. \qquad (5)$$

In this equation, $c_{\mathrm{Pso,\,free}}$ is the concentration of nonintercalated psoralen, $c_{\mathrm{DNA,\,free}}$ the concentration of nonoccupied base pairs and $c_{\mathrm{Pso,int}}$ the concentration of intercalated molecules. A low K_D value signifies a good intercalation affinity. K_D values depend on the intercalating psoralen and the specifics of DNA sample (15). For the sake of comparison with earlier studies, "AT-DNA," a synthetic sample composed of alternating adenine and thymine bases, was employed in all intercalation experiments. The K_D value was determined by a titration experiment relying on the hypochromic effect in the UV/Vis spectra of the psoralen derivatives upon intercalation (15,37). The total concentration of psoralen was kept constant while the concentration of DNA was gradually reduced. More details on this method are given in reference (15). As an example, the result of the titration experiment on $TMAPEM^+$ is given in Fig. 14. For low concentrations of DNA (green spectra), the spectra resemble the spectrum of only $TMAPEM^+$ in water. For higher DNA concentrations and thereby higher ratios of intercalated psoralens, a different spectral pattern reveals. A hypochromic effect around the maximum wavelength of 329 nm becomes discernable. At very high concentrations of DNA (brown spectra), the absorption is seen to increase again. It is possible that this effect is caused by an additional external binding process (38–41). This behavior was observed for $TMAPEM^+$ and $MPEM^+$ but not for MPM^+ and $TMAPM^+$. For the determination of the dissociation constant, only the absorption decrease for rather low DNA concentrations was taken into account (see Fig. 14, right). A fit based

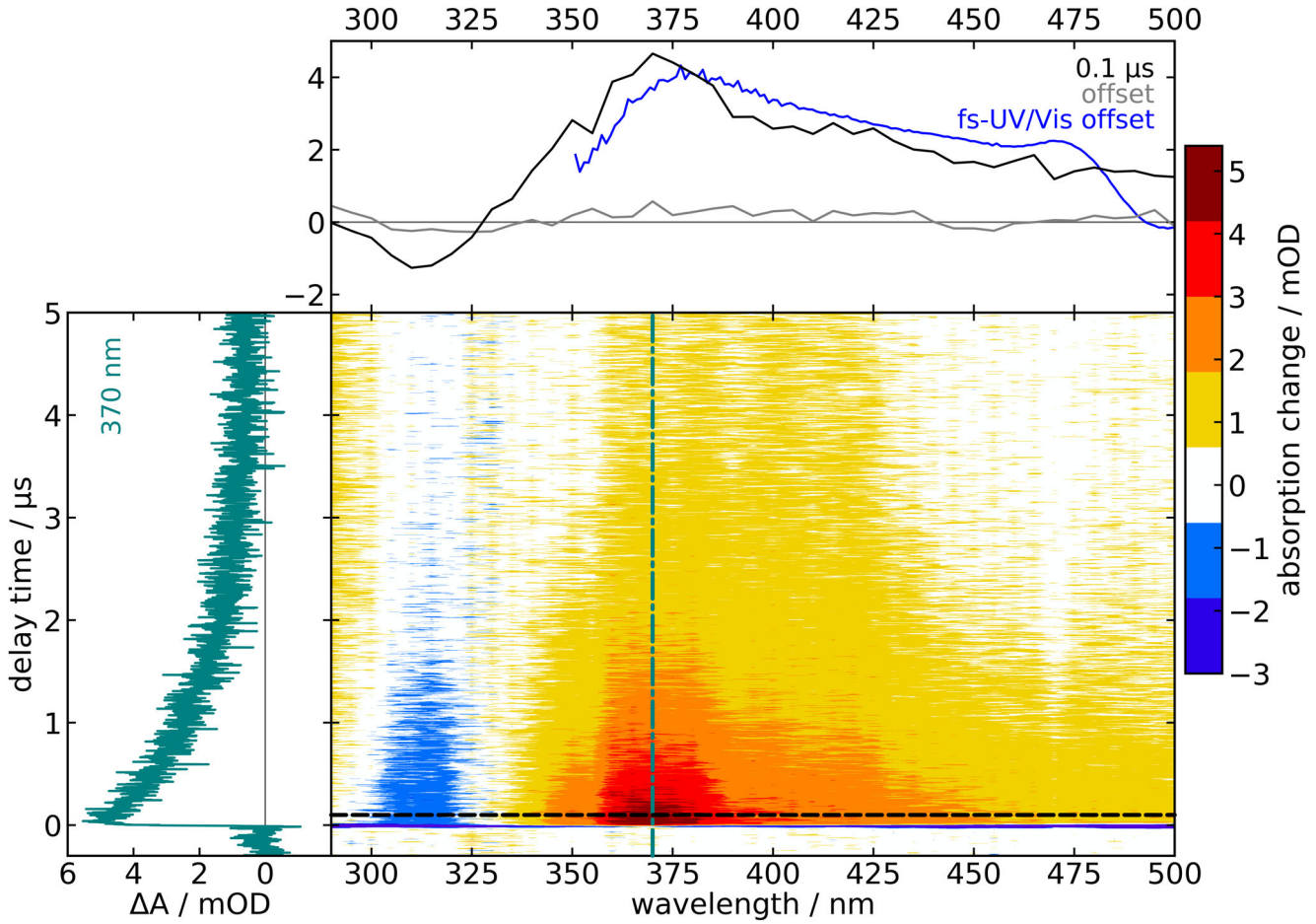

Figure 11. Nanosecond transient absorption of $TMAPM^+$ (60 µM) in air-saturated H_2O after excitation at 266 nm. The difference absorption of $TMAPM^+$ is color-coded. The vertical line in the contour plot gives the wavelength of the time trace shown on the left (turquois). The horizontal line gives the delay time of the transient spectrum depicted on top (black). For comparison, the fs-TA offset DADS (blue) of the measurement depicted in Fig. 10 is added.

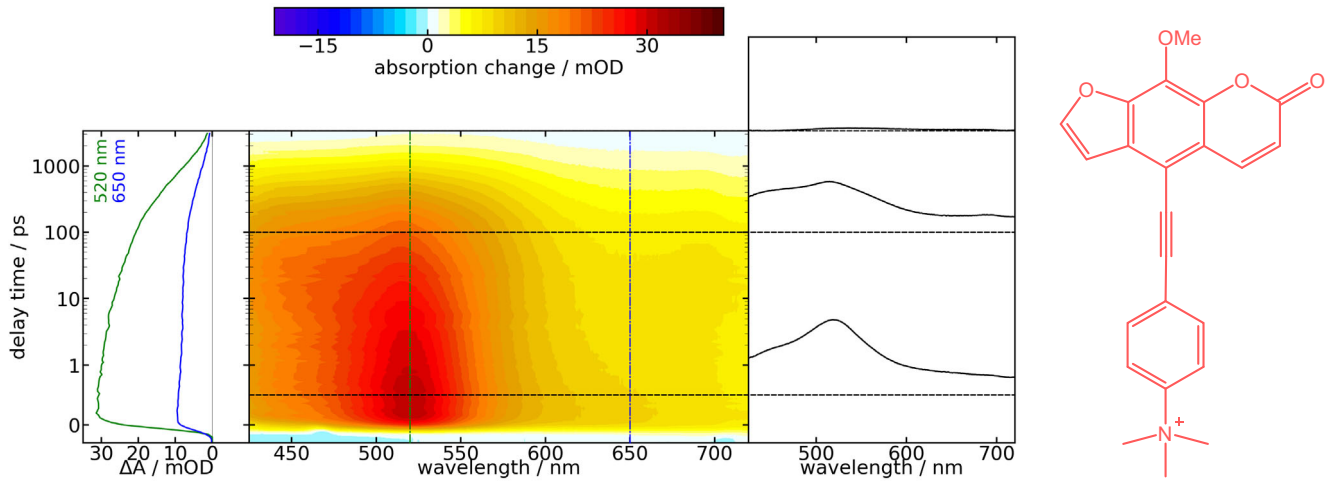

Figure 12. Femtosecond transient absorption of $TMAPEM^+$ (0.8 mM) in H_2O after excitation at 400 nm. The difference in absorption of $TMAPEM^+$ is color-coded. Vertical lines in the contour plot give the wavelengths of the time traces shown on the left. Horizontal lines give the delay time of the transient spectra depicted on the right.

on equation 5 yields the respective K_D values (for details see reference (15)). All K_D values are smaller than the one for 8-MOP implying higher intercalation affinity (see Table 2). This presumably relates with the positive charge of the derivatives (10). The bulky substituents in position 5 do not seem to impair the intercalation. Not only the absorption but also the

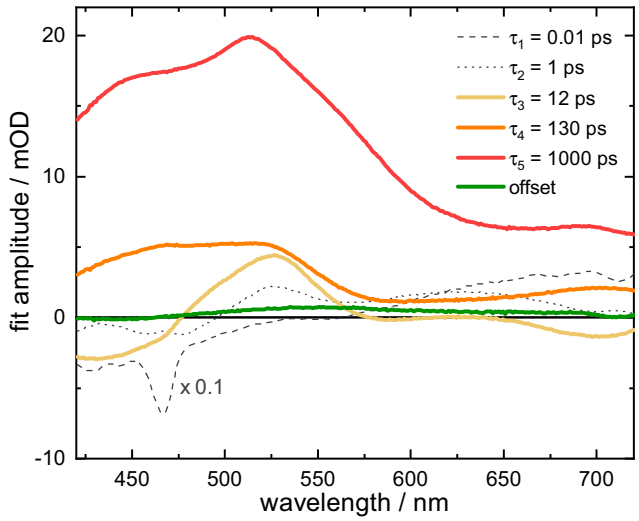

Figure 13. DADS retrieved for the femtosecond transient absorption experiment on TMAPEM$^+$ (Fig. 12).

fluorescence behavior changes due to intercalation. For 8-MOP as well as TMAPM$^+$ an increase in fluorescence quantum yield and a blueshift with respect to water can be detected for the psoralens intercalated in AT-DNA (see Supporting Information, not verified for the other derivatives). The blueshift is presumably due to the smaller dielectric response of the DNA interior as compared to water.

The reaction quantum yields of the photo-addition to DNA were determined for all four derivatives. A solution of the derivative as well as AT-DNA in water was illuminated with an LED emitting light in the UV-A (375 nm). The concentrations were chosen in a ratio so that most of the psoralens are intercalated. Changes to the absorption spectrum upon irradiation are solely due to the psoralen reacting, since the DNA does not absorb light in the UV-A. The resulting changes to the spectra

Table 2. K_D values (in M) for the intercalation of psoralens into AT-DNA.

MPM$^+$	MPEM$^+$	TMAPM$^+$	TMAPEM$^+$	8-MOP
$4.4{\cdot}10^{-4}$	$8.1{\cdot}10^{-5}$	$2.6{\cdot}10^{-4}$	$9.2{\cdot}10^{-6}$	$1.1{\cdot}10^{-3}$ (13)

are exemplified by TMAPEM$^+$ in Fig. 15. Small absorption contributions of the DNA below 320 nm were subtracted from the spectra. The irradiation intervals are given in minutes as well as photon equivalents (PE). A value of 1 PE signifies that on average each psoralen molecule absorbed one UV-A photon (see Materials and Methods). The absorption decreases between 308 and 418 nm and increases slightly beyond that. The typical absorption band of the furan monoadduct seen with 8-MOP or AMT with a maximum around 340 nm and a shoulder at ~ 350 nm cannot be seen (1,13). The pyrone monoadduct does not absorb in the UV-A region. It typically features a small absorption up to ~ 310 nm and could be a possible photoproduct here (1,42). A reaction quantum yield Φ_R of ~ 0.001 was computed. For all four psoralens, the yield Φ_R is below 0.005. These values range far below the ones of pharmaceutical psoralens 8-MOP (0.04), TMP (0.4) and 5-MOP (0.017) which we determined under similar experimental conditions before (13).

DISCUSSION

PUVA agents like 8-MOP experience PET quenching by the DNA base guanine (14,15). This reduces their therapeutic potency. The approach pursued here was to render this PET endergonic by lowering the excitation energy of 8-MOP *via* suitable substitution. For all four derivatives studied here, the absorption spectra are red-shifted from ~ 350 nm for 8-MOP to a maximum shift of ~ 400 nm for MPEM. This corresponds to a lowering of the vertical excitation energy of ~ 0.5 eV. Surprisingly, the fluorescence spectra of all derivatives and 8-MOP

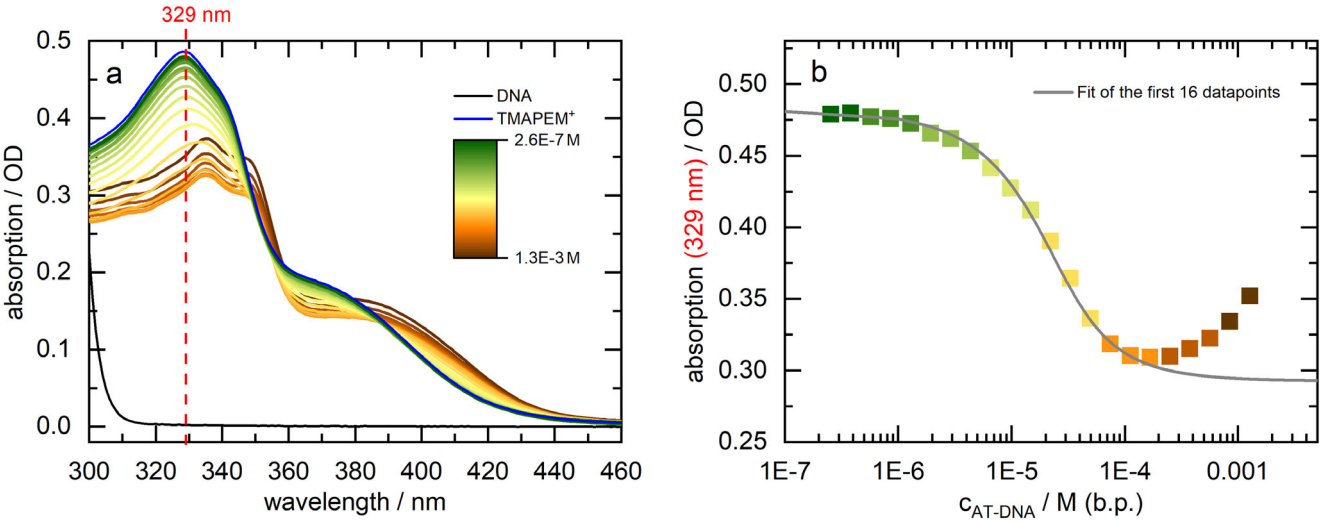

Figure 14. Determination of the DNA intercalation affinity of TMAPEM$^+$. a: UV/Vis absorption spectra of TMAPEM$^+$ (24 μM) with increasing concentration of AT-DNA in PBS buffer (green to brown). The contribution of DNA to the absorption was subtracted. Spectrum of pure TMAPEM$^+$ (24 μM) is shown in blue and AT-DNA ($1.3{\cdot}10^{-3}$ M) in black; b: Absorption at 329 nm versus the concentration of AT-DNA. A fit of the first 16 data points ($2.6{\cdot}10^{-7}$ M–$1.1{\cdot}10^{-4}$ M) yields the dissociation constant K_D of $9.2{\cdot}10^{-6}$ M.

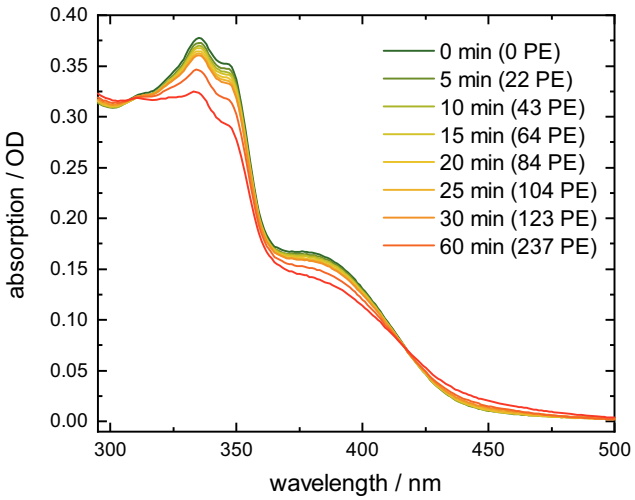

Figure 15. Irradiation of TMAPEM$^+$ (24 μM) with AT-DNA (0.5 mM) in PBS buffer (λ_{exc} = 375 nm, P = 10 mW, V = 3 mL, d = 1 cm). The irradiation times were converted to photon equivalents (PE).

feature similar peak wavelengths and the 0-0 energies are reduced by only ~ 0.2 eV. This small reduction cannot overcompensate the shift of reduction potentials $E^0(A/A^{-\cdot})$ of the psoralens toward more *positive* values caused by the cationic character of the substituents. For all derivatives studied, except TMAPEM$^+$, the ΔG^0_{CS} value for PET quenching by guanine is more negative than for 8-MOP. So, in terms of PET suppression TMAPEM$^+$ could be a promising PUVA agent. However, even compounds experiencing PET quenching like 8-MOP (15) are successfully employed in PUVA therapy. So, at this point, all derivatives described here might be potential PUVA agents. Thanks to their positive charge the derivatives feature water solubilities which are factor of 5 or more higher compared to 8-MOP. This charge presumably is also responsible for the increased intercalation affinity (10). The substituents at the 5 position, thus, do not seem to introduce a steric hindrance to the intercalation. Yet, all derivatives exhibit lower propensities to form photo-adducts with DNA. As the experiments were conducted with AT-only DNA, this cannot be attributed to *intermolecular* PET quenching by guanine.

The femtosecond transient absorption measurements on MPM$^+$ and MPEM$^+$ show that their S_1 state is effectively quenched by an *intramolecular* PET process. In this process, the 8-MOP moiety acts as an electron donor and the pyridinium part as an acceptor. As the PET involves an excited singlet state, it generates a singlet radical pair. In principle, this singlet radical pair might re-phase to the respective triplet one. However, in organic radical pairs this occurs on the time scale of tens of nanoseconds or longer (43–45). As shown here, the singlet radical pairs recombine on the picosecond time scale and no population of the triplet state is observed. The molecules under investigation in this study, thus, do not access their T_1 state, which is the precursor for the addition to DNA. So, a bit ironic, the attempt to suppress the *intermolecular* PET resulted in an *intramolecular* one. In both, MPM$^+$ and MPEM$^+$, the positive charge is located within the π-system of the chromophore. In TMAPM$^+$ and TMAPEM$^+$, the cationic residue is not in conjugation with the π-system. The femtosecond measurements show that in these derivatives no intramolecular PET quenching occurs. Their S_1 lifetimes are ~ 1 ns and thereby close to the one of 8-MOP. As with 8-MOP, the nanosecond decay goes along with the population of a species persisting for microseconds. The species is most likely the T_1 state of these derivatives. The triplet yield Φ_T of TMAPM$^+$ amounts to 0.15 and is higher than the one of 8-MOP (0.06 (8)). For TMAPEM$^+$, it is presumably smaller. The very small photo-addition quantum yields Φ_R < 0.005 indicate that the triplet states of TMAPM$^+$ and TMAPEM$^+$ differ from the one of 8-MOP concerning the reactivity. This is most likely not related to PET quenching by adenine. Upon intercalation into AT-DNA the fluorescence of TMAPM$^+$ increases. For PET quenching, of course, a decrease should occur (14). This leaves as a possible explanation the steric hindrance caused by the bulky substituent. Isaac et al. noticed a decrease in efficiency of covalent binding with increasing size of the substituent (10). Substitutions on position 5 seem to extend the distance between the intercalated psoralen (in particular the furan double bond) and the reactive double bond of thymine (46).

Despite the failure to find a PUVA agent not undergoing PET from guanine, the present study gives important guidelines for the optimization of psoralens. (i) Positive charge improves the water solubility and intercalation affinity, but can result in an intramolecular quenching of the S_1 state. Hereby, the location of this charge can be essential. In TMAPM$^+$ and TMAPEM$^+$ with the charge placed outside the π-system, no quenching was observed. (ii) A positive charge tends to shift the reduction potential of the psoralens toward more positive values enhancing the possibility of a PET from guanine. So, ways to increase water solubility and affinity without relying on cationic charge should be sought. (iii) Population of the triplet state does not guarantee high reaction quantum yields. Position, size and charge of the substituent need to be considered carefully.

Acknowledgements—This work has been supported by the Deutsche Forschungsgemeinschaft (grants GI 349/6-1 and MU 1088/14-1). Janina Bertling is grateful for a scholarship of the Jürgen Manchot Stiftung.

SUPPORTING INFORMATION

Additional supporting information may be found online in the Supporting Information section at the end of the article:

Figure S1. ^{1}H NMR spectrum of MPM$^+$ BF_4^- (500 MHz, DMSO-d_6, 293 K).

Figure S2. ^{13}C NMR spectrum of MPM$^+$ BF_4^- (125 MHz, DMSO-d_6, 293 K).

Figure S3. ^{1}H NMR spectrum of MPEM$^+$ BF_4^- (600 MHz, DMSO-d_6, 293 K).

Figure S4. ^{13}C NMR spectrum of MPEM$^+$ BF_4^- (151 MHz, DMSO-d_6, 293 K).

Figure S5. ^{1}H NMR spectrum of TMAPM$^+$ BF_4^- (600 MHz, DMSO-d_6, 293 K).

Figure S6. ^{13}C NMR spectrum of TMAPM$^+$ BF_4^- (151 MHz, DMSO-d_6, 293 K).

Figure S7. ^{1}H NMR spectrum of TMAPEM$^+$ BF_4^- (300 MHz, DMSO-d_6, 293 K).

Figure S8. ^{13}C NMR spectrum of TMAPEM$^+$ BF_4^- (75 MHz, DMSO-d_6, 293 K).

Figure S9. Normalized absorption and emission spectra of investigated psoralens recorded in dichloromethane.

Figure S10. Cyclic voltammograms on the reduction/oxidation of psoralen derivatives and building blocks studied here. The concentration was 2 mM in acetonitrile and the scan rate 0.1 V/s (except for $TMAPM^+$ with 0.05 V/s). The potentials were measured with an Ag/AgCl (sat. NaCl) electrode and shifted by +197 mV to yield the potentials vs NHE. Arrows indicate the direction of the scans. Vertical dashed lines indicate the half-wave ($E_{1/2}$) or cathodic/anodic peak potential (E_{ap}, E_{cp}). The representation follows the IUPAC convention.

Figure S11. Femtosecond transient absorption of 1-methylpyridinium iodide (MP^+I^-) (50 mM) and KI (50 mM) in H_2O after excitation at 320 nm. The absorption was set to 0.1 at excitation wavelength. The transient absorption is color coded. Vertical lines in the contour plot give the wavelengths of the time traces shown on the left. Horizontal lines give the delay time of the transient spectra depicted on the right.

Figure S12. Femtosecond transient absorption of 4-ethynyl-1-methylpyridinium triflate (MPE^+ triflate) (41 mM) and KI (50 mM) in H_2O after excitation at 317 nm. The absorption was set to 0.6 at excitation wavelength. The transient absorption is color coded. Vertical lines in the contour plot give the wavelengths of the time traces shown on the left. Horizontal lines give the delay time of the transient spectra depicted on the right.

Figure S13. Comparison of the difference absorption signal of $MPEM^+$ 0.4 ps after excitation at 400 nm and the fluorescence spectrum. The fluorescence spectrum was multiplied by the wavelength to the fourth power, λ^4, to obtain a stimulated emission signal, scaled and shifted vertically to match the bleach of the difference signal.

Figure S14. Time-correlated single photon counting on $MPEM^+$ in water. Blue dots represent experimental data, gray dots the instrumental response function (IRF) measured with scattered light. The solid blue line represents a multi-exponential fit convoluted numerically with the IRF.

Figure S15. Determination of the triplet difference absorption coefficient $\Delta\epsilon_T$ of $TMAPM^+$. The absorption spectrum of the ground state (red) is scaled and shifted to fit the DADS of the $TMAPM^+$ triplet (violet). The transient spectrum after 0.1 µs (gray) is depicted for comparison.

Figure S16. Comparison of the fluorescence spectra of 8-MOP (left) and $TMAPM^+$ (right) in absence (solid lines) and presence of AT-DNA (dashed lines).

Table S1. Experimental details of the synthesis of psoralen derivatives MPM^+, $MPEM^+$, $TMAPM^+$ and $TMAPEM^+$ by quaternization.

Table S2. Selected photophysical data of investigated psoralen derivatives in dichloromethane. Fluorescence quantum yields Φ_{fl} were determined with Coumarin 30 as a standard in acetonitrile ($\Phi_{fl} = 0.67$)

Table S3. Estimated standard potentials.

REFERENCES

1. Cimino, G. D., H. B. Gamper, S. T. Isaacs and J. E. Hearst (1985) Psoralens as photoactive probes of nucleic acid structure and function. *Annu. Rev. Biochem.* **54**, 1151–1193.
2. Kitamura, N., S. Kohtani and R. Nakagaki (2005) Molecular aspects of furocoumarin reactions: Photophysics, photochemistry, photobiology, and structural analysis. *J. Photochem. Photobiol. C Photochem. Rev.* **6**, 168–185.
3. Ling, T. C., T. H. Clayton, J. Crawley, L. S. Exton, V. Goulden, S. Ibbotson, K. McKenna, M. F. Mohd Mustapa, L. E. Rhodes, R. Sarkany and R. S. Dawe (2016) British Association of Dermatologists and British Photodermatology Group guidelines for the safe and effective use of psoralen-ultraviolet A therapy 2015. *Br. J. Dermatol.* **174**, 24–55.
4. Dall'Acqua, F., M. Terbojevich, S. Marciani, D. Vedaldi and M. Recher (1978) Investigation on the dark interaction between furocoumarins and DNA. *Chem. Biol. Interact.* **21**, 103–115.
5. Vowels, B. R., E. K. Yoo and F. P. Gasparro (1996) Kinetic analysis of apoptosis induction in human cell lines by UVA and 8-MOP. *Photochem. Photobiol.* **63**, 572–576.
6. Sloper, R. W., T. G. Truscott and E. J. Land (1979) The triplet state of 8-methoxypsoralen. *Photochem. Photobiol.* **29**, 1025–1029.
7. Kanne, D., K. Straub, H. Rapoport and J. E. Hearst (1982) Psoralen-Deoxyribonucleic acid photoreaction. Characterization of the monoaddition products from 8-methoxypsoralen and 4,5',8-trimethylpsoralen. *Biochemistry* **21**, 861–871.
8. Craw, M., R. V. Bensasson, J. C. Ronfard-Haret, M. T. S. Melo and T. G. Truscott (1983) Some photophysical properties of 3-carbethoxypsoralen, 8-methoxypsoralen and 5-methoxypsoralen triplet states. *Photochem. Photobiol.* **37**, 611–615.
9. Solar, S. and R. Quint (1992) Radiation induced primary processes of aqueous 8-methoxy-psoralen. A pulse radiolysis study. *Int. J. Radiat. Appl. Instrumentation. Part* **39**, 171–175.
10. Isaacs, S. T., C. Chun, J. E. Hyde, H. Rapoport and J. E. Hearst (1982) A photochemical characterization of reactions of psoralen derivatives with DNA. *Trends in Photobiology*, pp. 279–294. Springer US, Boston, MA.
11. Isaacs, S. T., C.-K.-J. Shen, J. E. Hearst and H. Rapoport (1977) Synthesis and characterization of new psoralen derivatives with superior photoreactivity with DNA and RNA. *Biochemistry* **16**, 1058–1064.
12. Diekmann, J., J. Gontcharov, S. Fröbel, C. Torres Ziegenbein, W. Zinth and P. Gilch (2019) The photoaddition of a psoralen to DNA proceeds via the triplet state. *J. Am. Chem. Soc.* **141**, 13643–13653.
13. Diekmann, J., I. Theves, K. A. Thom and P. Gilch (2020) Tracing the photoaddition of pharmaceutical psoralens to DNA. *Molecules* **25**, 5242.
14. Fröbel, S., A. Reiffers, C. Torres Ziegenbein and P. Gilch (2015) DNA Intercalated psoralen undergoes efficient photoinduced electron transfer. *J. Phys. Chem. Lett.* **6**, 1260–1264.
15. Fröbel, S., L. Levi, S. M. Ulamec and P. Gilch (2016) Photoinduced electron transfer between psoralens and DNA: Influence of DNA sequence and substitution. *ChemPhysChem* **17**, 1377–1386.
16. Weller, A. (1982) Photoinduced electron transfer in solution: Exciplex and radical ion pair formation free enthalpies and their solvent dependence. *Zeitschrift für Phys. Chemie* **133**, 93–98.
17. Geenen, S. R., L. Presser, T. Hölzel, C. Ganter and T. J. J. Müller (2020) Electronic finetuning of 8-methoxy psoralens by palladium-catalyzed coupling: Acidochromicity and solvatochromicity. *Chem. – A Eur. J.* **26**, 8064–8075.
18. Rubinsztajn, S., W. K. Fife and M. Zeldin (1992) Synthesis and reactivity of 1-Methyl-4-ethynylpyridinium triflate. *Tetrahedron Lett.* **33**, 1821–1824.
19. Dobek, K., J. Karolczak and J. Kubicki (2014) Temperature effects on excitation and deactivation processes of coumarin 102. A comparison with coumarin 153. *Dye. Pigment.* **100**, 222–231.
20. Rurack, K. and M. Spieles (2011) Fluorescence quantum yields of a series of red and near-infrared dyes emitting at 600–1000 nm. *Anal. Chem.* **83**, 1232–1242.
21. Mooney, J. and P. Kambhampati (2013) Get the basics right: Jacobian conversion of wavelength and energy scales for quantitative analysis of emission spectra. *J. Phys. Chem. Lett.* **4**, 3316–3318.
22. Parson, W. W. (2015) *Modern Optical Spectroscopy*, 2nd edn. Springer-Verlag, Berlin.
23. Fröbel, S., L. Buschhaus, T. Villnow, O. Weingart and P. Gilch (2015) The photoformation of a phthalide: a ketene intermediate traced by FSRS. *Phys. Chem. Chem. Phys.* **17**, 376–386.
24. Satzger, H. and W. Zinth (2003) Visualization of transient absorption dynamics - Towards a qualitative view of complex reaction kinetics. *Chem. Phys.* **295**, 287–295.
25. Fraser, P. J., W. R. Roper and F. G. A. Stone (1974) Cationic cyclic carbene complexes of iridium(III), nickel(II), palladium(II), and platinum(II). *J. Chem. Soc. Dalt. Trans*. 102–105.

26. Tatchen, J. and C. M. Marian (2006) Vibronic absorption, fluorescence, and phosphorescence spectra of psoralen: A quantum chemical investigation. *Phys. Chem. Chem. Phys.* **8**, 2133–2144.
27. Serrano-Pérez, J. J., R. González-Luque, M. Merchán and L. Serrano-Andrés (2008) The family of furocoumarins: Looking for the best photosensitizer for phototherapy. *J. Photochem. Photobiol. A Chem.* **199**, 34–41.
28. Strickler, S. J. and R. A. Berg (1962) Relationship between absorption intensity and fluorescence lifetime of molecules. *J. Chem. Phys.* **37**, 814–822.
29. Marciniak, H. and S. Lochbrunner (2014) On the interpretation of decay associated spectra in the presence of time dependent spectral shifts. *Chem. Phys. Lett.* **609**, 184–188.
30. Bagchi, B. and B. Jana (2010) Solvation dynamics in dipolar liquids. *Chem. Soc. Rev.* **39**, 1936.
31. Wood, P. D. and L. J. Johnston (1998) Photoionization and photosensitized electron-transfer reactions of psoralens and coumarins 1. *J. Phys. Chem. A* **102**, 5585–5591.
32. Gaudiello, J. G., D. Larkin, J. D. Rawn, J. J. Sosnowski, E. E. Bancroft and H. N. Blount (1982) On the mechanism of the electrochemical reduction of N-methylpyridinium ion. *J. Electroanal. Chem. Interfacial Electrochem.* **131**, 203–214.
33. Seidel, C. A. M., A. Schulz and M. H. M. Sauer (1996) Nucleobase-specific quenching of fluorescent dyes. 1. Nucleobase one-electron redox potentials and their Correlation with static and dynamic quenching efficiencies. *J. Phys. Chem.* **100**, 5541–5553.
34. Toyota, S. (2010) Rotational isomerism involving acetylene carbon. *Chem. Rev.* **110**, 5398–5424.
35. Okuyama, K., T. Hasegawa, M. Ito and N. Mikami (1984) Electronic spectra of tolan in a supersonic free jet: large-amplitude torsional motion. *J. Phys. Chem.* **88**, 1711–1716.
36. Klán, P. and J. Wirz (2009) *Photochemistry of organic compounds: From concepts to practice*. John Wiley & Sons, West Sussex.
37. Dougherty, G. and W. J. Pigram (1982) Spectroscopic analysis of drug-nucleic acid interaction. *Crit. Rev. Biochem.* **12**, 103–132.
38. Peacocke, A. R. and J. N. H. Skerrett (1956) The interaction of aminoacridines with nucleic acids. *Trans. Faraday Soc.* **52**, 261–279.
39. Hyde, J. E. and J. E. Hearst (1978) Binding of psoralen derivatives to DNA and chromatin: Influence of the ionic environment on dark binding and photoreactivity. *Biochemistry* **17**, 1251–1257.
40. Pérez-Flores, L., A. J. Ruiz-Chica, J. G. Delcros, F. M. Sánchez-Jiménez and F. J. Ramírez (2008) Effect of spermine conjugation on the interaction of acridine with alternating purine–pyrimidine oligodeoxyribonucleotides studied by CD, fluorescence and absorption spectroscopies. *Spectrochim. Acta Part A Mol. Biomol. Spectrosc.* **69**, 1089–1096.
41. van Holde, K. E., W. C. Johnson and P. S. Ho. (1998) Principles of Physical Biochemistry.
42. Anselmino, C., L. Voituriez and J. Cadet (1993) Characterization of the cis-syn and cis-anti Diastereoisomers of 5-Methoxypsoralen Pyrone-Side Monocycloadducts to Thymidine. *Chem. Res. Toxicol.* **6**, 858–865.
43. Rodgers, C. T. (2009) Magnetic field effects in chemical systems. *Pure Appl. Chem.* **81**, 19–43.
44. Eng, J. and T. J. Penfold (2020) Understanding and designing thermally activated delayed fluorescence emitters: beyond the energy gap approximation. *Chem. Rec.* **20**, 831–856.
45. Steiner, U. E. and T. Ulrich (1989) ChemInform abstract: Magnetic field effects in chemical kinetics and related phenomena. *Chem. Rev.* **89**, 51–147.
46. Demaret, J.-P., S. Brunie, J.-P. Ballini and P. Vigny (1989) Geometry of intercalation of psoralens in DNA approached by molecular mechanics. *Photochem. Photobiol.* **50**, 7–21.
47. Shim, S. C., H. K. Kang, S. K. Park and E. J. Shin (1987) Photophysical properties of some coumarin derivatives: 5,7-dimethoxycoumarin, 4',5'-dihydropsoralen, 8-methoxypsoralen (8-MOP) and 8-MOPTHD C4-cyclomonoadduct (THD thymidine). *J. Photochem.* **37**, 125–137.

3. Resümee

Im ersten Abschnitt dieses Kapitels sollen die Kernbotschaften der drei Veröffentlichungen resümiert werden. Im folgenden Abschnitt sind die Eigenschaften aller in dieser Arbeit untersuchten Psoralene gegenübergestellt. In den beiden letzten Abschnitten soll eine verwandte Gruppe, die der gewinkelten Psoralene vorgestellt und anschließend ein Blick in die Zukunft dieses Projekt geworfen werden.

3.1. Zusammenfassung der zentralen Ergebnisse

In der ersten Veröffentlichung wurde für das Psoralen-Derivat AMT die Photoanbindung an AT-DNA mittels verschiedener Techniken der stationären und zeitaufgelösten Spektroskopie sowie quantenchemischer Rechnungen untersucht. Die stationären Messungen im UV/Vis und IR zeigen die charakteristischen Banden der Edukt- und Produktabsorption im Grundzustand. In Nanosekunden-UV/Vis-Messungen ist eindeutig zu erkennen, dass die Anbindung im Mikrosekundenbereich stattfindet. Überlappende Signalbeiträge lassen allerdings keinen Rückschluss auf die involvierten transienten Spezies zu. Die Daten der Nanosekunden-IR-Spektroskopie dagegen zeigen scharfe, charakteristische Banden, welche eine Zuordnung ermöglichen. Mittels Lifetime Density Analysis kann die Anzahl an

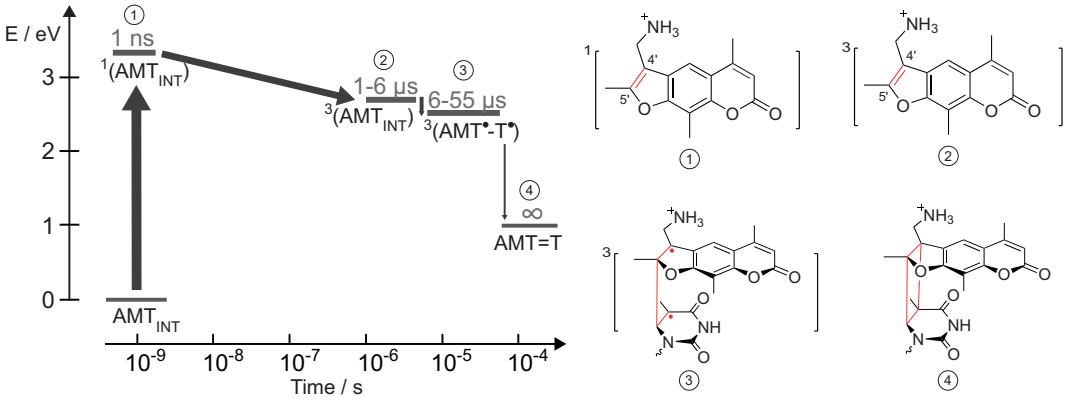

Abbildung 3.1. – Energieschema inklusive Lebensdauern der involvierten Spezies bei der Photoaddition von AMT an AT-DNA. Über die Breite der Pfeile sind die relativen Effizienzen für die Bildung der darauf folgenden Spezies ausgedrückt. Verändert entnommen aus Ref. [92].

Zeitkonstanten für den Anbindungsprozess auf mindestens drei Zeitkonstanten im Mikrosekundenbereich festgelegt werden. Gestützt durch quantenchemische Rechnungen ist die Zuordnung einer Zeitkonstante zum Zerfall des lokalen Triplettzustands von AMT und ei-

ne zum Zerfall eines Biradikals, bei welchem AMT über eine kovalente Bindung mit der Thymin-Base verbunden ist, möglich (siehe Abbildung 3.1). Die dritte Zeitkonstante ist vermutlich auf die Bildung von diastereomeren Produkten aufgrund von zwei unterschiedlichen Interkalationslagen zurückzuführen [93].

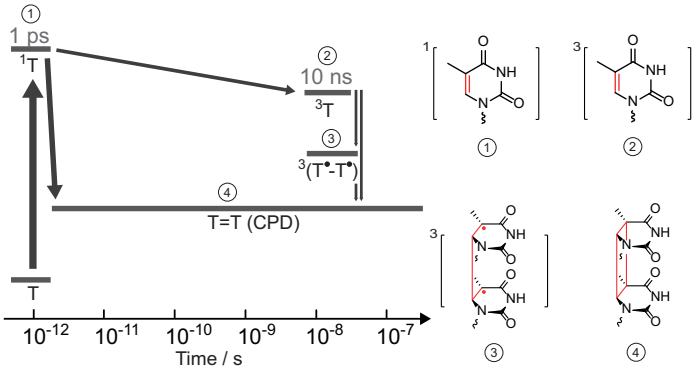

Abbildung 3.2. – Energieschema zur Entstehung des CPD-Schadens. Über die Breite der Pfeile sind die relativen Effizienzen für die Bildung der darauf folgenden Spezies ausgedrückt.

Eine weitere zentrale Aussage dieser Veröffentlichung kann durch die Gegenüberstellung der Photoaddition des Psoralens an die Thymin-Base mit der der Thymindimerisierung getroffen werden. Wie in Abschnitt 1.1 beschrieben, ist der häufigste direkte Photoschaden an der DNA die Entstehung eines Cyclobutan-Pyrimidin-Dimers (CPD). Aufgrund der strukturellen Ähnlichkeit beider Photoschäden, wäre zunächst auch ein ähnlicher Anbindungsprozess zu erwarten. Tatsächlich unterscheiden sich beide aber in vielerlei Hinsicht. Im Gegensatz zum Psoralen entsteht der CPD-Schaden hauptsächlich über den angeregten Singulettzustand (siehe Abbildung 3.2) [15]. Der Singulettzustand lebt nur ca. 1 ps. Obwohl der angeregte Singulettzustand von AMT mit ca. 1 ns drei Größenordnungen länger lebt, ist keine direkte Bildung des Photoprodukts aus diesem Zustand beobachtbar. Auch die Entstehung des CPD-Schadens kann, wenn auch mit geringen Ausbeuten, über den Triplettzustand ablaufen [94]. Als Gemeinsamkeit zum Psoralenphotoschaden, konnte auch hier mittels zeitaufgelöster IR-Spektroskopie die Entstehung eines intermediären Biradikals mit einer kovalenten Bindung zwischen den zwei Thymin-Molekülen festgestellt werden. Das Verstehen der Unterschiede und Gemeinsamkeiten dieser Prozesse kann wichtige Hinweise auf eine gezielte Steuerung von DNA-Photoreaktionen liefern.

Die zweite Veröffentlichung beschäftigt sich mit dem Anbindungsprozess der pharmazeutisch genutzten Psoralene, 8-MOP, TMP und 5-MOP, an die DNA. Stationäre Messungen im UV/Vis und IR zeigen wesentliche Unterschiede zwischen diesen Derivaten. Bei Betrachtung der Interkalationsaffinität sowie Reaktionsquantenausbeute ist das Derivat TMP dem am häufigsten applizierten Derivat 8-MOP überlegen. 8-MOP wiederum weist eine um zwei Größenordnungen höhere Wasserlöslichkeit auf. Für 5-MOP kann die Entstehung des Photoprodukts im UV-A-Bereich nicht verfolgt werden, da sich das dort absorbierende Furanmonoaddukt nicht bildet. Im IR können allerdings die Signaturen des Pyronmonoaddukts detektiert werden. Nanosekunden-UV/Vis-Messungen zeigen für 8-MOP und TMP eindeutig eine Anbindung über den Triplettzustand. Analog zu AMT, können auch hier

mehr als eine Zeitkonstante im Mikrosekundenbereich gefunden werden (siehe Abbildung 3.3). Dies deutet auf die Entstehung des intermediären Biradikals hin. Abschätzungen machen deutlich, dass die einmal populierten Triplettzustände mit hohen Effizienzen an die Thymin-Base der DNA binden. Dieses Ergebnis unterstreicht damit die Wichtigkeit des Triplettzustands für die Anbindung der Psoralene.

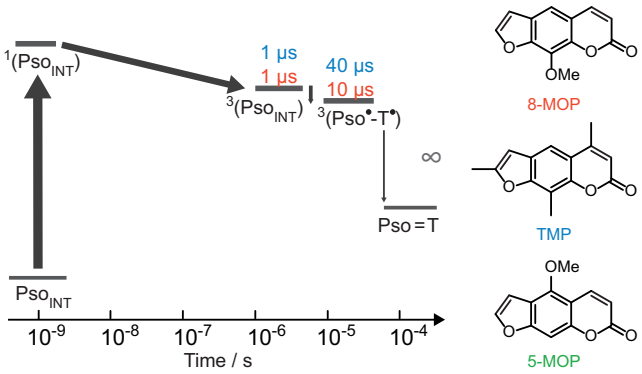

Abbildung 3.3. – Energieschema und Lebensdauern der involvierten Spezies bei der Photoaddition der rechts dargestellten Psoralene (Pso) an AT-DNA. Für das ebenfalls in der Studie untersuchte 5-MOP wird, anders als für 8-MOP und TMP, der Anbindungsprozess hauptsächlich über die Pyronseite vermutet. Zeitaufgelöste Daten liegen zu diesem Zeitpunkt noch nicht vor.

Die dritte Veröffentlichung behandelt die am Lehrstuhl für Organische Chemie unter der Leitung von Prof. Dr. Thomas J. J. Müller synthetisierten Psoralene. Die an Position 5 substituierten 8-MOP-Derivate (siehe Abbildung 3.4) zeigen in stationären UV/Vis Messungen eine eindeutige Rotverschiebung der Absorption. Wie in Abschnitt 1.5 beschrieben, wurde mit der Rotverschiebung das Ziel verfolgt, den PET von der Guanin-Base zum Psoralen zu unterdrücken. Zudem weisen die Psoralene durch das Einbringen einer positiven Ladung vergleichsweise hohe Wasserlöslichkeiten auf. Untersuchungen zur Anbindung an die DNA ergaben Reaktionsquantenausbeuten von unter 0.005 für alle vier Derivate. Femtosekunden-UV/Vis-Messungen zeigen für die Methylpyridinium-substituierten Derivate eine Erklärung für die niedrigen Reaktionsquantenausbeuten (siehe Abbildung 3.4, links). Ein schneller intramolekularer Elektrontransfer vom 8-MOP-Teil des Moleküls zum Substituenten löscht den angeregten S_1-Zustand. Der Rücktransfer findet ebenso im Pikosekundenbereich statt. Eine Population des Triplettzustands ist nicht zu erkennen. Für die beiden anderen Derivate (siehe Abbildung 3.4, rechts) ist die Erklärung nicht so eindeutig. Zeitaufgelöste Messungen deuten auf eine Population des Triplettzustands hin. Eine mögliche Erklärung für das Ausbleiben der Anbindung an die DNA ist die Interkalationslage von Position-5-substituierten Psoralenen. Wie zuvor beschrieben bildet das bekannte 5-substituierte 5-MOP aufgrund der Interkalationslage ausschließlich das Pyronmonoaddukt, da die Furandoppelbindung eine zu große räumliche Distanz zur Thymin-doppelbindung aufweist [95]. Die Botschaft dieser Studie ist daher, dass die Substitutionsposition sowie die Position der positiven Ladung entscheidenden Einfluss auf die Effizienz des Psoralens haben. Strategien zur Verbesserung der Eigenschaften sollen im folgenden Abschnitt noch einmal im Detail erläutert werden.

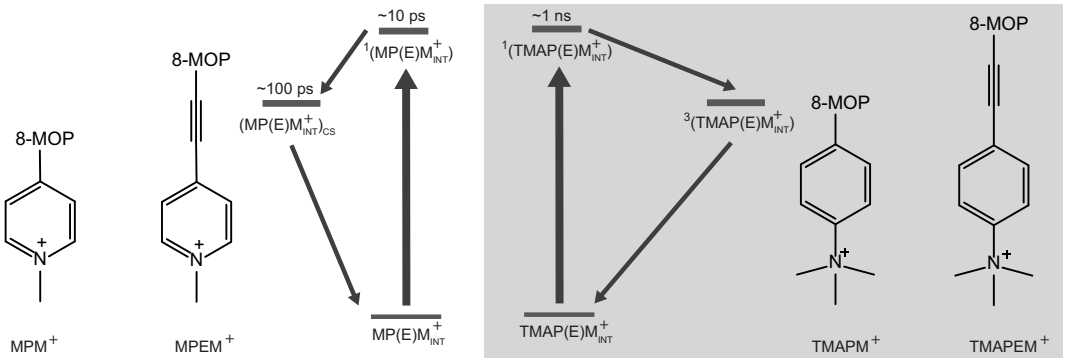

Abbildung 3.4. – Energieschema der involvierten Spezies nach UV-Anregung von MPM^+, $MPEM^+$, $TMAPM^+$ und $TMAPEM^+$. Der angeregte Singulettzustand der Methylpyridinium-substituierten Derivate (links) wird durch einen intramolekularen Elektronentransfer gelöscht. Bei den Trimethylaminophenyl-substituierten Derivaten (rechts) wird der Triplettzustand bevölkert. Eine signifikante Anbindung an die DNA ist für keines der Derivate zu beobachten.

3.2. Gibt es das „perfekte“ Psoralen?

Im Rahmen dieser Arbeit konnte der Anbindungsprozess eines Psoralens an die DNA aufgeschlüsselt und Kriterien für die Effizienz dieser Anbindung identifiziert werden. Wie in Kapitel 1 beschrieben sind Wasserlöslichkeit und Interkalationsaffinität zu DNA bekannte Kriterien für ein effizientes Psoralen. In dieser Arbeit konnte außerdem gezeigt werden, dass die Triplettquantenausbeute ebenso eine entscheidende Rolle spielt. Eine Verbesserung dieser Eigenschaften führt somit letztendlich zur Erhöhung der Reaktionsquantenausbeute für die Anbindung an DNA und steigert damit die Potenz des Psoralens. Außerdem sollte die Effektivität massiv steigen, wenn der PET mit Guanin verhindert werden kann. Für diese vier Kriterien gibt es jeweils Strategien zur Verbesserung dieser Eigenschaften.

Wasserlöslichkeit

Ein großer Bestandteil der Zelle ist Wasser. Das Psoralen muss sich also zunächst in Wasser lösen, um in die Nähe der DNA im Zellkern zu gelangen. Die verschiedenen Psoralen-Derivate weisen je nach Substitutions-Muster sehr unterschiedliche Wasserlöslichkeiten auf. Eine gute Übersicht bieten die Arbeiten von Isaacs et al. aus den Jahren 1977 [44] und 1982 [43]. Es zeigt sich der Trend, dass eine Substitution mit Methyl-Gruppen die Löslichkeit verringert, während die Einbringung einer positiven Ladung die Löslichkeit deutlich erhöht. Dieser Trend konnte auch für die in Abschnitt 2.3. beschriebenen, neuen Psoralene bestätigt werden. Die Wasserlöslichkeiten und weitere Eigenschaften der in dieser Arbeit behandelten Psoralene sind noch einmal zusammengefasst in Tabelle 3.1 zu finden.

Interkalationsaffinität

Die Interkalationsaffinität lässt sich mittels der Dissoziationskonstante K_D beschreiben. Je kleiner das Produkt aus freien Psoralen-Molekülen und DNA-Interkalationsstellen im Verhältnis zum Interkalations-Komplex, desto höher ist die Affinität des Psoralens zur DNA.

Auch hier lässt sich der Trend feststellen, dass eine positive Ladung zu einer hohen Interkalation führt (siehe Tabelle 3.1 und Ref. [43]). Im Gegensatz zur Wasserlöslichkeit scheint sich eine Methylierung allerdings auch positiv auf die Interkalationsaffinität auszuwirken. Dieser Effekt lässt sich ebenso für die gewinkelten Psoralene (siehe nächster Abschnitt) feststellen [96]. Begründet liegt dies in der Affinität der hydrophoben Methyl-Derivate zur hydrophoben Interkalationsumgebung innerhalb der DNA. Isaacs et al. stellten außerdem einen negativen Effekt auf die Interkalation durch das Einbringen von Hydroxymethyl- und Methoxymethyl-Gruppen an den Positionen 4’ und 5 fest [43]. Sie führten dies auf sterische Hinderung zurück.

Tabelle 3.1. – Übersicht zu ausgewählten Eigenschaften der in dieser Arbeit behandelten Psoralene. c_{sat} steht für die Sättigungskonzentration der Psoralene in Wasser, K_D ist die Dissoziationskonstante für die Interkalation in AT-DNA, Φ_T die Triplettquantenausbeute in Wasser, Φ_R die Reaktionsquantenausbeute für die Anbindung an AT-DNA, E_{00} die Übergangsenergie der Schwingungsgrundzustände von S_0 und S_1 und E^0_{Red} ist das Standardreduktionspotential gegen eine Normalwasserstoffelektrode (NHE) in Acetonitril.

	c_{sat} / mM	K_D / M	Φ_T	Φ_R	E_{00} / eV	E^0_{Red} / V
8-MOP	0.2 [43]	$1.1 \cdot 10^{-3}$	0.06 [97]	0.04	2.93 [74]	-1.7 [74]
5-MOP	0.03 [34]	$1.8 \cdot 10^{-4}$	< 0.01 [97]	0.017	-	-
TMP	0.003 [43]	10^{-4}	0.1 [98]*	0.4	-	-
AMT	34 [43]	$4.4 \cdot 10^{-4}$ [74]	0.2 [50]	0.12	3.21 [74]	-1.9 [74]
MPM^+	6	$4.4 \cdot 10^{-4}$	-	< 0.005	2.8	-0.82
$MPEM^+$	1	$8.1 \cdot 10^{-5}$	-	< 0.005	2.7	-0.7
$TMAPM^+$	3	$2.6 \cdot 10^{-4}$	0.15	< 0.005	2.9	-1.2
$TMAPEM^+$	4	$9.2 \cdot 10^{-6}$	-	< 0.005	2.7	-1.7

*in Methanol

Triplettquantenausbeute

Wie in Abschnitt 2.1 anhand von zeitaufgelösten Messungen eindeutig gezeigt wurde, findet die Anbindung des Psoralens AMT an die DNA über einen lokalen Triplettzustand von AMT statt. In Abschnitt 2.2 konnte auch für die Derivate 8-MOP und TMP gezeigt werden, dass die Population des Triplettzustands maßgeblich für die Anbindung ist. Eine hohe Triplettquantenausbeute ist daher ein entscheidender Faktor für die Effizienz des Psoralens im Hinblick auf die PUVA-Therapie. In Tabelle 3.1 sind die Triplettquantenausbeuten Φ_T der Derivate in Wasser gezeigt. Eine Abweichung der Ausbeuten von in DNA interkaliertem Psoralen ist allerdings nicht auszuschließen. Eine Abhängigkeit der Triplettquantenausbeute von der Polarität der Lösemittelumgebung konnte für einige Derivate beobachtet werden [97, 98]. In dieser Arbeit konnte außerdem gezeigt werde, dass die Effizienz zur Ausbildung des Photoprodukts aus dem Triplettzustand, das heißt der Anteil an Photoprodukt, der aus der Population des Triplettzustands folgt, sehr groß ist. Dies wird auch aus dem Vergleich der Triplettquantenausbeuten mit den Reaktionsquantenausbeuten Φ_R für die Anbindung sichtbar. Eine Ausnahme bildet das Derivat $TMAPM^+$. Trotz hoher Triplettquantenausbeu-

te konnte keine signifikante Photoproduktbildung festgestellt werden. Wie in Abschnitt 2.3 beschrieben, könnte das auf die Interkalationslage der an Position 5 substituierten Psoralene zurückzuführen sein. Diese Substitutionsstelle scheint eine Interkalation so zu beeinflussen, dass der Abstand der reaktiven Doppelbindung zur Thymin-Base signifikant größer und daher eine Anbindung um einiges unwahrscheinlicher wird. Demaret et al. begründen damit auch die Präferenz von 5-MOP zur Bildung des Pyron-Monoaddukts [62]. Die für andere Derivate bevorzugte Furandoppelbindung ist durch die geometrische Lage des Psoralens zwischen den Basen zu weit von der Thymin-Doppelbindung entfernt. Auch in der Studie von Isaacs et al. [43] schneiden die an Position 5 substituierten Psoralene um mindestens eine Größenordnung schlechter in der Reaktionsquantenausbeute ab im Vergleich zum nicht-substituierten Derivat.

PET mit Guanin

Befindet sich das interkalierte Psoralen in der Nähe einer Guanin-Base, so wird der angeregte Zustand des Psoralens durch einen schnellen photoinduzierten Elektronentransfer von Guanin aufs Psoralen gelöscht. Der Elektrontransfer tritt bei allen bisher untersuchten Derivaten auf und erklärt die geringen Reaktionsquantenausbeuten bei Verwendung von natürlicher bzw. Guanin-haltiger DNA [74]. Die in Abschnitt 1.5 beschriebene Strategie die E_{00}-Energie von 8-MOP durch geeignete Substitution zu senken war erfolgreich (siehe Tabelle 3.1). Allerdings hat sich das Standardreduktionspotential durch die Substitution ebenfalls geändert. Geschuldet ist dies vermutlich der positiven Ladung. Das Psoralen wird „leichter reduzierbar“ und damit steigt das Reduktionspotential. Einzig $TMAPEM^+$ ist in dieser Hinsicht vielversprechend. Da allerdings die Voraussetzung einer Anbindung an AT-DNA nicht gegeben ist, ist auch dieses Derivat für den Einsatz in der PUVA-Therapie ungeeignet. Allerdings könnte diese Substitutionsgruppe für eine andere Position, etwa Position 8 im Psoralen, in Betracht gezogen werden.

3.3. Eine verwandte Gruppe – die gewinkelten Psoralene

Angelicin ist der Grundkörper der Gruppe der gewinkelten Psoralene (siehe Abbildung 3.5). Gewinkelte Psoralene bilden, im Gegensatz zu den linearen Psoralenen, nur Monoaddukte mit DNA [96]. Sie werden daher auch monofunktionelle Psoralene genannt. Diese Eigenschaft, keine Crosslinks innerhalb der DNA bilden zu können, zeigte positive Eigenschaften für die Therapie. Während nach Anwendung der PUVA Therapie mit linearen Psoralenen unliebsame Nebenwirkungen durch Phototoxizität auf der Haut auftraten, wurde festgestellt, dass gewinkelte Psoralene kaum diese Wirkung zeigten [96, 99, 100]. Zunächst wurde an-

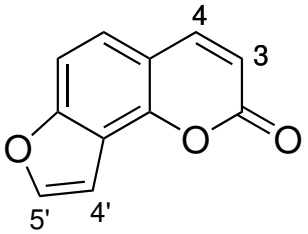

Abbildung 3.5. – Struktur von Angelicin.

genommen, dass Crosslinks für den gewünschten zellzerstörenden Effekt nötig sind. Diese These konnte aber von verschiedenen Gruppen widerlegt werden [101, 102]. Angelicin selbst weist allerdings nur eine sehr geringe Effizienz zur Photoanbindung an DNA auf. Die Substitution mit Methyl- und Methoxy-Gruppen kann aber zu einer starken Steigerung dieser führen [99, 103]. Die Methylierung an der 4'-Position [96, 100] und hier besonders das Derivat 4,4',6-Trimethylangelicin zeigt vielversprechende Eigenschaften, wie Bacchichetti et al. zeigten [104]. Als eine weitere außergewöhnliche Eigenschaft konnten Gia et al. zeigen, dass einige dieser gewinkelten Psoralene neben Thymin auch ähnlich effizient an Cytosin anzubinden scheinen [103]. Sie isolierten erfolgreich beide Addukte für das Derivat 4,4'-Dimethyl-5-methoxyangelicin mittels enzymatischer Zersetzung und anschließender Auftrennung mit HPLC. Diese beiden Derivate sind damit interessante Kandidaten für die Untersuchung ihrer photophysikalischer Eigenschaften mit den Methoden aus dieser Arbeit.

3.4. Ein Ausblick

Das Ziel dieser Arbeit war es, den Anbindungsmechanismus des Psoralens an die DNA aufzuklären. Dahingehend konnte wie in den Abschnitten 2.1 und 2.2 beschrieben die größten Fragestellungen geklärt werden. Außerdem konnten neue Erkenntnisse zur Synthese effektiverer Psoralen-Derivate gewonnen werden. Die in dieser Arbeit vorgestellten Derivate erfüllen noch nicht den Ansprüchen eines Medikaments für die PUVA-Therapie, aber es wird deutlich, welche Eigenschaften bei der Synthese potenter Psoralene zu beachten sind. Diese Eigenschaften bedingen sich teilweise und daher muss an den möglichen Stellschrauben geschickt gedreht werden. Besonders deutlich wird, dass eine Substitution an Position 5 vermieden werden sollte. Da große Substituenten keinen hinderlichen Einfluss auf die Interkalation zu nehmen scheinen, könnte eine Substitution der $TMAPM^+$- und $TMAPEM^+$-Substituenten an anderer Position in Betracht gezogen werden. Weiterhin könnte die Untersuchung und Substitution der gewinkelten Psoralene eine interessante Alternative bieten.

A. Anhang

The publication with the title „The Photoaddition of a Psoralen to DNA Proceeds via the Triplet State“ is reprinted with permission from Janina Diekmann, Julia Gontcharov, Sascha Fröbel, Christian Torres Ziegenbein, Wolfgang Zinth, and Peter Gilch, *Journal of the American Chemical Society* **2019** 141 (34), 13643-13653. doi: 10.1021/jacs.9b06521. Copyright 2019 American Chemical Society.

The publication titled „Tracing the Photoaddition of Pharmaceutical Psoralens to DNA“ is reprinted with permission and can be cited as Diekmann, J.; Theves, I.; Thom, K.A.; Gilch, P., *Molecules* **2020**, 25, 5242. doi: 10.3390/molecules25225242.

The publication titled „Synthesis and Photophysics of Water-Soluble Psoralens with Red-Shifted Absorption“ is reprinted with permission and can be cited as Bertling, J., Thom, K.A., Geenen, S., Jeuken, H., Presser, L., Müller, T.J.J. and Gilch, P., *Photochem Photobiol.* **2021** doi: 10.1111/php.13480

Supporting Information: The Photoaddition of a Psoralen to DNA proceeds via the Triplet State

Janina Diekmann,[†] Julia Gontcharov,[‡] Sascha Fröbel,[†,¶] Christian Torres Ziegenbein,[†,§] Wolfgang Zinth,[‡] and Peter Gilch[*,†]

†*Institut für Physikalische Chemie, Heinrich-Heine-Universität Düsseldorf, Universitätsstr. 1, 40225 Düsseldorf*

‡*Lehrstuhl für BioMolekulare Optik, Fakultät für Physik and Center for Integrated Protein Science Munich CIPSM, Ludwig-Maximilians-Universität München, Oettingenstrasse 67, 80538 München, Germany*

¶*Present address: Covestro Deutschland AG, Kaiser-Wilhelm-Allee 60, 51373 Leverkusen, Germany*

§*Present address: TÜV Rheinland Industrie Service GmbH, Am Grauen Stein, 51105 Köln, Germany*

E-mail: gilch@hhu.de

Contents

1 Experimental

1.1 Samples

AMT hydrochloride was synthesized from trioxsalen (TCI Europe, >98 %) as described before.[S1] Lyophilized DNA oligomers, 5'-$(TA)_{20}$-3' (HPLC purified), were purchased from IBA GmbH (Göttingen, Germany). H_2O (HPLC gradient grade) was purchased from Fisher Chemical and oxygen (99.998 %) from Air Liquide. All chemicals were used without further purifications. The DNA was dissolved in phosphate-buffered saline (Sigma-Aldrich, BioUltra, pH 7.2, 66 mM Na_2HPO_4/NaH_2PO_4 with 100 mM NaCl and 3 mM KCl added) or for measurements in the infrared in D_2O (purchased from Sigma-Aldrich with 99.9 atom % and buffered with 66 mM Na_2HPO_4/NaH_2PO_4, 100 mM NaCl and 3 mM KCl, pD 7.8). All DNA concentrations refer to base pairs (bp). Before each measurement annealing of the DNA strands was performed. The dissolved DNA was heated to about 90 °C in a water bath. The bath was then slowly cooled down to room temperature.

1.2 Steady-state spectroscopy

UV/Vis absorption spectra were recorded with a spectrometer from Perkin Elmer (Lambda 19). The solutions were measured in a fused silica cuvette (path length of 1 cm) from Hellma. A Vertex 80v FT-IR spectrometer from Bruker was used for steady-state measurements in the infrared. Custom-made cuvettes with CaF_2-windows (path length of 100 µm) were used. The steady-state measurements were performed at room temperature (20 - 21 °C). The impact of the photo-addition on the steady-state spectra was studied by illuminating the sample solution with an LED emitting at 375 nm (Nichia NSPU510CS) in the IR set-up and with the xenon lamp of a fluorimeter (Horiba, Fluoromax 4) at 370 nm for measurements in the UV/Vis. In the UV/Vis experiments the solutions were illuminated in 1 cm cuvettes with magnetic stirring. The light power P impinging on the sample amounted to 1.4 mW. With

this power and the illumination time t photon equivalents $PE(t)$ were computed *via*

$$PE(t) = \frac{n_{abs}(t)}{n_{AMT}} = \frac{I_0 \cdot \int_0^t 1 - 10^{-A_{Ex}(t)} dt}{n_{AMT}} = \frac{P \cdot \int_0^t 1 - 10^{-A_{Ex}(t)} dt}{h \cdot \frac{c}{\lambda_{Ex}} \cdot N_A \cdot n_{AMT}}.$$

The amount of substance n_{abs} refers to the absorbed photons, n_{AMT} is the total amount of AMT in the cuvette. $A_{Ex}(t)$ is the absorption of the solution at the excitation wavelength λ_{Ex}. Due to the progressing photo-addition it decreases with time. h is the Planck's constant, c the speed of light, and N_A Avogadro's number. A $PE(t)$ of one implies that after an illumination time t each AMT molecule has in average absorbed one photon. In the IR experiments, illumination was performed within the spectrometer with the LED output directed towards the IR cuvette. Since the light power absorbed by the sample could not be quantified precisely, no photon equivalents are reported.

1.3 Nanosecond flash photolysis

Probe light was obtained from a xenon lamp (L2273, Hamamatsu). Nanosecond transient absorption data were acquired with a LKS.60 spectrometer from Applied Photophysics in a right-angle geometry. The sum-frequency (355 nm) of the output of a Q-switched Nd:YAG laser (InnoLas, SpitLight 600) and its second harmonic was used for excitation. The pulses had a duration of 12 ns (full width at half maximum, FWHM) and a repetition rate of 1 Hz. The average pulse energy was 3 mJ. The spot diameter within the samples amounted to 5 mm. The solution was pumped through an all-quartz flow-through cuvette (176.766-QS, Hellma) with dimensions of 2 mm along the pump direction and 10 mm along the probe direction. Probe light transmitted through the flow cell was detected by a photomultiplier. At the excitation wavelength, the optical density was set to ~ 0.4 for a 1 cm path length. The time traces ranging from 300 to 600 nm were measured in 5 nm steps. For each time trace 10 consecutive measurements were averaged. All measurements were performed at room temperature (~ 21 °C).

1.4 Nanosecond UV Pump IR Probe spectroscopy

The time-resolved pump-probe set-up has been described previously.[S2] A femtosecond Ti:sapphire laser amplifier system (Tsunami/Spitfire Pro, Spectra Physics; repetition rate 1 kHz, pulse duration of $\sim$ 120 fs, wavelength 800 nm) generates tunable mid-IR (1375 cm^{-1} to 1750 cm^{-1}) probe pulses *via* a combination of non-collinear and collinear optical parametric amplifiers and subsequent difference-frequency mixing in $AgGaS_2$.[S3] The mid-IR pulses were analysed by a grating spectrometer (Chromex 250 IS, Bruker) and a 64-channel MCT array detector (IR-0144, Infrared Systems Development). Magic angle polarisations of the pump and the probe pulses were used. Nanosecond excitation pulses were supplied by an EKSPLA NT242 system (repetition rate 1 kHz, pulse duration 3 ns), synchronized to the IR-pulses from the femtosecond laser system.[S4,S5] At 355 nm pulse energies of ca. 3.4 µJ (spot diameter 170 µm x 170 µm) were used. The investigated solutions were kept in a flow-through cuvette (path length ca. 110 µm, CaF_2 windows). A peristaltic pump exchanged the sample volume between two successive pump pulses. All measurements were performed at ambient oxygen concentrations and room temperature (23 °C).

1.5 Data Analysis

Time dependent spectroscopic data were analyzed with two approaches. In the first approach, global lifetime analysis (GLA),[S6,S7] the wavelength λ (UV/Vis) or wavenumber $\tilde{\nu} = 1/\lambda$ (IR) and time dependent difference absorption $\Delta A(\lambda, t)$ is fitted with the following trial function

$$\Delta A(\lambda, t) = IRF \otimes \sum_{i=a}^{n} \Delta A_i(\lambda) \cdot e^{-\frac{t}{\tau_i}}.$$

$IRF\otimes$ stands for the convolution with the instrumental response function which is approximated by a Gaussian. Such a convolution was only performed for the UV/Vis experiment (FWHM of 12 ns). Due to an IRF with a FWHM of 3 ns the convolution was not necessary for the IR experiment. The fit yields the decay associated difference spectra (DADS) $\Delta A_i(\lambda)$

and the corresponding time constants τ_i.

The second approach, lifetime density analysis (LDA),[S7–S9] was applied to the IR data. In LDA, one attempts to express the experimental data $\Delta A(\tilde{\nu}, t)$ with this integral

$$\Delta A(\tilde{\nu}, t) = \int_0^\infty \Phi(\tilde{\nu}, \tau) \cdot e^{-\frac{t}{\tau}} d\tau.$$

Hereby, $\Phi(\tilde{\nu}, \tau)$ is a distribution function depending on the variables τ and $\tilde{\nu}$. For numerical reasons this integral is difficult to invert. The distribution function $\Phi(\tilde{\nu}, \tau)$ is therefore obtained using a fitting procedure with a large number (about 100) of fixed time constants τ_j evenly distributed on a logarithmic time axis and a regularization term. LDA as implemented in OPTIMUS[S7] was used. Amplitudes for 250 lifetimes spread on a logarithmic scale between 1 ns and 1 ms were calculated. For all wavenumbers, a fixed IRF of 3 ns was implemented. The upper limit of the time range in the LDA analysis (1 ms) exceeds the experimental one (70 µs). Therefore, signatures for lifetimes larger than 70 µs are the results of an extrapolation. The obtained signatures are similar to the DADS for "infinite" delay times in GLA. With a regularization factor of 0.98 an optimum between smoothing and residuals was obtained.

2 ns-IR: DADS of AMT with AT-DNA

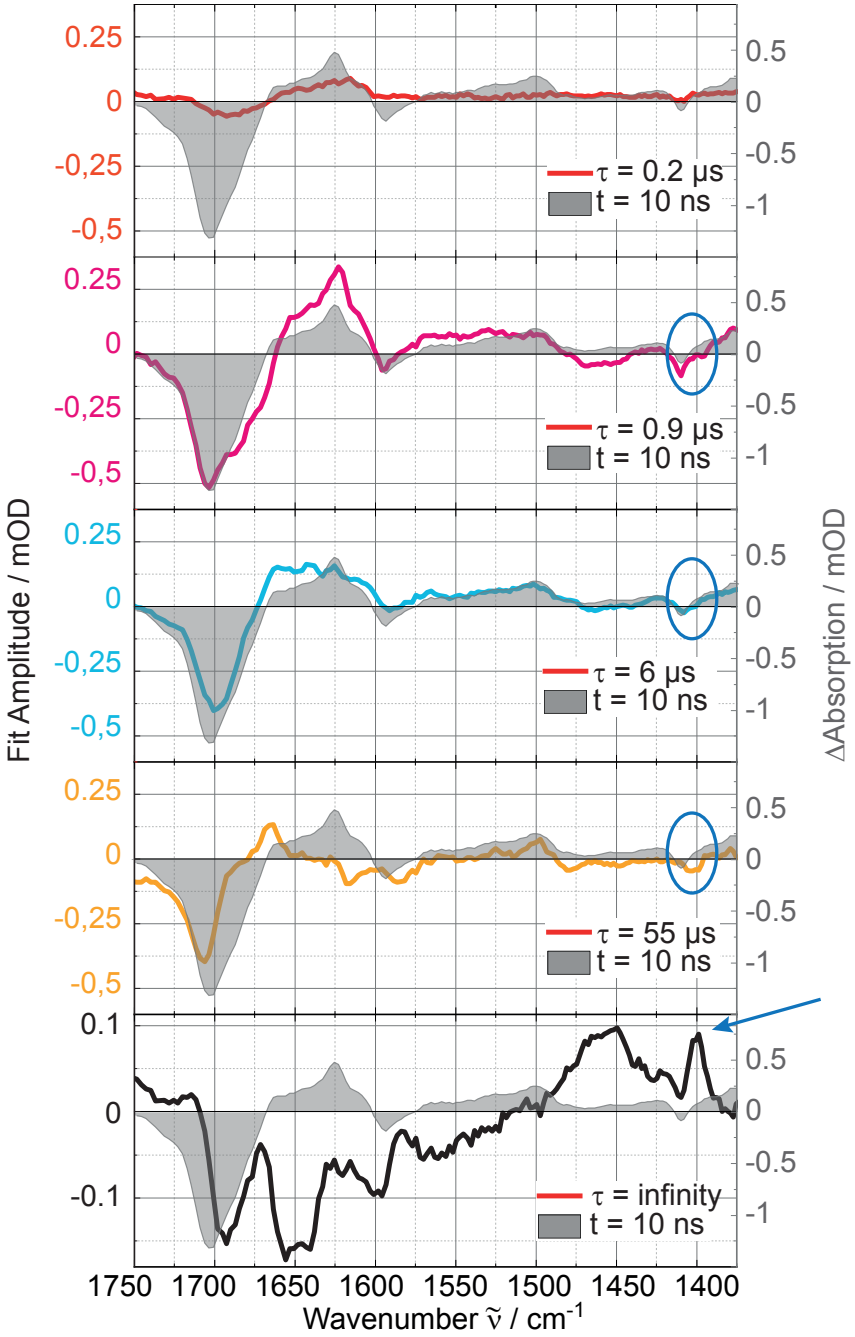

Figure S1: DADS of 0.2, 0.9, 6 and 55 µs in comparison with the transient spectrum after 10 ns of AMT with AT-DNA. The spectrum after 10 ns shows the signature of the triplet state. Bleaching bands at 1703, 1593 and 1410 cm^{-1} are visible. The bleaching band at 1410 cm^{-1} is highlighted by a blue circle. The DADS of 0.9 and 6 µs show a negative amplitude at this wavenumber indicating ground state recovery from these states. In the DADS of 55 µs a negative amplitude is detected at lower wavenumbers around 1400 cm^{-1}, pointing to the formation of the photoproduct band, marked with an arrow, from this state.

3 Computed IR spectra in Pyridine

Except for a different dielectric constant (13, value of pyridine), the same quantum chemical method was applied as for the data given in Figure 6 (main text). The IR spectra computed for the solvent pyridine (Figure S2) resemble the ones for water (Figure 6). In comparison to water, the carbonyl bands of all species are slightly up-shifted (by up to 12 cm^{-1}) in pyridine. Also the IR transition strength is slight affected, it is reduced by up 10 %.

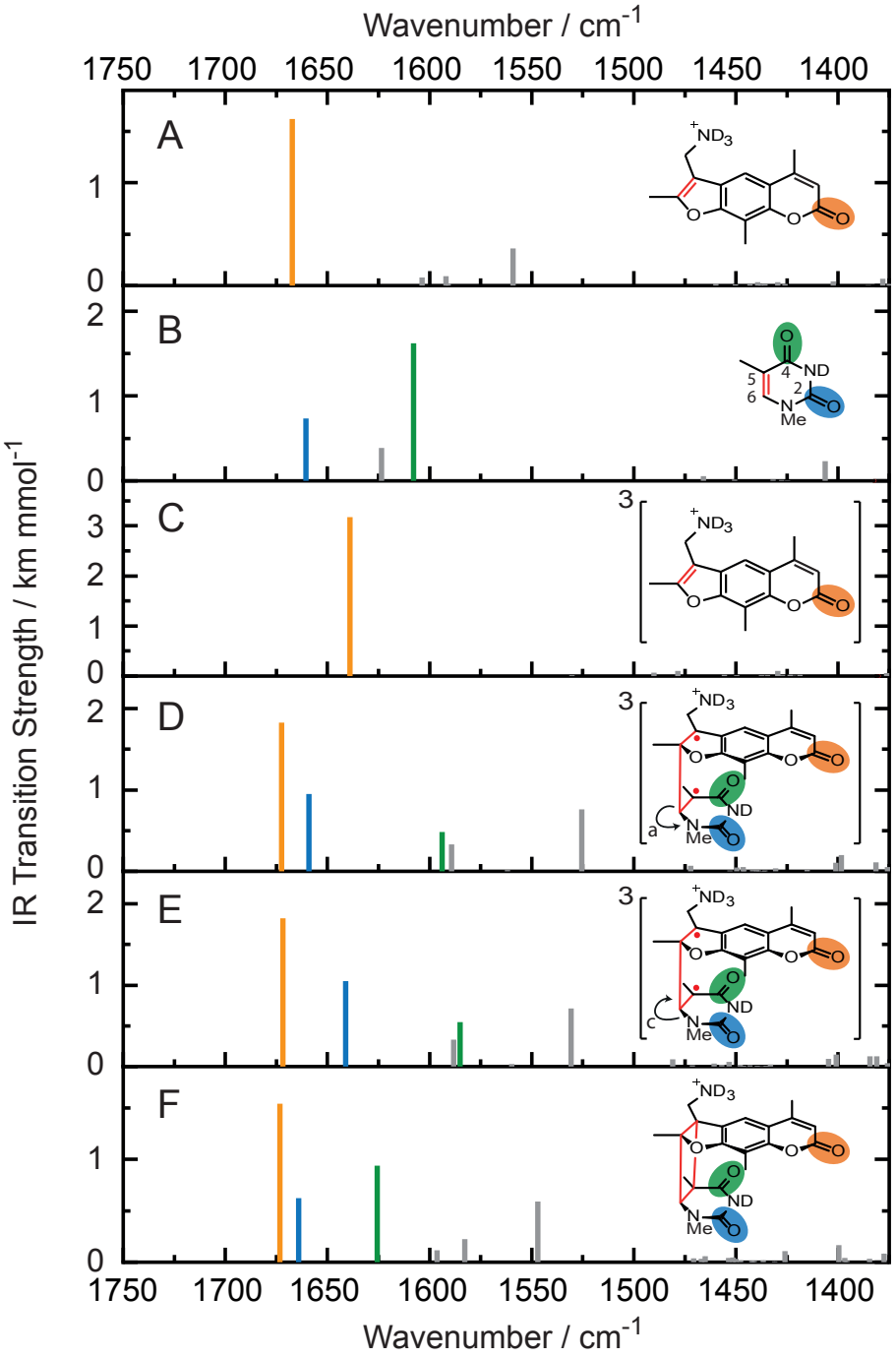

Figure S2: Computed IR stick spectra of AMT and 1-methylthymine derived species. The solvent environment was taken into account with the dielectric constant of pyridine (13). The positions of the bars represent the corrected (scaling factor of 0.96) wavenumbers and their heights the IR transition strength. In the structural formulas on the right the C=O bands contributing predominantly to the strongest IR bands are color coded.

4 Reaction efficiency of the triplet state η_R^T

The efficiency η_R^T, with which the $^3(\mathrm{AMT_{INT}})$ state forms the adduct is defined as the ratio of two concentrations

$$\eta_R^T = \frac{c_{PA}}{c_T}. \tag{1}$$

Hereby, the concentration of photo-adducts is given by c_{PA} and the one of the initially present $\mathrm{AMT_{INT}}$ in the triplet state by c_T. The ration of these concentrations is obtained *via*

$$\eta_R^T = \frac{\Delta A(\tilde{\nu}_{PA}, t=\infty)}{\Delta A(\tilde{\nu}_T, t=10\ ns)} \cdot \frac{\Delta\epsilon_T(\tilde{\nu}_T)}{\Delta\epsilon_{PA}(\tilde{\nu}_{PA})} = \frac{0.15\ mOD}{1.32\ mOD} \cdot \frac{1197\ M^{-1}cm^{-1}}{509\ M^{-1}cm{-}1} = 0.27. \tag{2}$$

The amount of photo-adducts is proportional to the amplitude spectrum for "infinite" delay times $\Delta A(\tilde{\nu}, t=\infty)$ (see Figure S3**A**). For the evaluation of the photo-adduct signature a detection wavenumber of 1693 $\mathrm{cm^{-1}}$ was chosen since here, the contribution of heated D_2O in ns-IR is small.[S10] At early delay times only the triplet state of $\mathrm{AMT_{INT}}$ contributes to the signal, therefore $\Delta A(\tilde{\nu}_T, t = 10$ ns) is proportional to its concentration (see Figure S3**B**). The difference absorption coefficients $\Delta\epsilon_{PA}(\tilde{\nu})$ of the photo-adduct were obtained from steady-state illumination (cf. Figure 3) (see Figure S3**C**). For the triplet state and its bleach contribution at 1704 $\mathrm{cm^{-1}}$, $\Delta\epsilon_T(\tilde{\nu}_T)$ was taken to equal $-\epsilon_G(\tilde{\nu}_{max})$. The respective absorption coefficient $\epsilon_G(\tilde{\nu})$ of the ground state is given in Figure S3**D**. With this input an efficiency η_R^T of 0.27 results.

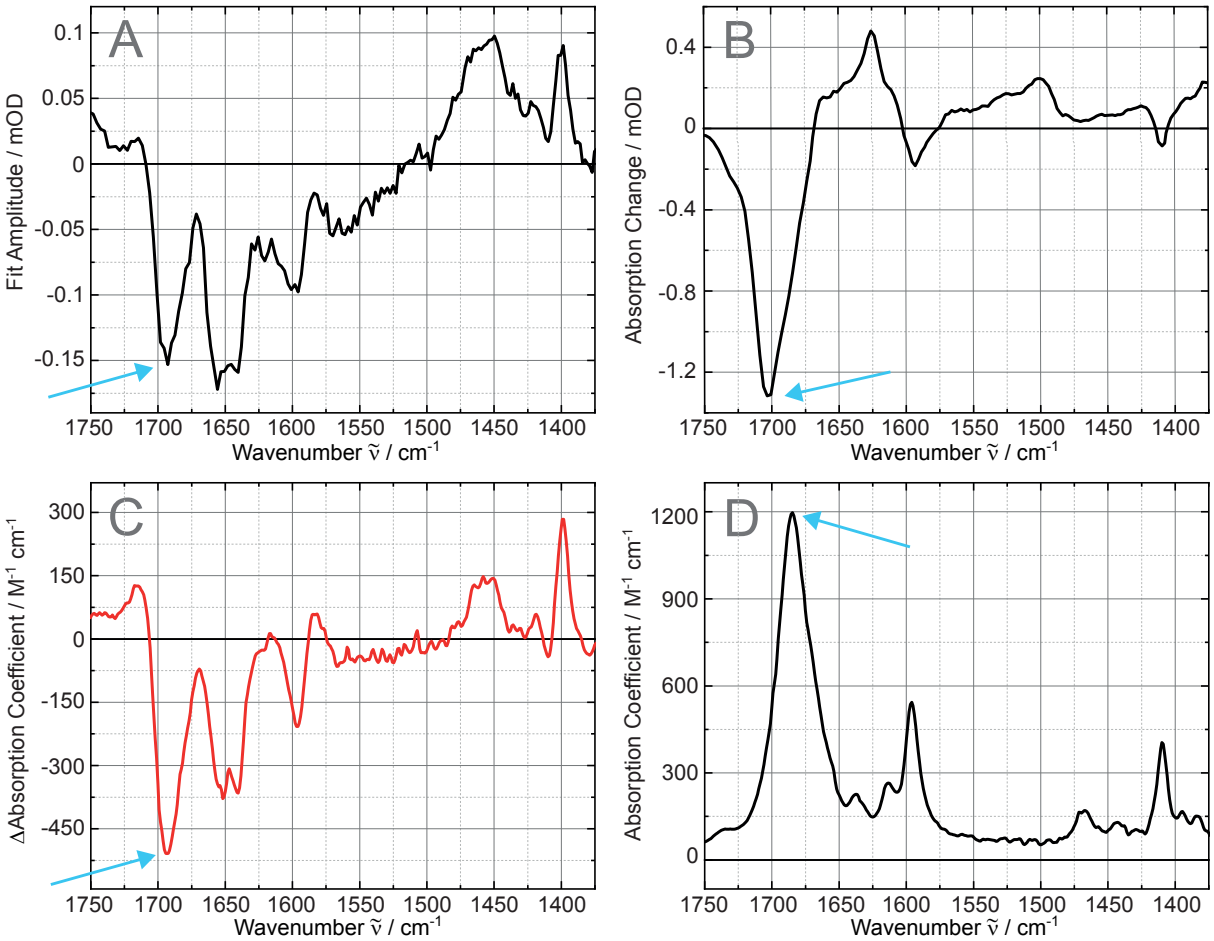

Figure S3: **A** The DADS for $\tau = \infty$ of AMT with AT-DNA. **B**: Difference spectrum at t = 10 ns of AMT with AT-DNA. **C**: Difference spectrum after exhaustive irradiation of AMT with AT-DNA. **D**: Absorption coefficients of AMT. The blue arrows mark the signal values entering the computation of the efficiency η_R^T.

References

(S1) Fröbel, S.; Reiffers, A.; Torres Ziegenbein, C.; Gilch, P. DNA Intercalated Psoralen Undergoes Efficient Photoinduced Electron Transfer. *The Journal of Physical Chemistry Letters* **2015**, *6*, 1260–1264.

(S2) Pilles, B. M.; Bucher, D. B.; Liu, L.; Clivio, P.; Gilch, P.; Zinth, W.; Schreier, W. J. Mechanism of the decay of thymine triplets in DNA single strands. *Journal of Physical Chemistry Letters* **2014**, *5*, 1616–1622.

(S3) Schrader, T.; Sieg, A.; Koller, F.; Schreier, W.; An, Q.; Zinth, W.; Gilch, P. Vibrational relaxation following ultrafast internal conversion: Comparing IR and Raman probing. *Chemical Physics Letters* **2004**, *392*, 358–364.

(S4) Ryseck, G.; Schmierer, T.; Haiser, K.; Schreier, W.; Zinth, W.; Gilch, P. The Excited-State Decay of 1-Methyl-2(1H)-pyrimidinone is an Activated Process. *ChemPhysChem* **2011**, *12*, 1880–1888.

(S5) Towrie, M.; Doorley, G. W.; George, M. W.; Parker, A. W.; Quinn, S. J.; Kelly, J. M. ps-TRIR covers all the bases – recent advances in the use of transient IR for the detection of short-lived species in nucleic acids. *The Analyst* **2009**, *134*, 1265.

(S6) Satzger, H.; Zinth, W. Visualization of transient absorption dynamics - Towards a qualitative view of complex reaction kinetics. *Chemical Physics* **2003**, *295*, 287–295.

(S7) Slavov, C.; Hartmann, H.; Wachtveitl, J. Implementation and Evaluation of Data Analysis Strategies for Time-Resolved Optical Spectroscopy. *Analytical Chemistry* **2015**, *87*, 2328–2336.

(S8) Croce, R.; Müller, M. G.; Bassi, R.; Holzwarth, A. R. Carotenoid-to-Chlorophyll Energy Transfer in Recombinant Major Light-Harvesting Complex (LHCII) of Higher Plants. I. Femtosecond Transient Absorption Measurements. *Biophysical Journal* **2001**, *80*, 901–915.

(S9) Dorlhiac, G. F.; Fare, C.; van Thor, J. J. PyLDM - An open source package for lifetime density analysis of time-resolved spectroscopic data. *PLoS computational biology* **2017**, *13*, e1005528.

(S10) Schreier, W. J.; Schrader, T. E.; Koller, F. O.; Gilch, P.; Crespo-Hernández, C. E.; Swaminathan, V. N.; Carell, T.; Zinth, W.; Kohler, B. Thymine dimerization in DNA is an ultrafast photoreaction. *Science* **2007**, *315*, 625–629.

Supporting Information: Synthesis and Photophysics of Water-Soluble Psoralens with Red-Shifted Absorption

Janina Bertling[1], Kristoffer A. Thom[1], Sarah Geenen[2], Hannah Jeuken[1], Lysander Presser[2], Thomas J. J. Müller*[2] and Peter Gilch*[1]

[1]*Institut für Physikalische Chemie, Heinrich-Heine-Universität Düsseldorf, Universitätsstr. 1, 40225 Düsseldorf, Germany*

[2]*Institut für Organische Chemie und Makromolekulare Chemie, Heinrich-Heine-Universität Düsseldorf, Universitätsstr. 1, 40225 Düsseldorf, Germany*

*Corresponding author e-mail: gilch@hhu.de (Peter Gilch)
ThomasJJ.Mueller@hhu.de (Thomas J.J. Müller)

Contents

1 General procedure (GP) for the synthesis and spectroscopic data

The 8-methoxypsoralen derivatives **1** or **2** were placed in an oven-dried Schlenk tube with a magnetic stir bar and dissolved in dry dichloromethane under nitrogen (for experimental details, see Table S1). The solution was cooled to 0 °C (ice water bath) and trimethyloxonium tetrafluoroborate was added and the reaction mixture was warmed to room temp. After full conversion, the reaction mixture was worked up.

Table S1: Experimental details of the synthesis of psoralen derivatives MPM^+, $MPEM^+$, $TMAPM^+$ and $TMAPEM^+$ by quaternization.

8-MOP derivatives **1** or **2**	$[Me_3O]^+[BF_4]^-$	CH_2Cl_2	T_1 (t_1)	T_2 (t_2)	Quaternized 8-MOP derivatives
154 mg of **1a** (0.560 mmol)	196 mg (1.32 mmol)	5.0 mL	0 °C (15 min)	23 °C (24 h)	142 mg (64%) of **MPM^+ BF_4^-**
107 mg of **1b** (0.338 mmol)	125 mg (0.84 mmol)	10.0 mL	0 °C (15 min)	23 °C (24 h)	108 mg (67%) of **$MPEM^+$ BF_4^-**
96.0 mg of **2a** (0.287 mmol)	103 mg (0.72 mmol)[a]	3.0 mL	0 °C (15 min)	23 °C (48 h)	80.0 mg(64%) of **$TMAPM^+$ BF_4^-**
134 mg of **2b** (0.373 mmol)	165 mg (1.12 mmol)	4.0 mL	0 °C (15 min)	23 °C (24 h)	107 mg (62%) of **$TMAPEM^+$ BF_4^-**

[a] After 24 h another batch of 42.5 mg (0.28 mmol) was added to the reaction mixture.

1.1 5-(1-Methylpyridinium-4-yl)8-methoxypsoralen tetrafluoroborate ($MPM^+ BF_4^-$)

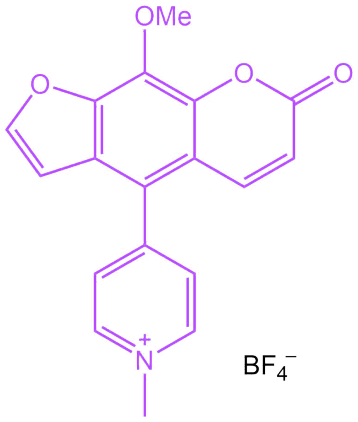

$C_{18}H_{14}BF_4NO_4$
[395.12]

According to the GP and after addition of diethylether and filtration, the residue was washed several time with portions of diethylether and dichloromethane and then dried in vacuo to give compound $MPM^+ BF_4^-$ (142 mg, 64%) as a yellow-green solid, Mp 277 °C (dec.).

^{1}H NMR (500 MHz, DMSO-d_6): $\delta = 4.30$ (s, 3 H), 4.43 (s, 3 H), 6.55 (d, $J = 9.9$ Hz, 1 H), 6.92 (d, $J = 2.3$ Hz, 1 H), 7.86 (d, $J = 9.9$ Hz, 1 H), 8.27–8.22 (m, 2 H), 8.29 (d, $J = 2.3$ Hz, 1 H), 9.16–9.08 (m, 2 H). ^{13}C NMR (125 MHz, DMSO-d_6): $\delta = 47.9$ (CH_3), 61.6 (CH_3), 106.0 (CH), 114.5 (C_{quat}), 116.1 (CH), 120.0 (C_{quat}), 126.0 (C_{quat}), 129.5 (CH), 133.8 (C_{quat}), 141.7 (CH), 143.3 (C_{quat}), 146.1 (CH), 146.2 (C_{quat}), 149.9 (CH), 151.5 (C_{quat}), 159.2 (C_{quat}). ESI-MS calcd. for $(C_{18}H_{14}NO_4)^+$ $m/z = 308.3$ (100 %); Found: 308.3 (100 %). IR: $\tilde{\nu}$ [cm^{-1}] = 1728 (s), 1643 (w), 1582 (s), 1526 (w), 1472 (w), 1423 (m), 1375 (w), 1314 (m), 1217 (w), 1192 (w), 1178 (m), 1153 (m), 1065 (s), 1047 (s), 1024 (s), 1011 (s), 984 (m), 968 (m), 951 (w), 885 (w), 839 (s), 791 (m), 760 (s), 652 (m). HR-MS (ESI): calcd. for $(C_{18}H_{14}NO_4)^+$ $m/z = 308.0917$; Found: 308.0921. HPLC (acetone): 98 % ($R_t = 1.7$ min).

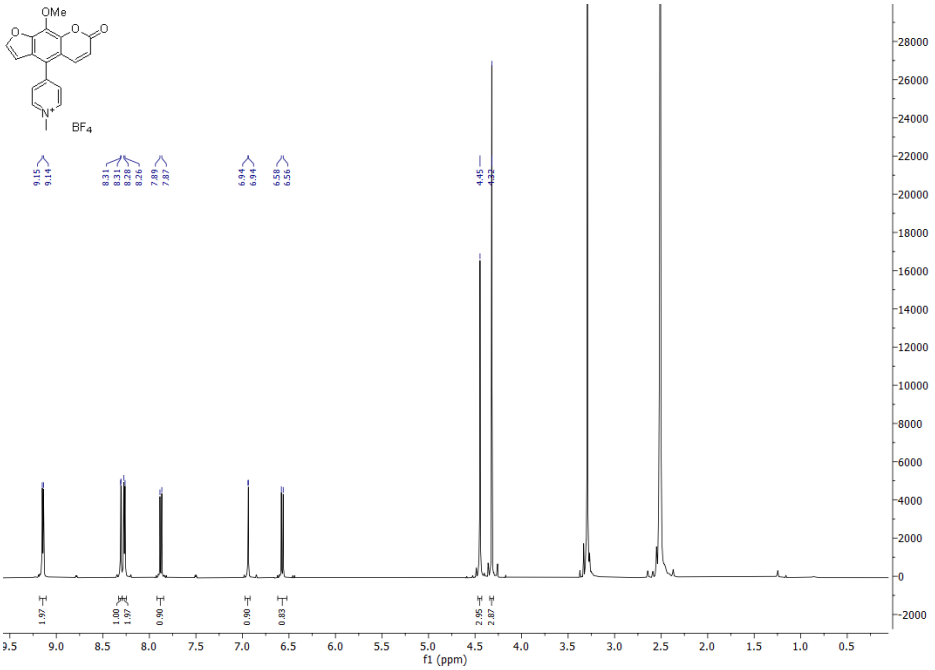

Figure S1: ^{1}H NMR spectrum of $MPM^{+}\ BF_4{}^{-}$ (500 MHz, DMSO-d_6, 293 K).

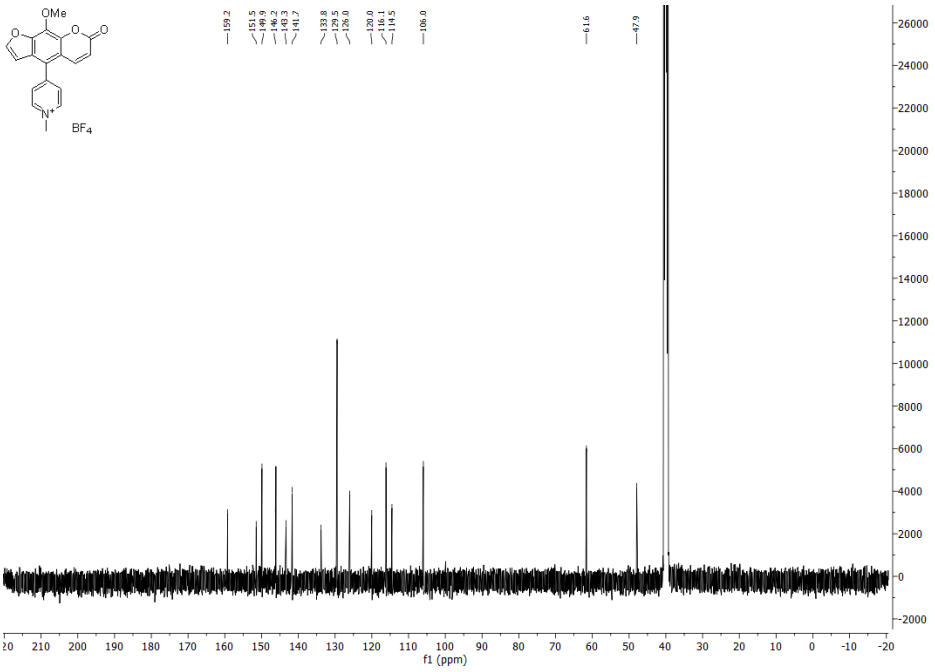

Figure S2: ^{13}C NMR spectrum of $MPM^{+}\ BF_4{}^{-}$ (125 MHz, DMSO-d_6, 293 K).

1.2 5-((1-Methylpyridinium-4-yl)ethynyl)8-methoxypsoralen tetrafluoroborate (MPEM$^+$ BF$_4^-$)

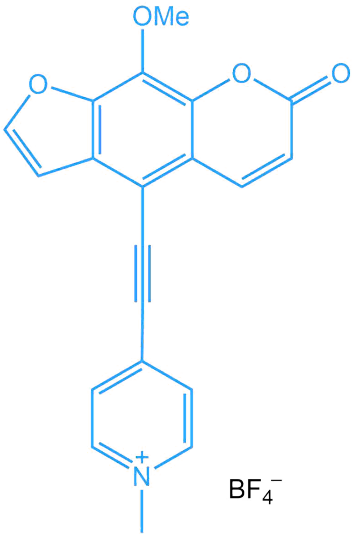

$C_{20}H_{14}BF_4NO_4$
[419.14]

According to the GP and after addition of diethylether and filtration, the residue was washed several time with portions of diethylether and dichloromethane and then dried in vacuo to give compound MPEM$^+$ BF$_4^-$ (108 mg, 67%) as an orange solid, Mp 185 °C (dec.).

^{1}H NMR (600 MHz, DMSO-d_6): δ = 4.33 (s, 3 H), 4.36 (s, 3 H), 6.67–6.58 (m, 1 H), 7.52 (dt, J = 3.4, 1.8 Hz, 1 H), 8.39 (t, J = 2.1 Hz, 1 H), 8.49 (d, J = 6.2 Hz, 2 H), 8.61–8.53 (m, 1 H), 9.06 (d, J = 6.4 Hz, 2 H). ^{13}C NMR (151 MHz, DMSO-d_6): δ 48.2 (CH_3), 61.6 (CH_3), 93.7 (C_{quat}), 96.4 (C_{quat}), 102.2 (C_{quat}), 107.2 (CH), 117.0 (CH), 119.0 (C_{quat}), 129.3 (CH), 130.8 (C_{quat}), 135.5 (C_{quat}), 138.3 (C_{quat}), 142.6 (CH), 142.7 (C_{quat}), 145.5 (C_{quat}), 145.9 (CH), 150.3 (CH), 159.5 (C_{quat}). IR: $\tilde{\nu}$ [cm^{-1}] = 2195 (m), 1713 (s), 1636 (w), 1618 (w), 1578 (s), 1522 (m), 1452 (w), 1423 (w), 1383 (m), 1323 (m), 1277 (w), 1184 (w), 1157 (m), 1123 (m), 1022 (s), 943 (w), 880 (w), 839 (m), 826 (m), 732 (w), 760 (m), 735 (w), 627 (w). HR-MS (ESI): calcd. for $(C_{20}H_{14}NO_4)^+$ m/z = 332.0917; Found: 332.0918. HPLC (acetone): 99 % (R_t = 2.6 min).

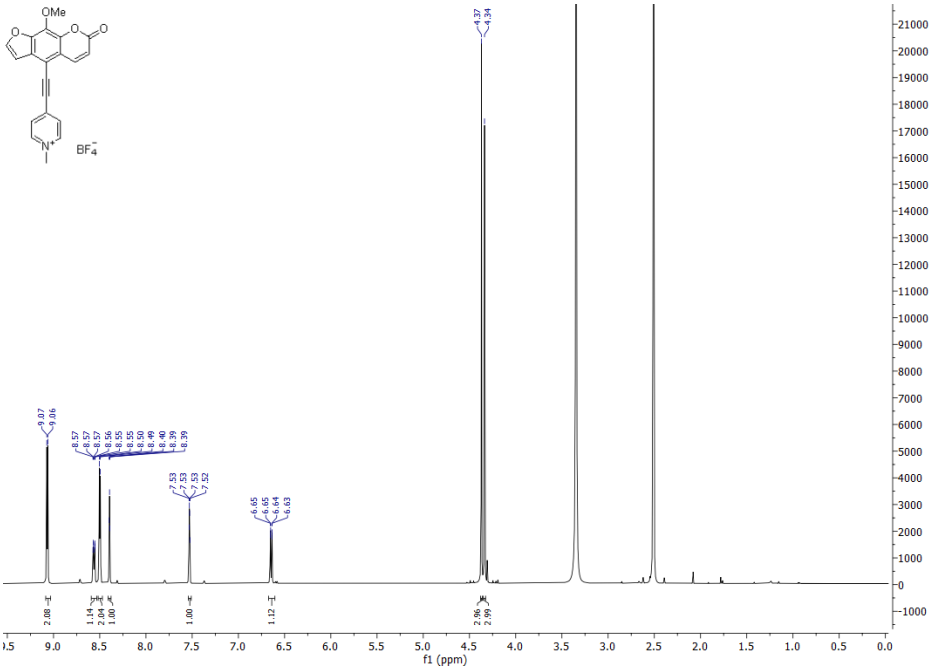

Figure S3: ^{1}H NMR spectrum of MPEM^{+} BF_4^{-} (600 MHz, DMSO-d_6, 293 K).

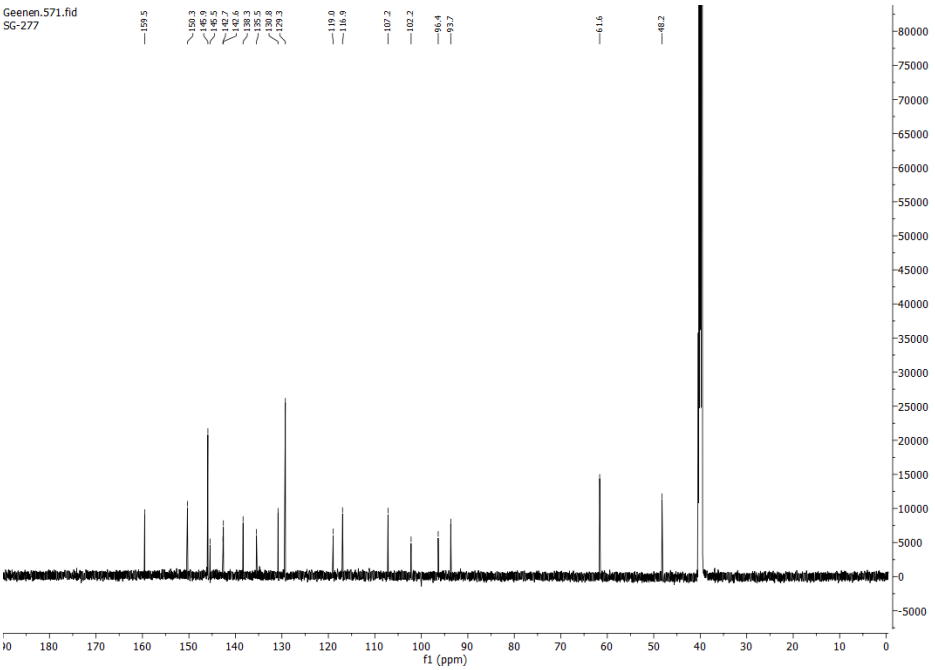

Figure S4: ^{13}C NMR spectrum of MPEM^{+} BF_4^{-} (151 MHz, DMSO-d_6, 293 K).

1.3 5-(4-*N,N,N*-Trimethylaminophenyl)8-methoxypsoralen tetrafluoroborate ($TMAPM^+ BF_4^-$)

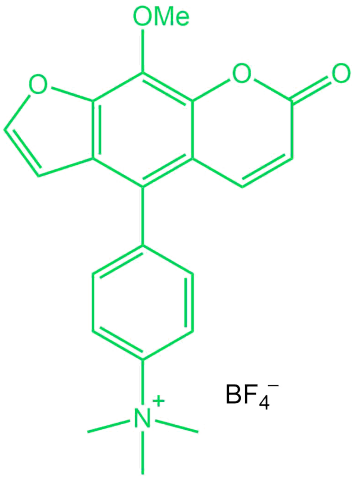

$C_{21}H_{20}BF_4NO_4$
[437.20]

According to the GP and after evaporation of the solvent in vacuo the residue was dissolved in deionized water (100 mL) and ethyl acetate (100 mL). The organic layer was extracted with water (3 x 30 mL). The combined aqueous layers were extracted with ethyl acetate (10 x 30 mL). The aqueous layer was concentrated and underlaid with dichloromethane and placed into the ultrasound bath for 5 min. The precipitate was collected and dried in vacuo to give compound $TMAPM^+ BF_4^-$ (80 mg, 64%) as a colorless solid, Mp 327 °C (dec.).

^{1}H NMR (600 MHz, DMSO-d_6): δ = 7.79 – 7.67 (m, 3 H), 3.69 (s, 9 H), 4.24 (s, 3 H), 6.48 (d, J = 9.9 Hz, 1 H), 6.74 (d, J = 2.2 Hz, 1 H), 7.79 – 7.67 (m, 3 H), 7.79 – 7.67 (m, 3 H). ^{13}C NMR (151 MHz, DMSO-d_6): δ = 56.5 (CH_3), 61.2 (CH_3), 99.5 (C_{quat}), 106.0 (CH), 114.0 (C_{quat}), 114.8 (CH), 121.1 (CH), 124.2 (C_{quat}), 125.5 (C_{quat}), 131.8 (CH), 136.7 (CH), 142.0 (CH), 143.1 (C_{quat}), 146.2 (C_{quat}), 146.9 (C_{quat}), 148.7 (C_{quat}), 159.3 (C_{quat}). IR: $\tilde{\nu}$ [cm^{-1}] = 1736 (m), 1736 (m), 1591 (m), 1474 (w), 1420 (w), 1373 (w), 1314 (w), 1153 (m), 1090 (s), 1028 (s), 961 (w), 941 (w), 905 (w), 885 (w), 866 (w), 847 (w), 826 (m), 760 (m), 723 (w), 631 (w). HR-MS (ESI): calcd. for $(C_{21}H_{20}NO_4)^+$ m/z = 350.1387; Found: 350.1391. HPLC (acetonitrile): 99 % (R_t = 3.1 min).

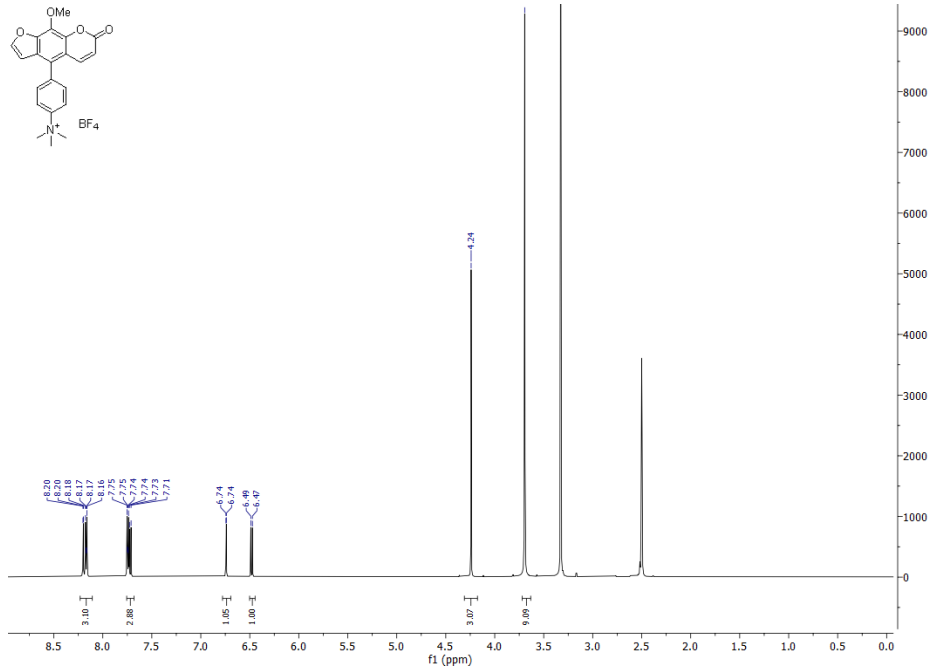

Figure S5: ^{1}H NMR spectrum of TMAPM^{+} BF_4^{-} (600 MHz, DMSO-d_6, 293 K).

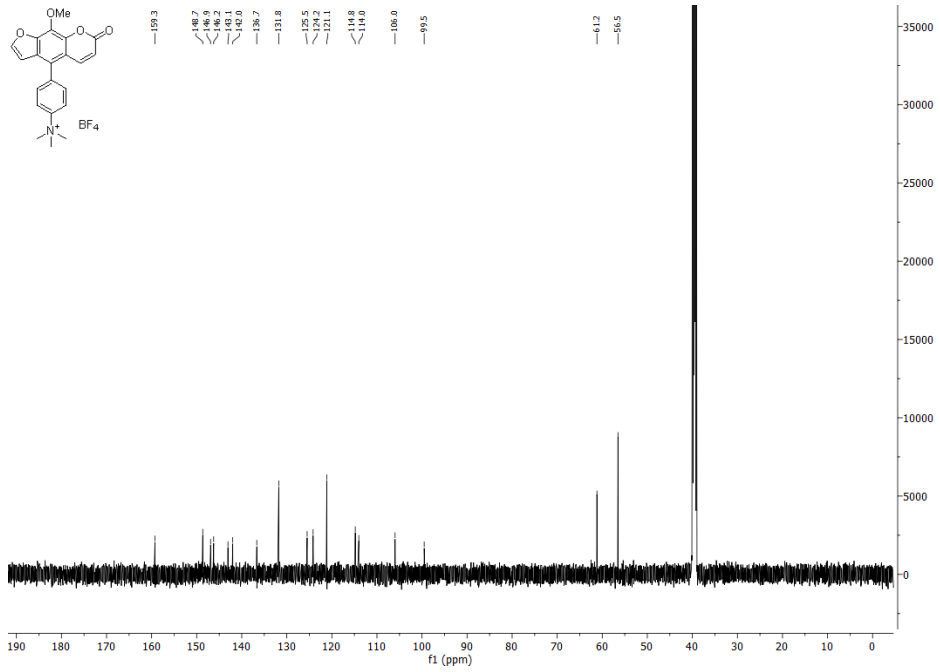

Figure S6: ^{13}C NMR spectrum of TMAPM^{+} BF_4^{-} (151 MHz, DMSO-d_6, 293 K).

1.4 5-((4-*N,N,N*-Trimethylaminophenyl)ethynyl)8-methoxypsoralen tetrafluoroborate (TMAPEM$^+$ BF_4^-)

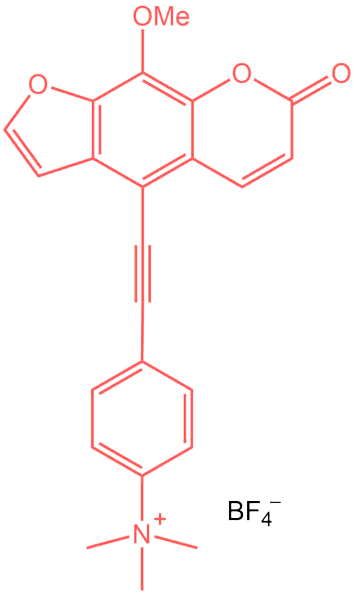

$C_{23}H_{20}BF_4NO_4$
[461.22]

According to the GP and after evaporation of the solvent in vacuo the residue was dissolved in deionized water (100 mL) and ethyl acetate (100 mL). The organic layer was extracted with water (3 x 30 mL). The combined aqueous layers were extracted with ethyl acetate (10 x 30 mL). The aqueous layer was concentrated and underlaid with dichloromethane and placed into the ultrasound bath for 5 min. The precipitate was collected and dried in vacuo to give compound TMAPEM$^+$ BF_4^- (107 mg, 62%) as a beige solid, Mp 259 °C (dec.).

^{1}H NMR (300 MHz, DMSO-d_6): δ = 3.64 (s, 9 H), 4.28 (s, 3 H), 6.57 (d, J = 9.8 Hz, 1 H), 7.36 (d, J = 2.2 Hz, 1 H), 8.13 – 7.98 (m, 4 H), 8.28 (d, J = 2.2 Hz, 1 H), 8.44 (d, J = 9.7 Hz, 1 H). ^{13}C NMR (75 MHz, DMSO-d_6): δ 56.5 (CH_3), 61.2 (CH_3), 85.2 (C_{quat}), 95.6 (C_{quat}), 104.5 (C_{quat}), 106.7 (CH), 115.8 (CH), 117.5 (C_{quat}), 121.2 (CH), 123.8 (C_{quat}), 128.9 (C_{quat}), 133.1 (CH), 133.3 (C_{quat}), 142.5 (CH), 145.6 (C_{quat}), 147.2 (C_{quat}), 149.1 (CH), 159.3 (C_{quat}). IR: $\tilde{\nu}$ [cm^{-1}] = 1709 (s), 1585 (m), 1514 (w), 1491 (w), 1474 (w), 1425 (w), 1379 (w), 1317 (m), 1207 (w), 1159 (w), 1126 (m), 1031 (s), 959 (w), 937 (w), 880 (w), 829 (m), 746 (m), 716 (w), 689 (w). HR-MS (ESI): calcd. for $(C_{23}H_{20}NO_4)^+$ m/z = 374.1387; Found: 374.1386. HPLC (acetonitrile): 99 % (R_t = 4.3 min).

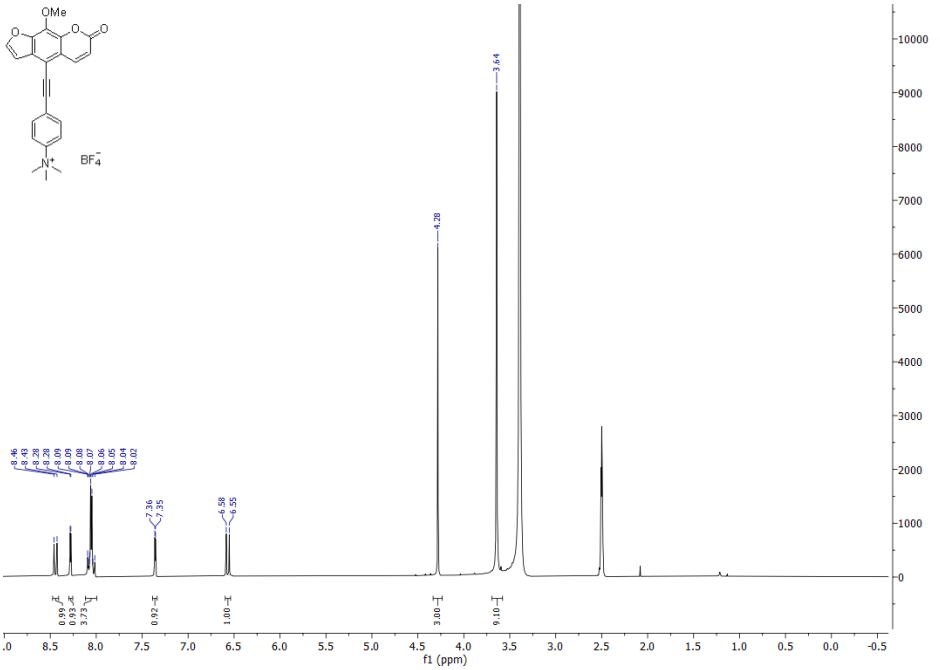

Figure S7: ^{1}H NMR spectrum of TMAPEM^{+} BF_4^{-} (300 MHz, DMSO-d_6, 293 K).

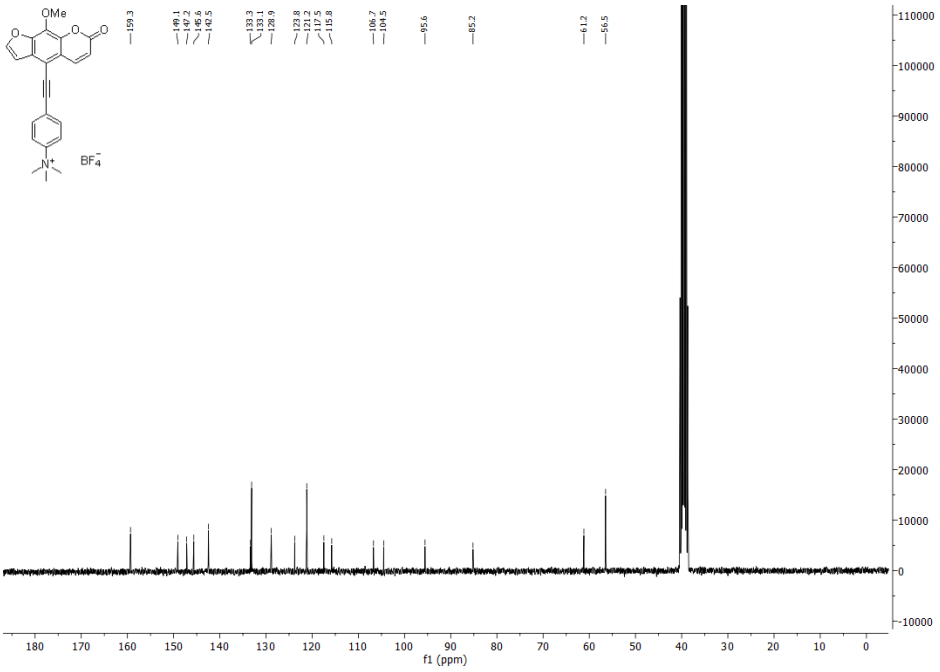

Figure S8: ^{13}C NMR spectrum of TMAPEM^{+} BF_4^{-} (75 MHz, DMSO-d_6, 293 K).

2 Photophysical behavior in dichloromethane

The absorption and emission spectra of the cationic psoralens MPM^+, $MPEM^+$, $TMAPM^+$ and $TMAPEM^+$ were recorded in dichloromethane at room temperature and fluorescence quantum yields Φ_{fl} were determined using Coumarin 30 as a standard in acetonitrile (see Table S2, Figure S9).

Table S2: Selected photophysical data of investigated psoralen derivatives in dichloromethane. Fluorescence quantum yields Φ_{fl} were determined with Coumarin 30 as a standard in acetonitrile (Φ_{fl}= 0.67 [1])

	$\lambda_{max,abs}$ / nm$^{(a)}$ (ϵ / M^{-1} cm^{-1})	$\lambda_{max,em}$ / nm$^{(b)}$ (Φ_{fl})	Stokes shift $\tilde{\nu}$ / cm^{-1}
MPM^+	355 (6000)	**393** (5900sh)	517 (0.05)	6100
$MPEM^+$	375 (3700)	**434** (5500)	551 (<0.01)	4900
$TMAPM^+$	307 (13400)	**359** (6000sh)	465 (<0.01)	6300
$TMAPEM^+$	342 (19900)	**372** (10000)	455 (<0.01)	4900

$^{(a)}$ $c = 10^{-5}$ M $^{(b)}$ $c = 10^{-7}$ M

MPM^+ has the highest fluorescence quantum yield in this series (0.05). Alkynyl expansion of compound $MPEM^+$ increases the conjugated π-system and causes a bathochromic shift of the longest wavelength absorption band to 434 nm and likewise for the emission maximum. The fluorescence quantum yield is lower than 0.01. Trimethylammonium substitution of compounds $TMAPM^+$ and $TMAPEM^+$ causes a clear blue shift of the absorption and emission maxima in comparison to the pyridinium derivatives. The qualitative comparison of pyridinium (MPM^+ and $MPEM^+$) and trimethylammonium ($TMAPM^+$ and $TMAPEM^+$) psoralens supports the rationale that the latter are stronger inductive acceptor functionalities and lead to hypsochromic shifts of both absorption and emission bands.

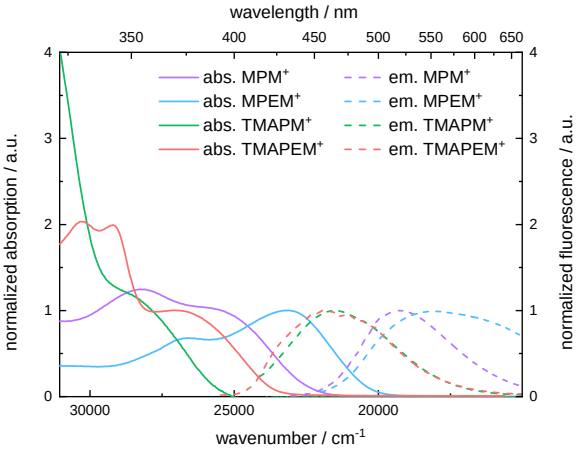

Figure S9: Normalized absorption and emission spectra of investigated psoralens recorded in dichloromethane.

3 Cyclic voltammograms

Cyclic voltammograms were recorded as described in the main text. The reduction of MPM^+ is chemically reversible (see Figure S10, dark blue). For this compound, the half peak potential $E_{1/2}$ is taken to equal the standard potential E^0. All other compounds exhibit chemically irreversible reductions and oxidations, that is the radicals generated electrochemically decompose. For chemically irreversible processes, the cathodic (E_{CP}) or anodic peak potentials (E_{AP}) were first determined (see Figure S10, light blue). Assuming that the radicals generated electrochemically decompose in a first order process with rate constants k_f, estimates concerning the standard potentials E^0 can be made based on equations (1) and (2) [2].

$$E^0 = E_{CP} - \underbrace{\frac{RT}{2nF}\left(\ln\left(\frac{k_f RT}{\nu nF}\right) - 1.56\right)}_{>0} \tag{1}$$

$$E^0 = E_{AP} + \underbrace{\frac{RT}{2nF}\left(\ln\left(\frac{k_f RT}{\nu nF}\right) - 1.56\right)}_{>0} \tag{2}$$

R stands for the gas constant, T the temperature, ν the scan rate, $n = 1$ the number of transferred electrons and F the Faraday constant. Note that these equations are only valid for the condition, $k_f \gg \frac{\nu nF}{RT}$ ($\frac{\nu nF}{RT}$ here amounts to $\sim 4\ s^{-1}$). For this situation, the terms marked by the brackets in eqn. (1) and (2) are positive. This implies that the peak potentials E_{CP} and E_{AP} are shifted towards 0 V with respect to the standard potentials E^0. Evaluation of these shifts requires knowledge of the rate constants k_f. For the compounds studied here, these are not available. The radical anion formed from the psoralen derivative AMT [3] has a lifetime of about 10 µs which corresponds to a rate constant of $10^5\ s^{-1}$. For this lifetime a shift of -0.1 V can be estimated via equation (1) for a scan rate ν of 0.1 V s^{-1}. If the radicals treated here featured comparable lifetimes, the standard potential E^0 for reductions ought to be $\sim$ 0.1 V more negative and the ones for oxidation $\sim$ 0.1 V more positive. The resulting estimated standard potentials are listed in Table S3.

Table S3: Estimated standard potentials.

	E^0_{Red} / V	E^0_{Ox} / V
MPM^+	-0.815	1.9
MP^+	-1.2	
$MPEM^+$	-0.7	1.9
MPE^+	-0.7	
$TMAPM^+$	-1.2	
$TMAPEM^+$	-1.7	

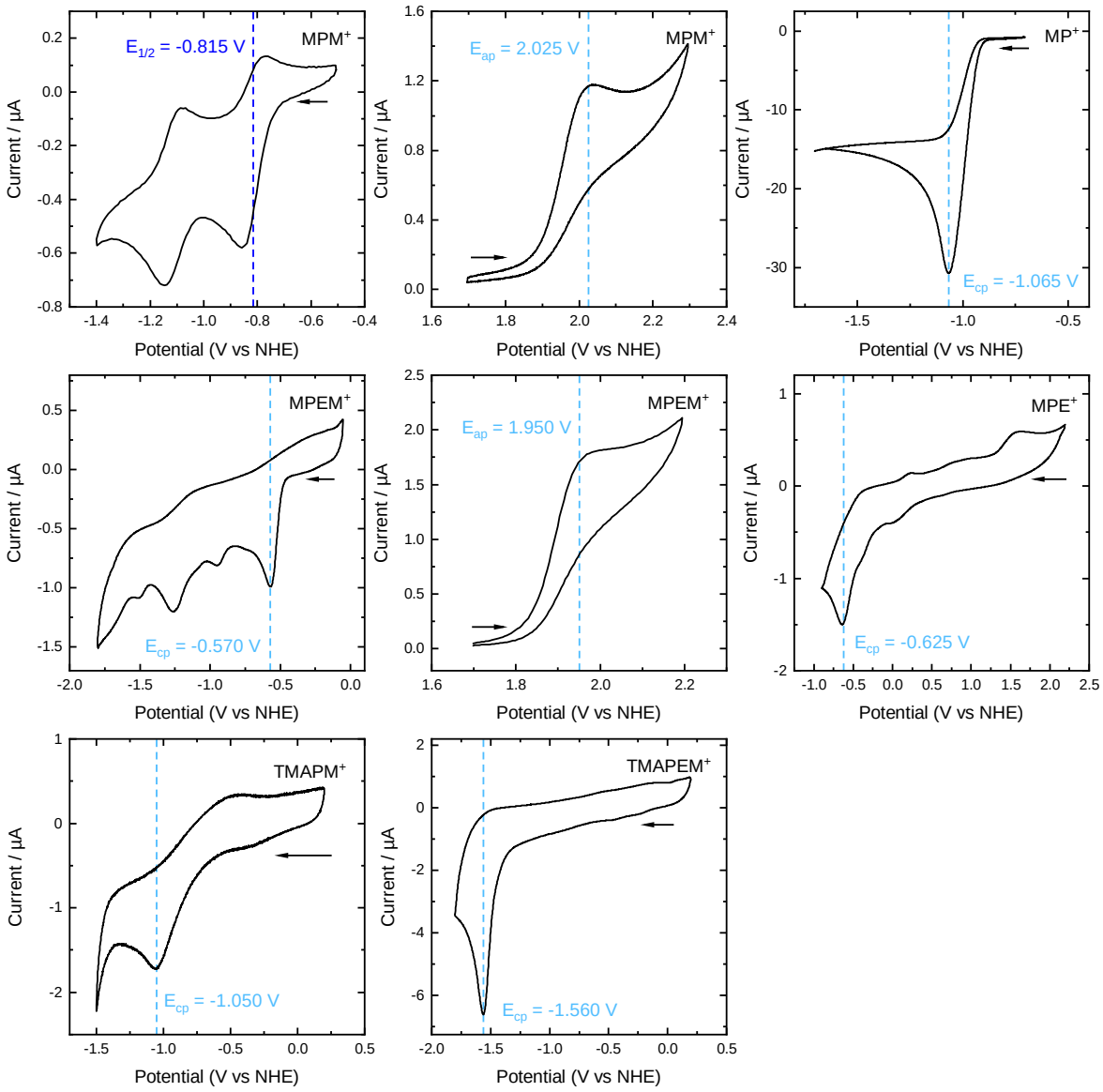

Figure S10: Cyclic voltammograms on the reduction/oxidation of psoralen derivatives and building blocks studied here. The concentration was 2 mM in acetonitrile and the scan rate 0.1 V/s (except for TMAPM with 0.05 V/s). The potentials were measured with an Ag/AgCl (sat. NaCl) electrode and shifted by +197 mV to yield the potentials vs NHE [4]. Arrows indicate the direction of the scans. Vertical dashed lines indicate the half-wave ($E_{1/2}$) or cathodic/anodic peak potential (E_{ap}, E_{cp}). The representation follows the IUPAC convention [5].

4 Generation and signature of the MP and MPE radical

Solutions of pyridinium cations and iodide I^- feature intermolecular charge transfer (CT) bands [6, 7]. Excitation into these bands reduces the pyridinium cations to the respective neutral radical. For MP^+I^- and MPE^+I^- dissolved in water the respective CT band is located at around 320 nm. Femtosecond laser pulses in resonance with their transition caused the difference absorption signatures depicted in Figures S11 and S12. The low absorption at the excitation wavelength for MP^+I^- resulted in a strong time zero artifact due to the simultaneous absorption of pump and probe photons [8]. Shortly afterwards, a band peaking at 450 nm is discernible which persists for ≈ 10 ps. We assign this band to the radical MP. In the experiment on MPE^+I^- (Figure S12) the absorption at the excitation wavelength was higher and therefore no time zero artifact is observed. Immediately after the excitation, a positive difference signal with peaks at 535 nm and 630 is detected. It persists for ≈ 100 ps and is assigned to the radical MPE.

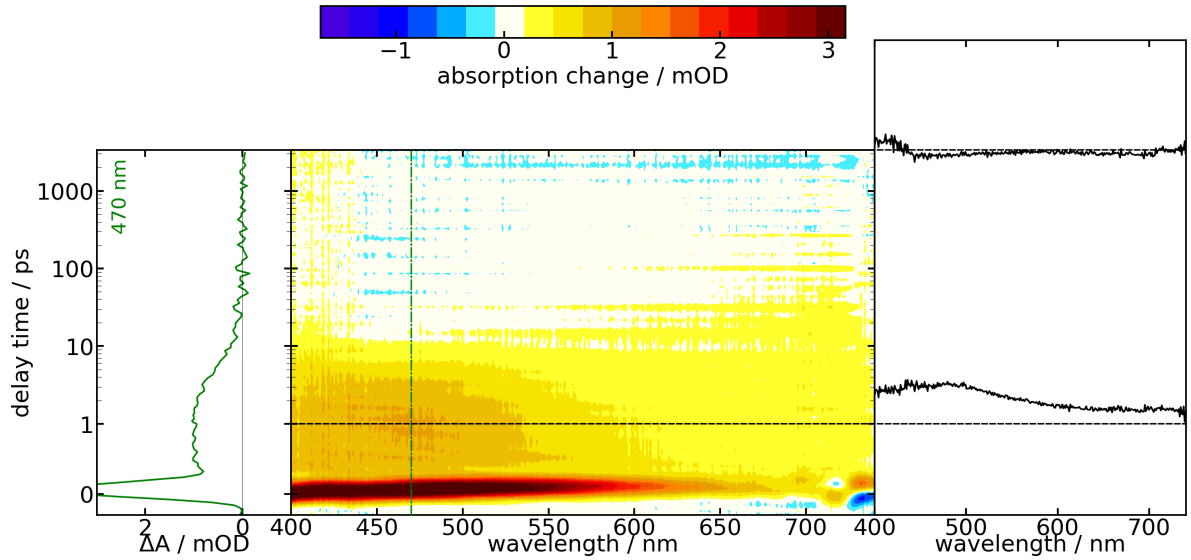

Figure S11: Femtosecond transient absorption of 1-methylpyridinium iodide (MP^+I^-) (50 mM) and KI (50 mM) in H_2O after excitation at 320 nm. The absorption was set to 0.1 at excitation wavelength. The transient absorption is color coded. Vertical lines in the contour plot give the wavelengths of the time traces shown on the left. Horizontal lines give the delay time of the transient spectra depicted on the right.

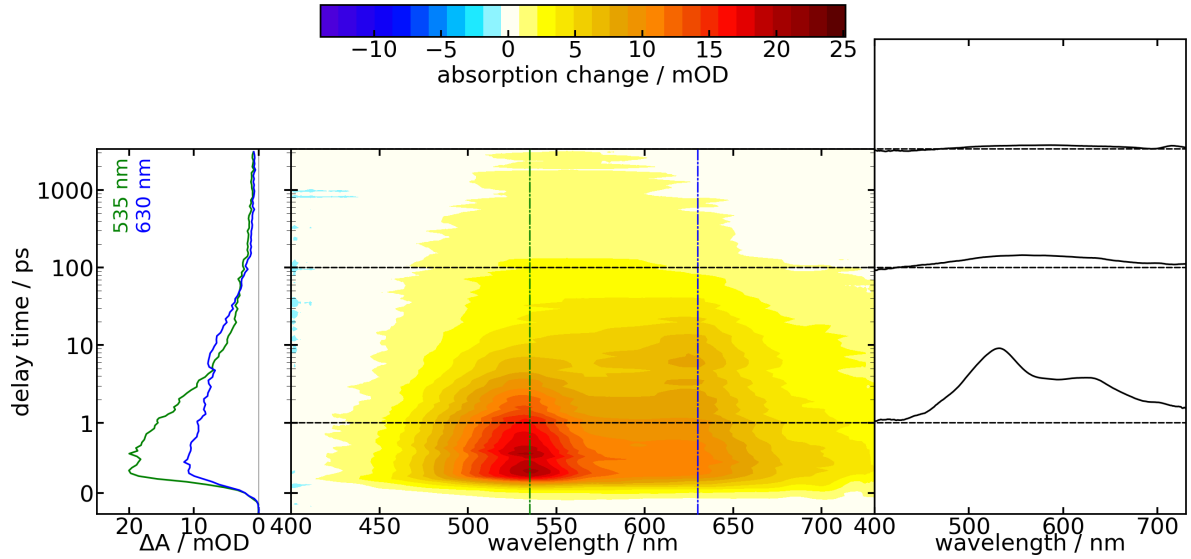

Figure S12: Femtosecond transient absorption of 4-ethynyl-1-methylpyridinium triflate (MPE^+ triflate) (41 mM) and KI (50 mM) in H_2O after excitation at 317 nm. The absorption was set to 0.6 at excitation wavelength. The transient absorption is color coded. Vertical lines in the contour plot give the wavelengths of the time traces shown on the left. Horizontal lines give the delay time of the transient spectra depicted on the right.

5 Comparison of bleach signal with fluorescence spectrum of $MPEM^+$

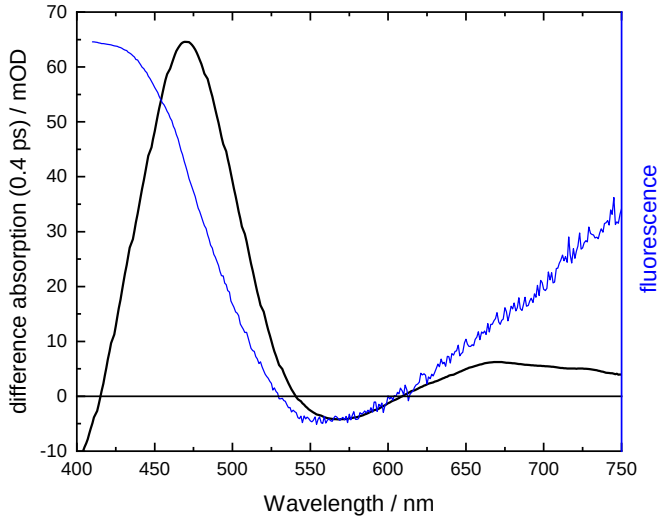

Figure S13: Comparison of the difference absorption signal of $MPEM^+$ 0.4 ps after excitation at 400 nm and the fluorescence spectrum. The fluorescence spectrum was multiplied by the wavelength to the fourth power, λ^4, [9] to obtain a stimulated emission signal, scaled and shifted vertically to match the bleach of the difference signal.

6 TCSPC

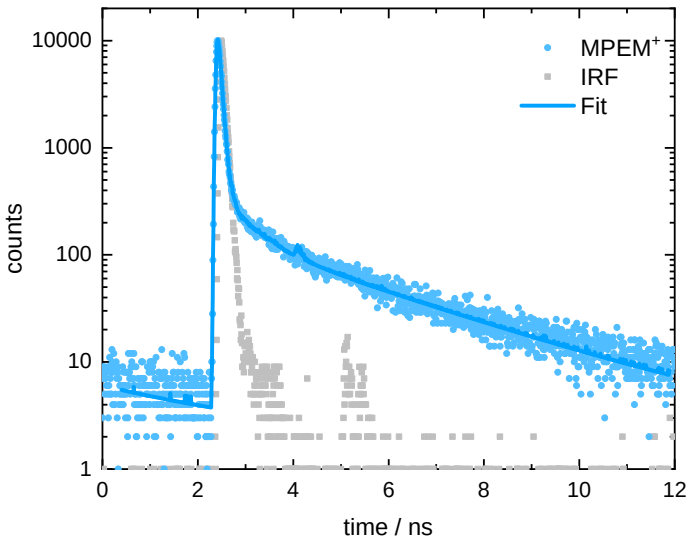

Figure S14: Time-correlated single photon counting on $MPEM^+$ in water. Blue dots represent experimental data, gray dots the instrumental response function (IRF) measured with scattered light. The solid blue line represents a multi-exponential fit convoluted numerically with the IRF.

7 Determination of the triplet quantum yield Φ_T of TMAPM$^+$

The determination of the triplet quantum yield Φ_T of TMAPM$^+$ relied on a method described in ref. [10] This method entails the quantification of the triplet difference absorption coefficient $\Delta\epsilon_T$ by "trimming" the inverted ground state spectrum into the bleach contribution of the respective DADS (Figure S15). Using the known triplet quantum yield $\Phi_T^{ref} = 0.6$ [11] of the reference thioxanthone in methanol and its difference absorption coefficient $\Delta\epsilon_T^{ref}$ (600 nm) = 23000 $M^{-1}cm^{-1}$ [10]. The triplet yield Φ_T can be computed via

$$\Phi_T = \frac{\Delta A_{t=0}^{TMAPM^+}}{\Delta\epsilon_T^{TMAPM^+}} \cdot \frac{\Delta\epsilon_T^{ref}}{\Delta A_{t=0}^{ref}} \cdot \Phi_T^{ref} \tag{3}$$

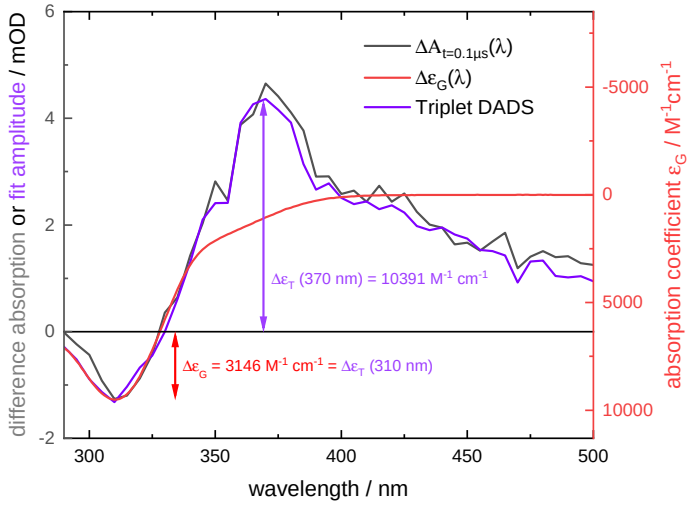

Figure S15: Determination of the triplet difference absorption coefficient $\Delta\epsilon_T$ of TMAPM$^+$. The absorption spectrum of the ground state (red) is scaled and shifted to fit the DADS of the TMAPM$^+$ triplet (violet). The transient spectrum after 0.1 µs (grey) is depicted for comparison.

8 Emission behaviour in presence of DNA

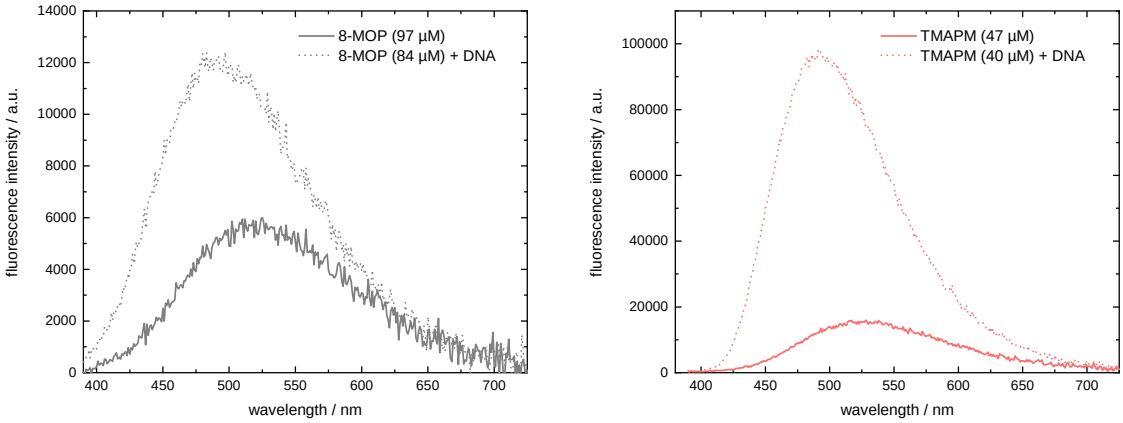

Figure S16: Comparison of the fluorescence spectra of 8-MOP (left) and $TMAPM^+$ (right) in absence (solid lines) and presence of AT-DNA (dashed lines).

References

[1] G. Jones, W. R. Jackson, C. Y. Choi, and W. R. Bergmark, "Solvent effects on emission yield and lifetime for coumarin laser dyes. Requirements for a rotatory decay mechanism," *The Journal of Physical Chemistry*, vol. 89, no. 2, pp. 294–300, Jan. 1985. DOI: 10.1021/j100248a024.

[2] O. Hammerich and B. Speiser, "Chapter 2: Techniques for Studies of Electrochemical Reactions in Solution," in *Organic Electrochemistry*, O. Hammerich and B. Speiser, Eds., 5th ed., CRC Press, 2015, pp. 97–168.

[3] S. Fröbel, L. Levi, S. M. Ulamec, and P. Gilch, "Photoinduced Electron Transfer between Psoralens and DNA: Influence of DNA Sequence and Substitution," *ChemPhysChem*, vol. 17, no. 9, pp. 1377–1386, May 2016. DOI: 10.1002/cphc.201500889.

[4] L. Meites, *Handbook of Analytical Chemistry*. New York: McGraw-Hill, 1963.

[5] N. Elgrishi, K. J. Rountree, B. D. McCarthy, *et al.*, "A Practical Beginner's Guide to Cyclic Voltammetry," *Journal of Chemical Education*, vol. 95, no. 2, pp. 197–206, 2018. DOI: 10.1021/acs.jchemed.7b00361.

[6] E. M. Kosower, "The Effect of Solvent on Spectra. I. A New Empirical Measure of Solvent Polarity: Z-Values," *Journal of the American Chemical Society*, vol. 80, no. 13, pp. 3253–3260, Jul. 1958. DOI: 10.1021/ja01546a020.

[7] E. M. Kosower and L. Lindqvist, "Flash photolysis of a pyridinium iodide through the charge-transfer band," *Tetrahedron Letters*, vol. 6, no. 50, pp. 4481–4485, Jan. 1965. DOI: 10.1016/S0040-4039(01)89049-3.

[8] M. Lorenc, M. Ziolek, R. Naskrecki, *et al.*, "Artifacts in femtosecond transient absorption spectroscopy," *Applied Physics B: Lasers and Optics*, vol. 74, no. 1, pp. 19–27, Jan. 2002. DOI: 10.1007/s003400100750.

[9] J. Furthner and A. Penzkofer, "Emission spectra and cross-section spectra of neodymium laser glasses," *Optical and Quantum Electronics*, vol. 24, no. 5, pp. 591–601, May 1992. DOI: 10.1007/BF00619758.

[10] A. Reiffers, C. Torres Ziegenbein, A. Engelhardt, *et al.*, "Impact of Mono-Fluorination on the Photophysics of the Flavin Chromophore," *Photochemistry and Photobiology*, vol. 94, no. 4, pp. 667–676, 2018. DOI: 10.1111/php.12921.

[11] T. Villnow, G. Ryseck, V. Rai-Constapel, C. M. Marian, and P. Gilch, "Chimeric behavior of excited thioxanthone in protic solvents: I. Experiments," *Journal of Physical Chemistry A*, vol. 118, no. 50, pp. 11 696–11 707, 2014. DOI: 10.1021/jp5099393.

Literaturverzeichnis

[1] J. D. Watson und F. H. C. Crick, „Molecular Structure of Nucleic Acids: A Structure for Deoxyribose Nucleic Acid“, *Nature*, Jg. 171, Nr. 4356, S. 737–738, Apr. 1953. DOI: 10.1038/171737a0.

[2] J. M. Berg, J. L. Tymoczko, G. J. Gatto Jr. und L. Stryer, *Biochemistry*, 8. Aufl. New York: W. H. Freeman, 2015.

[3] H. R. Drew, R. M. Wing, T. Takano u. a., „Structure of a B-DNA dodecamer: conformation and dynamics.“, *Proceedings of the National Academy of Sciences*, Jg. 78, Nr. 4, S. 2179–2183, Apr. 1981. DOI: 10.1073/pnas.78.4.2179.

[4] D. Sehnal, A. S. Rose, J. Koča, S. K. Burley und S. Velankar, „Mol*: Towards a Common Library and Tools for Web Molecular Graphics“, in *Proceedings of the Workshop on Molecular Graphics and Visual Analysis of Molecular Data*, Ser. MolVA '18, Brno, Czech Republic: Eurographics Association, 2018, S. 29–33.

[5] E. C. Friedberg, L. D. McDaniel und R. A. Schultz, „The role of endogenous and exogenous DNA damage and mutagenesis“, *Current Opinion in Genetics & Development*, Jg. 14, Nr. 1, S. 5–10, Feb. 2004. DOI: 10.1016/j.gde.2003.11.001.

[6] T. Lindahl, „An N-Glycosidase from Escherichia coli That Releases Free Uracil from DNA Containing Deaminated Cytosine Residues“, *Proceedings of the National Academy of Sciences*, Jg. 71, Nr. 9, S. 3649–3653, Sep. 1974. DOI: 10.1073/pnas.71.9.3649.

[7] A. Sancar und W. D. Rupp, „A novel repair enzyme: UVRABC excision nuclease of Escherichia coli cuts a DNA strand on both sides of the damaged region“, *Cell*, Jg. 33, Nr. 1, S. 249–260, 1983. DOI: 10.1016/0092-8674(83)90354-9.

[8] R. Lahue, K. Au und P. Modrich, „DNA mismatch correction in a defined system“, *Science*, Jg. 245, Nr. 4914, S. 160–164, Juli 1989. DOI: 10.1126/science.2665076.

[9] W. J. Schreier, P. Gilch und W. Zinth, „Early Events of DNA Photodamage“, *Annual Review of Physical Chemistry*, Jg. 66, Nr. 1, S. 497–519, 2015. DOI: 10.1146/annurev-physchem-040214-121821.

[10] J. Cadet, S. Mouret, J. L. Ravanat und T. Douki, „Photoinduced damage to cellular DNA: Direct and photosensitized reactions“, *Photochemistry and Photobiology*, Jg. 88, Nr. 5, S. 1048–1065, 2012. DOI: 10.1111/j.1751-1097.2012.01200.x.

[11] R. P. Sinha und D.-P. Häder, „UV-induced DNA damage and repair: a review“, *Photochemical & Photobiological Sciences*, Jg. 1, Nr. 4, S. 225–236, Apr. 2002. DOI: 10.1039/b201230h.

[12] J. Cadet und P. Vigny, „The photochemistry of nucleic acids“, in *Bioorganic Photochemistry*, H. Morrison, Hrsg., New York: John Wiley & Sons, 1990, S. 1–272.

[13] T. Douki, „Effect of denaturation on the photochemistry of pyrimidine bases in isolated DNA“, *Journal of Photochemistry and Photobiology B: Biology*, Jg. 82, Nr. 1, S. 45–52, Jan. 2006. DOI: 10.1016/j.jphotobiol.2005.08.009.

[14] T. Douki, „The variety of UV-induced pyrimidine dimeric photoproducts in DNA as shown by chromatographic quantification methods“, *Photochemical and Photobiological Sciences*, Jg. 12, Nr. 8, S. 1286–1302, 2013. DOI: 10.1039/c3pp25451h.

[15] W. J. Schreier, T. E. Schrader, F. O. Koller u. a., „Thymine Dimerization in DNA Is an Ultrafast Photoreaction“, *Science*, Jg. 315, Nr. 5812, S. 625–629, Feb. 2007. DOI: 10.1126/science.1135428.

[16] D. E. Godar, „UVA1 Radiation Triggers Two Different Final Apoptotic Pathways“, *Journal of Investigative Dermatology*, Jg. 112, Nr. 1, S. 3–12, Jan. 1999. DOI: 10.1046/j.1523-1747.1999.00474.x.

[17] B. R. Vowels, E. K. Yoo und F. P. Gasparro, „Kinetic Analysis of Apoptosis Induction in Human Cell Lines by UVA and 8-MOP“, *Photochemistry and Photobiology*, Jg. 63, Nr. 5, S. 572–576, Mai 1996. DOI: 10.1111/j.1751-1097.1996.tb05658.x.

[18] R. Johnson, L. Staiano-Coico, L. Austin u. a., „PUVA treatment selectively induces a cell cycle block and subsequent apoptosis in human T-lymphocytes“, *Photochemistry and Photobiology*, Jg. 63, Nr. 5, S. 566–571, 1996. DOI: 10.1111/j.1751-1097.1996.tb05657.x.

[19] D. Pathirana, A. Ormerod, P. Saiag u. a., „European S3-Guidelines on the systemic treatment of psoriasis vulgaris“, *Journal of the European Academy of Dermatology and Venereology*, Jg. 23, Nr. SUPPL. 2, S. 1–70, Okt. 2009. DOI: 10.1111/j.1468-3083.2009.03389.x.

[20] A. Menter, N. J. Korman, C. A. Elmets u. a., „Guidelines of care for the management of psoriasis and psoriatic arthritis“, *Journal of the American Academy of Dermatology*, Jg. 62, Nr. 1, S. 114–135, Jan. 2010. DOI: 10.1016/j.jaad.2009.08.026.

[21] R. Sidbury, D. M. Davis, D. E. Cohen u. a., „Guidelines of care for the management of atopic dermatitis“, *Journal of the American Academy of Dermatology*, Jg. 71, Nr. 2, S. 327–349, Aug. 2014. DOI: 10.1016/j.jaad.2014.03.030.

[22] A. Taieb, A. Alomar, M. Böhm u. a., „Guidelines for the management of vitiligo: the European Dermatology Forum consensus“, *British Journal of Dermatology*, Jg. 168, Nr. 1, S. 5–19, Jan. 2013. DOI: 10.1111/j.1365-2133.2012.11197.x.

[23] N. Oiso, T. Suzuki, M. Wataya-kaneda u. a., „Guidelines for the diagnosis and treatment of vitiligo in Japan“, *The Journal of Dermatology*, Jg. 40, Nr. 5, S. 344–354, Mai 2013. DOI: 10.1111/1346-8138.12099.

[24] E. A. Olsen, E. Hodak, T. Anderson u. a., „Guidelines for phototherapy of mycosis fungoides and Sézary syndrome: A consensus statement of the United States Cutaneous Lymphoma Consortium“, *Journal of the American Academy of Dermatology*, Jg. 74, Nr. 1, S. 27–58, Jan. 2016. DOI: 10.1016/j.jaad.2015.09.033.

[25] T. C. Ling, T. H. Clayton, J. Crawley u. a., „British Association of Dermatologists and British Photodermatology Group guidelines for the safe and effective use of psoralen-ultraviolet A therapy 2015“, *British Journal of Dermatology*, Jg. 174, Nr. 1, S. 24–55, 2016. DOI: 10.1111/bjd.14317.

[26] T. B. Fitzpatrick und M. Pathak, „Part IV: Basic Considerations of the Psoralens: Historical Aspects of Methoxsalen and Other Furocoumarins“, *Journal of Investigative Dermatology*, Jg. 32, Nr. 2, S. 229–231, Feb. 1959. DOI: 10.1038/jid.1959.40.

[27] M. A. Pathak und T. B. Fitzpatrick, „The evolution of photochemotherapy with psoralens and UVA (PUVA): 2000 BC to 1992 AD“, *Journal of Photochemistry and Photobiology, B: Biology*, Jg. 14, Nr. 1-2, S. 3–22, 1992. DOI: 10.1016/1011-1344(92)85080-E.

[28] H. Hönigsmann, „History of phototherapy in dermatology“, *Photochem. Photobiol. Sci.*, Jg. 12, Nr. 1, S. 16–21, 2013. DOI: 10.1039/C2PP25120E.

[29] H. Kuske, „Experimentelle Untersuchungen zur Photosensibilisierung der Haut durch pflanzliche Wirkstoffe“, *Archiv für Dermatologie und Syphilis*, Jg. 178, Nr. 2, S. 112–123, Okt. 1938. DOI: 10.1007/BF02068442.

[30] I. R. Fahmy und H. Abu-Shady, „Ammi Majus Linn.; Pharmacognostical Study and Isolation of a Crystalline Constituent, Ammoidin“, *Q J Pharm Pharmacol.*, Jg. 20, Nr. 3, S. 281–291, 1947.

[31] A. M. El Mofty, „A preliminary clinical report on the treatment of leukoderma with Ammi majus Linn“, *J. R. Egypt Med. Assoc.*, Jg. 31, S. 651–665, 1948.

[32] J. A. Parrish, T. B. Fitzpatrick, L. Tanenbaum und M. A. Pathak, „Photochemotherapy of Psoriasis with Oral Methoxsalen and Longwave Ultraviolet Light“, *New England Journal of Medicine*, Jg. 291, Nr. 23, S. 1207–1211, Dez. 1974. DOI: 10.1056/NEJM197412052912301.

[33] R. S. Stern, L. A. Thibodeau, R. A. Kleinerman, J. A. Parrish und T. B. Fitzpatrick, „Risk of Cutaneous Carcinoma in Patients Treated with Oral Methoxsalen Photochemotherapy for Psoriasis“, *New England Journal of Medicine*, Jg. 300, Nr. 15, S. 809–813, Apr. 1979. DOI: 10.1056/NEJM197904123001501.

[34] L. Musajo, G. Rodighiero, G. Colombo, V. Torlone und F. Dall'Acqua, „Photosensitizing furocoumarins: Interaction with DNA and photo-inactivation of DNA containing viruses“, *Experientia*, Jg. 21, Nr. 1, S. 22–24, Jan. 1965. DOI: 10.1007/BF02136362.

[35] R. Dodd, G. Moroff, S. Wagner u. a., „Inactivation of viruses in platelet suspensions that retain their in vitro characteristics: comparison of psoralen-ultraviolet A and merocyanine 540-visible light methods“, *Transfusion*, Jg. 31, Nr. 6, S. 483–490, Juli 1991. DOI: 10.1046/j.1537-2995.1991.31691306242.x.

[36] J. Kaiser-Guignard, G. Canellini, N. Lion u. a., „The clinical and biological impact of new pathogen inactivation technologies on platelet concentrates“, *Blood Reviews*, Jg. 28, Nr. 6, S. 235–241, Nov. 2014. DOI: 10.1016/j.blre.2014.07.005.

[37] R. Edelson, C. Berger, F. Gasparro u. a., „Treatment of Cutaneous T-Cell Lymphoma by Extracorporeal Photochemotherapy“, *New England Journal of Medicine*, Jg. 316, Nr. 6, S. 297–303, Feb. 1987. DOI: 10.1056/NEJM198702053160603.

[38] R. Knobler, G. Berlin, P. Calzavara-Pinton u. a., „Guidelines on the use of extracorporeal photopheresis“, *Journal of the European Academy of Dermatology and Venereology*, Jg. 28, S. 1–37, Jan. 2014. DOI: 10.1111/jdv.12311.

[39] R. L. Edelson, „Photopheresis: Present and future aspects“, *Journal of Photochemistry and Photobiology B: Biology*, Jg. 10, Nr. 1-2, S. 165, Juli 1991. DOI: 10.1016/1011-1344(91)80221-3.

[40] H. T. Greinix, R. M. Knobler, N. Worel u. a., „The effect of intensified extracorporeal photochemotherapy on long-term survival in patients with severe acute graft-versus-host disease“, *Haematologica*, Jg. 91, Nr. 3, S. 405–408, 2006.

[41] M. Sasaki, F. Meguro, E. Kumazawa u. a., „Evidence for uptake of 8-methoxypsoralen and 5-methoxypsoralen by cellular nuclei“, *Mutation Research/Fundamental and Molecular Mechanisms of Mutagenesis*, Jg. 197, Nr. 1, S. 51–58, Jan. 1988. DOI: 10.1016/0027-5107(88)90139-X.

[42] I. M. Schmitt, S. Chimenti und F. P. Gasparro, „Psoralen-protein photochemistry — a forgotten field“, *Journal of Photochemistry and Photobiology B: Biology*, Jg. 27, Nr. 2, S. 101–107, Feb. 1995. DOI: 10.1016/1011-1344(94)07101-S.

[43] S. T. Isaacs, C. Chun, J. E. Hyde, H. Rapoport und J. E. Hearst, „A Photochemical Characterization of Reactions of Psoralen Derivatives with DNA“, in *Trends in Photobiology*, Boston, MA: Springer US, 1982, S. 279–294. DOI: 10.1007/978-1-4615-9203-7_24.

[44] S. T. Isaacs, C.-K. J. Shen, J. E. Hearst und H. Rapoport, „Synthesis and characterization of new psoralen derivatives with superior photoreactivity with DNA and RNA“, *Biochemistry*, Jg. 16, Nr. 6, S. 1058–1064, März 1977. DOI: 10.1021/bi00625a005.

[45] J. Tatchen und C. M. Marian, „Vibronic absorption, fluorescence, and phosphorescence spectra of psoralen: A quantum chemical investigation“, *Physical Chemistry Chemical Physics*, Jg. 8, Nr. 18, S. 2133–2144, 2006. DOI: 10.1039/b518436c.

[46] W. W. Mantulin und P.-S. Song, „Excited states of skin-sensitizing coumarins and psoralens. Spectroscopic studies“, *Journal of the American Chemical Society*, Jg. 95, Nr. 16, S. 5122–5129, Aug. 1973. DOI: 10.1021/ja00797a004.

[47] S. Fröbel, „Ultraschnelle Prozesse bei der therapeutisch genutzten Photochemie von Psoralenen in DNA“, Dissertation, Institut für Physikalische Chemie II der Heinrich-Heine-Universität Düsseldorf, 2016.

[48] A. Andreoni, R. Cubeddu, F. Dall'Acqua, C. N. Knox und T. G. Truscott, „Fluorescence lifetimes of furocoumarins. Psoralens“, *Chemical Physics Letters*, Jg. 114, Nr. 3, S. 329–333, März 1985. DOI: 10.1016/0009-2614(85)80925-8.

[49] R. V. Bensasson, E. J. Land und C. Salet, „Triplet excited state of furocoumarins: reaction with nucleic acid bases and amino acids.“, *Photochemistry and photobiology*, Jg. 27, Nr. 3, S. 273–80, März 1978. DOI: 10.1111/j.1751-1097.1978.tb07600.x.

[50] C. Salet, T. Macedo De Sa E Melo, R. Bensasson und E. J. Land, „Photophysical properties of aminomethylpsoralen in presence and absence of DNA“, *Biochimica et Biophysica Acta (BBA) - Nucleic Acids and Protein Synthesis*, Jg. 607, Nr. 2, S. 379–383, Apr. 1980. DOI: 10.1016/0005-2787(80)90090-8.

[51] J. Tatchen, N. Gilka und C. M. Marian, „Intersystem crossing driven by vibronic spin–orbit coupling: a case study on psoralen“, *Physical Chemistry Chemical Physics*, Jg. 9, Nr. 38, S. 5209, 2007. DOI: 10.1039/b706410a.

[52] S. Caffieri, „Furocoumarin photolysis: chemical and biological aspects“, *Photochemical & Photobiological Sciences*, Jg. 1, Nr. 3, S. 149–157, März 2002. DOI: 10.1039/b107329j.

[53] L. Lerman, „Structural considerations in the interaction of DNA and acridines“, *Journal of Molecular Biology*, Jg. 3, Nr. 1, 18–IN14, Feb. 1961. DOI: 10.1016/S0022-2836(61)80004-1.

[54] G. Dougherty und W. J. Pigram, „Spectroscopic Analysis of Drug-Nucleic Acid Interaction“, *Critical Reviews in Biochemistry*, Jg. 12, Nr. 2, S. 103–132, Jan. 1982. DOI: 10.3109/10409238209108704.

[55] J. B. Lepecq und C. Paoletti, „A fluorescent complex between ethidium bromide and nucleic acids. Physical-Chemical characterization“, *Journal of Molecular Biology*, Jg. 27, Nr. 1, S. 87–106, 1967. DOI: 10.1016/0022-2836(67)90353-1.

[56] N. C. Garbett, P. A. Ragazzon und J. B. Chaires, „Circular dichroism to determine binding mode and affinity of ligand–DNA interactions“, *Nature Protocols*, Jg. 2, Nr. 12, S. 3166–3172, Dez. 2007. DOI: 10.1038/nprot.2007.475.

[57] F. Dall'Acqua, M. Terbojevich, S. Marciani, D. Vedaldi und M. Recher, „Investigation on the dark interaction between furocoumarins and DNA“, *Chemico-Biological Interactions*, Jg. 21, Nr. 1, S. 103–115, Apr. 1978. DOI: 10.1016/0009-2797(78)90071-6.

[58] E. C. Long und J. K. Barton, „On demonstrating DNA intercalation“, *Accounts of Chemical Research*, Jg. 23, Nr. 9, S. 271–273, Sep. 1990. DOI: 10.1021/ar00177a001.

[59] G. Wiesehahn und J. E. Hearst, „DNA unwinding induced by photoaddition of psoralen derivatives and determination of dark-binding equilibrium constants by gel electrophoresis“, *Proceedings Of The National Academy Of Sciences Of The United States Of America*, Jg. 75, Nr. 6, S. 2703–2707, 1978. DOI: 10.1073/pnas.75.6.2703.

[60] J. E. Hyde und J. E. Hearst, „Binding of psoralen derivatives to DNA and chromatin: influence of the ionic environment on dark binding and photoreactivity“, *Biochemistry*, Jg. 17, Nr. 7, S. 1251–1257, Apr. 1978. DOI: 10.1021/bi00600a019.

[61] S. Fröbel, A. Reiffers, C. Torres Ziegenbein und P. Gilch, „DNA Intercalated Psoralen Undergoes Efficient Photoinduced Electron Transfer“, *The Journal of Physical Chemistry Letters*, Jg. 6, Nr. 7, S. 1260–1264, Apr. 2015. DOI: 10.1021/acs.jpclett.5b00307.

[62] J.-P. Demaret, S. Brunie, J.-P. Ballini und P. Vigny, „Geometry of Intercalation of Psoralens in DNA Approached by Molecular Mechanics“, *Photochemistry and Photobiology*, Jg. 50, Nr. 1, S. 7–21, Juli 1989. DOI: 10.1111/j.1751-1097.1989.tb04124.x.

[63] G. D. Cimino, H. B. Gamper, S. T. Isaacs und J. E. Hearst, „Psoralens as photoactive probes of nucleic acid structure and function“, *Annual Review of Biochemistry*, Jg. 54, S. 1151–1193, 1985.

[64] N. Kitamura, S. Kohtani und R. Nakagaki, „Molecular aspects of furocoumarin reactions: Photophysics, photochemistry, photobiology, and structural analysis“, *Journal of Photochemistry and Photobiology C: Photochemistry Reviews*, Jg. 6, Nr. 2-3, S. 168–185, Okt. 2005. DOI: 10.1016/j.jphotochemrev.2005.08.002.

[65] D. Kanne, H. Rapoport und J. E. Hearst, „8-Methoxypsoralen-nucleic acid photoreaction. Effect of methyl substitution on pyrone vs. furan photoaddition“, *Journal of Medicinal Chemistry*, Jg. 27, Nr. 4, S. 531–534, Apr. 1984. DOI: 10.1021/jm00370a017.

[66] G. Rodighiero, L. Musajo, F. Dall'acqua u. a., „Mechanism of skin photosensitization by forucoumarins“, *Biochimica et Biophysica Acta (BBA) - Nucleic Acids and Protein Synthesis*, Jg. 217, Nr. 1, S. 40–49, Sep. 1970. DOI: 10.1016/0005-2787(70)90120-6.

[67] P. C. Beaumont, B. J. Parsons, S. Navaratnam, G. O. Phillips und J. C. Allen, „The reactivities of furocoumarin exicted states with DNA in solution. A laser flash photolysis and fluorescence study“, *Biochimica et Biophysica Acta*, Jg. 608, Nr. 2, S. 259–265, Juli 1980. DOI: 10.1016/0005-2787(80)90171-9.

[68] P. C. Beaumont, B. J. Parsons, G. O. Philips und J. C. Allen, „A laser flash photolysis and fluorescence study of aminomethyltrimethylpsoralen in the presence and absence of DNA“, *Photobiochem. Photobiophys*, Jg. 5, S. 359–364, 1983.

[69] J. J. Serrano-Pérez, L. Serrano-Andrés und M. Merchán, „Photosensitization and phototherapy with furocoumarins: A quantum-chemical study“, *Chemical Physics*, Jg. 347, Nr. 1-3, S. 422–435, Mai 2008. DOI: 10.1016/j.chemphys.2007.10.011.

[70] J. J. Serrano-Pérez, M. Merchán und L. Serrano-Andrés, „Photoreactivity of Furocoumarins and DNA in PUVA Therapy: Formation of Psoralen-Thymine Adducts“, *The Journal of Physical Chemistry B*, Jg. 112, Nr. 44, S. 14 002–14 010, Nov. 2008. DOI: 10.1021/jp805523d.

[71] S. Omar und L. A. Eriksson, „Interaction and photobinding between 8-methoxypsoralen and thymine“, *Chemical Physics Letters*, Jg. 471, Nr. 1-3, S. 128–132, März 2009. DOI: 10.1016/j.cplett.2009.02.010.

[72] X. Huang und R. Zhang, „A Theoretical Rationale why Furan-side Monoadduct is More Favorable Toward Diadduct Formation in 8-Methoxypsoralen and Thymine Complexes“, *Photochemistry and Photobiology*, Jg. 89, Nr. 4, S. 891–899, Juli 2013. DOI: 10.1111/php.12067.

[73] E. Sage und E. Moustacchi, „Sequence context effects on 8-methoxypsoralen photobinding to defined DNA fragments“, *Biochemistry*, Jg. 26, Nr. 12, S. 3307–3314, Juni 1987. DOI: 10.1021/bi00386a010.

[74] S. Fröbel, L. Levi, S. M. Ulamec und P. Gilch, „Photoinduced Electron Transfer between Psoralens and DNA: Influence of DNA Sequence and Substitution“, *ChemPhysChem*, Jg. 17, Nr. 9, S. 1377–1386, Mai 2016. DOI: 10.1002/cphc.201500889.

[75] S. R. Geenen, L. Presser, T. Hölzel, C. Ganter und T. J. J. Müller, „Electronic Fine-tuning of 8-Methoxy Psoralens by Palladium-Catalyzed Coupling: Acidochromicity and Solvatochromicity“, *Chemistry – A European Journal*, Jg. 26, Nr. 36, S. 8064–8075, Juni 2020. DOI: 10.1002/chem.201905676.

[76] S. R. Geenen, T. Schumann und T. J. J. Müller, „Fluorescent Donor–Acceptor Psoralen Cruciforms by Consecutive Suzuki–Suzuki and Sonogashira–Sonogashira One-Pot Syntheses“, *The Journal of Organic Chemistry*, Jg. 85, Nr. 15, S. 9737–9750, Aug. 2020. DOI: 10.1021/acs.joc.0c01059.

[77] S. R. Geenen, „Synthese und Eigenschaften neuartiger Donor-Akzeptor-Psoralen-Chromophore“, Dissertation, Institut für Organische Chemie und Makromolekulare Chemie der Heinrich-Heine-Universität Düsseldorf, 2020.

[78] A. Weller, „Photoinduced Electron Transfer in Solution: Exciplex and Radical Ion Pair Formation Free Enthalpies and their Solvent Dependence“, *Zeitschrift für Physikalische Chemie*, Jg. 133, Nr. 1, S. 93–98, Jan. 1982. DOI: 10.1524/zpch.1982.133.1.093.

[79] T. Villnow, „Schnelle Interkombination aromatischer Carbonylverbindungen am Beispiel von Thioxanthon und Anthrachinon“, Dissertation, Institut für Physikalische Chemie II der Heinrich-Heine-Universität Düsseldorf, 2015.

[80] C. Torres Ziegenbein, „Effziente blaue OLED Emitter durch reverse Interkombination in aromatischen Carbonylverbindungen?“, Dissertation, Institut für Physikalische Chemie II der Heinrich-Heine-Universität Düsseldorf, 2018.

[81] A. Reiffers, „Zeitaufgelöste Spektroskopie zur Photophysik und Photochemie von Phthalimiden“, Dissertation, Institut für Physikalische Chemie II der Heinrich-Heine-Universität Düsseldorf, 2020.

[82] K. A. Thom, „Direkte und sensibilisierte Untersuchung von aromatischen Carbonylen als neuartige OLED-Emitter“, Dissertation, Institut für Physikalische Chemie II der Heinrich-Heine-Universität Düsseldorf, 2021.

[83] I. H. van Stokkum, D. S. Larsen und R. van Grondelle, „Global and target analysis of time-resolved spectra“, *Biochimica et Biophysica Acta (BBA) - Bioenergetics*, Jg. 1657, Nr. 2-3, S. 82–104, Juli 2004. DOI: 10.1016/j.bbabio.2004.04.011.

[84] H. Satzger und W. Zinth, „Visualization of transient absorption dynamics - Towards a qualitative view of complex reaction kinetics“, *Chemical Physics*, Jg. 295, Nr. 3, S. 287–295, 2003. DOI: 10.1016/j.chemphys.2003.08.012.

[85] R. Croce, M. G. Müller, R. Bassi und A. R. Holzwarth, „Carotenoid-to-Chlorophyll Energy Transfer in Recombinant Major Light-Harvesting Complex (LHCII) of Higher Plants. I. Femtosecond Transient Absorption Measurements“, *Biophysical Journal*, Jg. 80, Nr. 2, S. 901–915, Feb. 2001. DOI: 10.1016/S0006-3495(01)76069-9.

[86] M. G. Müller, J. Niklas, W. Lubitz und A. R. Holzwarth, „Ultrafast Transient Absorption Studies on Photosystem I Reaction Centers from Chlamydomonas reinhardtii. 1. A New Interpretation of the Energy Trapping and Early Electron Transfer Steps in Photosystem I“, *Biophysical Journal*, Jg. 85, Nr. 6, S. 3899–3922, 2003. DOI: 10.1016/S0006-3495(03)74804-8.

[87] A. R. Holzwarth, M. G. Muller, M. Reus u. a., „Kinetics and mechanism of electron transfer in intact photosystem II and in the isolated reaction center: Pheophytin is the primary electron acceptor“, *Proceedings of the National Academy of Sciences*, Jg. 103, Nr. 18, S. 6895–6900, 2006. DOI: 10.1073/pnas.0505371103.

[88] A. R. Holzwarth, M. G. Müller, J. Niklas und W. Lubitz, „Ultrafast Transient Absorption Studies on Photosystem I Reaction Centers from Chlamydomonas reinhardtii. 2: Mutations near the P700 Reaction Center Chlorophylls Provide New Insight into the Nature of the Primary Electron Donor“, *Biophysical Journal*, Jg. 90, Nr. 2, S. 552–565, Jan. 2006. DOI: 10.1529/biophysj.105.059824.

[89] V. A. Lórenz-Fonfría und H. Kandori, „Transformation of Time-Resolved Spectra to Lifetime-Resolved Spectra by Maximum Entropy Inversion of the Laplace Transform“, *Applied Spectroscopy*, Jg. 60, Nr. 4, S. 407–417, Apr. 2006. DOI: 10.1366/000370206776593654.

[90] C. Slavov, H. Hartmann und J. Wachtveitl, „Implementation and Evaluation of Data Analysis Strategies for Time-Resolved Optical Spectroscopy“, *Analytical Chemistry*, Jg. 87, Nr. 4, S. 2328–2336, Feb. 2015. DOI: 10.1021/ac504348h.

[91] G. F. Dorlhiac, C. Fare und J. J. van Thor, „PyLDM - An open source package for lifetime density analysis of time-resolved spectroscopic data.“, *PLoS computational biology*, Jg. 13, Nr. 5, T. Poisot, Hrsg., e1005528, Mai 2017. DOI: 10.1371/journal.pcbi.1005528.

[92] J. Diekmann, J. Gontcharov, S. Fröbel u. a., „The Photoaddition of a Psoralen to DNA Proceeds via the Triplet State“, *Journal of the American Chemical Society*, Jg. 141, Nr. 34, S. 13 643–13 653, Aug. 2019. DOI: 10.1021/jacs.9b06521.

[93] D. Kanne, K. Straub, H. Rapoport und J. E. Hearst, „Psoralen-Deoxyribonucleic Acid Photoreaction. Characterization of the Monoaddition Products from 8-Methoxypsoralen and 4,5',8-Trimethylpsoralen“, *Biochemistry*, Jg. 21, Nr. 5, S. 861–871, 1982. DOI: 10.1021/bi00534a008.

[94] L. Liu, B. M. Pilles, J. Gontcharov, D. B. Bucher und W. Zinth, „Quantum Yield of Cyclobutane Pyrimidine Dimer Formation Via the Triplet Channel Determined by Photosensitization“, *Journal of Physical Chemistry B*, Jg. 120, Nr. 2, S. 292–298, 2016. DOI: 10.1021/acs.jpcb.5b08568.

[95] J. P. Demaret, J. P. Ballini und P. Vigny, „Molecular mechanics and dynamics study of DNA-furocoumarins complexes: Effect of methylation of the angular derivati-

ves on the intercalation geometry“, *Journal of Computer-Aided Molecular Design*, Jg. 7, Nr. 6, S. 683–698, 1993. DOI: 10.1007/BF00125326.

[96] F. Bordin, F. Dall'acqua und A. Guiotto, „Angelicins, angular analogs of psoralens: Chemistry, photochemical, photobiological and phototherapeutic properties“, *Pharmacology and Therapeutics*, Jg. 52, Nr. 3, S. 331–363, 1991. DOI: 10.1016/0163-7258(91)90031-G.

[97] M. Craw, R. V. Bensasson, J. C. Ronfard-Haret, M. T. S. Melo und T. G. Truscott, „Some Photophysical Properties of 3-Carbethoxypsoralen, 8-Methoxypsoralen and 5-Methoxypsoralen Triplet States“, *Photochemistry and Photobiology*, Jg. 37, Nr. 6, S. 611–615, Juni 1983. DOI: 10.1111/j.1751-1097.1983.tb04529.x.

[98] P. C. Beaumont, B. J. Parsons, G. O. Phillips und J. C. Allen, „A laser flash photolysis study of the reactivities of the triplet states of 8-methoxypsoralen and 4,5',8-trimethylpsoralen with nucleic acid bases in solution“, *Biochimica et Biophysica Acta (BBA) - Nucleic Acids and Protein Synthesis*, Jg. 562, Nr. 2, S. 214–221, Apr. 1979. DOI: 10.1016/0005-2787(79)90167-9.

[99] F. Dall'Acqua, D. Vedaldi, A. Guiotto u. a., „Methylangelicins: New Potential Agents for the Photochemotherapy of Psoriasis. Structure-Activity Study on the Dark and Photochemical Interactions with DNA“, *Journal of Medicinal Chemistry*, Jg. 24, Nr. 7, S. 806–811, 1981. DOI: 10.1021/jm00139a008.

[100] F. Dall'Acqua, D. Vedaldi, F. Bordin u. a., „4'-Methylangelicins: new potential agents for the photochemotherapy of psoriasis“, *Journal of Medicinal Chemistry*, Jg. 26, Nr. 6, S. 870–876, Juni 1983. DOI: 10.1021/jm00360a016.

[101] G. Rodighiero, F. Dall'Acqua, S. Marciani u. a., „Studies on the reactivation of bacteria photodamaged by an angular furocoumarin: Angelicin“, *Biophysik*, Jg. 8, Nr. 1, S. 1–8, März 1971. DOI: 10.1007/BF01194255.

[102] M. J. Ashwood-Smith und E. Grant, „Conversion of psoralen DNA monoadducts in E. coli to interstrand DNA cross links by near UV light (320-360 nm): Inability of angelicin to form cross links, in vivo“, *Experientia*, Jg. 33, Nr. 3, S. 384–386, 1977. DOI: 10.1007/BF02002841.

[103] O. Gia, A. Anselmo, M. T. Conconi u. a., „4'-Methyl derivatives of 5-MOP and 5-MOA: Synthesis, photoreactivity, and photobiological activity“, *Journal of Medicinal Chemistry*, Jg. 39, Nr. 22, S. 4489–4496, 1996. DOI: 10.1021/jm960117r.

[104] F. Baccichetti, F. Carlassare, F. Bordinα u. a., „4,4',6-Trimethylangelicin, a New very Photoreactive and non Skin-Phototoxic Monofunctional Furocoumarin“, *Photochemistry and Photobiology*, Jg. 39, Nr. 4, S. 525–529, Jan. 1984. DOI: 10.1111/j.1751-1097.1984.tb03887.x.

,